Massachusetts Institute of Technology
Department of Civil Engineering
Constructed Facilities Division
Cambridge, Massachusetts 02139

ON THE USE OF SIMPLE MODELS IN NONLINEAR DYNAMIC ANALYSIS

by

JAVIER R. PIQUE

Supervised by

José M. Roesset

September 1976

Sponsored by the National Science Foundation
Division of Advanced Environmental Research and Technology
Grant GI-43106

Research Report R76-43 Order No. 559

50272-101

REPORT DOCUMENTATION PAGE	1. REPORT NO. NSF/RA-761701	2.	3. Recipient's Accession No.

4. Title and Subtitle
On the Use of Simple Models in Nonlinear Dynamic Analysis

5. Report Date
September 1976

6.

7. Author(s)
J. R. Pique

8. Performing Organization Rept. No.
R76-43

9. Performing Organization Name and Address
Massachusetts Institute of Technology
School of Engineering
Department of Civil Engineering
Cambridge, Massachusetts 02139

10. Project/Task/Work Unit No.
Order No. 559

11. Contract(C) or Grant(G) No.
(C)
(G) GI43106

12. Sponsoring Organization Name and Address
Engineering and Applied Science (EAS)
National Science Foundation
1800 G Street, N.W.
Washington, D.C. 20550

13. Type of Report & Period Covered

14.

15. Supplementary Notes

16. Abstract (Limit: 200 words)
An evaluation of simple models to predict the inelastic dynamic response of frames is presented. Two types of models were considered, a shear-beam model with the floor springs determined on the basis of an incremental static analysis, and an equivalent one-degree-of-freedom system resulting from the same analysis. Three heights of frames were studied, a four-story frame designed by UBC, three ten-story frames (one designed by UBC, Anderson's frame, and Kamil's frame). Analyses were performed under El Centro 1940 (N-S) earthquake for different intensities and Taft (N69W).

The simple models can provide a reasonable approximation to the response with largest discrepancies of the order of 27%. Solutions obtained with the equivalent single-degree-of-freedom system are comparable to those of the shear-beam model, or even better for the four- and ten-story frames. For the taller structure, however, the response deteriorates slightly. Changes in motion intensity did not seem to alter the degree of accuracy of the response; neither did the different ground motions. The structural responses were, however, very different for the two earthquakes.

17. Document Analysis a. Descriptors
Nonlinear systems
Dynamic structural analysis
Elastic properties
Degrees of freedom
Framed structures
Frames

b. Identifiers/Open-Ended Terms
Nonlinear dynamic analysis

c. COSATI Field/Group

18. Availability Statement
NTIS

19. Security Class (This Report)

20. Security Class (This Page)

21. No. of Pages
284

22. Price
A13-A01

ABSTRACT

An evaluation of simple models to predict the inelastic dynamic response of frames is presented. Two types of models were considered, a shear-beam model with the floor springs determined on the basis of an incremental static analysis, and an equivalent one-degree-of-freedom system resulting from the same analysis. Three heights of frames were studied, a four-story frame designed by UBC, three ten-story frames (one designed by UBC, Anderson's frame, and Kamil's frame). Analyses were performed under El Centro 1940 (N-S) earthquake for different intensities and Taft (N69W).

The simple models can provide a reasonable approximation to the response with largest discrepancies of the order of 27%. Solutions obtained with the equivalent single-degree-of-freedom system are comparable to those of the shear-beam model, or even better for the four- and ten-story frames. For the taller structure, however, the response deteriorates slightly. Changes in motion intensity did not seem to alter the degree of accuracy of the response; neither did the different ground motions. The structural responses were, however, very different for the two earthquakes.

When the bending yield criterion was used, an improvement in the agreement of the responses was obtained.

Local member ductilities were estimated based on the predictions from the simple models and the static analysis. The results show reasonable agreement with the point-hinge model response.

PREFACE

The work described in this report is based on the thesis by Javier Piqué, presented to the Civil Engineering Department at M.I.T. in partial fulfillment of the requirements for the degree of Doctor of Philosophy. The research was supervised by Professor José M. Roesset and was made possible through Grant GI-43106 from the National Science Foundation, Division of Advanced Environmental Research and Technology.

This is the fourth of a series of reports published under this grant. The first three were:

1. Research Report R76-37, by Tarek S. Aziz: "Inelastic Dynamic Analysis of Building Frames," August 1976.

2. Research Report R76-38, by Kenneth Mark: "Nonlinear Dynamic Response of Reinforced Concrete Frames," August 1976.

3. Research Report R76-42, by Samir Sehayek: "Effect of Ductility On Response Spectra for Elasto-Plastic Systems," September 1976.

A mis padres , a quienes todo les debo

TABLE OF CONTENTS

Table of Contents (Continued)

Table of Contents (Continued)

LIST OF FIGURES

LIST OF TABLES

LIST OF SYMBOLS

A	Cross-sectional Area
B	Square Diagonal Matrix (nxn) with terms $2\beta_i\omega_i$ for viscous damping in Mode D
C	Damping Matrix
D	Width of Building in the Direction of Earthquake
E	Modulus of Elasticity
F	Vector of Lateral Forces
F_i	Force in story "i"
F_t	Additional Concentrated Lateral Force on top story
F_y	Yield Stress for material Yield Force on floor spring
G	Shear Modulus
h	Story Height or Total Building Height
h_i	Height from story "i" to the ground
I	Unit Vector
I_c	Inertia Column
I_g	Inertia girder
i	Subscript to indicate story number
j	Subscript to indicate net deflected shape number "j"
K	Equivalent Stiffness of E.S.D.O.F.
K_c	I_c/h Relative Stiffness of Columns
K_{ga}	I_{ga}/ℓ Relative Stiffness of girders above floor under consideration
K_{gb}	I_{gb}/ℓ Relative Stiffness of girders below floor under consideration
K	Equivalent Stiffness of E.S.D.O.F.

List of Symbols Continued

K	Floor Stiffness or Stiffness Matrix
K_1	Inition Floor Stiffness
K_2	Second Branch Stiffness
k	Stiffness of Elastoplastic Component in Multilinear Spring
k_{tj}	Tangent Stiffness of Branch j or E.S.D.O.F. Multilinear Spring
ℓ	Girder Span
M	Equivalent Mass of E.S.D.O.F.
M	Bending Moment Mass Matrix
M_y	Yield Moment in a Bilinear Moment-Rotation Curve
M_p	Plastic Moment ZF_y
M_{pc}	Plastic Moment Columns
M_{pg}	Plastic Moment Girders
P	Member Axial Load or Vector of Lateral Load Increments
P_y	Axial Load Capacity
p	Percentage of Initial Slope Used for Second Branch of a Bilinear Curve, or of dual component model
Q	Square Matrix Containing Modal Shapes
$( )^T$	Indicates Transpose Matrix
U	Relative Floor Displacements Deflected Shapes
U'	Net Deflected Shapes $U_{j+1} - U_j$
$\ddot{U}$	Vector of Relative Floor Accelerations
u	Incremental Horizontal Joint Displacement. Relative Displacement on E.S.D.O.F.
$\ddot{u}_G$	Ground Acceleration

List of Symbols Continued

V	Base Shear, Story Shear
v	Incremental Vertical Joint Displacements
W_i	Weight of floor "i"
x, y	Joint Coordinates
Z	Plastic Modulus
β	Percentage of Critical Damping
Δ	Interstory Displacement or Distortion. Also Denotes Increment
δ	Lateral Floor Displacement, Respect to the Ground
δ_t	Lateral Displacement of Top Floor
ϕ	Curvature
μ_θ	Rotation Ductility
μ_M	Moment Ductility

CHAPTER 1

INTRODUCTION

1.1 MODELS FOR INELASTIC DYNAMIC ANALYSIS

Modern engineered buildings are expected to have deformations in the inelastic range during the occurrence of strong earthquakes. This is a fact accepted by present design philosophies based primarily on two considerations, i.e., the relatively small probability of occurrence of the design earthquake during the lifetime of the structure and the

supposedly excessive cost of designing the building to remain elastic under such excitation. Thus the necessity to develop procedures of analysis to predict the response of buildings in the inelastic range under seismic ground motions. Several ways of modeling structural frames for nonlinear dynamic analysis have been presented, varying in the level of sophistication. They can be grossly classified in three groups: simple models, point-hinge models, and fiber models.

The cost of the analysis increases substantially from the simple models towards the fiber models. As a research tool, the fiber models should give, when properly implemented, the most accurate picture of the dynamic behavior of a building. In this sense, they could serve as the measure against which the other models are compared. Practically for larger structures this becomes, however, prohibitive, and the point-hinge models have been used for this purpose instead.

A very short overall descriptive view of these models is presented next, and in section 1.1.4 a summary of findings by other researchers concerning the shear-beam models is included.

1.1.1 Simple Models

Most of the models developed in this category are the ones known as shear-beam models. Initially developed and used for one-degree-of-freedom systems [1]*, they have been extended to multi-degree-of-freedom systems or multistory frames [2,3]. These models have been used to

---

*(*) Numbers in brackets indicate reference number at the end of the text.

represent the behavior of plane frames [1,3], or as presented by Anagnostopoulos an entire building [2], combining the different elements (plane frames, shear walls or elevator cores) spatially distributed into an equivalent system with only three degrees of freedom per floor.

The basic characteristic of the shear-beam models is the substitution of the whole assembly of girders and columns that constitute a story of a frame by a single spring. This means that for plane frames only one degree of freedom per floor is considered, namely, a lateral floor translation.

For three-dimensional structures the three degrees of freedom at each floor level can be resolved into a single component in the plane of each constitutive frame or element in order to compute the corresponding restoring force [2]. Another important distinction of these models is that they are close-coupled systems, which implies that the behavior of any floor is influenced only by the two adjacent ones, above and below. The one exception is the "bending spring" used in reference [2] for shear-wall elements. A wide variety of force-deformation relations has been used for these models, their choice being determined by the type of frame or element they were supposed to represent. Thus, the first studies were performed with elastoplastic [1] springs, and then bilinear, trilinear [2,4], and a whole array of other springs were used with either stiffness or strength degrading characteristics, or with both of them. (See for example references [2,5,6,7]).

Another model that falls into this category is the one presented by Takizawa [4]. In this case the structure is not directly substituted

by a spring per floor, but instead by a superposition of collapse mechanisms. These are thought to correspond to different stages of plastification in the building. For the case of a "single-degree-of-freedom mechanism" for the overall structural deformation, the system is reduced to an equivalent single-degree-of-freedom inelastic system. The basic idea had already been presented and applied by Biggs (see Ch. 5 [8]), for dynamic loads, although not for cyclic behavior.

1.1.2 Point-Hinge Models

Inelastic dynamic analyses using these models are carried out at the member level. That is, the structure (a building frame, usually) is discretized into prismatic members: girders and columns. In some formulations the joints are also treated as a separate element. An increasing number of variations have been developed. Among these are the studies by Clough and Benuska [9], Anderson and Bertero [10], Giberson [11], Goel [12], Kamil [13], Fukada [14], Takeda et al. [15], Aziz [16]. All of these deal only with plane frames. Kubori, Minai and Fujiwara [36] have presented an approach to solve tri-dimensional framed structures.

The general denomination of point hinge to this type of modeling derives from the fact that once a member yields, a hinge is assumed to have formed at the point where the capacity was exceeded and not over a continuous length of the member. Aziz' formulation [16] accounts fora "plastification length" to be taken away from the original member length, but it is a given input, not a measure of the plastic incursions

of the member. Provisions have been introduced to consider members with end rigid zones [16,17] to model girders ending in shear walls and also bar elements of the truss type [17]. In all cases, however, yielding occurs at a given section or a point along the longitudinal axis of the member.

Yield criterion for these models is either a bending or an interaction yield line [16,17,18]. In the first case yield is reached when the bending moment in a section of the member exceeds the plastic moment capacity Mp. This may occur for any direction of the moment (positive or negative). In most formulations this check is done at the member ends. By subdividing a beam into several elements it is possible to account for hinge formation along the member [17], although they would always form at prespecified points. The interaction yield criterion defines a yield line (for plane prismatic members) as a function of the ultimate axial load and moment capacities. The shape of this curve varies for steel [19] and concrete members [20], but in either case yield is reached when a combination of moment and axial load defines a point in or over the yield line capacity of the member. Actually, a reduced plastic moment capacity is computed as a function of the axial load and compared with the applied moment. Member idealization has been done in different ways. Clough [4] introduced a dual component model and Giberson [11] a single component model. Aziz [16] implemented both and presented a "generalized single component model." In the dual component model the member is thought to be constituted of an elastic member and an elasto-plastic member, both acting simultaneously. The single

component model is an elastic member with two springs at the ends which can have different force-deformation characteristics.

A range of hysteretic laws is available to represent the behavior of the joints or end sections of a member. Bilinear [9], bilinear with stiffness degradation [16], trilinear with stiffness degradation [15], and Ramberg-Osgood laws [12] are used with models of the dual component type. These are really moment-rotation relationships, since the analysis provides only rotations of the member ends and the constitutive relations used in the structural analysis are moment-rotation relations. Aziz [16] has an additional stiffness and strength degradation spring to be used--as the other spring types--with the single component model. It must be mentioned that in this case the moment at one end is only a function of the rotation at that same end, and independent, thus, from the rotation at the other end. The moment-rotation relationship is then fully reproduced.

1.1.3 Fiber Models

These models were developed initially for steel structures by Pérez and Roesset [21] and also by Latona [22] and Adams [23]. They have been extended to model reinforced concrete frames in a work by Mark [24].

The structure is first discretized at the member level as in the point hinge models. Then every member--girder or column--is divided into several segments, each of which is made up of a series of parallel fibers.

The stiffness of each member is obtained by integrating along the member the segments whose properties were computed from the section level [22,23]. The characteristics of the entire structure are then computed in the traditional way, based on member properties.

Force-deformation characteristics are assumed to be known for each fiber, and strains and stresses computed at every step of the analysis throughout the structure. Yielding of a fiber is here a precisely defined phenomenon and allows to keep track of the spreading of plasticity across a segment and along the member length.

1.1.4 Models' Performance

Anagnostopoulos [2] found reasonable agreement on the average for maximum floor displacements between a trilinear shear-beam model and results by Clough [9] using a point-hinge model. Clough's analysis was performed with a bending model without including the effects of the gravity loads, either in the member capacity or P-Δ effects. Anagnostopoulos' trilinear was defined in terms of the member properties for each floor with the following formulas:

Initial stiffness (after Biggs)

$$K_1 = \frac{24E}{h^2} \frac{1}{\frac{2}{\Sigma K_c} + \frac{1}{\Sigma K_{ga}} + \frac{1}{\Sigma K_{gb}}} \qquad (1\text{-}1)$$

Ultimate strength

$$F_{y_{max}} = \min \left\{ 2 \frac{\Sigma M_{pc}}{h} , \; 2 \frac{\Sigma M_{pg}}{h} \right\} \qquad (1\text{-}2)$$

where E = Modulus of Elasticity

h = Story height

$\Sigma K_c = \Sigma \frac{I}{h}$ for all columns in the story

$\Sigma K_{ga} = \Sigma \frac{I}{\ell}$ for all girders in floor above

$\Sigma K_{gb} = \Sigma \frac{I}{\ell}$ for all girders in floor below

ℓ = Girder length

ΣM_{pc} = Sum of plastic moment capacities for all columns in the floor

ΣM_{pg} = Sum of plastic moment capacities for all girders in the floor

The first yield or end of the first branch was taken as one-half of $F_{y_{max}}$. The slope of the second branch, K_2 was taken as twenty percent of K_1.

Aziz [16], on the other hand, found substantial differences between the response predicted by his point-hinge model and the shear-beam model, the properties of the latter being computed as described above. The envelope of maximum floor displacements predicted by the shear-beam model in most cases tended to follow that of the first mode shape of a shear beam, thus overestimating the displacements of the lower stories and underestimating them in the upper stories. Unemura, Aoyama and Takizawa found similar discrepancies between a point-hinge model analysis and shear-beam models whose properties were computed by three different procedures [4,25].

It must be noted that the way the spring parameters are computed in the original presentation by Anagnostopoulos does not reflect the interaction between different stories of a frame. This may explain some of the observed differences in the predicted response.

1.2 OUTLINE OF PRESENT RESEARCH

1.2.1 Purpose and Objectives

The shear-beam model is an appealing procedure of inelastic, dynamic analysis to be used as a design aid and can handle a complete building with a variety of elements and include torsional effects, as opposed to the more complex models which normally solve only plane frames. Storage requirements are relatively small and the cost involved is reasonable. Unsatisfactory performance of the shear-beam model has been, however, reported as discussed in section 1.1.4. In order to use this model with confidence it is thus necessary to determine whether observed discrepancies are due to the shear-beam simplification (close coupling of the masses) or are instead the result of inadequate estimation of the spring parameters. This calls for another way of defining these properties that reflects the interaction between stories on floor stiffness and yield strength.

Another approach is to develop and implement an alternate simple model. Abandoning for that purpose the shear-beam idealization, it is intended to reduce the whole multistory frame to an equivalent single-degree-of freedom system, as suggested by Biggs and Takizawa. The advantage provided by the simplicity and economy of this model should make it a useful tool for design.

In summary, the objectives of the present research are:

1) To evaluate the validity of the shear-beam model.
2) To develop an improved way of obtaining the parameters of the floor springs.
3) To develop and evaluate an alternate analysis procedure based on an equivalent single degree of freedom (s.d.o.f.).

1.2.2 Scope

To meet these objectives a group of buildings were selected. Three of them were designed according to the U.B.C. Code specifically as part of this research. The criterion was to use buildings as close to actual typical buildings as possible. It was assumed, therefore, that a design based on U.B.C. was the common engineering practice to date.

The choice was restricted to steel moment-resisting frames. In addition to these buildings, two other frames used by previous investigators were analyzed. Both of them were steel moment-resisting frames also. The initial step was to subject these frames to a set of incremental lateral loads using a nonlinear inelastic static analysis. Different distributions of these loads along the height of the building were selected and used in order to compare their influence on the spring parameters. These analyses provide force (story shear)-deformation (interstory-displacement) relations that reflect floor interactions. Subsequently these curves were used to define multilinear shear-interstory displacement (distortion) hysteretic loops, one per floor. A set of simpler springs were also fitted through these curves following bilinear and trilinear hysteretic models.

Dynamic analyses of the structures under consideration using the newly computed spring properties were performed. In order to be able to use existing computer programs for the dynamic analysis of shear-beam-type models, a simple algorithm was used to convert the multilinear springs into simpler and already implemented models. This same tool was later used for the modeling of the equivalent multilinear spring in the s.d.o.f. system.

Another set of parallel dynamic analysis was performed using the point-hinge formulation developed by Aziz [16] and later expanded by Roesset et al. [26]. Comparisons between the predicted response of both models were carried out. The envelopes of maximum floor displacements and of maximum distortion were used as reference.

Predicted ductilities were also studied. Since the shear-beam models provide only floor ductilities, an approximate estimation of member ductilities was made using the floor response predicted by them and the corresponding member ductilities resulting from the incremental static analysis.

The equivalent s.d.o.f. system was developed based on the envelopes of lateral floor displacement from the static analysis. As hinges started to form in the members resulting in different mechanisms, the lateral "deformed shape" of the building also changed its configuration. Based on these sets of "shapes" and their corresponding loading, an equivalent multilinear spring for the entire building was computed. An equivalent mass and initial stiffness (actually the first branch of the spring) were also obtained. A dynamic analysis was then performed for this s.d.o.f. system and the incremental floor displacements and distortions calculated using the appropriate deformed shape of the building.

An estimation of local ductilities was also made in this case relating the static incremental analysis and the overall displacements predicted by the s.d.o.f. system.

1.2.3 Organization

In Chapter II the incremental inelastic static analysis is presented. A description of the buildings used in the analysis is included; the steps followed in the design are described in detail in Appendix A. Next, the lateral load distributions used as incremental loading are discussed, followed by an evaluation of their influence on the resulting shear-distortion curves. The effects of gravity loads in the stiffness and strength are discussed.

In Chapter III the results of the dynamic analyses using multilinear shear springs for the floors are presented. A presentation of the criterion to define the corresponding multilinear spring from the shear-distortion curves is made. This is followed by a description of the procedure to resolve the multilinear model into a set of elastoplastic springs. Then, a comparison of the response predicted by both the point-hinge model and these multilinear shear springs is presented. A procedure to obtain member ductilities from the static and shear-beam dynamic analyses is described, and the results compared to the ductilities predicted by the point-hinge model.

Chapter IV contains the results of the dynamic analysis using the traditional--but improved--shear springs: bilinear and trilinear. First a description of how these springs were obtained is presented, and then the predicted response using these is evaluated against the results presented in Chapter III for the point-hinge model and the multilinear spring. A comparison with the results using the springs computed following Anagnostopoulos' rules is also included.

In Chapter V an equivalent single-degree-of-freedom system for inelastic dynamic analysis is described. The formulation is presented first followed by a discussion and evaluation of the results as compared to the other models. Member ductilities computed by using results from both the incremental static analysis and dynamic analyses using this model are compared to the ones predicted by the point-hinge model. Chapter VI summarizes the conclusions reached and contains recommendations for continuing research in the area.

CHAPTER 2

INCREMENTAL INELASTIC STATIC ANALYSIS

2.1 INTRODUCTION

One of the objectives of this research is to establish a better way of obtaining the parameters that define a floor spring. The approximate formulas used so far (Eqs. 1.1 and 1.2) do not accurately reflect the properties of all the floors contributing to the characteristics of a given story. Also, they assume a floor mechanism which may not be possible for the frame to develop. In this Chapter an alternative way

of determining floor spring parameters using an incremental inelastic static analysis is presented. In this way, the entire structure is solved for every increment of load and the shear and interstory displacement (distortion) for a specific story are obtained, reflecting accurately the influence (or lack of it) of every other floor. In addition the limit strength (yield) for each story will be the result of a combined mechanism for the entire frame instead of an isolated floor mechanism.

The analyses were performed for different lateral load distributions. Their influence in the shear-distortion curves was evaluated, and--after performing dynamic analysis--it was possible to determine which load distribution gave the best agreements.

A description of the buildings used for this study is presented first. This includes the basis for the design of the frames for this research. Then, the different types of lateral load distributions are discussed. Next, the inelastic static analysis is presented, with a discussion of the treatment of gravity loads, incremental lateral loads, yield criterion, ductility definitions and additional nonlinear effects such as P-Δ and change in geometry. Section 2.5 presents a sample of shear-distortion curves obtained as a result of this analysis and a discussion of their main characteristics. These curves, one per floor, are the basis for an approximation of the floor spring parameters on a later stage. The two following sections discuss in detail the influence of the lateral load distribution on these curves and also of the gravity loads. Finally the conclusions are summarized in section 2.8.

2.2 BUILDING FRAMES USED

The influence of the number of stories and height of the building on the performance of the shear-beam model was of interest. It was decided to investigate for which type of buildings the response could be predicted with better reliability; or if the conclusions reached for a low-height frame would remain valid for a medium-height or tall building. In order to have a reasonable range of building heights it was decided to choose three basic numbers of stories: four, ten, and sixteen stories, thus having frames in the short range, intermediate and taller ranges. With these choices it was expected to cover a wide range of common buildings built today. All frames used in this research are steel moment-resisting frames. Since the primary objective at this stage was to investigate the validity of the shear-beam model, it would have been of little help to include additional parameters in the member modeling (stiffness degradation, for instance). Work including these other variables, important for reinforced concrete frames, should be undertaken in the future.

Following these criteria, it was decided to select buildings with four, ten, and sixteen stories. One frame of each kind was designed specifically for this study, and two other frames used by other investigators were selected: a single-bay ten-story steel frame by Anderson [10] and a three-bay ten-story frame by Kamil [13].

The following considerations and specifications were used in the design of the three frames used herein:

- The proportion of the spans and heights was chosen so as to represent typical building structures of their kind, taking into account that structures of different heights have generally different uses, and have common architectural dimensions.

- A plan for each building was selected and a typical frame spacing was chosen. The analysis will be restricted to an interior frame, assuming all the others are equal, thus disregarding any effects due to torsion.

- All designs were based on the Uniform Building Code (U.B.C.) [27] of 1973. According to this:

- The design was based on allowable working stress for dead plus live load or a combination of dead, live and earthquake loads, in which case the allowable stresses were increased by thirty-three percent.

- Earthquake forces were computed according to U.B.C. for buildings located in zone three.

- Proportioning of member sections, girders and columns was done following the specifications of the American Institute of Steel Construction (AISC), part I [19]. The yield stress of the material (F_y) was taken as 36 ksi and the Modulus of Elasticity (E) as 30,000 ksi.

- The loads used in the design were: eighty pounds per square foot (psf) for dead load in all three buildings, and a live load of forty psf for a typical floor of the four-story building and twenty psf for the roof. In both the ten- and sixteen-story frames the live load was fifty psf for a typical floor and twenty psf for the roof.

- All designs were also checked for a combination of dead, live and wind loads with the same increase in allowable stress per-

mitted by the U.B.C. code. Wind load for the four-story frame was taken as uniform twenty psf. For the ten-story frame wind pressure was twenty psf constant along the height, and for the sixteen-story frame twenty psf for the first three stories, twenty-five from floors four to eight, and thirty psf from floors nine to sixteen. These forces were all computed from the U.B.C. for buildings located in California [37].

- Drift requirements were enforced in all three buildings when required. A maximum interstory drift and a maximum overall drift for the whole frame were selected.

$$\frac{\Delta_i}{h_i} \leq \frac{1}{350} \qquad \frac{\delta_T}{h_T} \leq \frac{1}{350} \qquad \text{for wind loads}$$

$$\frac{\Delta_i}{h_i} \leq \frac{1}{500} \qquad \frac{\delta_T}{h_T} \leq \frac{1}{500} \qquad \text{for earthquake loads (after reference [8])}$$

Δ_i = interstory displacement for floor i, due to lateral load
h_i = height of story "i"
δ_T = lateral floor displacement of top floor
h_T = total height of building.

For column design the building was assumed to be fully braced out of plane, and therefore sidesway was prevented. K-factors for the columns were thus taken as 1. In the plane of the frame, though, sidesway was not prevented and the AISC slenderness criterion was applied to compute equivalent lengths. Girders for a given floor were all taken equal according to the section where maximum effects were encountered. It was decided that this would reflect a more realistic, practical design than changing section profiles from span to span. Since it was

intended to design buildings as close to actual structures as possible, that criterion was followed in all three designs.

Column sections were maintained for at least two contiguous stories. It was thought impractical--and almost always avoided in actual practice, due to increased costs--to change column sections at shorter intervals. This criterion resulted, however, in some columns being over-proportioned.

2.2.1 Four-Story Frame

Figures 2.1 and 2.2 show the plan and elevation view of the four-story building used in this study. From now on this frame will be referred to as "4-story UBC." Section denominations are shown in Fig. 2.2. The properties used are presented in more detail in Appendix A.

This frame was proportioned to have the central span shorter than the two exterior ones; it was thought to be a typical apartment building where this is usually the case. Also all heights were chosen to be equal and ten feet each, a rather typical value for a low-rise apartment building.

With the exception of the interior columns of the first story, all sections were proportioned for dead plus live load (D+L). The combination of dead, live, and lateral load (either earthquake (Q) or wind (W) was not critical. Drift requirements for both lateral loads were satisfied without having to increase member sizes.

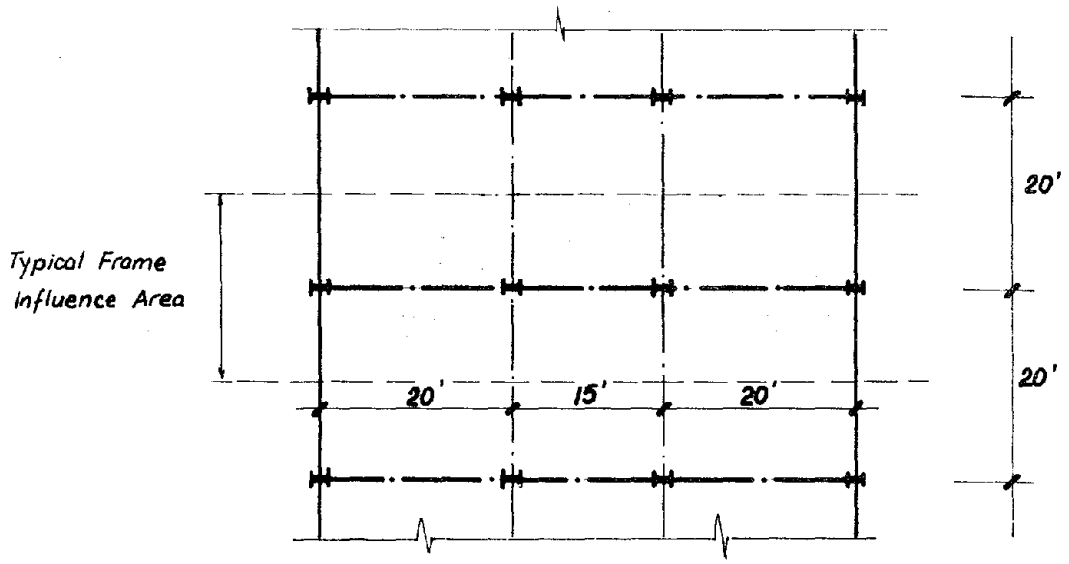

FIGURE 2.1 - PLAN 4-STORY BUILDING

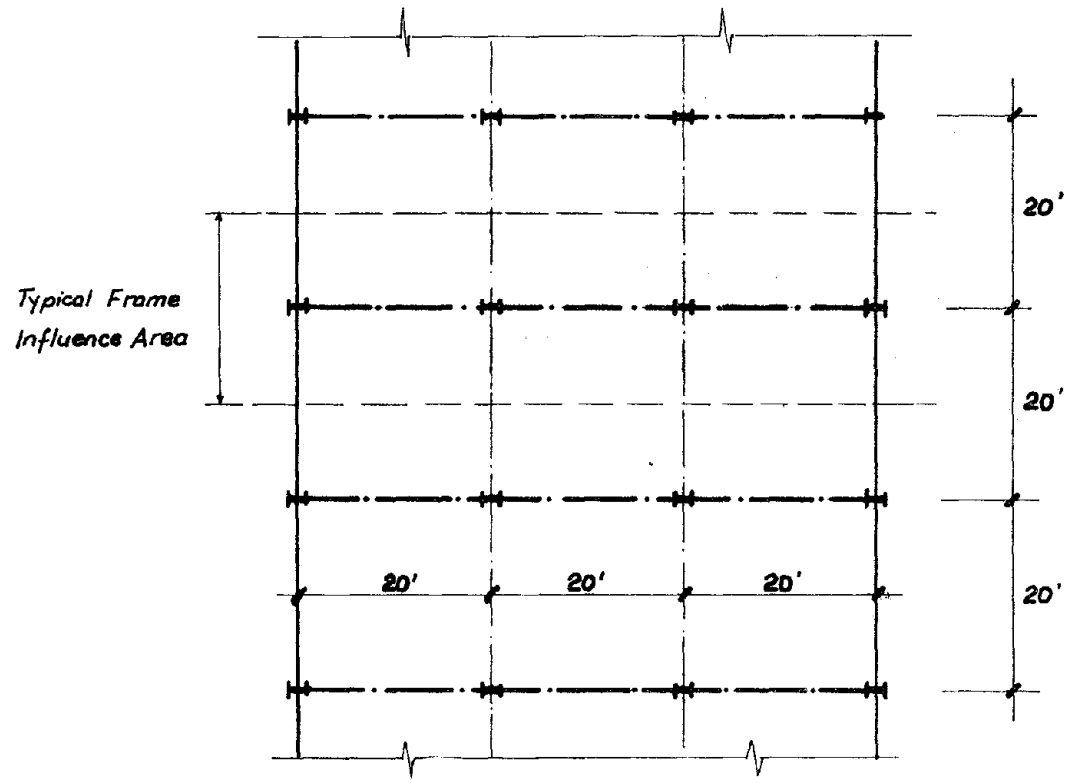

FIGURE 2.3 - PLAN 10-STORY BUILDING BY UBC AND 16- STORY BUILDING

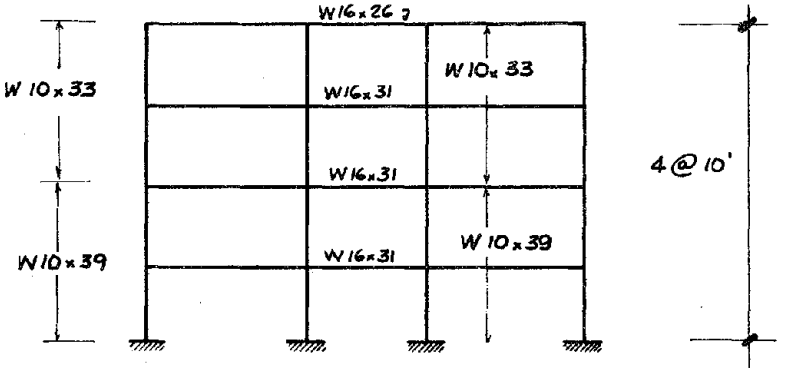

FIGURE 2.2 - FOUR STORY FRAME BY U.B.C.

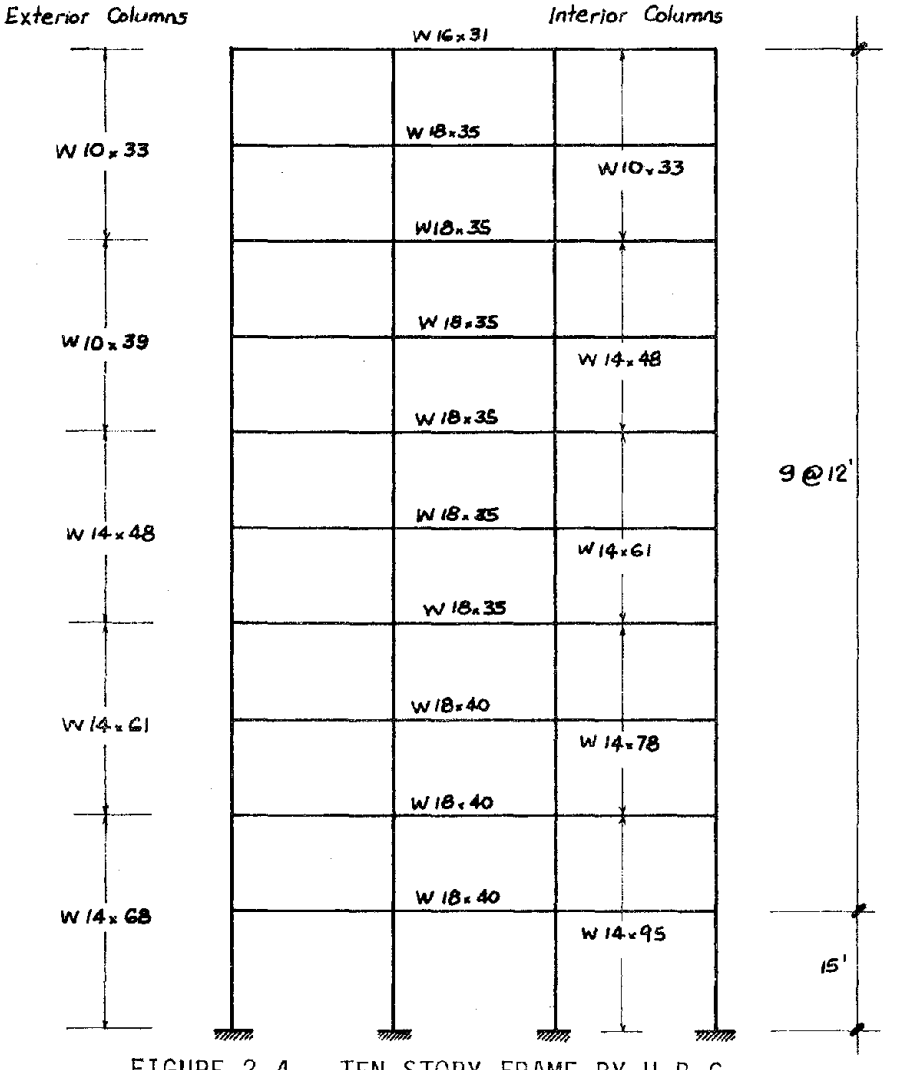

FIGURE 2.4 - TEN STORY FRAME BY U.B.C.

2.2.2 Ten-Story Frames

Ten-Story U.B.C.

The first ten-story frame that was used is shown in Figs. 2.3 and 2.4. It was proportioned to represent a typical office building of medium height. Story heights were also chosen as are more commonly encountered: a taller first story (15 feet) and all the rest of equal height, twelve feet. This figure (12 ft.) was thought to be used frequently for this type of construction. The frame has three spans of twenty feet each (all equal). Girder design was controlled by D + L + Q in the first seven stories except the third, where D + L + W was dominant; and by D + L in the three top stories. No changes were necessary due to drift requirements. Columns in the first six stories were proportioned for D + L + Q and for D + L in the top four. No changes were required by drift either. This frame will be referred to as "10-story UBC."

Anderson Frame

The second ten-story frame used was one presented by Anderson and Bertero [10]. This is a one-bay ten-story moment-resisting frame shown in Fig. 2.5. Although it has an unusual configuration for a frame of this height, it was considered useful for comparison purposes.

Kamil Frame

The third ten-story frame is one presented by Kamil [13]. This is a three-bay ten-story, unsymmetrical moment-resisting frame. Section properties and configuration are shown in Fig. 2.6.

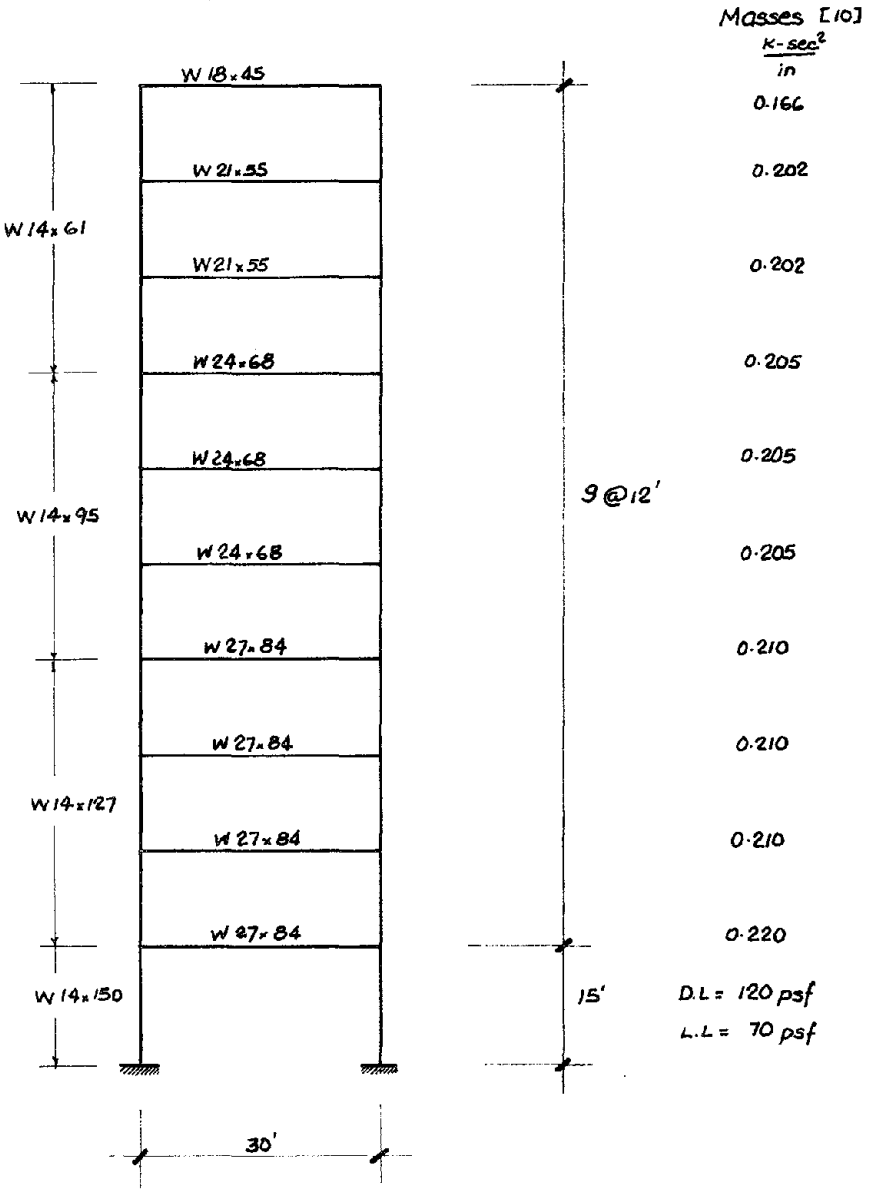

FIGURE 2.5 - ANDERSON FRAME

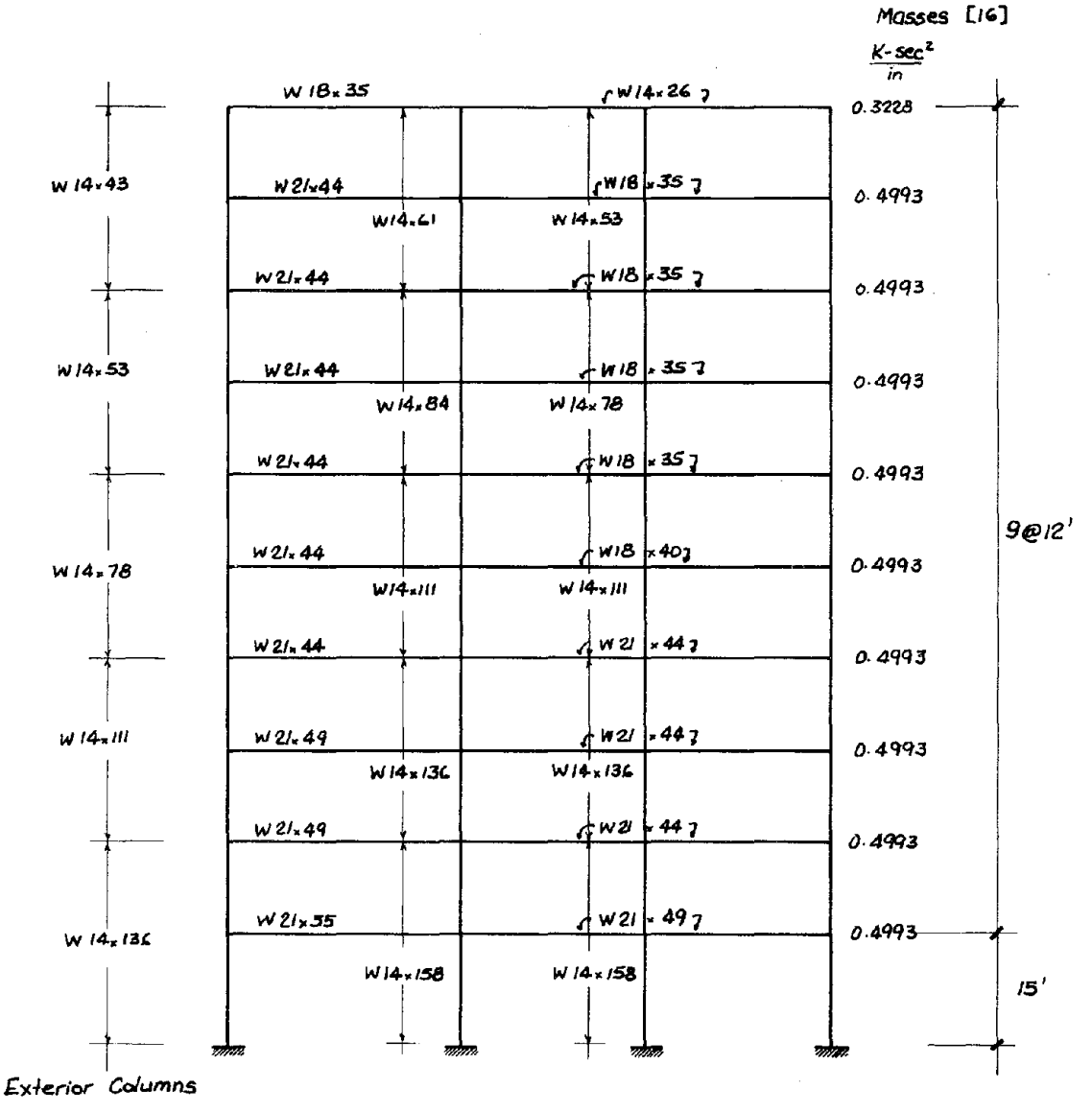

FIGURE 2.6 - KAMIL FRAME

2.2.3 Sixteen-Story Frame

This frame was proportioned following the same criterion as for the 10-story UBC frame, except for the increased number of stories. This resulted in a height-to-depth (h/D) ratio larger than three, forcing the addition of a concentrated lateral force at the top floor according to UBC. Sixteen stories were thought to be a reasonable number of stories for a tall building and a good compromise to limit computational expenses.

The plan view is shown in Fig. 2.3 and elevation in Fig. 2.7. Girder design was initially controlled by the combination D + L + W in the first thirteen stories; the top three floors were controlled by D + L. Later the girders of the first and second floors were increased in size to satisfy story drift requirements demanded by wind. Column design was controlled almost entirely by the combination D + L + W, except in the two top stories, fifteen and sixteen. The third- and fourth-story columns had to be increased to satisfy drift requirements as imposed by wind.

2.3 TYPES OF LOADS

The shear-distortion curves that define a floor spring in the shear-beam model depend on the relative deformation of the floor and its members. That is, for a given configuration of floor displacements a given set of shear-distortion curves would be obtained. Theoretically then the curves to be used as input for a dynamic analysis using the shear-beam model should change as the dynamic deflected shape of

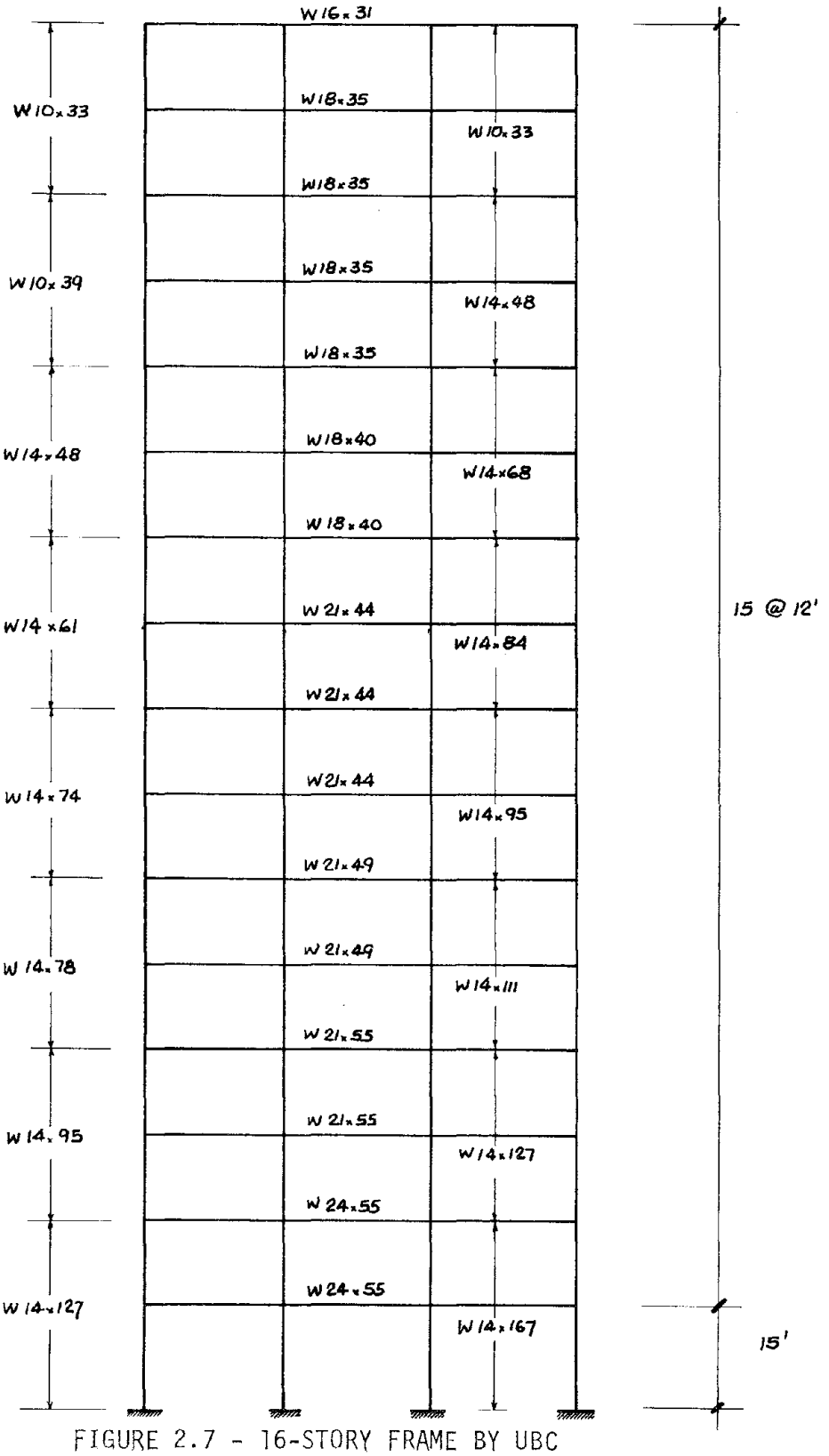

FIGURE 2.7 - 16-STORY FRAME BY UBC

the building changes (for deflected shape is meant the envelope of lateral floor displacements). This is of course infeasible.

The choice of deflected shape or lateral load distribution to obtain the shear-distortion curves has to be independent of time. The logical choice is then to select an envelope of maximum floor displacements or an envelope of maximum lateral forces and to compute the corresponding curves. It was opted to select a group of lateral force distributions that represent maximum expected values according to different criteria. An attempt was made to use a linear distribution of floor displacements in height, but the results proved to be impractical and the idea was abandoned.

The lateral load distributions used were (Fig. 2.8):

- U.B.C. code distribution
- Following the first mode shape
- Following the shape that results in story shears according to the square root of the sum of the squares (SRSS) of all the modes
- Uniform along height
- Applied Technology Council, ATC-3 distribution.

U.B.C. Code

For all the frames considered in this study, a distribution in height of the total base shear according to the U.B.C. code [24] was computed. That is,

$$F_i = \frac{W_i\, h_i}{\Sigma W_i\, h_i}\,(V - F_t) \qquad (2\text{-}1)$$

$$F_t = 0.004V\,\left(\frac{h}{D}\right)^2 < .15V \quad \text{for } \frac{h}{D} > 3 \qquad (2\text{-}2)$$

If the weight of each floor is equal, this results in a triangular distribution.

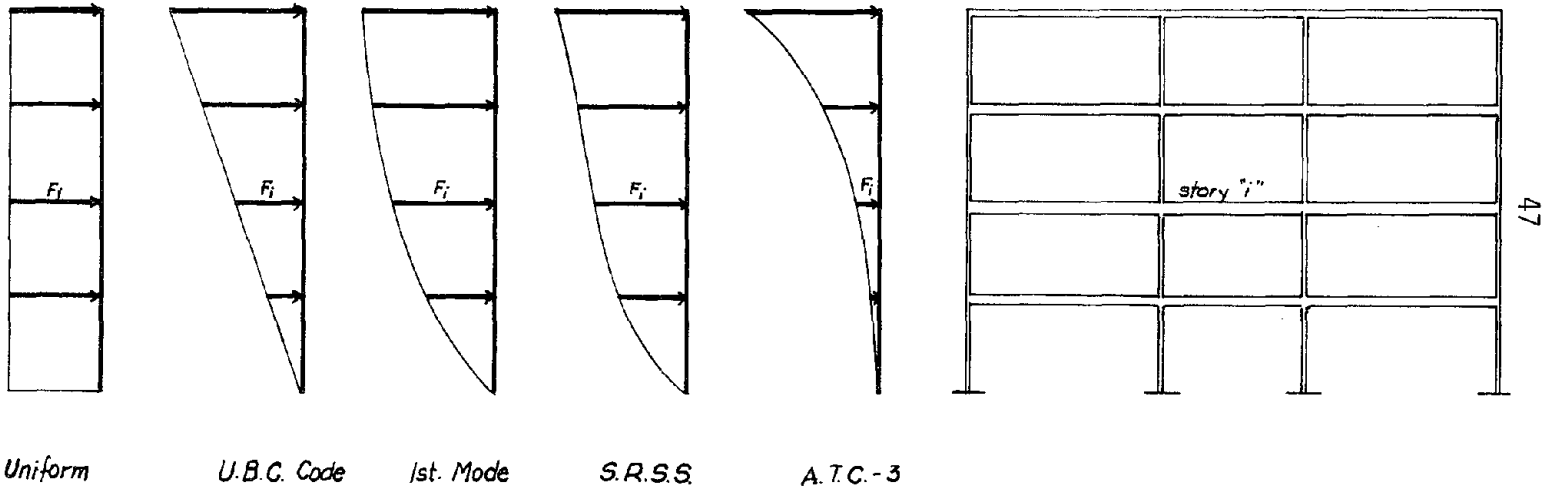

FIGURE 2.8 - LATERAL LOAD DISTRIBUTIONS

First Mode Shape

A dynamic analysis of the three frames designed according to the U.B.C. was performed using APPLE PIE [30]. The first mode shape was then used to distribute the base shear proportionally to it.

SRSS of All Modes

From the same dynamic analysis, the SRSS shears were used to compute equivalent story forces. The base shear was then distributed proportionally to the shape given by these equivalent SRSS story forces.

Uniform

A set of lateral forces uniformly distributed along height was also used, mainly because of its simplicity and in order to evaluate whether the results thus obtained would compare with the ones using more sophisticated shapes.

ATC-3

For the taller buildings where bending type deformation may be significant, the Applied Technology Council (ATC) [29] in its draft report number three suggest a parabolic distribution:

$$F_i = \frac{W_i \, h_i^2}{\Sigma W_i \, h_i^2} \qquad (2\text{-}3)$$

This distribution was used in order to determine if it would give better results than traditional distributions in the case of taller buildings.

2.4 INCREMENTAL INELASTIC STATIC ANALYSIS

The incremental inelastic static analyses were performed using a modified version of a computer program prepared as part of Adams' dissertation [23]. A detailed presentation of element stiffness matrices and solution scheme can be found in the same reference. What follows is a summary of the criteria and procedures applied in the present study.

2.4.1 General

The analysis procedure follows an incremental displacement formulation that assumes linear behavior during a given increment of load. The direct stiffness method is used to generate the system stiffness matrix starting from the member level [31,32]. All members are assumed to be prismatic and may have an arbitrary configuration in the plane. (The program in its present version is restricted to plane structures). Although initially all members are considered fix-ended in the stiffness generation, appropriate modifications to the member matrix are introduced to account for hinge formation at either or both ends [23]. Hinges may be specified at desired locations, even in the initial stage, by reading an indicator with the input data. The proper modifications are then introduced in the stiffness matrix of the member under consideration. Three degrees of freedom per joint are considered in the analysis: a horizontal displacement, a vertical displacement, and a rotation, all in the global reference frame. Axial and bending deformations are taken into account, but shear deformations are neglected.

2.4.2 Gravity Loads

Gravity loads can be considered in the analysis if desired. They can be either member loads, in which case they are restricted to uniformly distributed loads; or they can be nodal forces, in which case they can be vertical or horizontal concentrated load or a joint moment. These nodal values or the corresponding ones from distributed loads are assembled directly into the force vector at the moment they are read.

2.4.3 Incremental Lateral Loads

By this, reference is made to both lateral loads or prescribed lateral displacements. Actually, as mentioned in the section above, any joint load can be given directly, and this extends also to any joint displacement. The reason to discuss it in this separate section is that loads or prescribed nodal displacements can be applied incrementally in any desired direction. That is, in order to facilitate the tracking of member hinge formations, the magnitude and sign of lateral loads increment, instead of the full value, is given together with the number of times this increment will be applied. This results in a cumulative lateral load with the same distribution in height as its incremental components.

The analysis is performed then as many times as increments, taking in each case only the values of the incremental loads but superimposing the forces, moments, and displacements of each step on the ones accumulated up to the preceding step. At the beginning of a new cycle, each member is checked for exceedance of its capacity according to one of

two yield criteria (Sec. 2.4.5), and if that is the case, appropriate modifications are introduced into the member stiffness matrix to account for hinge formation.

2.4.4 P-Δ and Nonlinear Geometry Effects

The analysis procedure being described has the capability of including nonlinear effects due to change in geometry and gravity loads (P-Δ). The first is accomplished in the following manner. At the end of each step of incremental loading, the joint coordinates are modified to include the incremental joint displacements (horizontal u, and vertical v) obtained in that step. This means that for the following step a completely new geometry will be used to generate element and system matrices. The new joint coordinates for step "n" would be,

$$x_i^n = x_i^{n-1} + u^n \qquad \text{for joint "i"}$$

$$y_i^n = y_i^{n-1} + v^n$$

At every step new member lengths are computed and also the new orientation, thus resolving member forces into the global reference system using the appropriate rotation transformations. It must be noted, however, that no changes in the value of the loads due to the modified geometry are introduced, nor second-order effects other than P-Δ. P-Δ effects are introduced as a correction to the stiffness matrix of the column members to simulate a fictitious equivalent lateral force applied at both ends. Since the magnitude of this force is directly

proportional to Δ, the amount P/h is subtraced from the corresponding term in the stiffness matrix.

Figure 2.9 illustrates this approximation by assuming a straight line chord rotation instead of the actual double curvature deformed shape.

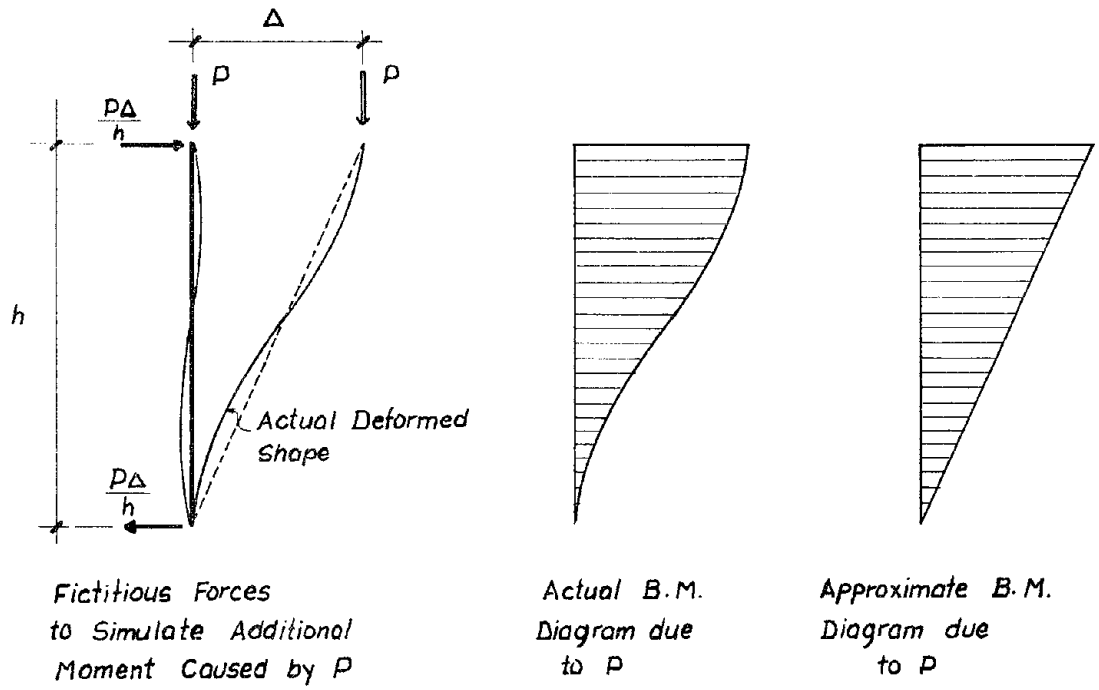

FIGURE 2.9 - P-Δ EFFECT

2.4.5 Yield Criteria

A bilinear moment-rotation diagram is assumed for each member end. The second slope is taken as a fraction of the initial stiffness. As shown in Fig. 2.10, yielding is reaced at an end section when M_y is exceeded. Two criteria can be used to estimate the Yield Moment capacity of a member in terms of its properties. The first criterion is

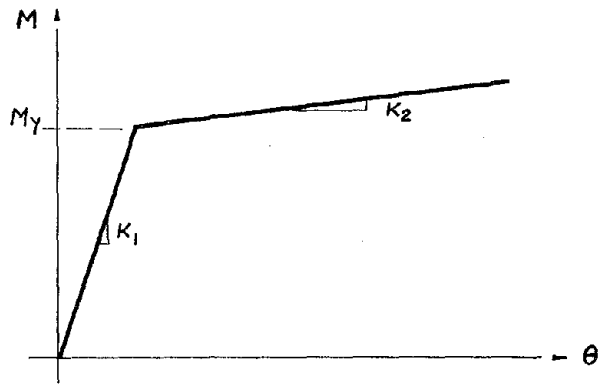

FIGURE 2.10 - BILINEAR MOMENT-ROTATION RELATION FOR END MEMBER SECTION

known as the "Bending Model." In this case, the yield moment capacity of the member always equals its Plastic Moment, M_p, independently of the magnitude of the axial load acting at that time.

$$M_y = M_p \tag{2-4}$$

The second criterion is known as the "Interaction Model" and in this case M_y is a function of both Plastic Moment and the Axial Load Capacity. The yield line is defined according to Part II of the AISC Specifications [19] and is illustrated in Fig. 2.11. The yield capacity is given

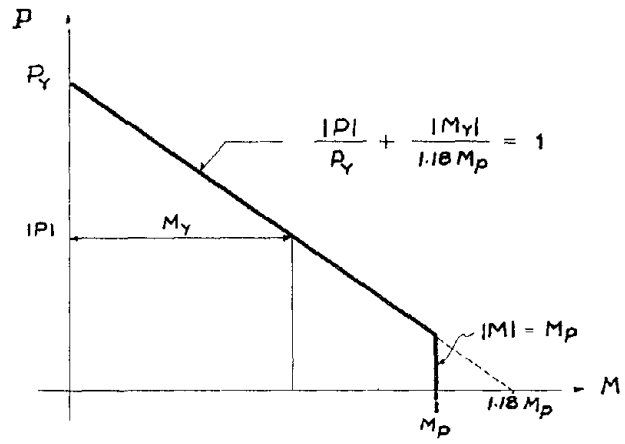

FIGURE 2.11 - INTERACTION DIAGRAM FOR STEEL SECTIONS (AISC)

by any of the following expressions:

$$M_y = \left(\frac{P_y - |P|}{P_y}\right) 1.18\, M_p \qquad (2\text{-}5)$$

$$M_y \leq M_p \qquad (2\text{-}6)$$

Whenever the cumulative bending moment at the end section of a member exceeds M_y (computed according to either criterion) a hinge is declared to have formed and the member stiffness matrix for the next step will be computed for that particular situation. If a reversal occurs due to change in the direction of the loads and the bending moment is less than that in the preceding step, the section is assumed to behave elastically until yielding is reached in the opposite direction.

2.4.6 Definitions of Ductility

Two definitions of ductility were introduced in the analysis, one based on moments, the other one based on rotations. Both have been used previously by other investigators [9,10,17].

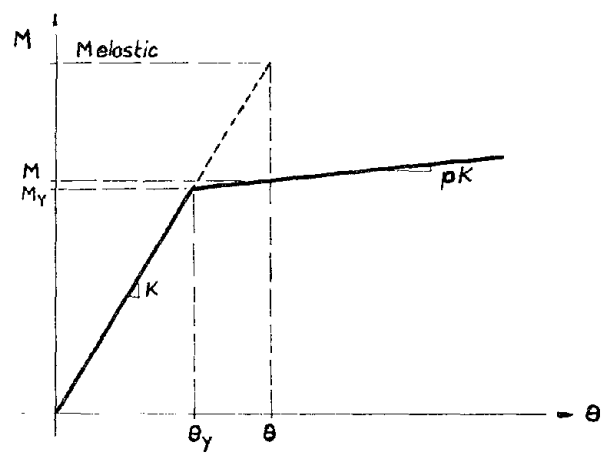

FIGURE 2.12 - DUCTILITY BASED ON MOMENTS

Moment ductility is defined as (Fig. 2.12)

$$\mu_M = \frac{M_{elastic}}{M_y} \tag{2-7}$$

$$\mu_M = 1 + \frac{M - M_y}{p \cdot M_y} \tag{2.8}$$

where M = Actual Bending Moment at a given section

M_y = Yield Moment Capacity according to either yield criteria

p = Percentage of first branch slope used for second branch.

This definition has been considered equivalent to a ductility based on curvatures [10,17]. It must be noted, however, that this would be the case only if an explicit moment-curvature relationship were available for any section, and the constitutive relations were given in terms of curvature ($M = f(\phi)$). Since there is no explicit way of enforcing a bilinear relationship between moments and curvatures, the only variables being end rotations and moments, equation (2-3) must be regarded as no more than it is: an estimation of ductility based on moments. The yield moment capacity M_y is a function of the axial load for the case of the interaction model. The higher the value of P, the lower the yield capacity (Fig. 2.13). This implies that as the analysis progresses, ductilities are computed based on variable reference levels and for the same value of the moment a different ductility will be obtained if P changes its magnitude. Although this criterion may be debatable, it will be used in this study for at this stage of research it seems to be as meaningful as any other.

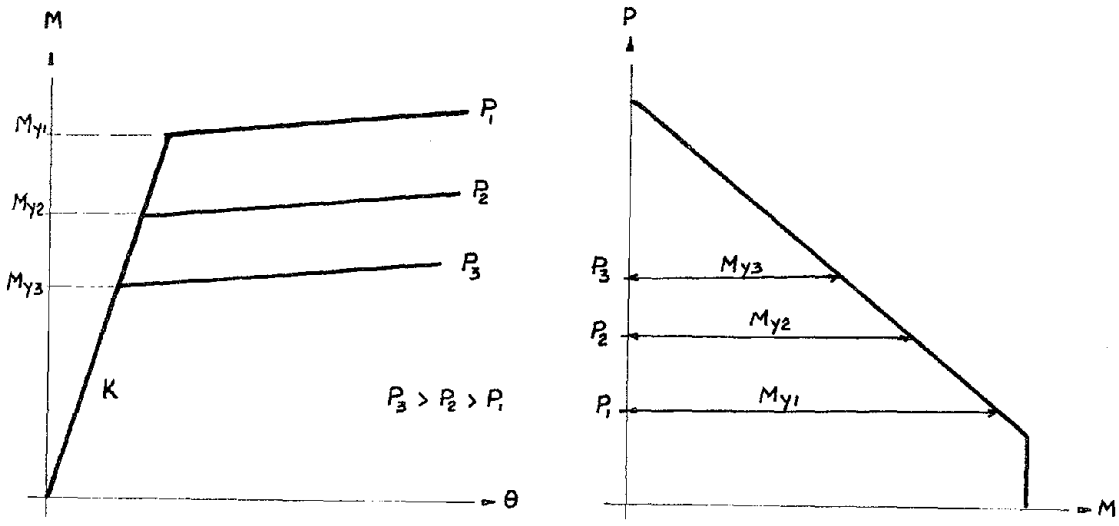

FIGURE 2.13 - MOMENT-ROTATION RELATIONS FOR DIFFERENT AXIAL LOADS

Rotation ductility is defined as

$$\mu_\theta = 1 + \frac{\theta_{plastic}}{\theta_y} \qquad (2\text{-}9)$$

where θ_y is the yield rotation and $\theta_{plastic}$, the plastic rotation at the moment μ_θ is evaluated.

For any given member θ_y may take different values depending upon the end support conditions and the applied loads. The actual deflected shape of the member in a frame structure is therefore a function of the loads and the stiffness distribution of the other components. A commonly used assumption is an antisymmetrical deformed shape [9,10,17] which requires equal moments at both ends of a simply supported member (Fig. 2.14). This of course is not the case when gravity loads are applied (which is expected in any real structure) and generally for a frame, with more than one bay or for the columns in most frames. Again this criterion is taken as a normalizing value, but without claiming a

true representation of a real situation. M_y is also a function of axial loads for the interaction model, and the appropriate value is used whenever μ_θ is computed.

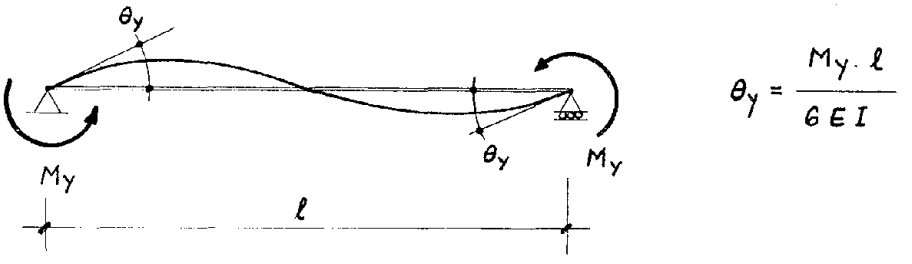

FIGURE 2.14 - ANTISYMMETRICAL DEFORMED SHAPE

2.5 STORY SHEAR VS. INTERSTORY DISPLACEMENT CURVES

The main output of this incremental inelastic static analysis was a set of curves representing story shear (V) vs. interstory displacement or distortion (Δ). For each structure one curve per floor was obtained. The following procedure was used to perform these analyses.

- First, the total base shear as required by the U.B.C. code of 1973 (V_c) was computed. The bases for this estimation were the same as for the design, and were reported in section 2.2.
- This base shear was then distributed along the height of the frames, according to the code specifications, and also following the other distributions.

- The forces thus obtained were divided by seven in the four-story building and by 10 for the other buildings in order to obtain the incremental forces for the analysis. (Other load increments were investigated and the results are reported in section 2.6). In addition, each floor force was equally distributed among the nodes of each floor to avoid the effect of the axial deformation of the girders.

- The buildings were loaded in three stages; uniformly distributed loads due to gravity were applied first. Only dead loads were used for this purpose, since no live loads were supposed to be present when earthquake loads were applied. The U.B.C. code specifies that the weight of the building considered in computing base shear be that of dead loads only (for structures other than storage warehouses), and therefore the above criterion was followed. A second loading stage was the application of the lateral loads following the code distribution and in separate but similar analyses the other distributions presented in section 2.3. In each case the total base shear applied in this stage was normalized to the value of the base shear computed according to the code: that is, V_c. This normalization allowed comparisons to be made based on fixed multiples of V_c, the only variable left being the distribution in height by itself. In all cases it was expected that the frame would remain elastic beyond this magnitude of load. Kamil's frame was an exception, and this stage had to be modified applying lateral load in small increments immediately after the dead loads were applied.

  The third stage was the continuation of lateral loading, but now in small increments according to the procedure described before, section 2.4.3. Fifty to sixty increments of load were applied in order to achieve yielding in most floors. In some cases, however, the top floor remained elastic even after very large deformations had accumulated from the floors below.

- Story shears were computed as the summation of the column shears and distortions were computed from the overall floor displacements. The horizontal displacement of all the joints in a given floor were averaged to obtain a unique value for the story.

- Ductilities for all the members were computed at the end of each incremental step using both definitions, moments and rotations.

Figure 2.15 illustrates the three loading stages for the four-story frame. The shear-distortion curve for each story is produced as loads are progressively applied to the structure. When dead loads are acting, no resulting story shear is obtained, nor lateral displacements, since the frame is symmetric and symmetrically loaded. After lateral loads are applied, the V-Δ curve starts to take shape (Fig. 2.15(b), and 2.15 (c)). A change in slope will be registered on the curves every time a new hinge is formed in the structure. The location of the hinge does not have to be in the same floor as that of the curve being observed, since interaction is appropriately reflected when solving the entire frame. Deflected shapes corresponding to known levels of lateral force are obtained simultaneously as part of the analysis. Their configurations vary as hinges formed throughout the frame (Fig. 2.15 (c)). The output of these analyses is used in two ways: the V-Δ curves are used to estimate new floor springs for the shear-beam model and the deflected shapes and their corresponding loads are used to generate an equivalent multilinear single degree-of-freedom system. In addition ductilities computed at this stage are used in combination with the dynamic analysis to predict local ductilities due to the ground excitations.

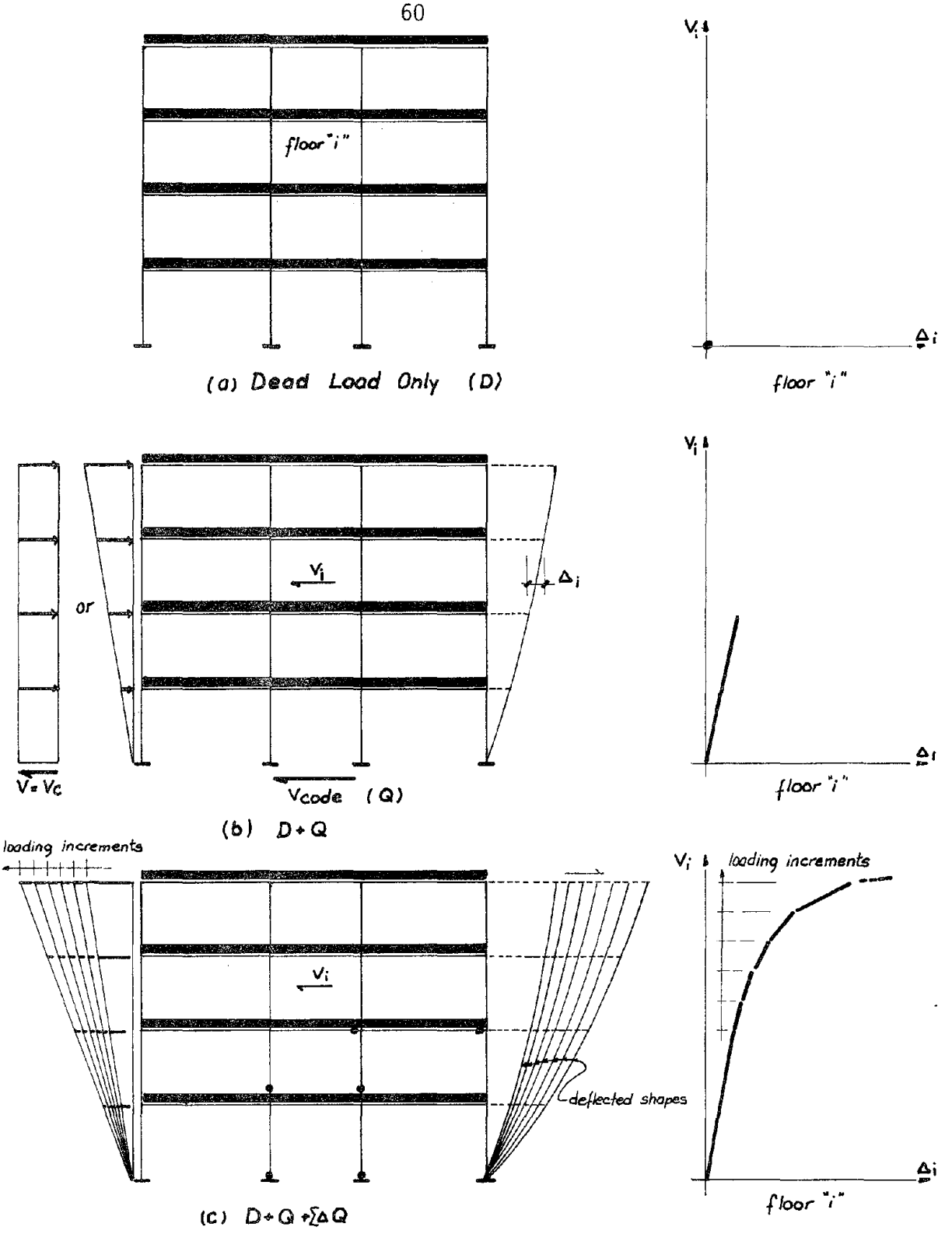

FIGURE 2.15 - INCREMENTAL STATIC ANALYSIS

Next, a selected group of shear-distortion curves will be presented to illustrate some general characteristics. These analyses were performed using the interaction model, gravity loads due to dead load, and UBC code lateral forces. Fig. 2.16 shows the shear-distortion curve for the first floor of the four-story frame. The first branch remains elastic up to 65% of the apparently straight initial portion. The transition towards ultimate yield is progressive, and therefore a precise initial yield point is difficult to identify. Beyond values of distortion of 9.6 inches a plateau is reached whose slope is 2% of the initial slope. This was to be expected, since the analysis was performed using a second slope of 2% for the bilinear moment-rotation relation. Actually the range on which the curve is used in the dynamic analysis is limited to the ordinate defined by 4.8 inches of distortion. The rest of the curve was obtained because of the necessity to increase the loads and enforce yielding in the upper stories. This was also the case for the other buildings. Note that the final slope in the range of interest defined above is larger than the actual ultimate slope.

Figures 2.17, 2.18 and 2.19 show the shear-distortion curves corresponding to floors three, six and nine of the 10-story UBC frame. The basic difference between these curves and the preceding one is that there are much more clear, abrupt, changes in stiffness. Although the inclination of the curve does not show a large change initially, the actual change in stiffness (slope) can be of the order of 50%. The approach to the last branches of the curve is sharper than for the curve in Fig. 2.16. For the ninth story curve the transition is marked more

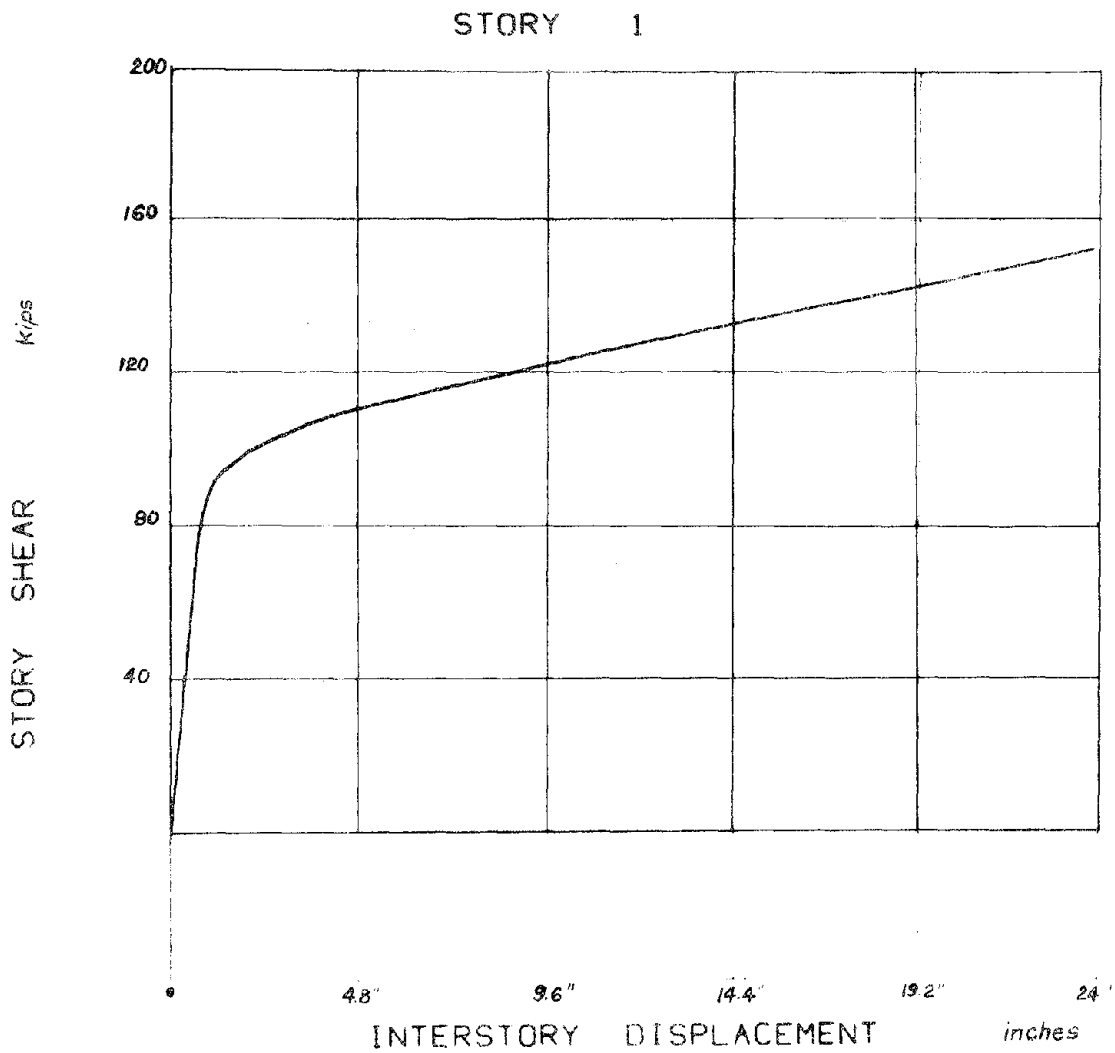

FIGURE 2.16 - 4-STORY UBC FRAME: V-Δ CURVE, 1ST. STORY

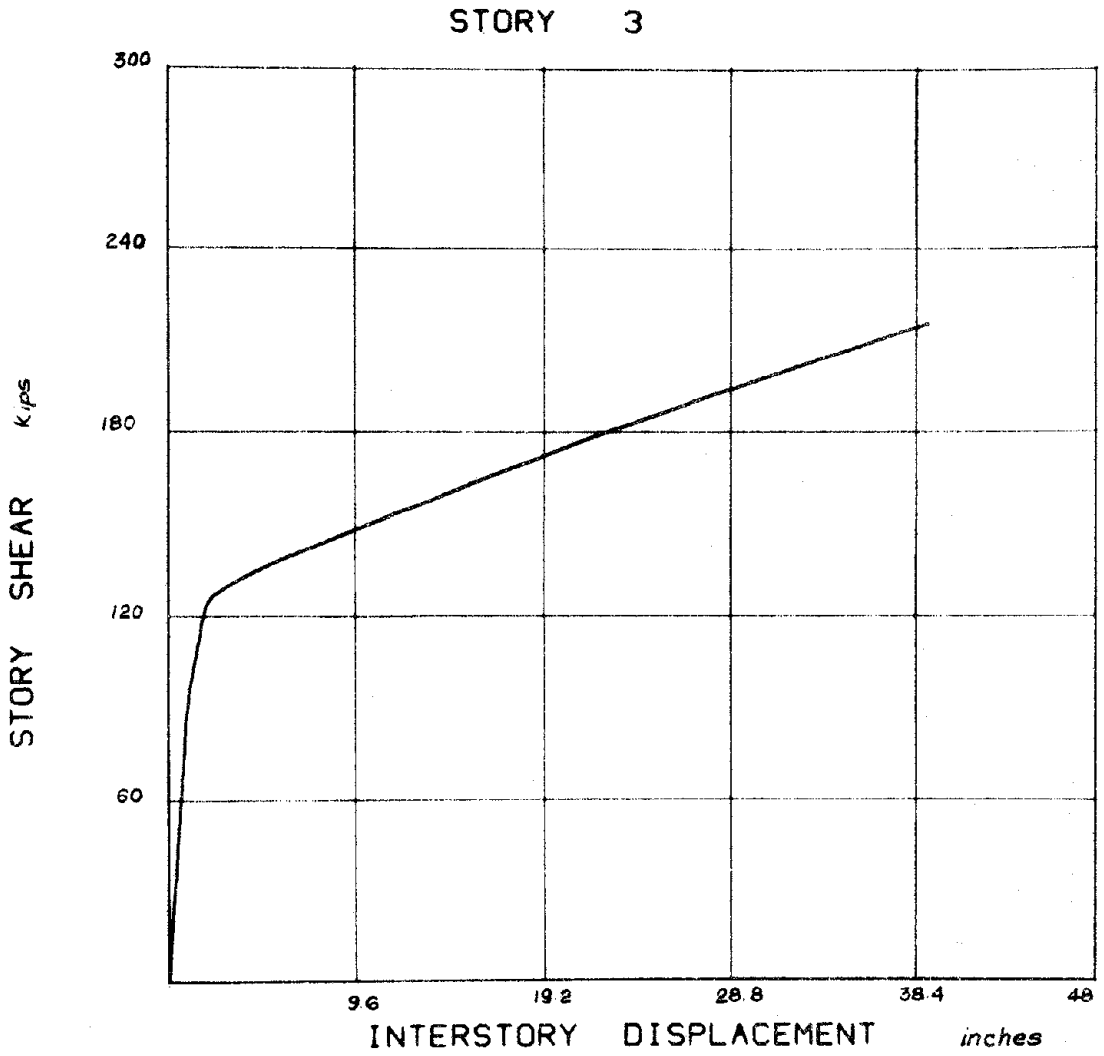

FIGURE 2.17 - 10-STORY UBC FRAME: V-Δ CURVE, 3RD. STORY

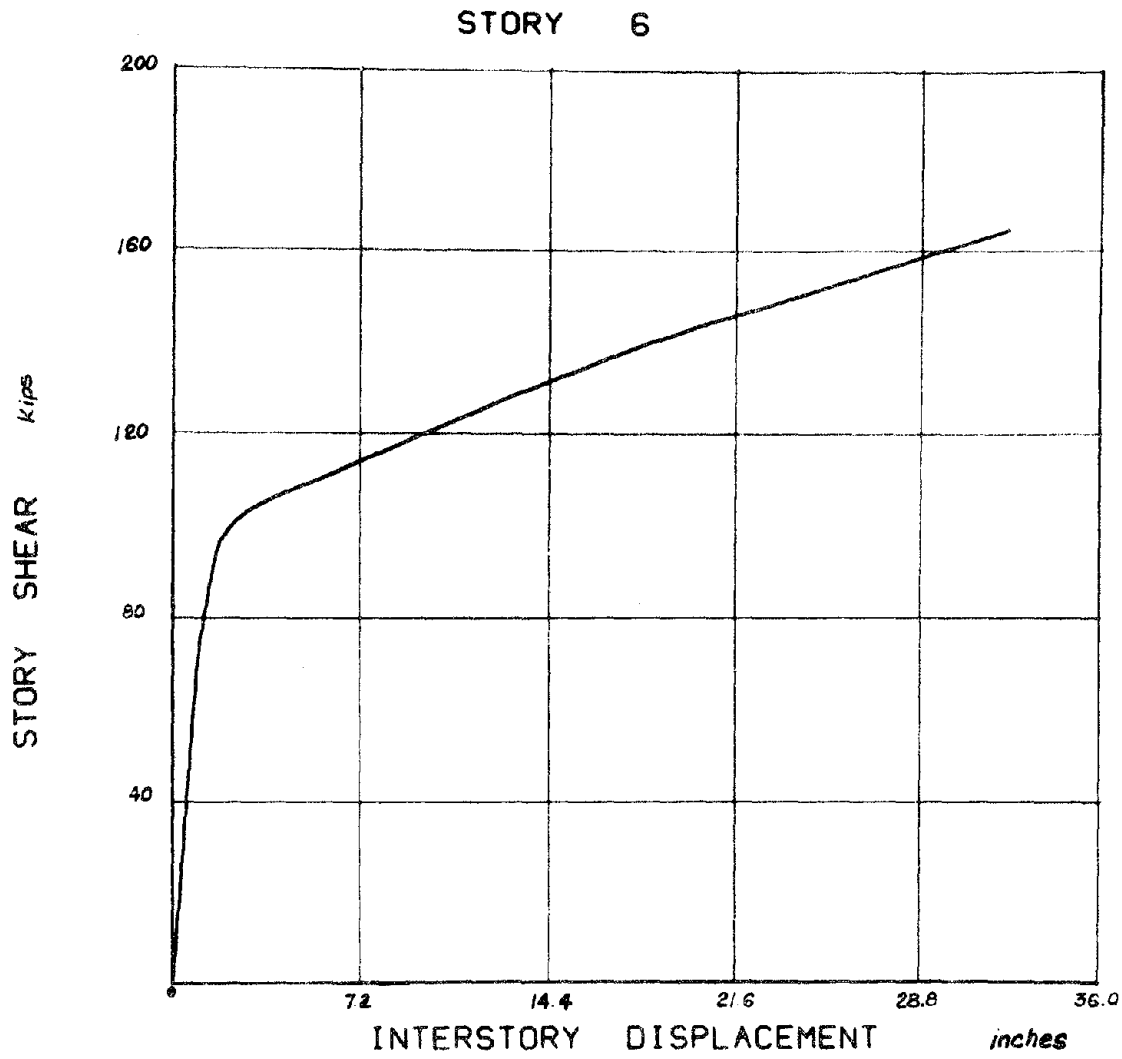

FIGURE 2.18 - 10-STORY UBC FRAME: V-Δ CURVE, 6TH. STORY

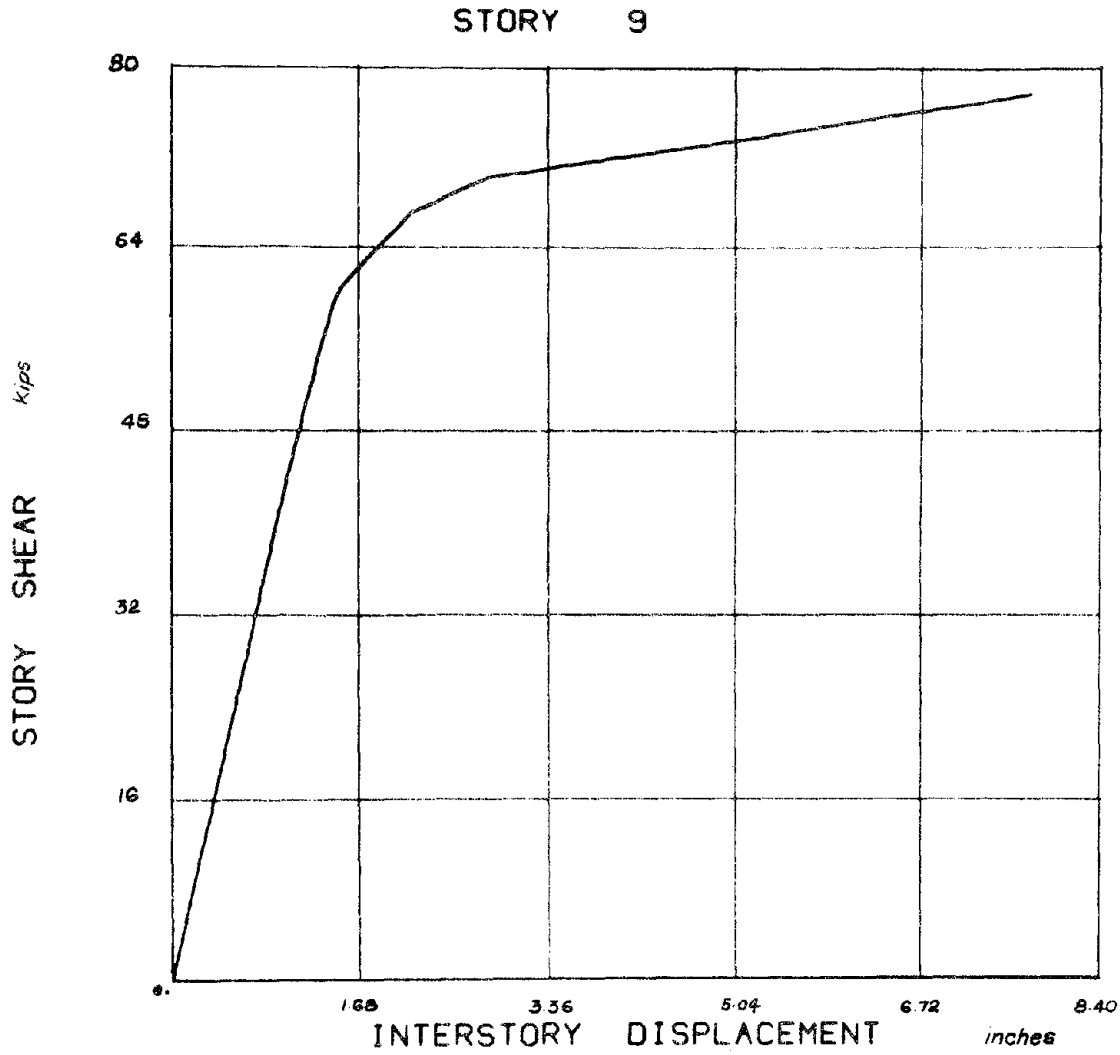

FIGURE 2.19 - 10-STORY UBC FRAME: V-Δ CURVE, 9TH. STORY

clearly, although it seems at a relative higher shear value. Figure 2.20 shows the curve for floor three of Anderson's Frame. The interesting feature about this plot is the sharp changes in slope, defining a clear trilinear relationship. Anderson's frame has only one bay and therefore fewer elements intervene in defining yielding. Figures 2.21, 2.22 and 2.23 show V-Δ curves for floors two, seven and fifteen of the 16-story U.B.C. frame. The three curves show different characteristics which are maintained for low, intermediate and upper stories. In Figure 2.21 transition is progressive initially, but a clearly defined zone of constant slope appears before ultimate yielding. In the seventh floor curve (Fig. 2.22) changes in slope are abrupt, but sections of constant stiffness can be visualized. The curve for the fifteenth story (Fig. 2.23) shows a progressive transition towards ultimate yielding with almost no portions where the slope is constant for more than one loading increment.

2.6 EFFECTS OF LOAD DISTRIBUTION

In order to evaluate the effects of load distribution on stiffness and strength (yield level) the three frames designed by U.B.C. (four, ten and sixteen stories) were analyzed for all the load types described in section 2.2.

These analyses were performed using the interaction yield criterion (section 2.4.5) or "interaction model" as it will be referred to herein. To facilitate the comparisons, a bilinear force-deformation relationship was fitted to the shear-distortion curves as described below. The initial slope of the curves (or first branch) was prolonged until encounter-

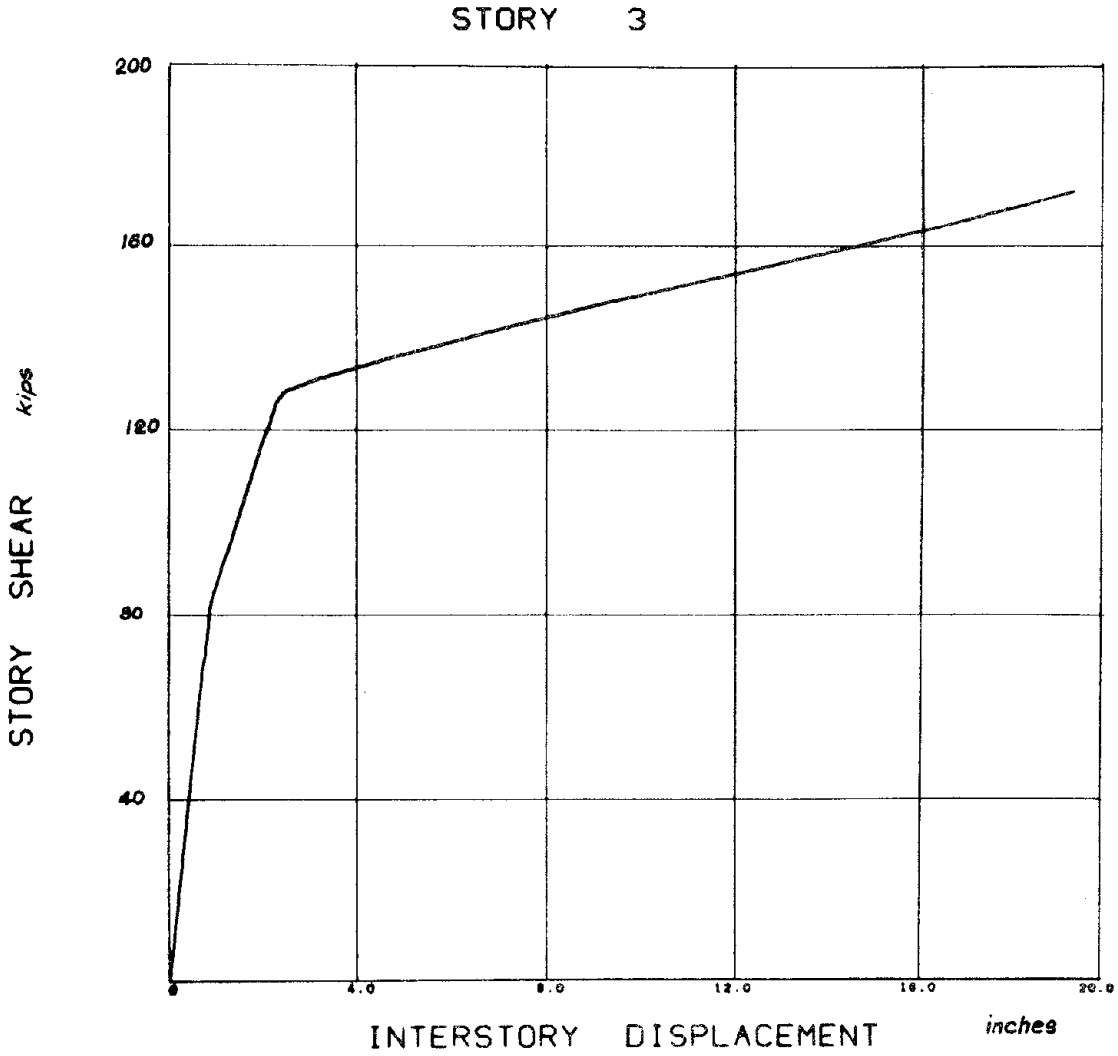

FIGURE 2.20 - ANDERSON FRAME: V-Δ CURVE, 3RD. STORY

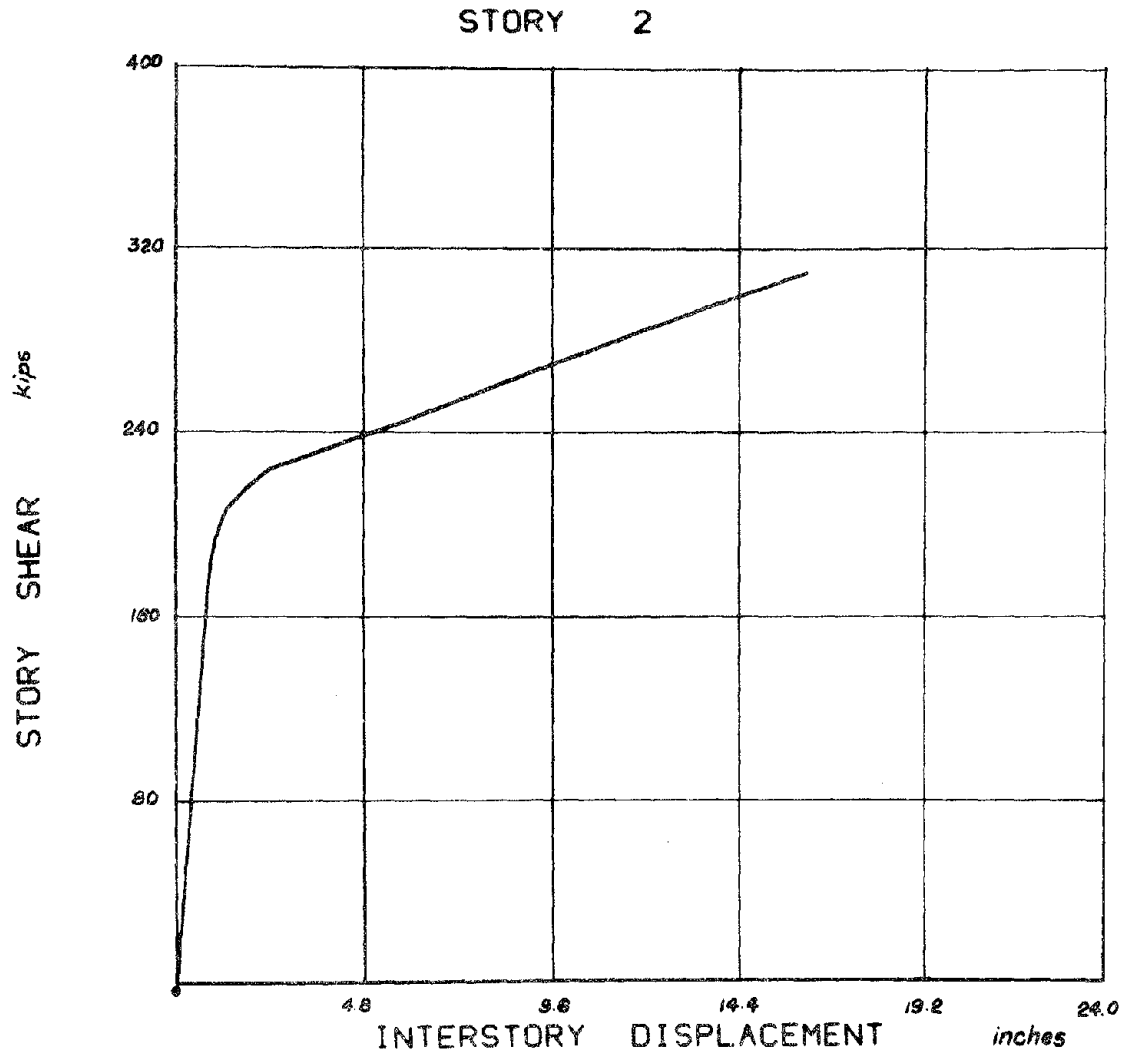

FIGURE 2.21 - 16-STORY UBC FRAME: V-Δ CURVE, 2ND. STORY

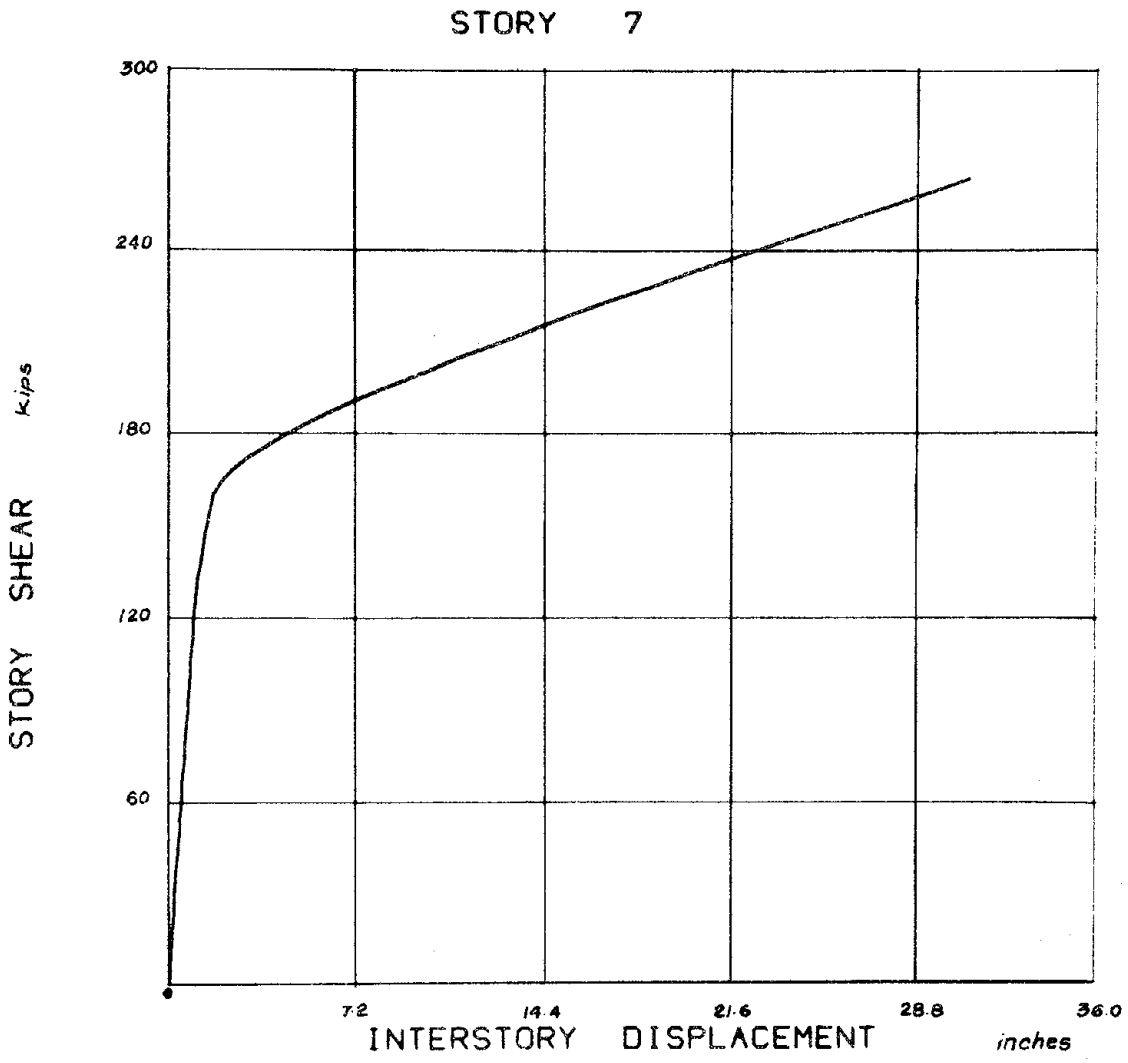

FIGURE 2.22 - 16-STORY UBC FRAME: V-Δ CURVE, 7TH. STORY

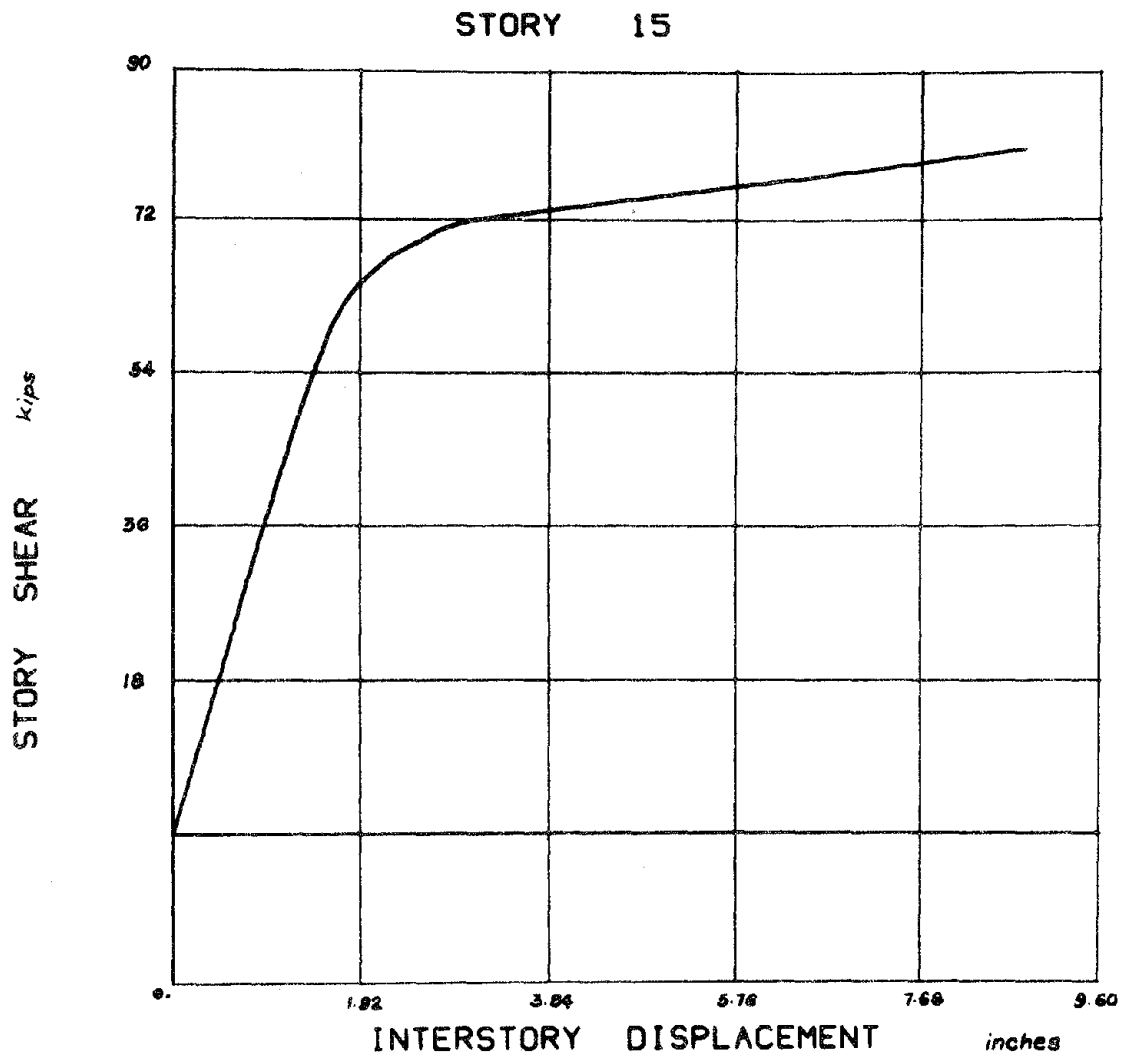

FIGURE 2.23 - 16-STORY UBC FRAME: V-Δ CURVE, 15 TH. STORY

ing a line traced back from the ultimate slope or last branch. Fig. 4.1 illustrates how this approximation was carried out. A yield point was defined as the intersection of these two lines.

Stiffness

The slope at any point of the shear-distortion curve is the lateral floor stiffness. This is a value representing a change in story shear per unit floor distortion, but not the traditional stiffness definition of force per unit floor displacements, while all the other floors are kept fixed. The stiffness used here is a function of the lateral loads applied and implies a known distribution of floor forces with height.

$$K_{\text{floor "i"}} = \frac{\text{Change in } V_i}{\text{Change in } \Delta_i} \qquad (2\text{-}10)$$

Yield Value

In most curves there is a clearly defined point where the curve becomes asymptotic, reaching the ultimate slope. This point is defined as the theoretical ultimate yield. Actually in the approximations introduced by the bilinear or trilinear springs a fictitious ultimate yield is used. For the trilinear one, ultimate yield is defined from the intersection of the second branch with the last branch of the ultimate slope (Fig. 4.1).

Table 2.1 shows initial stiffnesses and yield values for the different load distributions on the four-story building. It can be seen that on the whole, variations on yield force and stiffness are relatively small. In the first floor, for example, the maximum difference in stiffness is of the order of four percent, and on the top floor it is of the

FOUR-STORY U.B.C. FRAME

LATERAL LOAD DISTRIBUTION	UNIFORM		FIRST MODE		UBC CODE		SRSS	
FLOOR	K	F_y	K	F_y	K	F_y	K	F_y
1	1337	107	1289.7	101	1290.8	101.5	1293.7	102
2	883.2	88	897.3	93	894.1	93	892	93
3	769.4	70	790.3	75	789.9	76	787.4	77
4	710.4	69*	731.1	63*	742.8	70*	749.8*	72

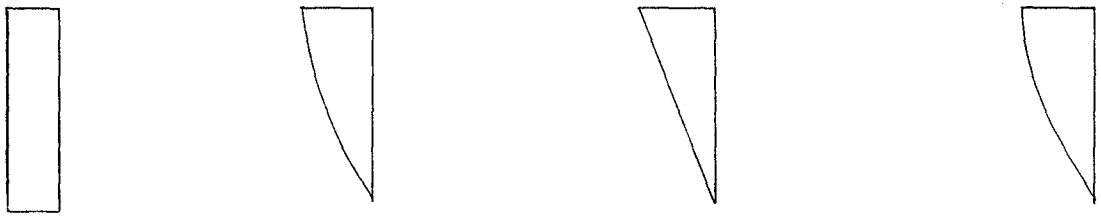

K in Kips/ft., F_y in Kips, N.A. = Not Available, (*) Estimated.

TABLE 2.1 - FOUR-STORY U.B.C. FRAME. BILINEAR SPRINGS

order of six percent. Yield values change only for the uniform distribution and remain almost unaffected for the other three. It is interesting to notice that the changes in stiffness show a certain correlation with the slope of the lateral load distribution. That is, stiffnesses increase when the slope of the force distribution is larger, except for the first floor with uniform load.

Table 2.2 shows the stiffnesses and yield values for the ten-story UBC frame. In this case also, only a small variation in stiffness is registered. In the first floor the change is smaller than four percent, while in the other stories the differences are even smaller, except for the ninth and tenth stories, where the variations are five and twelve percent. Yield values vary somewhat more, but the changes are small for the code, first mode and SRSS distributions. The extremes are in all cases within ten percent of each other. Results for the uniform distribution tend to indicate a departure from the trend showed by the other distributions in relation to stiffnesses; for example, values are always the highest in the bottom story and the smallest in most of the rest. The same is found for yield values. It seems as though a uniform lateral load distribution does not result in appropriate spring parameters. Results from the ATC-3 force distribution are also somewhat different, although not as much as the ones from the uniform distribution. In this case, values for yield and stiffness are lowest of all in the bottom stories, but similar or slightly higher in the upper stories.

A similar trend was encountered for the sixteen-story UBC frame. Table 2.3 shows stiffnesses and yield values for all five distributions on this building. The top floors show again the widest range of stiff-

TEN-STORY U.B.C. FRAME

LAT. LOAD DISTRIBUTION	UNIFORM		FIRST MODE		UBC CODE		SRSS		ATC-3	
FLOOR	K	F_y	K	F_y	K	F_y	K	F_y	K	F_y
1	1370.7	144	1333.1	135	1334.8	136	1343.5	140	1324.5	130
2	1233.5	134	1228.6	134	1228.6	133	1229	133	1220.5	127
3	1121.4	122	1123.5	128	1122.8	128	1116.2	125	1117.08	124.8
4	1046.3	111	1050	121	1049.1	120.5	1039.5	118	1045.1	120
5	906.7	98	915.7	113	914.6	112	906.8	110	914.3	116
6	884.7	88	894.7	100.5	894.0	100	887.3	102	897.2	108
7	748.5	NA	758.5	87.5	758.2	87	756.8	92	763.1	96
8	729.0	NA	741.5	90	742.6	92	745.6	92	751.1	92
9	498.1	NA	508.4	68	509.5	68	522.9	75	517.2	72
10	426.3	NA	439.7	58	444.4	58	480.8	64*	459.2	NA

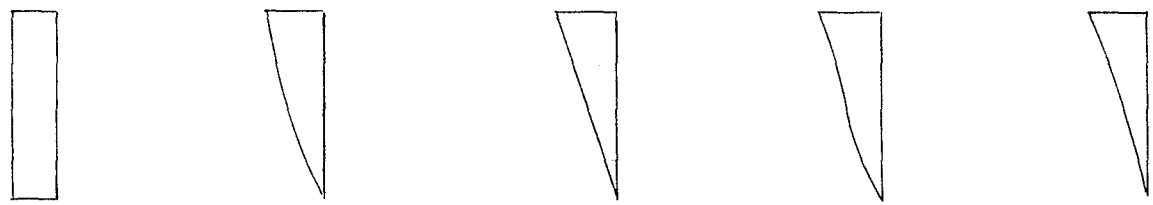

K in Kips/ft, F_y in Kips, N.A. = Not Available, (*) Estimated

TABLE 2.2 - TEN-STORY U.B.C. FRAME. BILINEAR SPRINGS

SIXTEEN-STORY U.B.C. FRAME

DISTRI-BUTION	UNIFORM		FIRST MODE		UBC CODE		SRSS		ATC-3	
FLOOR	K	F_y	K	F_y	K	F_y	K	F_y	K	F_y
1	2751	248	2692	220	2696	222	2709	230	2683	215
2	2541	228	2515	215	2518	216	2522	220	2502	210
3	2137	212	2118	200	2118	199	2116	209	2104	204
4	1982	196	1966	192	1965	188	1955	194	1952	193
5	1757	182	1745	184	1743	182	1730	182	1731	176
6	1637	168	1629	176	1626	170.5	1610	172	1617	170
7	1475	154	1472	168	1468	161	1452	161	1462	165
8	1385	144	1389	156	1385	150	1369	152	1382	157
9	1276	130	1284	146	1280	140	1266	146	1281	149
10	1147	116	1158	135	1153	132	1142	136	1157	138
11	954	108	969	124	965	118.5	962	126	972	128
12	872	96	891	107	889	106	892	115	899	116
13	684	83.2	701	92	702	90.5	708	103	711	100
14	644	NA	666	85	671	85.5	686	93	682	88
15	435	NA	454	67	462	64	489	79	469	71
16	342	NA	365	59*	402	58	438	62	399	60*

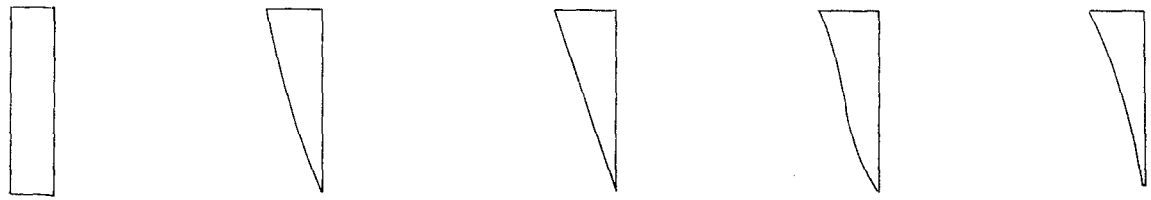

K in Kips/ft., F_y in Kips, N.A. = Not Available, (*) Estimated.

TABLE 2.3 - SIXTEEN-STORY UBC FRAME. BILINEAR SPRINGS

ness with differences being up to eleven percent in the fifteenth floor and twenty-two percent in the sixteenth. The highest values for stiffness are given by the SRSS force distribution (except in the first floor) as it happened for the ten-story frame. The uniform distribution also gives the largest difference.

For yield strengths there is a scatter of fifteen and ten percent in the first two stories; then, only smaller differences can be noticed up to the eighth floor when it rises to ten percent and continues with this value (or increases in some cases) up to the upper floors. Yield values for the three upper stories when using the uniform distribution of forces were not obtained because those floors remained elastic even for very large deformations of lower floors and the entire frame. But judging from yield values of the lower stories, it seemed that there was a trend for these strengths to be the lowest of all and to be at least fifteen percent below the maximum given by SRSS. This fact was also observed for the ten-story frame as discussed above, suggesting an undesirable disparity with the others.

A characteristic of the curves that remain practically unchanged for all the force distributions was the shape itself. If there were changes in stiffness or yield for a given floor, the curves were clearly proportional in all other points.

First Yield

For a given V-Δ curve, there is always a point where the behavior becomes nonlinear. Theoretically this would be the shear and distortion for which first yield occurs. However, in some stories this change in

slope can be the result of yielding in lower stories propagated when solving the entire frame, rather than some member of that or adjacent floors having yielded. It is not clear whether this value should be used directly, or whether an equivalent first yield should be defined. It also must be noted that some numerical changes in slope do not become explicit in the drawn curve, this point being usually hidden in an apparently straight segment. Therefore a criterion had to be adopted that in some way reflected local floor behavior as well as the interaction between floors. In Chapter IV two ways of defining first yield from the V-Δ curves are discussed for trilinear approximations.

None of them, however, takes the point where the first change in stiffness occurs. The first (defined as trilinear A) is the best-fitted trilinear to the shear-distortion curves. This one will be used in this section to present some results regarding first yield.

Several factors affected the location of first yield: the force distribution, the rate of loading, the use of gravity loads in the analysis, the yield criterion used. From all of these the force distribution was the least influential factor, the others having considerable importance.

Analyses were carried out for larger increments of load and they showed the first yield always over-estimated because of "overshooting" in the incremental solution. That is, linear behavior was assumed during a loading step and yielding would occur for lower values of the load than those at the end of the step. At the same time the transitions in stiffness would be much sharper than for smaller loading steps. It was found appropriate to use loading increments between one-seventh and one-tenth

FOUR-STORY UBC FRAME

FLOOR	FIRST YIELD	ULT. YIELD
1	92	106
2	80	96.5
3	68	78
4	47	70

TEN-STORY UBC FRAME

FLOOR	FIRST YIELD	ULT. YIELD
1	100	137
2	98	135
3	91	130
4	98	122.5
5	81	114
6	69	101
7	63	87.5
8	60.5	93
9	59	69.5
10	47	62

SIXTEEN-STORY UBC FRAME

FLOOR	FIRST YIELD	ULT. YIELD
1	199	225
2	201	224
3	180	201
4	163.5	190.5
5	152	184.5
6	145	173.5
7	131	164
8	120	153
9	111	14
10	102.5	134.5
11	97.5	120.6
12	90	107.6
13	71	92
14	67	88
15	55.5	66
16	60	60

TABLE 2.4 - YIELD VALUES FOR TRILINEAR SPRING
DEAD PLUS CODE LATERAL LOAD. INTERACTION MODEL.
(Units: Kips)

of the code base shear. For even taller frames, smaller increments may be necessary to appropriately track yielding propagation on the members. Using the "bending model" as yield criterion resulted generally, as expected, in higher values for first yield since the capacity of the columns was independent of axial loads and there they remained elastic until larger loads were reached.

Table 2.4 shows values of first and ultimate yield strengths for the four-, ten- and sixteen-stories UBC frames. These correspond to a fitted trilinear on the curves obtained for a combination of dead plus code lateral loads, all using the interaction model. (Ultimate values are slightly different from those of the bilinear springs.) On the average, first yield occurs at eighty-one percent of the ultimate for the four-story frame, at seventy-two percent for the ten-story frame and at eighty-two percent for the sixteen-story frame. These are surprisingly high values if compared with the criterion used by Anagnostopoulos [2] of fifty percent. This varies for other cases of course, but it is rarely below two-thirds of the ultimate strength.

2.7 EFFECTS OF GRAVITY LOADS

Analyses were performed for the four-, ten- and sixteen-story UBC frames with and without initial gravity loads. Only dead loads were included. Since the different load distributions resulted in similar values for stiffness and yield, it was decided to study the influence of gravity loads by using the distribution obtained from the UBC code only. The interaction model was used as the yield criterion.

FOUR-STORY UBC FRAME

FLOOR	FIRST YIELD	ULT. YIELD
1	96	110
2	91	101
3	74.5	80
4	NA	NA

TEN-STORY FRAME

FLOOR	FIRST YIELD	ULT. YIELD
1	129	144
2	125	141
3	121	134
4	113	127
5	105	119
6	92.5	105
7	86	94
8	72	94
9	64	71.5
10	NA	NA

SIXTEEN-STORY FRAME

FLOOR	FIRST YIELD	ULT. YIELD
1	206	231
2	204	229
3	196	203
4	180	194
5	175	188
6	165	179
7	160	170
8	150	159
9	186	150
10	180	139
11	118	126
12	102.5	110
13	91	97
14	73	91
15	61	70
16	NA	NA

TABLE 2.5 - YIELD VALUES FOR TRILINEAR SPRING CODE LATERAL LOAD ONLY. INTERACTION MODEL.
(Units: Kips)

Stiffness

Initial stiffnesses in all cases remained unchanged for both situations. Since the applied lateral force in both cases is the same, this fact indicated that lateral displacements were not affected by the gravity loads when the structure behaved elastically.

First Yield

Tables 2.4 and 2.5 present yield values for trilinear approximations with and without gravity loads. First yield occurred at lower shear values when gravity loads were used. For the four-story frame an increase ranging from five to thirteen percent was found when using only lateral loads. For the ten-story UBC frame, increase varied from ten to thirty percent in some cases, and for the sixteen-story frame, increases varied from ten to twenty-three percent. It must be noted that the second branch of the trilinear springs for the case without gravity loads was very short, springs being almost bilinear.

Ultimate Yield

After first yielding had occurred, hinge formation became more accelerated when gravity loads were present, resulting in accentuated earlier nonlinear behavior. This resulted in lower values for ultimate strength because the curves would become asymptotic at lower shear values. Fig. 2.24 shows the curves for story 5 of the ten-story UBC frame. This is a typical situation, repeated for all frames and stories. It must be noted that the reduction of shear capacity is not as large as could be imagined. This can be explained due to the difference in signs between gravity loads moments and lateral loads moments. In some cases they have

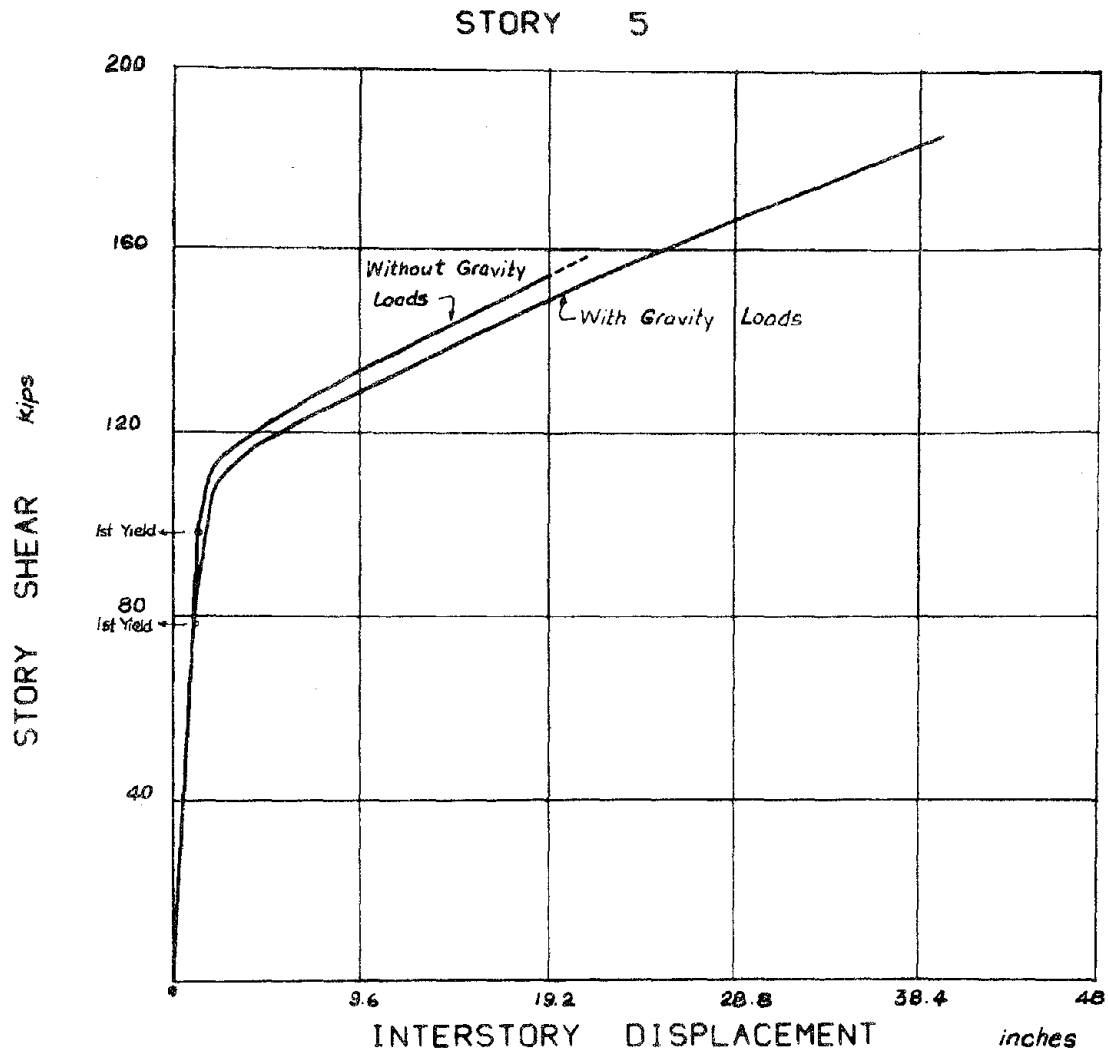

FIGURE 2.24 - INFLUENCE OF GRAVITY LOADS. INTERACTION MODEL.

5TH. STORY. 10-STORY UBC FRAME

equal signs, thereby reducing substantially the remaining capacity of that member, but where they have opposite signs, the capacity is actually increased, resulting in an average reduced floor capacity rather moderate. This is illustrated for both ends of a typical girder in figure 2.25.

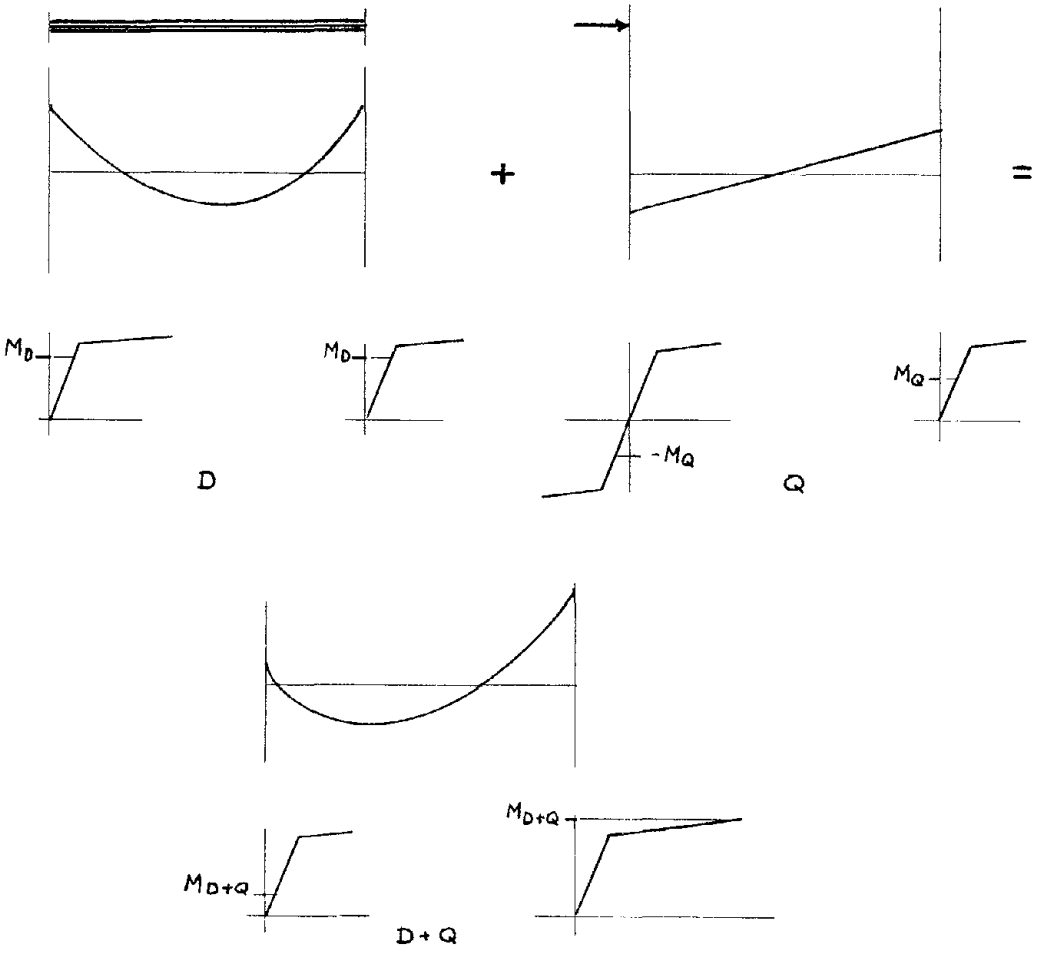

FIGURE 2.25 - INITIAL GRAVITY LOADS EFFECTS

Besides, the interaction model results in additional reduction of the member capacity due to the initial presence of axial loads due to gravity. From Tables 2.4 and 2.5 it can be seen that ultimate yield decreases

by about four percent on the average when gravity loads are used. For the four-story frame it is about four percent average, five percent for the ten-story frame, and three percent for the sixteen-story frame. Similar comparisons were done using the bending model. Figure 2.26 shows the curves for the ninth floor of the 10-story UBC frame as a typical illustration that the gravity load had no effect on the initial stiffness and on the ultimate yield. Both curves eventually converged to the same ultimate slope. The only difference is on the occurrence of first yield. When gravity loads are considered, yielding occurs at a lower level of shear and nonlinearities after that are more pronounced than for the case with no gravity loads. This trend is similar in all floors and for all buildings. On the average this difference is of the order of ten to fifteen percent. In comparison with the interaction model, however, first yield values were around ten percent higher in both situations of loading.

2.8 CONCLUSIONS

The conclusions for this chapter can be summarized as follows:

- It is feasible to use an incremental static analysis to obtain shear-distortion curves. This solution reflects interaction between the floors and accounts for propagation of yielding as the load increases. By using these curves, approximate floor springs can be derived to use in an inelastic dynamic analysis.

- The influence of the assumed lateral force distribution on initial stiffness is small. There were slight variations in the values of stiffness for different load distributions. The scatter was always larger in the top stories. Also it could be noticed that

the taller the building, the larger the differences. Overall, it can be concluded that stiffness is not significantly affected by the force distribution

- Ultimate yield strength is more sensitive to load distribution, although the range of variation is always below twenty percent, within ten percent in most cases, and if the uniform distribution is not considered, differences are even smaller.

- The uniform load distribution seemed to give consistently different results than the rest of them, suggesting it would not be desirable to use it.

- First yield as defined in Chapter IV was found to be sensitive to the rate of loading, to the yield criterion used, and to the presence of gravity laods in the analysis. For the case where the variables above were maintained constant, the first yield was between sixty-five to eighty percent of the ultimate yield.

- The shape of the shear-distortion curves was practically unaffected by the lateral force distribution, but it was changed due to gravity loads.

- The presence of gravity loads--when using the interaction model--resulted in no change for initial stiffness. First yielding occurs at a lower shear value when gravity loads are included, yield propagation is accelerated, and nonlinearities in the V-Δ curve are more pronounced. Ultimate yield was about four percent smaller on the average when gravity loads were used.

- When the bending model is used, the presence of gravity loads initiates yielding at a lower value of the story shear. This difference is on the average of ten to fifteen percent of the ultimate yield value. The transition from first yield to ultimate yield is smaller for the case where lateral loads are used. But besides these two changes the curves are very similar: the same initial and ultimate stiffness and the same ultimate yield value.

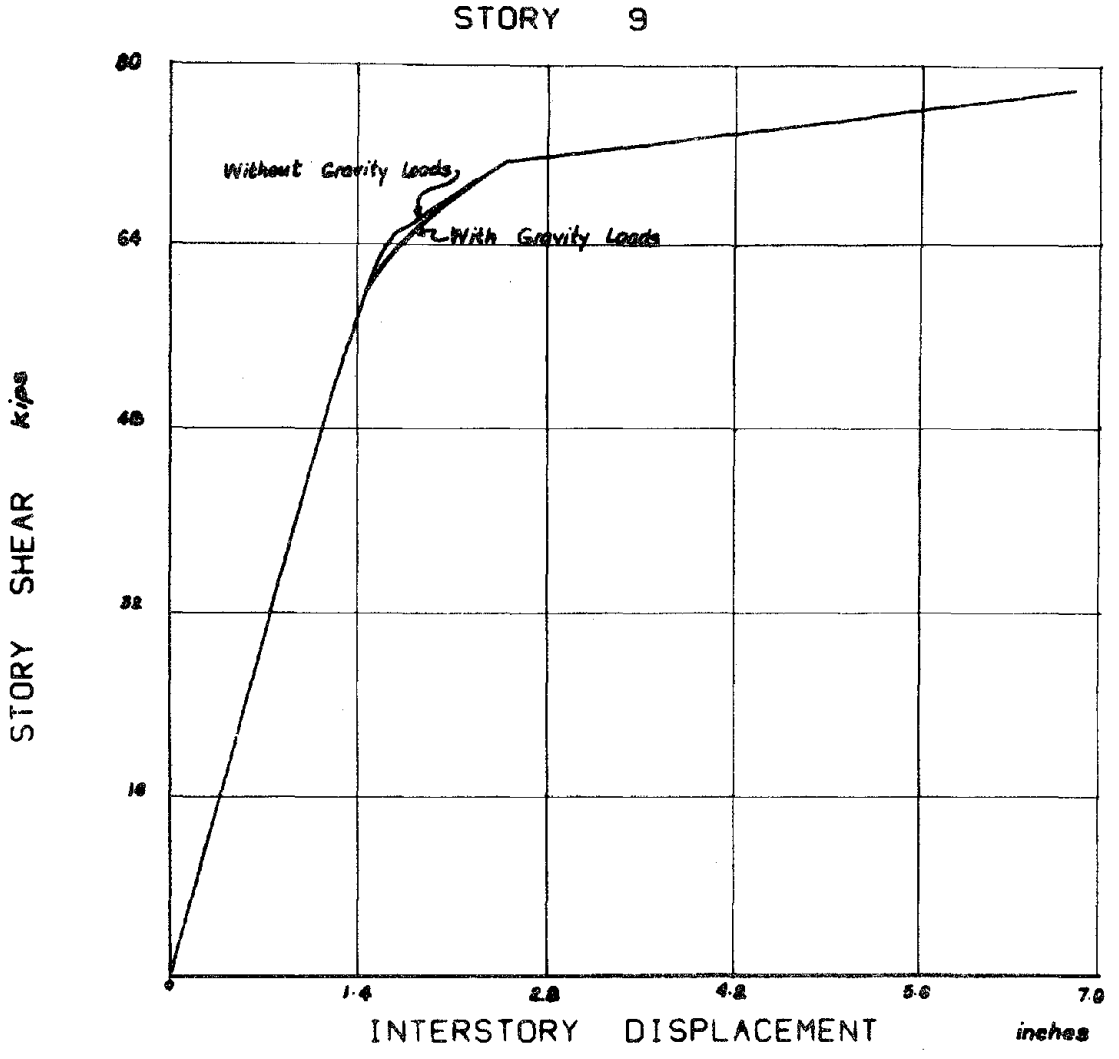

FIGURE 2.26 - INFLUENCE OF GRAVITY LOADS. BENDING MODEL.

9TH. STORY. 10-STORY UBC FRAME

CHAPTER 3

INELASTIC DYNAMIC ANALYSIS WITH MULTILINEAR SHEAR SPRINGS

3.1 INTRODUCTION

In this Chapter, an evaluation of the response predicted by the shear beam approximation using the shear distortion curves obtained as floor springs in Chapter 2 is presented.

The curves are made up of a string of straight segments. When the behavior is elastic or no additional hinges are formed in a particular moment, longer linear segments are formed. Over the complete range studied

the number of segments is, however, rather large for all to be considered in a practical analysis. In most cases only the initial part of the curve may be of interest, if the interstory distortions from the dynamic analysis are expected to be smaller than a given value. Some approximations may be made in any case to reduce the number of segments to a small (bilinear or trilinear springs) value. At this point, however, an evaluation of the shear beam hypothesis was the objective, and therefore it was important to reproduce the shear-distortion curves as closely as possible. It was decided, therefore, to substitute or approximate the V-Δ curves by a series of straight segments following closely shear actual shape and forming a multilinear curve.

From each of the static analyses performed, a set of multilinear curves were obtained in order to investigate which one would give the best agreements with the point-hinge model. Thus for the four-, ten- and sixteen-story UBC frames, analyses were done for a combination of dead load plus uniform, first mode shape, UBC code, SRSS of all modes and ATC-3 lateral force distributions (not for the four-story frame). For the ten-story frames by Anderson and Kamil only the combination of dead plus lateral code forces was used. All these analyses were done using the interaction model. In addition, analyses using the bending model and no dead loads were performed for all the frames mentioned. Only code lateral loads were used in these cases. (These analyses were done because other evaluations of the shear beam model have in the past used the bending model and no gravity loads.)

The following section describes the procedure used to obtain the

multilinear floor springs and their resolution into a series of elasto-plastic springs (needed to use Anagnostopoulos' solution procedure, Ref. 2). Section 3.3 contains the results of all the dynamic analyses and comparisons of the predicted responses. A short presentation of the base for the dynamic analysis using the point-hinge model is given at the beginning of the section, followed by the results for the four-, ten-, and sixteen-stories frames. An evaluation of the influence in the dynamic response of the different load distributions and earthquake intensity is presented in sections 3.3.5 and 3.3.6. The section is closed with a description of the steps followed to compute local ductilities from the shear beam responses.

An overall evaluation of the response predicted by the shear beam model is presented in section 3.4. The conclusions are summarized in section 3.5.

3.2 MODELING OF MULTILINEAR SPRINGS

The actual shear-distortion curves were plotted directly by the computer, one curve per floor in every case. These are nearly continuous curves, although made up of smaller straight segments from the assumption of linear behavior during a loading step. Each of them was transformed into an equivalent multilinear curve. By using more than two or three branches (hence the denomination of multilinear), it was possible to closely model almost any shape of V-Δ curve.

3.2.1 Multilinear Springs after Actual Shear-Distortion Curves

Figure 3.1 illustrates a typical approximation of an actual V-Δ curve by a multilinear one. The straight segments are always defined by

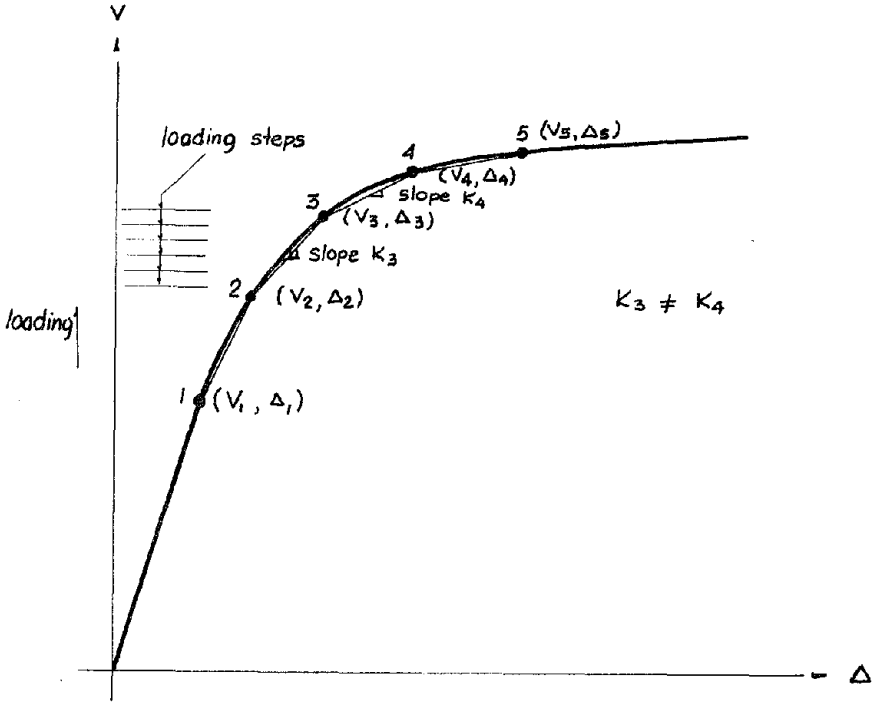

FIGURE 3.1 - ACTUAL CURVILINEAR SHEAR-DISTORTION CURVE

points that lie in the actual curve and only in between the curve is replaced by a straight line. As part of the output of the incremental static analysis, the equivalent floor stiffness and the story shear force and distortion are printed. These values in conjunction with the plots made by the computer are the guidelines to the approximation. One direct way of proceeding is to superimpose on the real curve straight segments that follow the curve as closely as possible and then to read off the

the corresponding coordinates (V,Δ) for the points where the slope changes. This procedure is rather inaccurate. It was decided instead to use both the curves, as a reference, and the printed output as the exact actual values, because substantial changes in stiffness (slope of the curve) are overlooked in the plots due to the scale and steepness of the lines. (For a change from 85° to 80°, for example, the slope is reduced in half). From the printed output, then, and for a given floor, a set of points were read off (V,Δ) every time a reasonable change in slope occurred. For instance, the first point read was that where the behavior stopped being elastic. This was immediately recognized when the initial slope computed at the first step of lateral loading began to change. Then, for another number of increments--sometimes as small as two or one in extreme cases--the slope would remain at the same value. The point before the next change in stiffness occurred was then recorded as the limit of the second segment and so on. (See the third segment in Figure 3.1, for example.) This is a straight line with slope K_3 replacing a curvilinear section of the curve where small changes in stiffness were occurring as the load increased. Only after a reasonable change in slope was in evidence, another segment of slope K_4 was defined, and the coordinates of point 3 were read off (V_3, Δ_3) from the computer printout. This process was repeated until the section of the curve which was of interest was all included. The number of points read and segments defined varied according to the shape of the curve. For some cases where the curve itself was made up by four or five straight segments it was only necessary to identify those limiting points where stiffness changed. In

other cases, however, where there was a continuous change in stiffness, only significant variations were considered or straight segments interpolated every certain number of loading increments. The number of segments used varied from five to thirteen.

3.2.2 Resolution of Multilinear Curves with Elastoplastic Components

The computer program developed by Anagnostopoulos [2] for inelastic analysis using the shear beam formulation can accept bilinear and trilinear springs for the components. It also accepts other degrading springs, but it is not implemented to handle springs with more than three branches. It can, however, superimpose several springs for a given floor simulating the different components of the building. This feature was exploited in order to model a multilinear spring by decomposing it into a set of elastoplastic springs in parallel; since they could be modeled in the program as a bilinear with zero second slope. A typical multilinear hysteretic loop with four segments is shown in Fig. 3.2. After the last

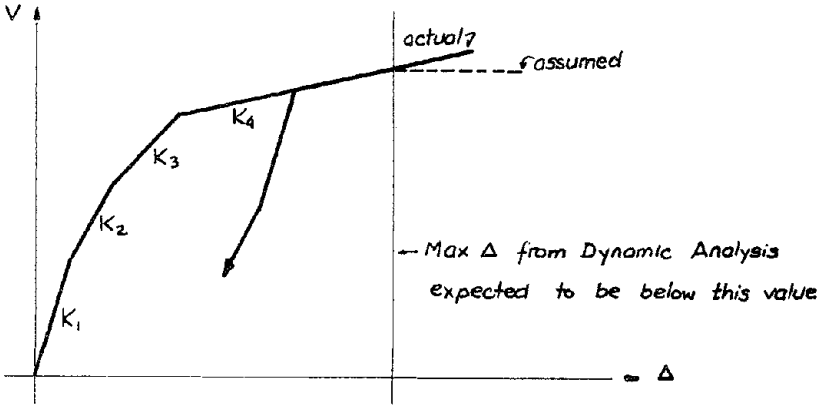

FIGURE 3.2 - MULTILINEAR HYSTERETIC LOOP FOR FLOOR SPRING

segment a zero slope is assumed. This portion is never reached because in all cases the last point is taken as corresponding to a distortion value much larger than the one expected from the dynamic analysis.

Referring again to Figure 3.1, the restoring characteristics of this fictitious multilinear spring can be replaced by the superposition of four springs with a hysteretic elastoplastic force-deformation relation acting in parallel. That is, for a given level of distortion in the real spring, all components experience the same deformation as if held by a rigid plate at both ends (Figure 3.3). By equilibrium then,

$$F(\Delta) = F_1(\Delta) + F_2(\Delta) + F_3(\Delta) + F_4(\Delta) \qquad (3\text{-}1)$$

where $F_i(\Delta)$ represents an elastoplastic hysteretic relationship (Figure (3.4), and each elastoplastic spring is fully defined when the yield force F_y and the initial slope K are known. The stiffness of the last spring "n" is taken as the slope of the last branch "n".

$$k_n = K_n \qquad (3\text{-}2)$$

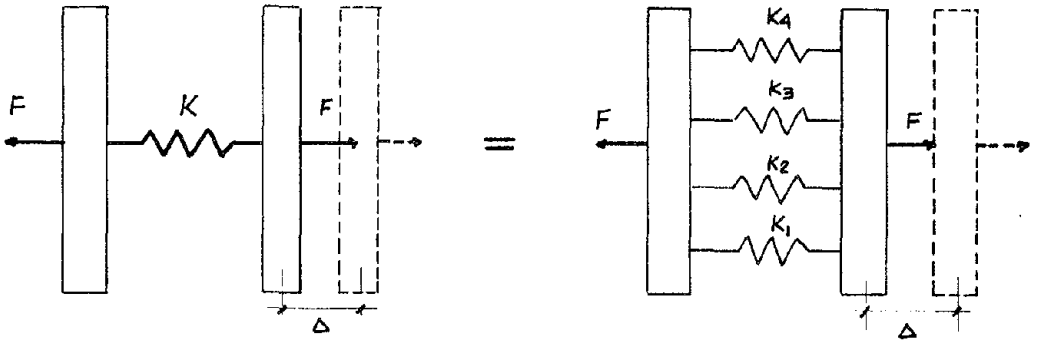

FIGURE 3.3 - PARALLEL SUPERPOSITION OF SPRINGS

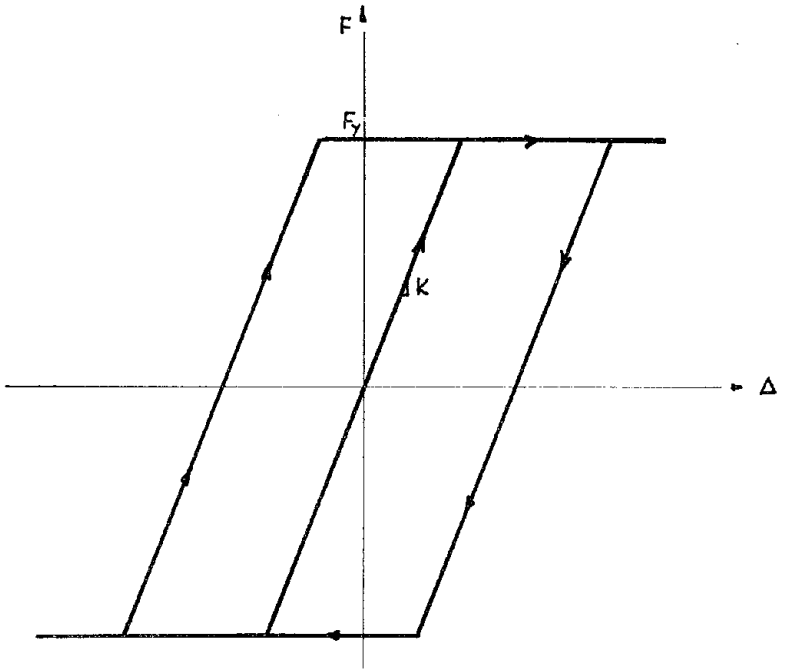

FIGURE 3.4 - ELASTOPLASTIC HYSTERETIC LOOP

Next the yield force F_{yn} has to be computed. This is

$$F_{yn} = k_n \Delta_n \tag{3-3}$$

Spring n is fully defined. Up to this step spring M has been divided into two components, an elastoplastic and the multilinear M', which is the difference between M and spring IV, as can be seen in Figure 3.5(a). Spring M' is made up of three segments, or (n-1) in the general case, and the new force ordinates of points that define it are calculated by subtracting k_{IV} times the corresponding distortion Δ from the original ordinates. That is

$$F'_i = F_i - k_n \Delta_i \qquad \begin{array}{l}\text{for point } i \\ i = 1, (n-1)\end{array} \tag{3-4}$$

where F'_i = Force ordinate at point i of first reduced multilinear M' after subtracting spring "n".

F_i = Force ordinate at point i of original multilinear spring.

k_n = Slope of elastoplastic spring number "n" equal to slope of last branch of original multilinear spring

Δ_i = Distortion abscissa at point i, unchanged from the original.

Notice that the values of the abscissa Δ_i remain unchanged at all times, since this decomposition is in parallel.

The next step is to start with the reduced multilinear M' and to calculate the following elastoplastic spring, in this case spring III, (n-1) in the general case. Again the stiffness of spring III (k_{III}) is taken as the slope of the last branch of multilinear M',

$$k_{III} = K'_3 \qquad (3.5)$$

The yield $F_{y\ III}$ is then $F_{y\ III} = k_{III} \cdot \Delta_3$

Multilinear M" with two branches only is defined by computing the new ordinates F''_i in a similar manner as for M', using Eq. (3.4), except that F_i becomes F'_i and F'_i becomes F''_i. "i" varies from 1 to (n-2). Figures 3.5(c) and 3.5(d) illustrate the following steps to compute springs II and I.

Although this procedure makes it simple to visualize how the elastoplastic components can be obtained, a rather direct approach was used to actually compute their properties.

From Eq. (3-2) $k_{IV} = K_4$

From Eq. (3-5) $k_{III} = K'_3$

but actually $K'_3 = K_3 - K_4 \qquad (3\text{-}6)$

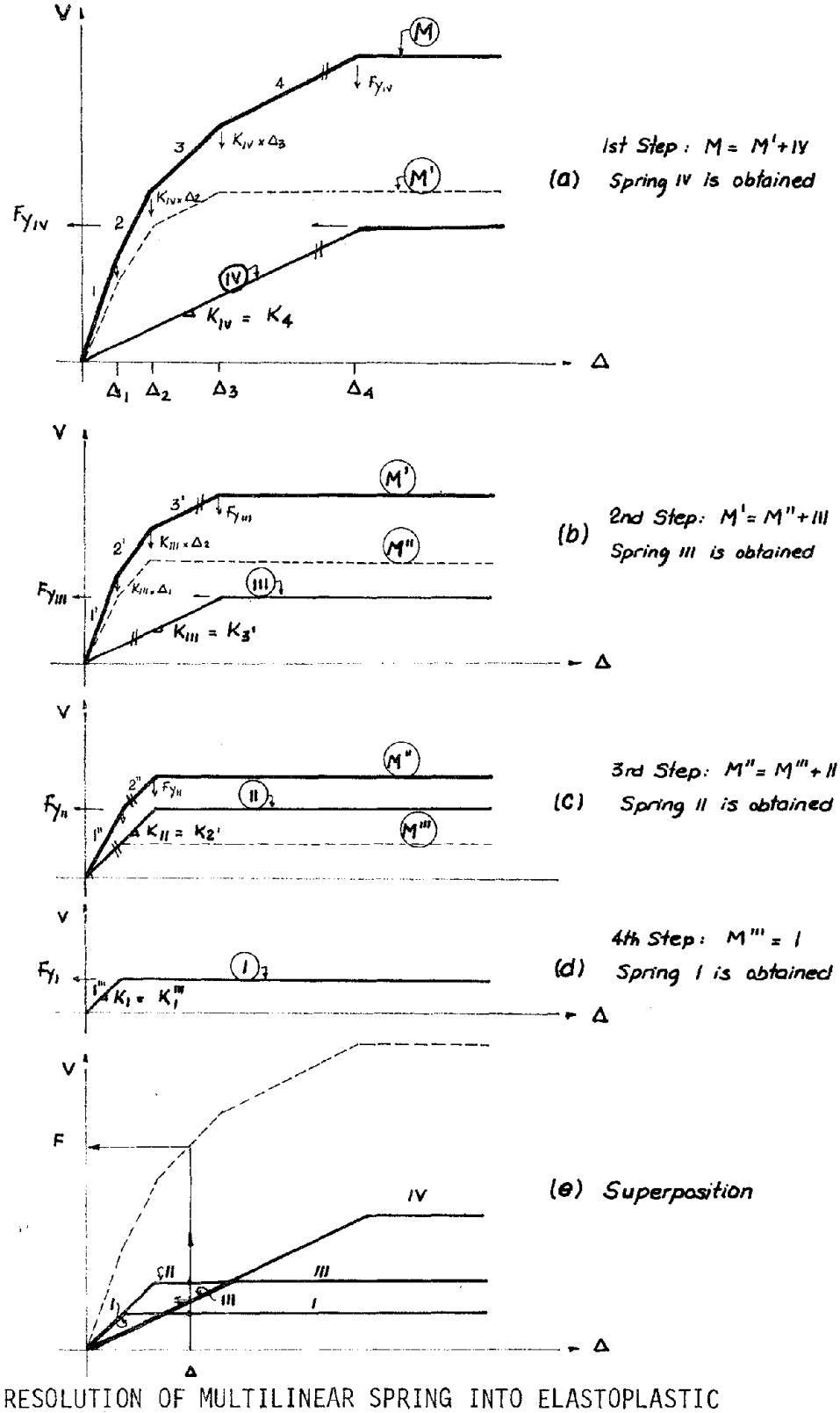

FIGURE 3.5 - RESOLUTION OF MULTILINEAR SPRING INTO ELASTOPLASTIC COMPONENTS IN PARALLEL

being K_3 and K_4 stiffnesses of branch 3 and 4 in the original multilinear, so

$$k_{III} = K_3 - K_4$$

and in general

$$k_n = K_n - K_{n+1} \tag{3-7}$$

where

k_n = stiffness of elastoplastic component 'n'

K_n = stiffness of branch 'n' of multilinear spring being resolved

K_{n+1} = stiffness of branch 'n+1' of multilinear spring being resolved.

Yield values are then computed by

$$F_{yn} = k_n \Delta_n \tag{3-8}$$

Figure 3.6 illustrates how the total restoring force F in the multilinear spring for a given distortion Δ is computed using Eq. (3-1) as the sum of the forces in each elastoplastic spring for the same value of Δ.

3.3 COMPARISONS OF RESPONSES PREDICTED BY POINT-HINGE AND MULTILINEAR SHEAR BEAM MODELS

The formulation and numerical solution used in this study for the shear beam type dynamic analysis is that presented by Anagnostopoulos in reference [2]. The shear beam approximation reduces the entire structure to a lumped mass system with three degrees of freedom per floor (for the tridimensional case) and a set of floor springs with different shear-distortion relations. Figure 3.7 illustrates the shear beam type idealization. The system is close-coupled.

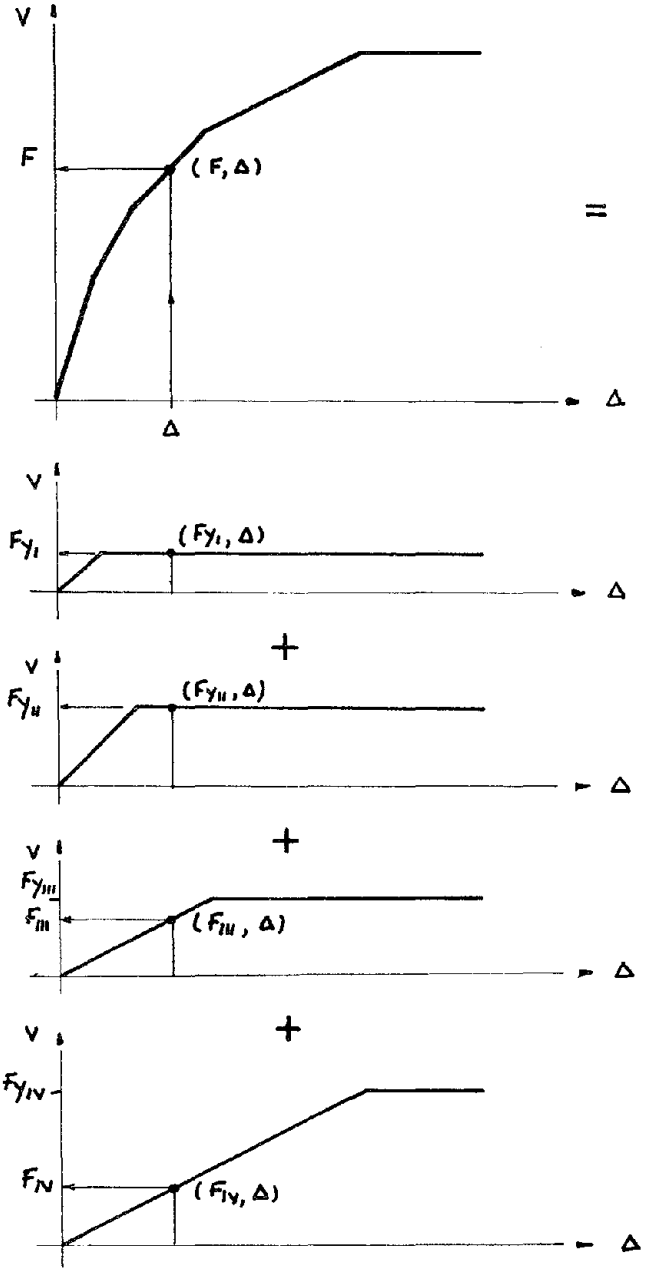

FIGURE 3.6 - RESTORING FORCE FROM ELASTOPLASTIC SPRINGS IN PARALLEL

Each floor has a hysteretic nonlinear shear-distortion curve that defines a restoring force for a given level of deformation. The incremental differential equations of motion to be integrated over time are

$$M\ \ddot{U} + C\ \dot{U} + F(U) = -\ M\ I\ \ddot{u}_G(t) \qquad (3\text{-}9)$$

where M, C are mass and damping matrices, U a vector of relative displacements, $\dot{U}$ and $\ddot{U}$, velocity and acceleration vectors, I a column vector of unit values, $\ddot{u}_G$ ground acceleration, F(U) a vector of restoring forces.

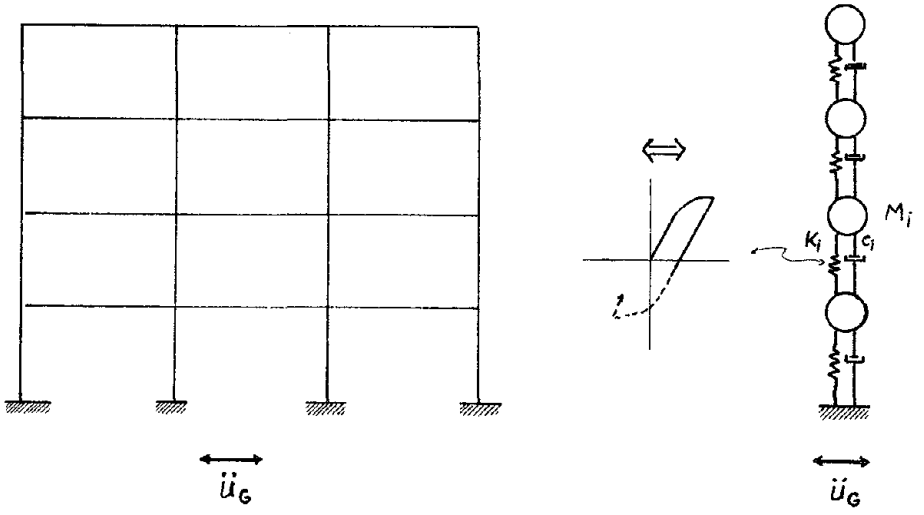

FIGURE 3.7 - SHEAR BEAM MODEL OF A MULTISTORY FRAME (CLOSE-COUPLED SYSTEM)

The mass matrix M is a diagonal matrix: element 'i' is the mass of floor 'i'. If the problem is tridimensional, the order of the matrix is 3n x 3n and all the floor masses are grouped in diagonal submatrices for each direction. For the plan rotation the mass moment of inertia of

the floors J_i are used instead. The Damping Matrix is given by [33]:

$$C = M\,Q\,B\,Q^T\,M \qquad (3\text{-}10)$$

where M = mass matrix

Q = matrix with c lumns containing the modal shapes (normalized with respect to M, $\phi^T M\phi = 1$)

B = diagonal matrix with elements $2\beta_i\omega_i$

β_i = percentage of critical damping in the i^{th} mode.

F(U) is a vector of forces computed every time step from the shear springs as a function of the level of deformation of the floor. It includes the summation of all resisting forces on the floor if there is more than one spring.

Equation (3-9) was integrated in time using the "constant velocity method" [8]. This procedure can be considered as an application of the central difference formula [34]. The recurrence formulas for step n are:

$$\left.\begin{aligned} \dot{U}_n &= \frac{1}{2\Delta t}\,(U_{n+1} - U_{n-1}) \\ U_n &= \frac{1}{\Delta t^2}\,(U_{n+1} - 2U_n + U_{n-1}) \end{aligned}\right\} \qquad (3\text{-}11)$$

For the dynamic analyses performed here, the effects of gravity loads were implemented in the computer program following the approximation described in section 2.4.4. It must be noted that this option was not used when performing the static analysis, because for large deformations the slope of the shear-distortion became negative. Instead it was decided to use it when performing the dynamic analysis. A constant

value of damping for all the modes was used equal to two percent.

The floor masses were computed including dead load only, consistently with the loads used in the static analysis to obtain the shear-distortion curves. Live loads were not included following the UBC criterior to compute earthquake forces.

Two earthquake records were used for all dynamic analyses with both formulations: El Centro of 1940 N-S component, and Taft 1952 N69W component. The first six seconds of El Centro were used, and the first ten seconds of Taft. Both versions were digitized at 0.01 seconds. El Centro's peak acceleration is 0.314g and Taft's 0.157g.

3.3.1 Point-Hinge Model Dynamic Analysis

Dynamic Analyses of all frames were performed using the computer program FRIEDA [26]. This is a solution based on a point-hinge modeling of frames developed by Aziz [16]. The version used for this research was the one reported in Ref. [26], which is an update of the original. The formulation and solution scheme are reported in detail there.

The structure is modeled as a set of columns and girders assembled to constitute a plane frame. In the present version this program is limited to this type of frames only.

Member stiffness matrices and the assemblage of the total stiffness matrix are almost identical with the procedure followed in the static a analysis of Chapter 2, the only exception being that FRIEDA has the option of including shear deformation for the columns and does not take axial deformation for the girders into account. Once the total stiffness

matrix is formed, both a kinematic and a static condensation are performed to obtain the lateral stiffness matrix and reduce the dynamic degrees of freedom to a lateral displacement per floor. The equations of motion solved are of the same form as equation (3-9).

$$M \ddot{U} + C \dot{U} + \sum K \Delta U = - M I \ddot{U}_g \qquad (3\text{-}12)$$

where K is the lateral stiffness matrix obtained by condensation at every time step; the other terms are similar to the ones defined for the shear beam model.

The constant velocity method [8] is also used here for the numerical integration of the equations of motion. The first time step, however, is integrated using a 4^{th} order Kunge-Kutta method. The same is true for the shear beam analysis.

Each member is idealized as a dual component model (Fig. 3.8) as proposed by Clough [9]. One component remains always elastic and the other is elastoplastic. Both act in parallel. The program also implemented a single component model as proposed by Giberson [11], but in all analysis performed for this study, only the dual component model was used.

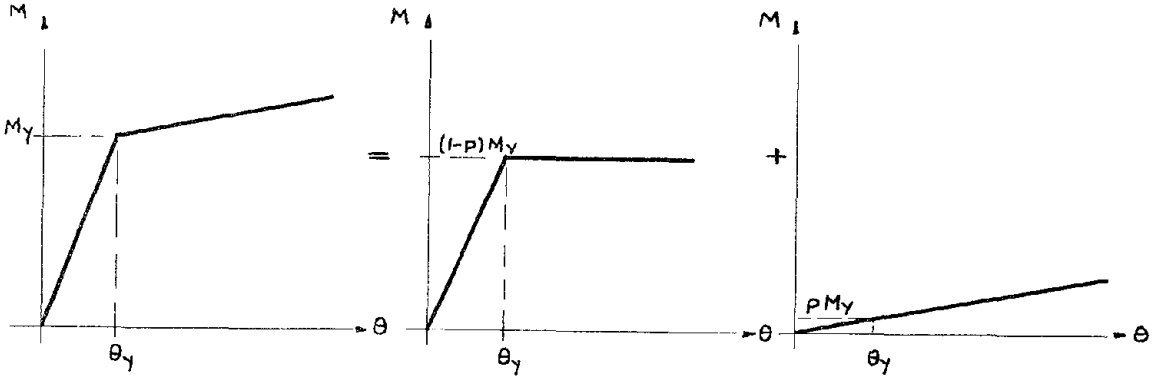

FIGURE 3.8 - DUAL COMPONENT MODEL

Yield criteria are the same as the ones used in the static analysis, interaction and bending models. This program, however, has the capability of dealing with nonsymmetrical interaction diagrams as for reinforced concrete and also accepts different positive or negative plastic moment capacities for a given section.

During a time step the behavior is assumed to be elastic and equations (3-12) applied. At the end of every time step all members are scanned for exceedance of their capacity. If that is the case, a hinge is placed at the appropriate end, and the corresponding stiffness matrix is modified accordingly. If a reversal has occurred, then the member is assumed to be elastic again, and its stiffness matrix reinstated to its original form. This implies that the total stiffness matrix is modified and the condensation process repeated whenever there is a change of member status.

The definitions of ductility used in this program are essentially the same as the ones used in the static analysis, the only difference being that the moment capacity of the columns M_y when computing rotation ductility is not reduced by the magnitude of the axial loads.

Several damping options are available in FRIEDA: constant damping in each mode; damping proportional to the stiffness matrix; damping proportional to the mass matrix, and a linear combination of both stiffness and mass matrices (the so-called Rayleigh damping). In this study a constant value of damping in all the modes was used equal to two percent of critical damping. This value was assumed to be reasonable, since additional damping was expected to be introduced due to the energy dissipa-

tion of the hysteretic loops. A second slope of two percent was used for the moment rotation diagram in the dual component model. This is the same value used in the static analyses.

P-Δ effects are considered in the analysis in different ways: modifying the stiffness matrices of the columns as in section 2.4.4 or by stability functions. The first option was used herein whenever this effect was included.

3.3.2 Four-Story Frame

Comparisons were made of floor displacements relative to the ground and of interstory displacements (distortions) as predicted by both models.

Figure 3.9 shows plots of both responses for the elastic case. This was achieved for a peak acceleration of 0.0785g, which is one quarter of the El Centro record. The agreement is quite good for displacements and for distortions.

Figures 3.10 and 3.11 show the response when using the springs from the UBC code and uniform distributions and when using the first mode shape and SRSS of all modes distributions. Peak acceleration in this case was 0.314g, the standard peak of the record. P-Δ was included in all cases.

The shape of both envelopes for floor displacement is very similar. Interestingly enough, even the point hinge model predicts a curve that has a curvature similar to that of a shear beam. The values for displacement of the top are of the order of 5 inches, or about one percent of the

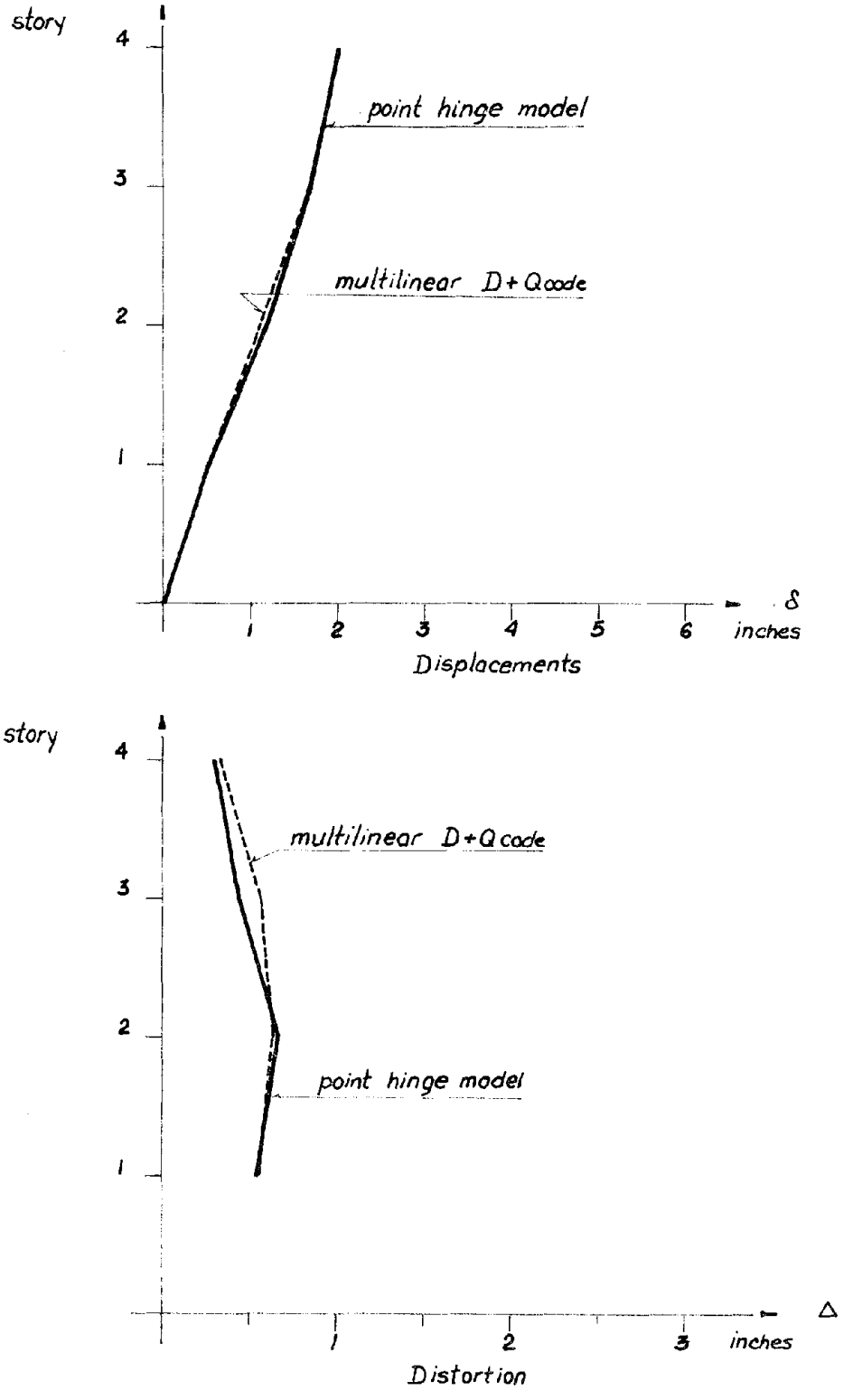

FIGURE 3.9 - 4-STORY UBC FRAME: POINT HINGE VS. MULTILINEAR SPRING. $D+Q_{code}$. INTERACTION. ELASTIC. 1/4 EL CENTRO. P-Δ

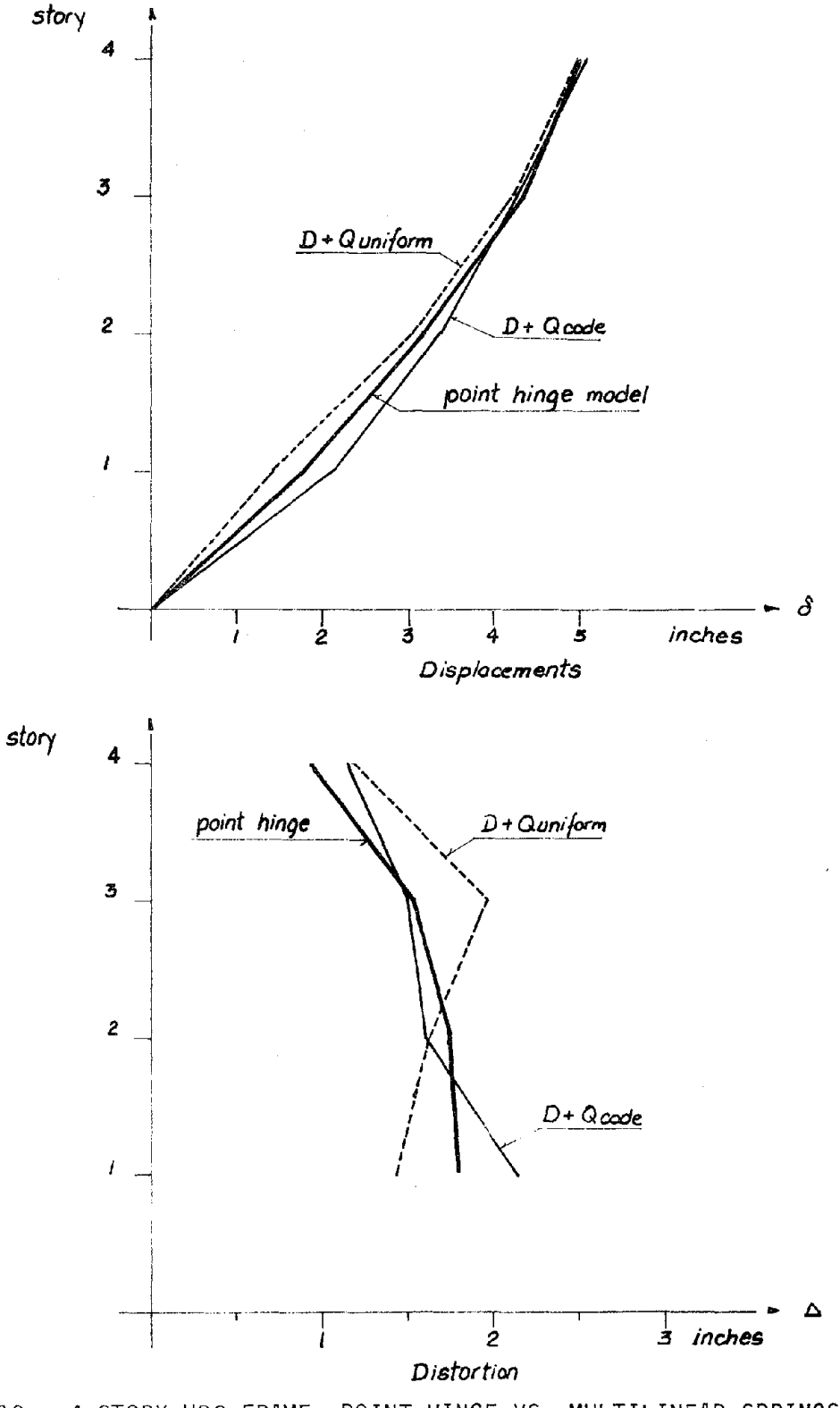

FIGURE 3.10 - 4-STORY UBC FRAME: POINT HINGE VS. MULTILINEAR SPRINGS. $D+Q_{uniform}$. $D+Q_{code}$. INTERACTION. EL CENTRO. P -Δ

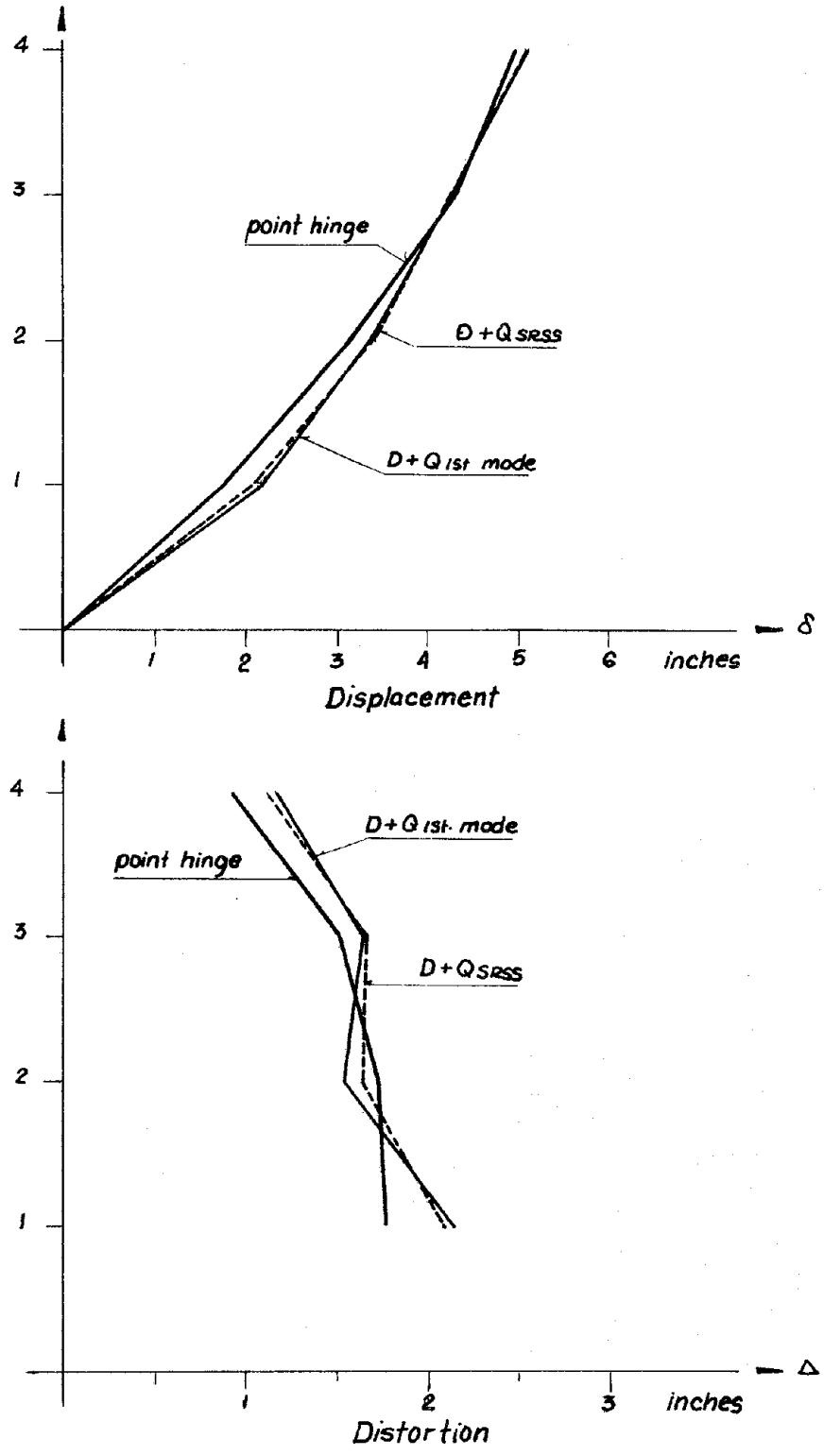

FIGURE 3.11 - 4-STORY UBC FRAME: POINT HINGE VS. MULTILINEAR SPRINGS. $D+Q_{1st.\ mode}$. $D+Q_{SRSS}$. INTERACTION. EL CENTRO. P-Δ

total height of the building. On Figure 3.12 hinges that have formed at least one time during the analysis are shown. Most yielding occurs in the columns which explains the shape of the envelope of maximum displacements. The agreement in general is very good, and the maximum differences are of twenty percent on the first floor.

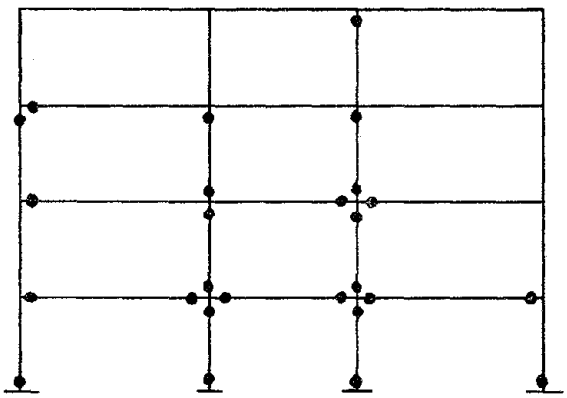

FIGURE 3.12 - MECHANISM CORRESPONDING TO MAXIMUM DISPLACEMENTS
(4-Story UBC Frame)

The shape of the distortion envelopes differ from the point-hinge curve, although the basic trend of larger values in the lower stories is maintained. For the shear beam model the envelopes are more jagged and vary with load distribution. The maximum values reach two inches, which is about 1.7% of the story height. These values are larger than the ones corresponding to floor displacements by comparison, which is explained by the fact that they do not occur at the same time. All but the uniform load distribution give the largest value at the bottom story.

Figure 3.13 shows the comparison for the same building and motion, but without P-Δ. There is not much difference with the former cases, suggesting small influence of this effect over floor displacements and distortions.

Figure 3.14 shows the results for the Taft earthquake. A scaling of this record had to be made since the peak acceleration is smaller than El Centro's. The criterion used was to equate the intensities of both earthquakes as defined by Arias [37]. This resulted in a factor of 1.87 by which Taft accelerations were multiplied. The agreement is even better than for El Centro. It must be noted, however, that the extent of yielding was smaller for this case. The magnitude of displacements and distortions is smaller too.

Figure 3.15 presents the results of analyses performed for different peak accelerations using El Centro. This was restricted to the point-hinge model and the shear springs from UBC code distributions. P-Δ effects were not included for this comparison. The first set of curves is for one quarter El Centro when behavior is elastic, the second for one El Centro, and the third for twice El Centro.

For all cases the agreement between both models remains practically the same and as expected the magnitude of the deformations does not increase proportionally with the peak ground acceleration.

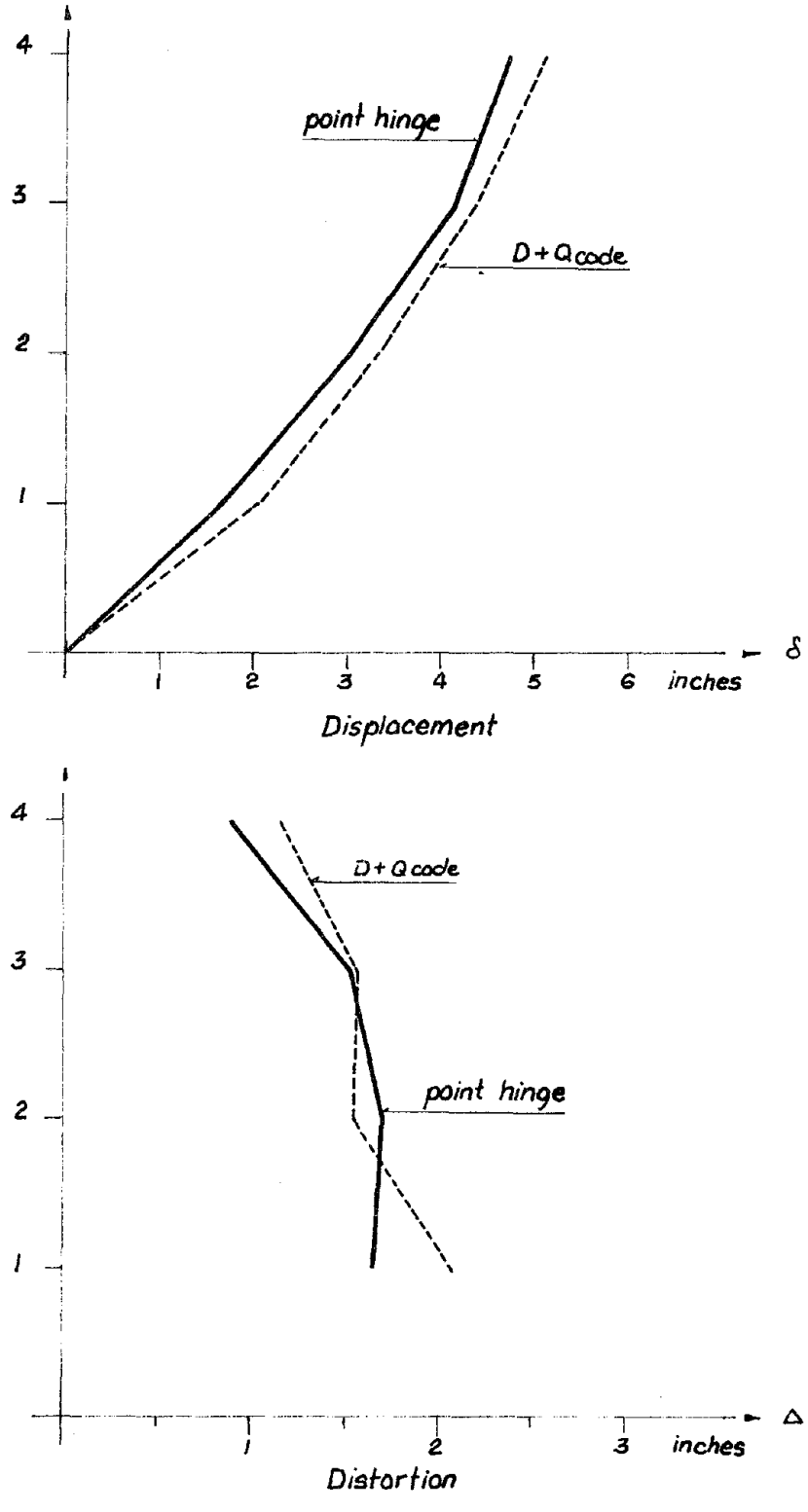

FIGURE 3.13 - 4-STORY UBC FRAME: POINT HINGE VS. MULTILINEAR. $D+Q_{code}$. INTERACTION. EL CENTRO. NO P-Δ

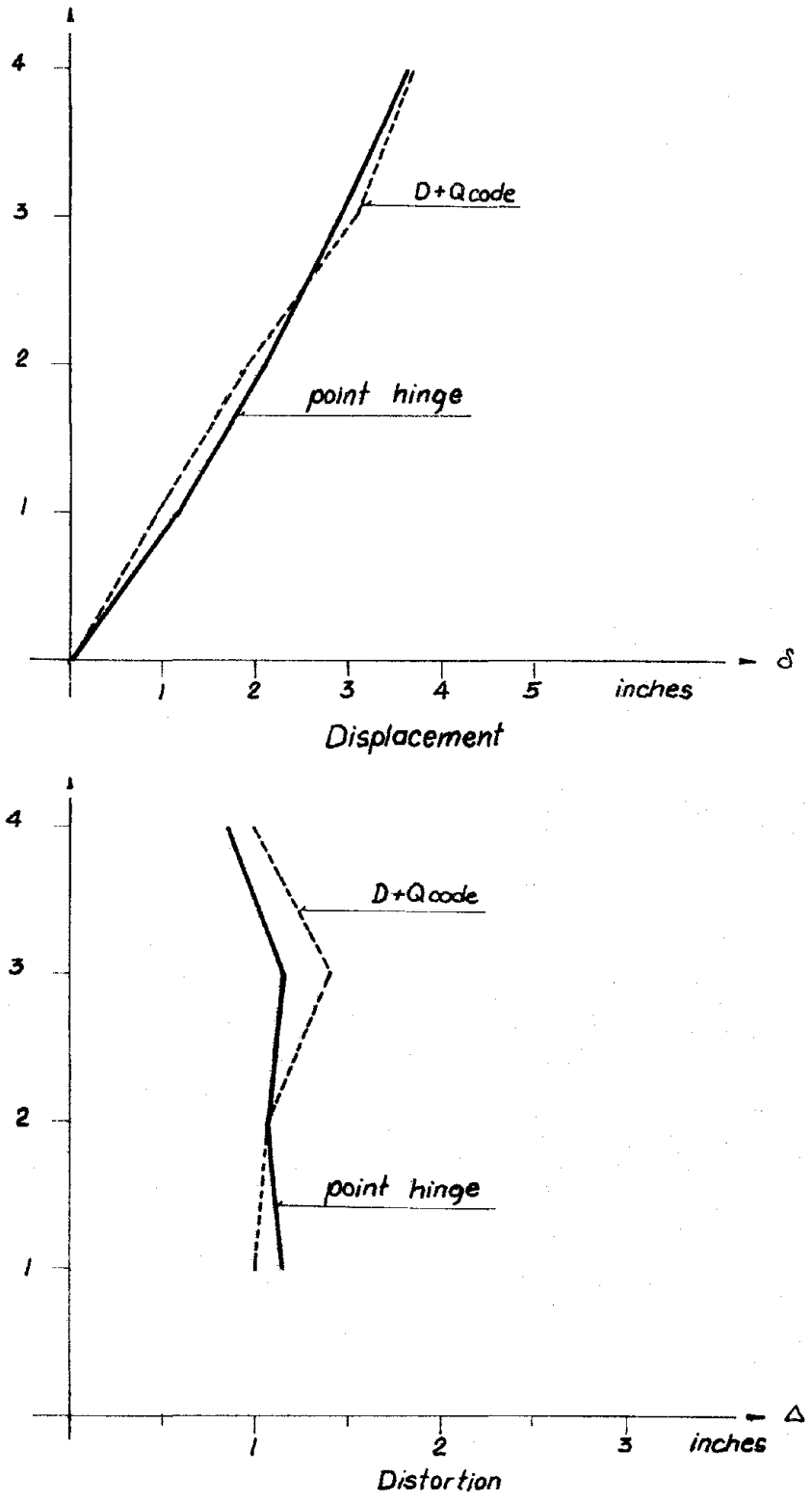

FIGURE 3.14 - 4-STORY UBC FRAME: POINT HINGE VS. MULTILINEAR. $D+Q_{code}$. INTERACTION. 1.87 x TAFT. NO P-Δ

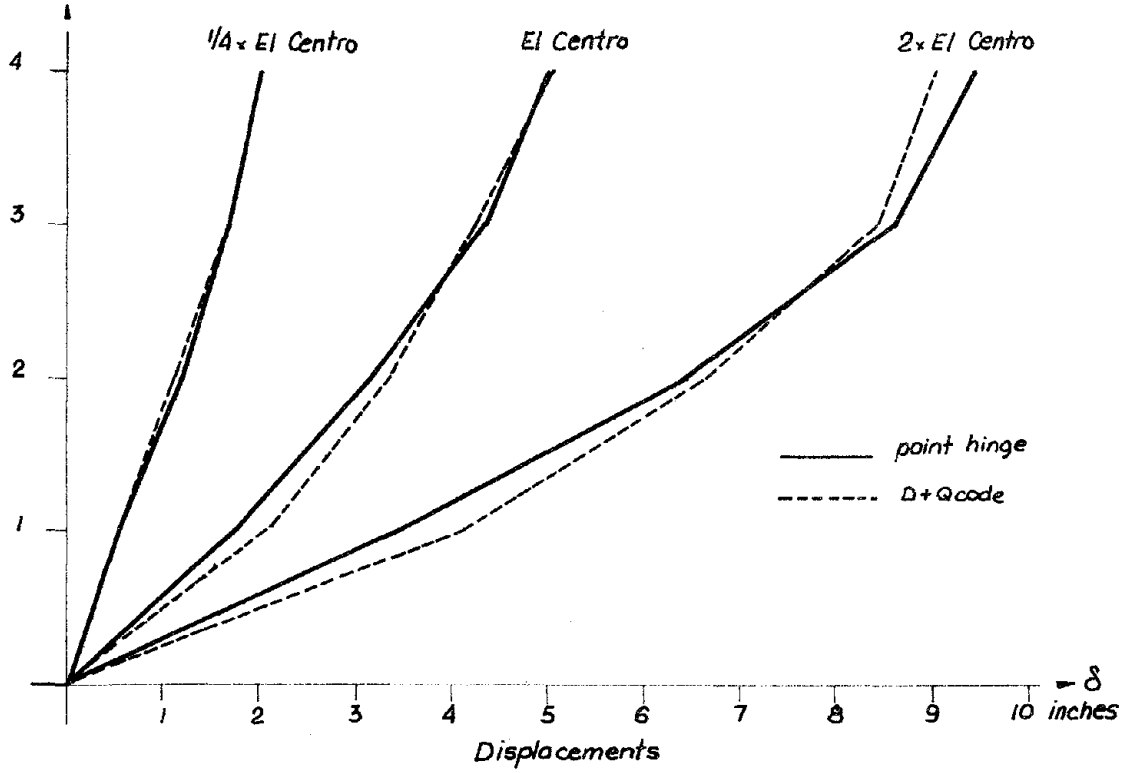

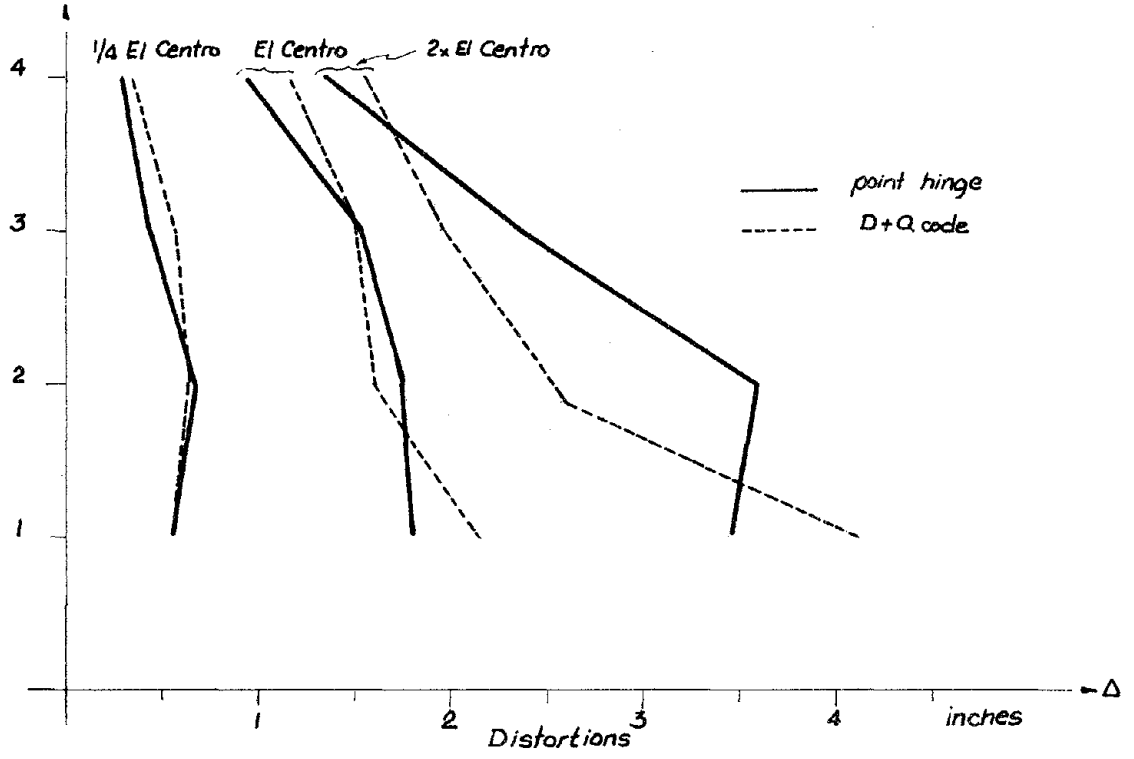

FIGURE 3.15 - 4-STORY UBC FRAME: POINT HINGE VS. MULTILINEAR FOR DIFFERENT PEAK ACCELERATIONS. $D+Q_{code}$. INTERACTION

3.3.3 Ten-Story Frames

Ten-Story UBC Frame

Figure 3.16 shows the envelopes of maximum floor displacement and maximum distortion predicted by the point-hinge and the multilinear shear beam model under elastic behavior. The peak acceleration used was one quarter of El Centro. Shear springs were obtained using the UBC code lateral force distribution.

The shape of the floor displacements envelope departs from the shear beam curve, having an inflection point at about the third floor and another one at the seventh floor. It is interesting to note that the analysis using the improved shear springs is capable of modeling a behavior of this type while previously the envelopes obtained with this model resulted in a curve following the first mode shape of a shear beam.

A maximum floor displacement of five inches is obtained at the top floor and the distortions are almost constant along height, oscillating around 0.6 inches. The agreement in both cases is excellent. Figure 3.17 shows the comparisons between the point-hinge response and the shear-beam response using springs resulting from the UBC code distribution, a uniform distribution and the ATC-3 distribution; all for El Centro. Figure 3.18 shows similar results using the first mode and SRSS of all modes distributions, as well as curves obtained using trilinear springs as defined by Anagnostopoulos [2] (Equations (1-1, 1-2)) (plotted for reference.)

Consistently all of the improved springs give smaller floor displacements than the point-hinge model; the shape of the curves is, however, proportional along height. For distortions, the shear springs predict smaller

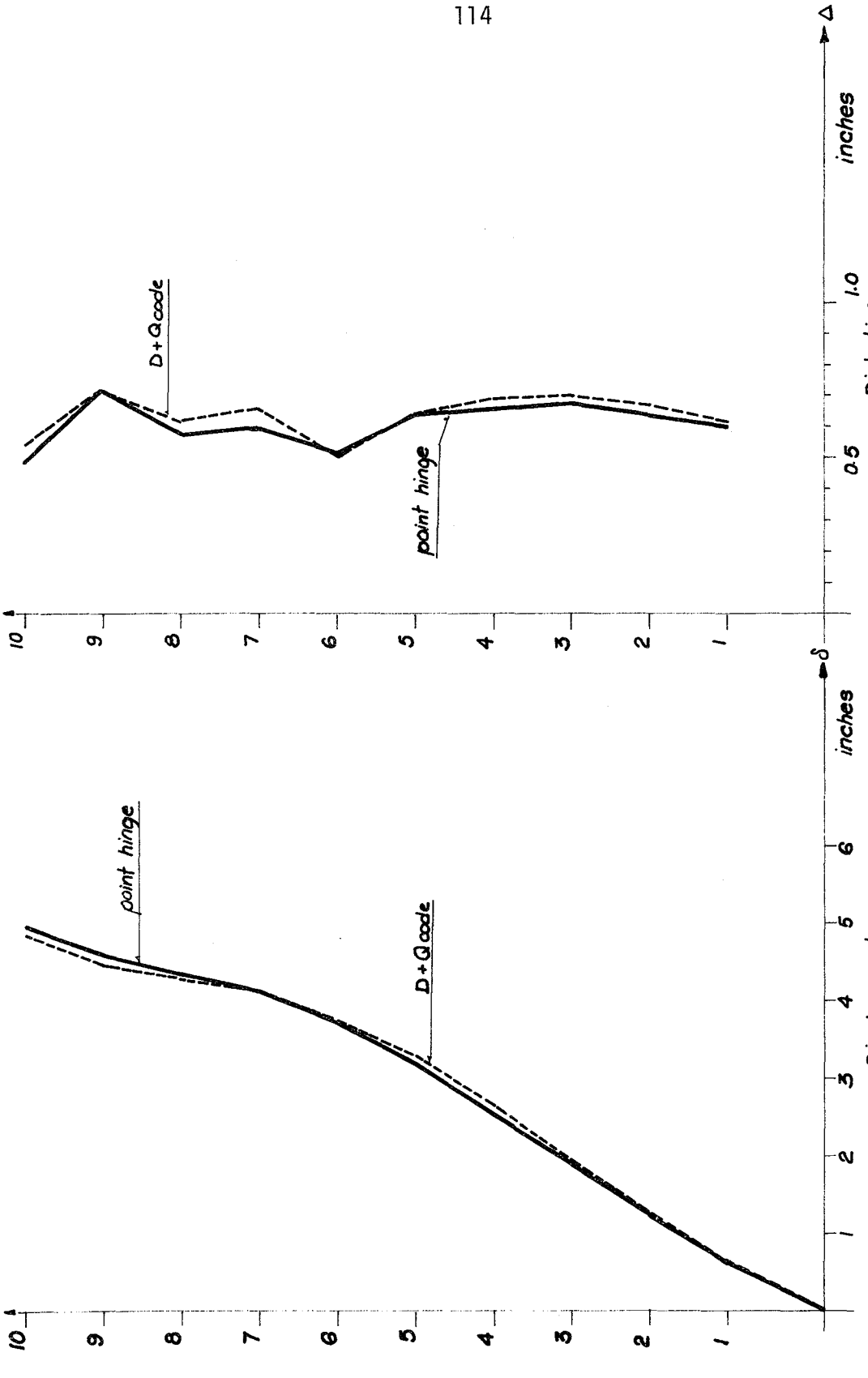

FIGURE 3.16 - 10-STORY UBC FRAME: POINT HINGE VS. MULTILINEAR. $D+Q_{code}$. ELASTIC. 1/4 EL CENTRO. INTERACTION. NO P-Δ

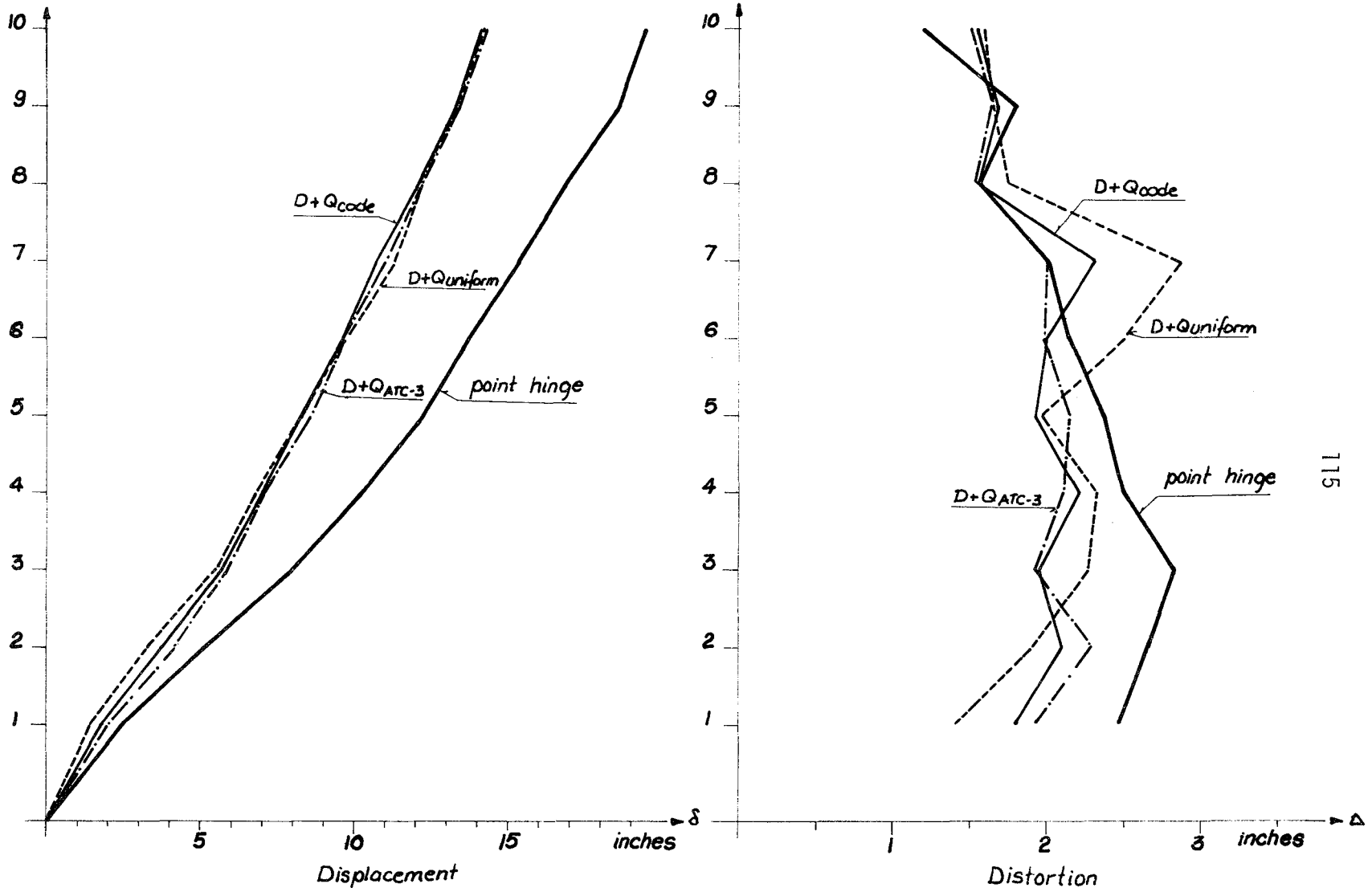

FIGURE 3.17 - 10-STORY UBC FRAME: POINT HINGE VS. MULTILINEAR. $D+Q_{code}$. $D+Q_{uniform}$. $D+Q_{ATC-3}$. EL CENTRO. P-Δ

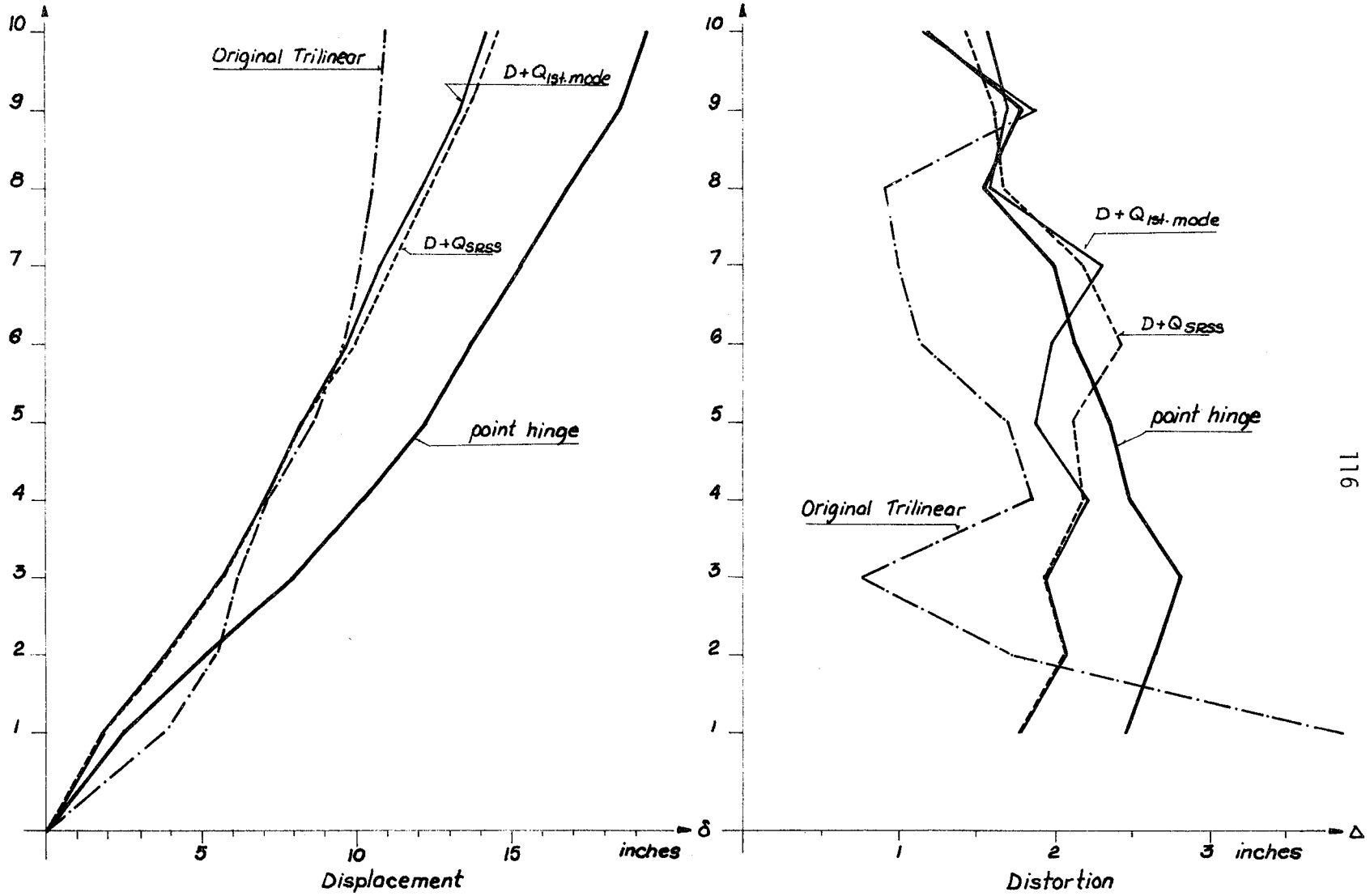

FIGURE 3.18 - 10-STORY UBC FRAME: POINT HINGE VS. MULTILINEAR. $D+Q_{1st.\ mode}$. $D+Q_{SRSS}$. INTERACTION. EL CENTRO. P-Δ

values on the lower half of the structure and then follow rather closely the point-hinge model on the upper half. As expected, the shape of the displacement envelope using Anagnostopoulos' trilinear is very similar to that of a shear beam, and in this particular case it underestimates the capacity of the lower stories and overestimates it at the upper stories. Distortions predicted by this model do not follow a pattern consistently and show large discrepancies with the other springs.

The maximum displacement predicted by FRIEDA was 19 inches at the top, a rather large value for a structure of this height. However, there was not large inelastic action on the members, suggesting that the structure itself was quite flexible. The shear springs predicted a maximum of 14.2 inches, which is smaller by 27 percent. The same difference was maintained along the height of the building with only small variations. Clearly the first-story distortion was underestimated by the shear springs for this level of inelastic action.

On the average the point-hinge model predicts distortions of the order of two inches. The shear springs also predict an average distortion of two inches. The agreement is acceptable if an average criterion were to be used. However, there are significant discrepancies that reach up to 28 percent in some cases. (The envelopes for uniform distribution are not being considered in these comparisons, because they seem to produce a response consistently worse than the other distributions.)

A different type of mechanism was formed in this case as compared to the four-story frame. Most inelastic action was developed by the girders and only the bottom story, seventh and ninth floor columns went

inelastic. Figure 3.19 illustrates the formation of hinges in the members corresponding to maximum ductilities.

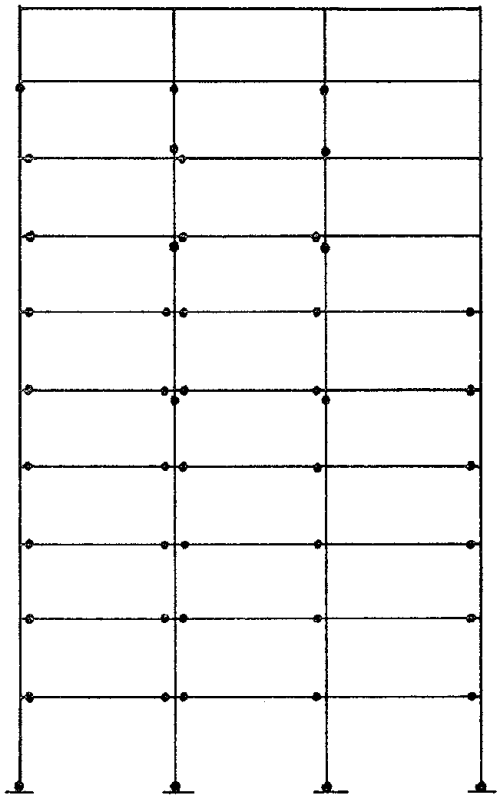

FIGURE 3.19 - HINGE MEMBER DISTRIBUTION

Figure 3.20 illustrates the responses without P-Δ effect. The shear springs used were those obtained for the UBC code distribution; both analyses performed under El Centro. For the point-hinge model, the top displacement diminishes by half an inch, while it increases slightly

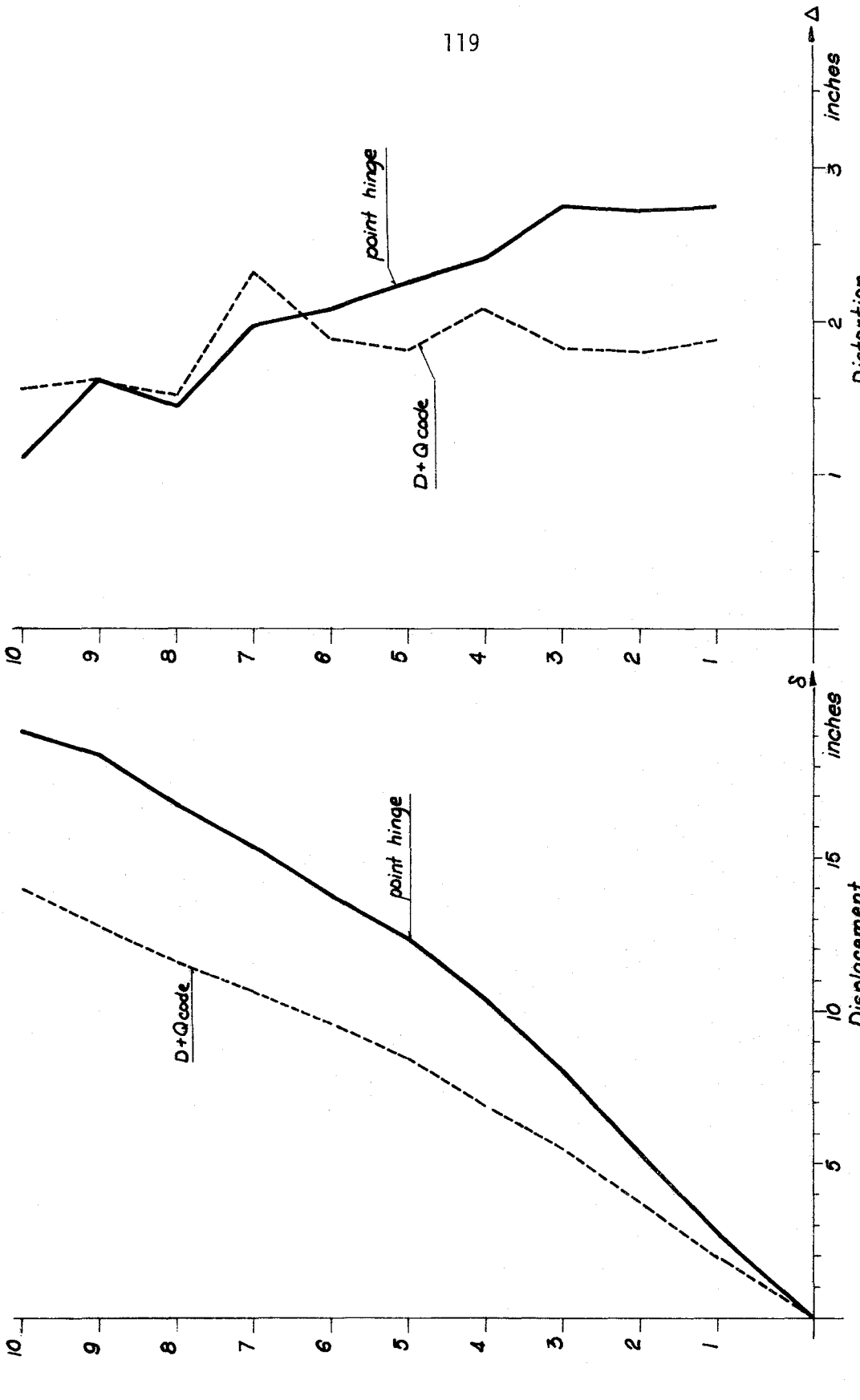

FIGURE 3.20 - 10-STORY UBC FRAME: POINT HINGE VS. MULTILINEAR. D+Q code. NO P-Δ . EL CENTRO

on the first five floors, and particularly in the first floor (13%). From the sixth to the eighth floor there is no change. Distortions are slightly smaller (6%) in all floors except the first, where it increases by 13%. For the multilinear spring, displacement in the first floor increases and then remains unchanged until the seventh floor, where it is smaller thereafter. Distortions are smaller from the second to the seventh floor and then remain unchanged. The first-floor distortion is only slightly larger. Overall for this frame, changes due to the P-Δ effect are minimum. The agreement between both models is the same as reported for the case where P-Δ was included.

A more significant change is observed when the same two cases are analyzed using the bending model for yield criterion and no initial gravity loads. Figure 3.21 illustrates these results. A much better agreement is observed for floor displacements, since all values for the point-hinge model decrease, and all values for the shear-beam model increase. In the case of distortions the point-hinge model predicts smaller values in all floors, the largest difference being in the first (30%) and second floor. Distortions predicted by the shear-beam show the same basic pattern as for the case with interaction, but the changes are not consistent along height. The agreement between the two is no different than before; that is, good on the average, with maximum discrepancies of 27%.

On Figure 3.22 results are presented for both analyses, using 1.87 Taft. The comparisons were made using the springs from UBC code distribution, the interaction yield criterion, and without P-Δ effect.

The top displacement is 9.7 inches, which is quite small for a

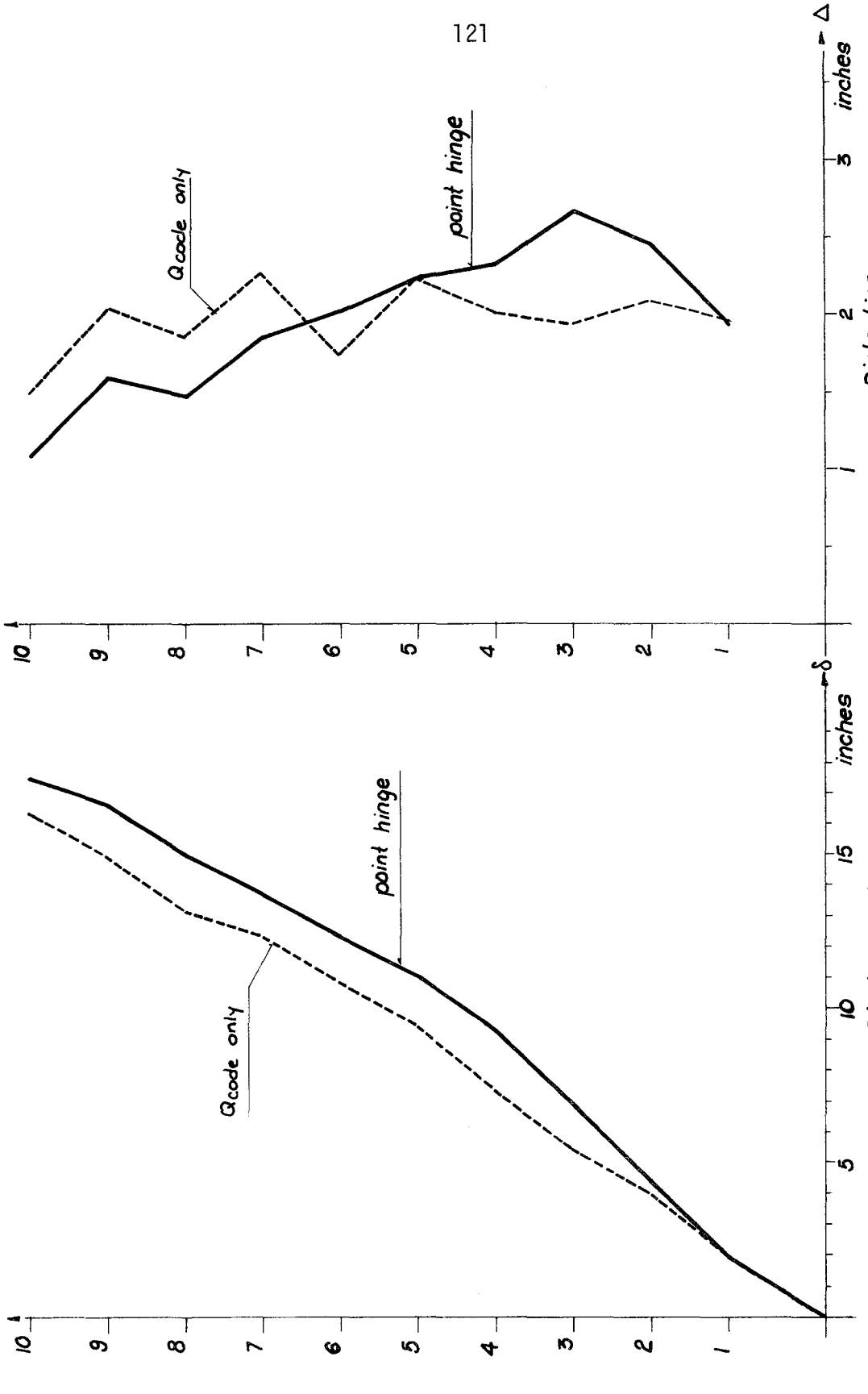

FIGURE 3.21 - 10-STORY UBC FRAME: POINT HINGE VS. MULTILINEAR. Q_{code} ONLY. BENDING MODEL. NO GRAVITY LOADS. EL CENTRO

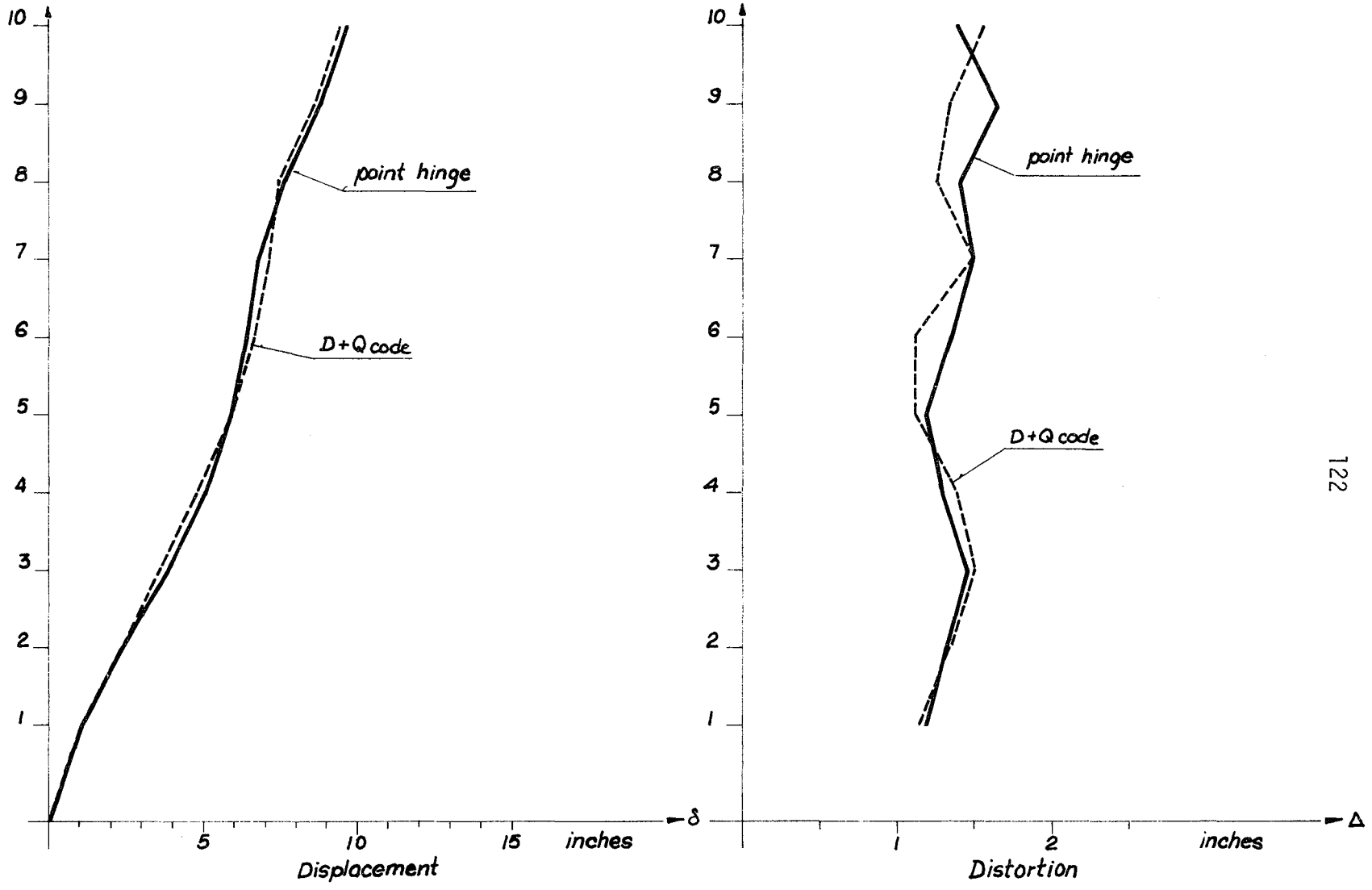

FIGURE 3.22 - 10-STORY UBC FRAME: POINT HINGE VS. MULTILINEAR. $D+Q_{code}$. INTERACTION. 1.87xTAFT. NO P-Δ

motion with the same Arias' intensity of El Centro, if compared with the 19 inches resulting for the latter. In the present case the agreement between the two models is very good, both for displacements and distortions. The shape and magnitude of displacements are properly reproduced by the shear-beam model. It must be noted that there is less inelastic action developed in the frame under Taft, and most of it occurs in the girders. An important consideration arises from this comparison. For two motions with the same intensity the responses differ by 70%, suggesting that uncertainties in the ground excitation are a larger source of variations than the difference in response due to the model used in the analysis.

On Figures 3.23 and 3.24 comparisons are presented for three levels of peak acceleration using El Centro. In the elastic case the agreement is very good for both displacements and distortions. For El Centro standard acceleration, the floor displacements predicted by the shear-beam model are smaller by 26% all along height. The distortions are smaller up to the sixth floor by a maximum of 30% and slightly larger thereafter. For twice El Centro the agreement is better. In this case the shear-beam model predicts larger displacements for all floors, and also larger distortions except for floor nine. The differences reach a maximum of 15 percent, but are usually much smaller. It is interesting to note that the top displacement predicted by the shear-beam model goes from 14 to 23.4 inches for once and twice El Centro, but the one predicted by the point-hinge model goes from 19 to 22.6 only, a much smaller increase.

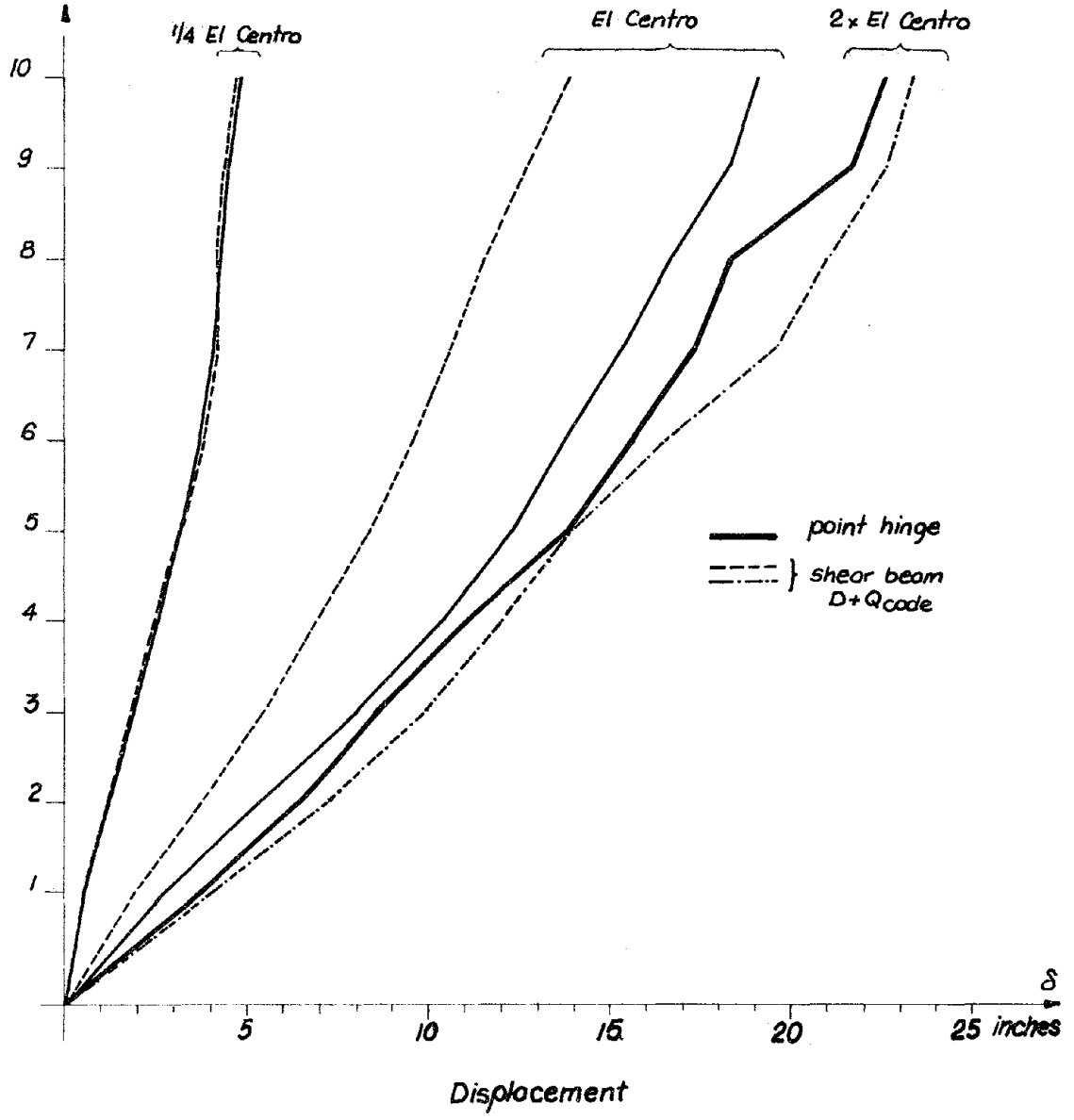

FIGURE 3.23 - 10-STORY UBC FRAME, MAX. DISPLACEMENTS. POINT HINGE VS. MULTILINEAR. INTERACTION. $D+Q_{code}$. FOR DIFFERENT PEAK ACCELERATIONS. EL CENTRO. NO P-Δ

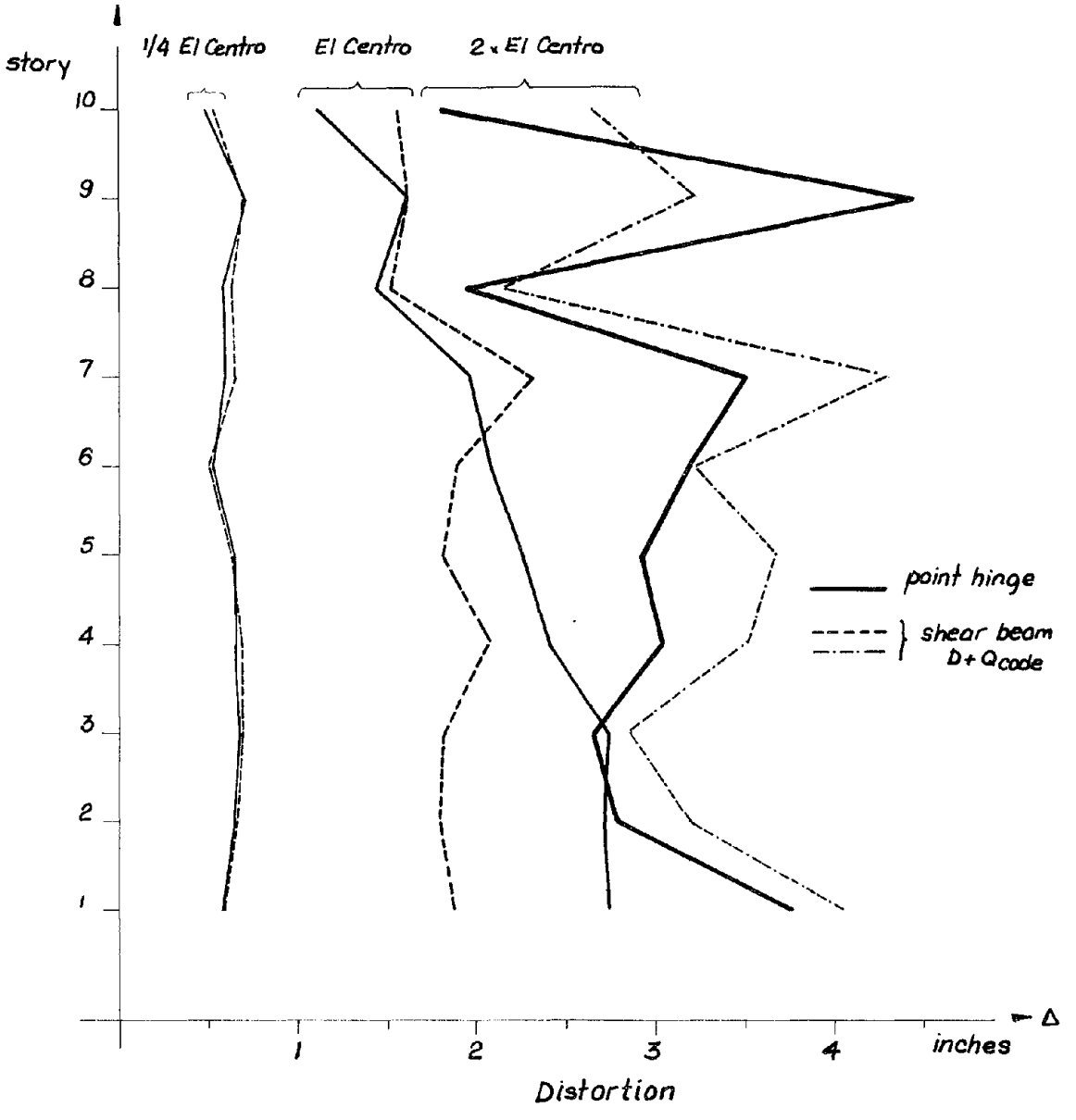

FIGURE 3.24 - 10-STORY UBC FRAME, MAX. DISTORTIONS. POINT HINGE VS. MULTILINEAR. INTERACTION. $D+Q_{code}$. FOR DIFFERENT PEAK ACCELERATIONS. EL CENTRO. NO P-Δ

Anderson Frame

On Figure 3.25 the results for Anderson's frame are compared. This case includes P-Δ effects and was analyzed under El Centro. The multilinear springs used were those obtained from the UBC code lateral force distribution. The shape of both curves is similar all along the height of the building. However, the shear-beam model predicts consistently lower values for displacements and for distortions up to the ninth floor, where they become larger. The discrepancies for displacements are between 25 and 30 percent, and for distortions from 10 to 27%, except for the first floor (38%). This behavior appears to be similar to that reported for the 10-story UBC frame for similar conditions (P-Δ, interaction, El Centro). However, on Figure 3.26 a substantial change in the response is observed in the case where no P-Δ effects are included. The top displacement predicted by the shear-beam model, for example, decreases from 16.4 to 13.8 inches (16%), and in some other floors (fifth floor, for instance) up to 18 percent. This indicates an important role played by the P-Δ effect for this building. The top displacement predicted by the shear-beam model decreases from 12.6 to 11.8 inches--seven percent, and even less for the other floors. The effect of P-Δ does not seem to be reflected in the same way by the shear-beam model (the way it is implemented) and the point-hinge model. For this case, then, the agreement between the two models is much better, and the maximum discrepancies are less than eighteen percent. The shape of both curves is similar at all floors, even though this building has only one bay, making it prone to behave as a bending beam.

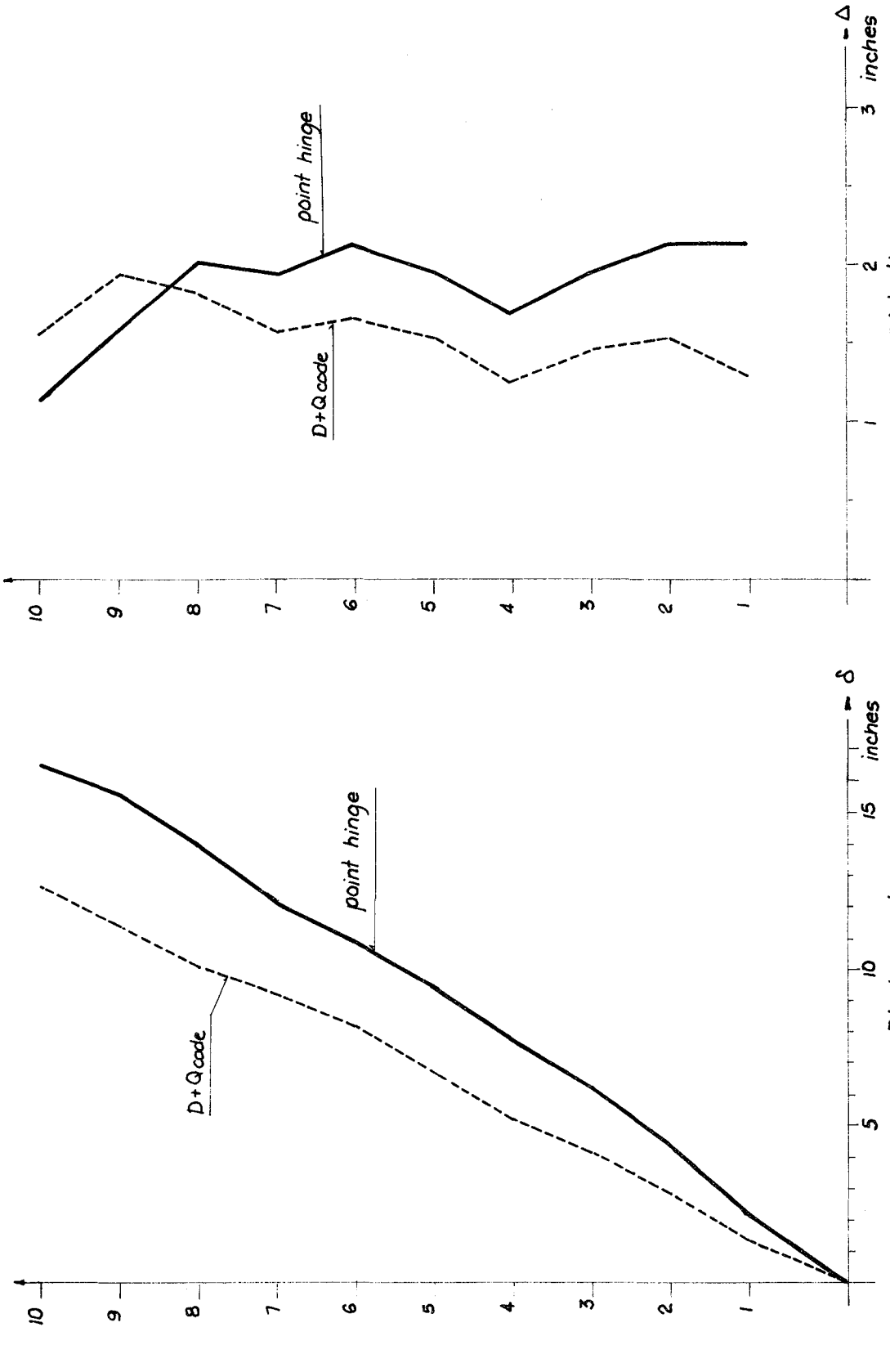

FIGURE 3.25 - ANDERSON FRAME: POINT HINGE VS. MULTILINEAR. $D+Q_{code}$. INTERACTION. EL CENTRO. P- Δ

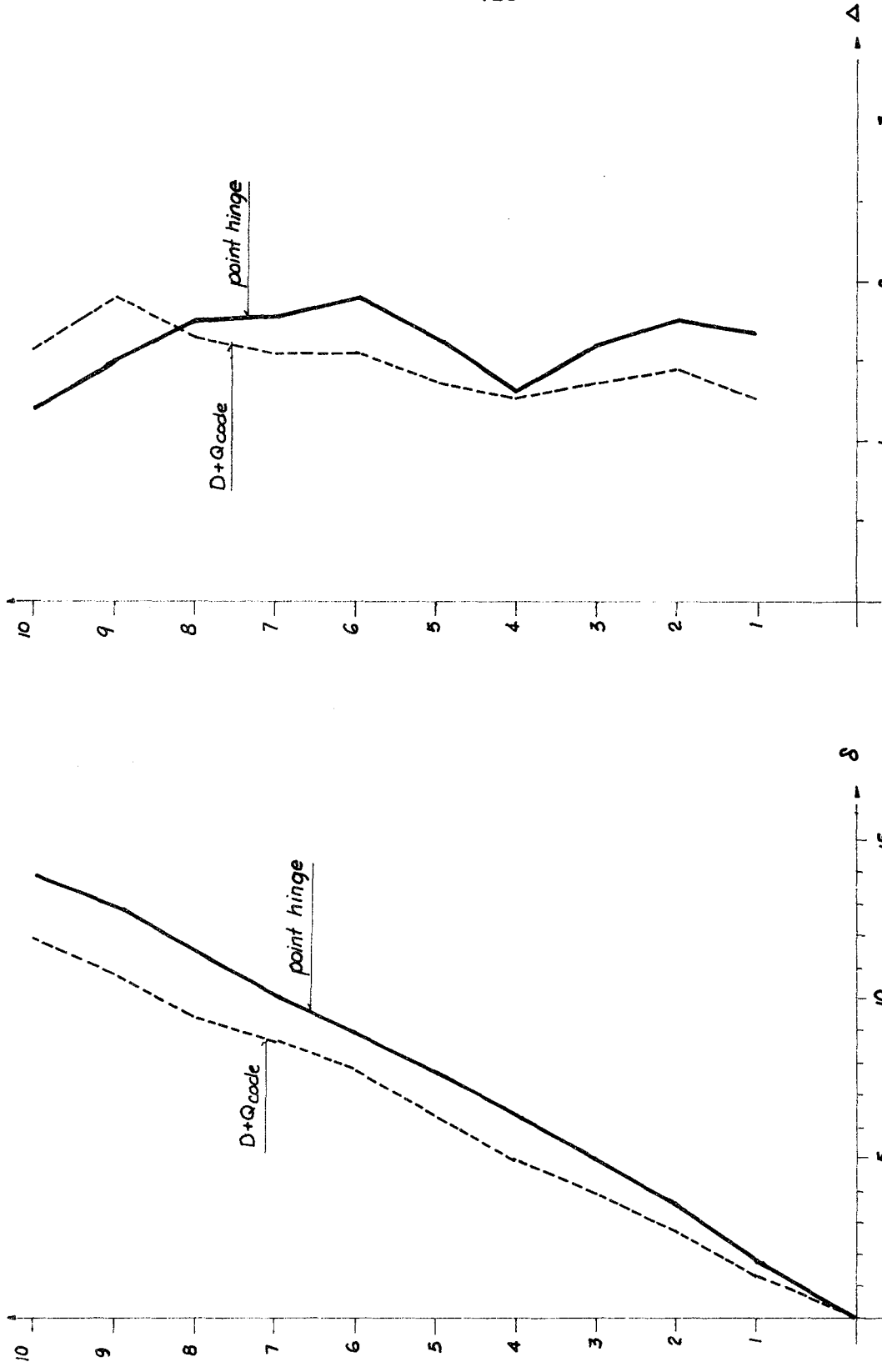

FIGURE 3.26 - ANDERSON FRAME: POINT HINGE VS. MULTILINEAR. $D+Q_{code}$. INTERACTION. EL CENTRO NO P-Δ

The agreement on distortions is also improved, having a maximum difference of 24% in the first floor, but less than 18% in the rest. Figure 3.27 illustrates the formation of hinges on the frame for the maximum displacements.

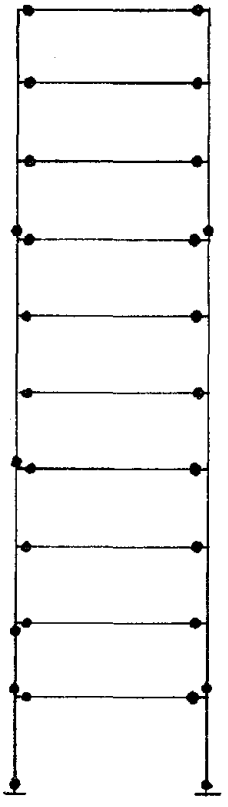

FIGURE 3.27 - ANDERSON FRAME. HINGE FORMATION

On Figure 3.28 results for the two models are presented using the bending yield criterion, without P-Δ effects and initial gravity loads. The agreement for displacements is excellent up to the fifth floor, and on the upper stories a maximum difference of 8% is registered. Overall the shear-beam model matches shape and values very well. On the average the agreement on distortions is also good, although there are some local

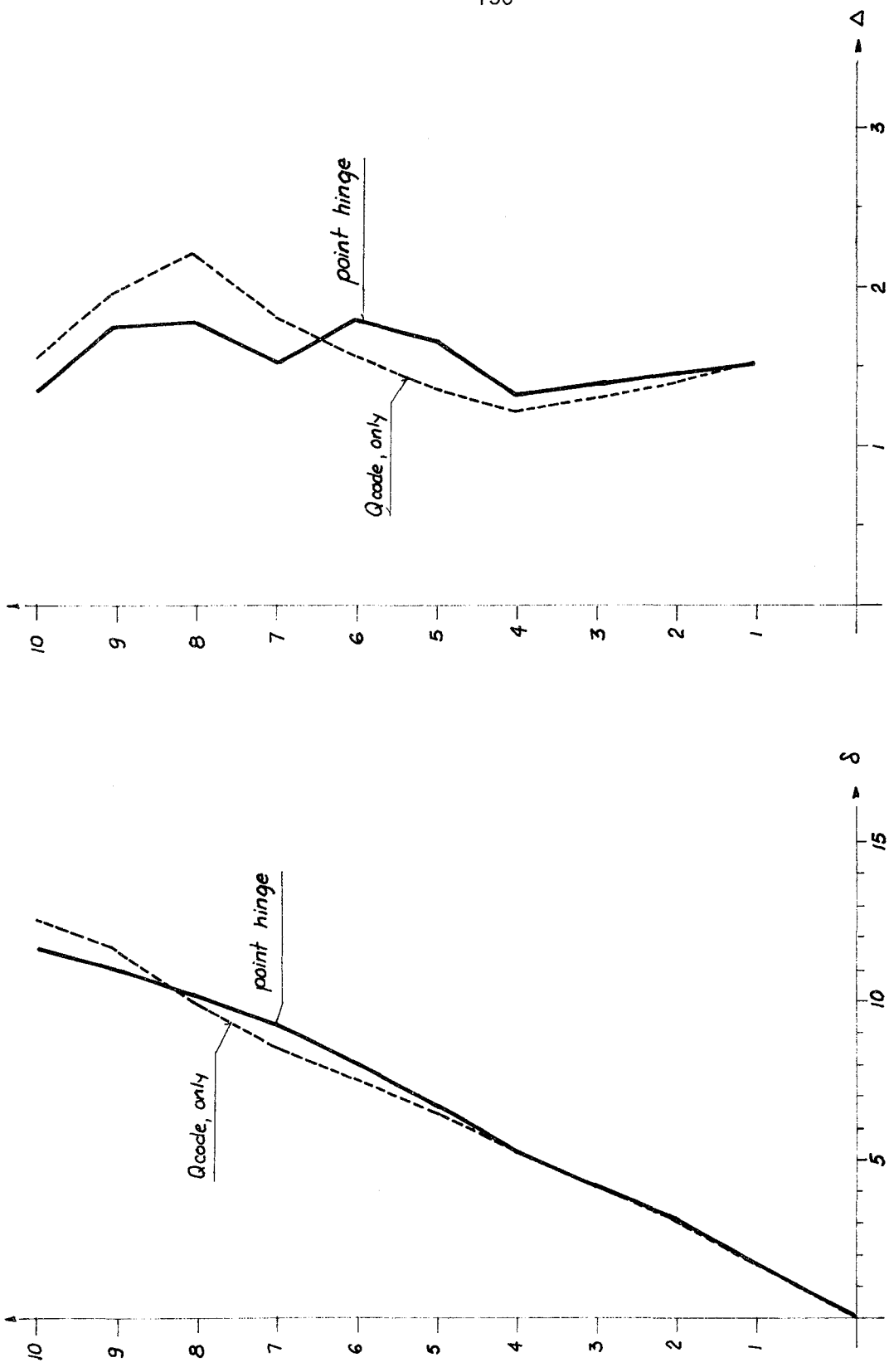

FIGURE 3.28 - ANDERSON FRAME: POINT HINGE VS. MULTILINEAR. Q_{code}. BENDING. EL CENTRO. NO P-Δ

discrepancies of up to 22%. The shape of this envelope as given by the shear springs is not properly reproduced on the region of stories four to seven.

Kamil Frame

Figure 3.29 shows the envelopes of maximum displacements and distortions for Kamil's frame obtained using El Centro, the interaction yield criterion, and including P-Δ effect. The curves for displacements match very well in the upper five stories, but the shear-beam model predicts smaller displacements in the lower stories. Differences are not, however, very large in absolute terms. The shape of the curves is essentially similar in both cases, departing from the classical shear-beam shape. This is an asymmetrical frame, and in order to discard any discrepancies on the shear springs due to the direction of lateral loading, both cases were analyzed. No significant differences were encountered either in floor stiffness or in strength due to loading direction.

The distortion envelopes follow approximately the same curved shape with larger discrepancies at both ends, first and top floors. On these stories the shear-beam model predicts smaller values (50% less).

Figure 3.30 shows results for the same building, but without P-Δ effects considered. An even more accentuated tendency as reported for the Anderson frame is found here. The response predicted by the shear-beam model almost does not change the displacements envelope, and only the upper four stories distortions increase. But displacements predicted by the point-hinge model decrease in all floors an average of 15%. However, distortions decrease up to the seventh floor, and then

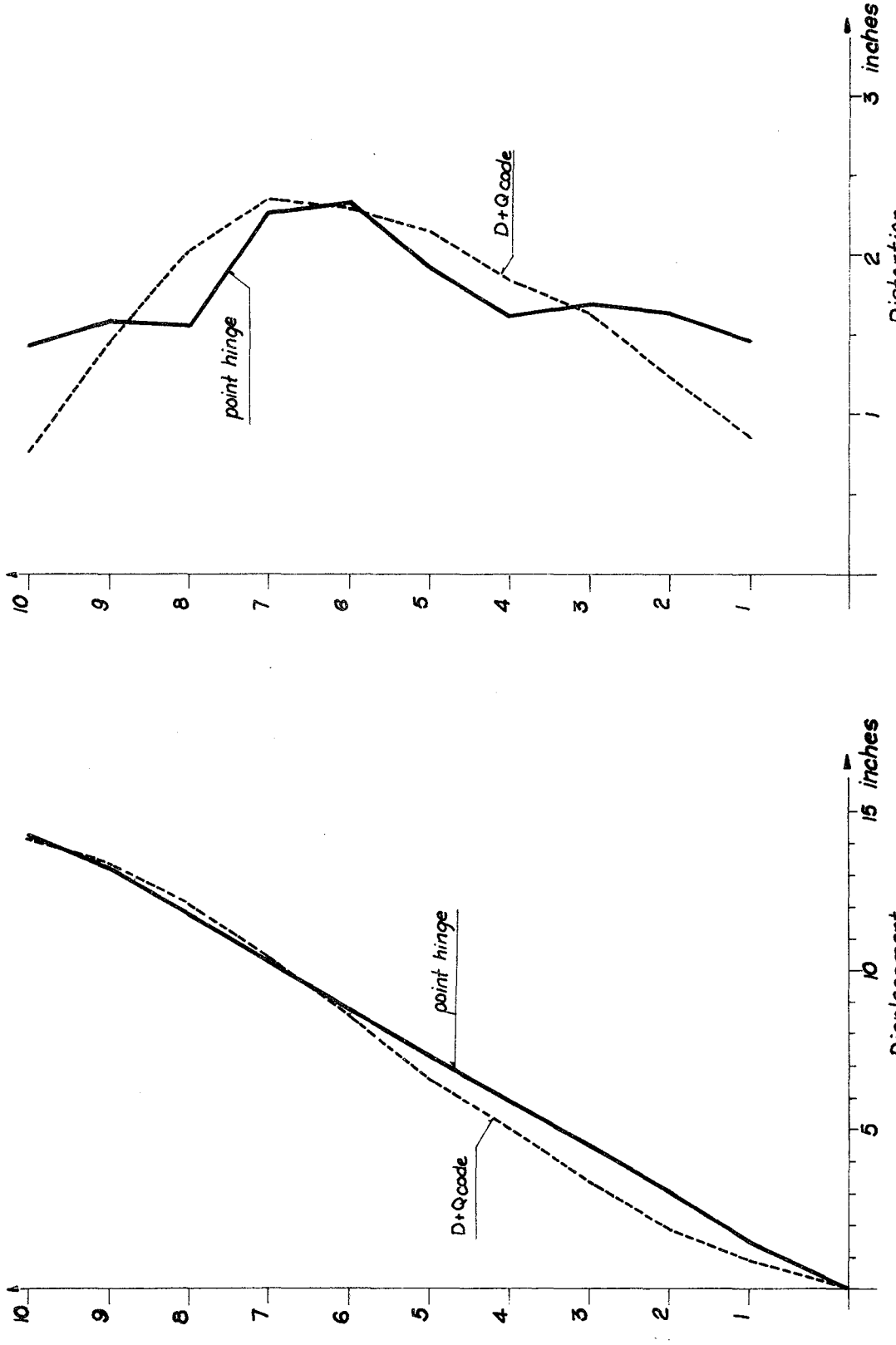

FIGURE 3.29 - KAMIL'S FRAME: POINT HINGE VS. MULTILINEAR. $D+Q_{code}$. INTERACTION. P-Δ. EL CENTRO

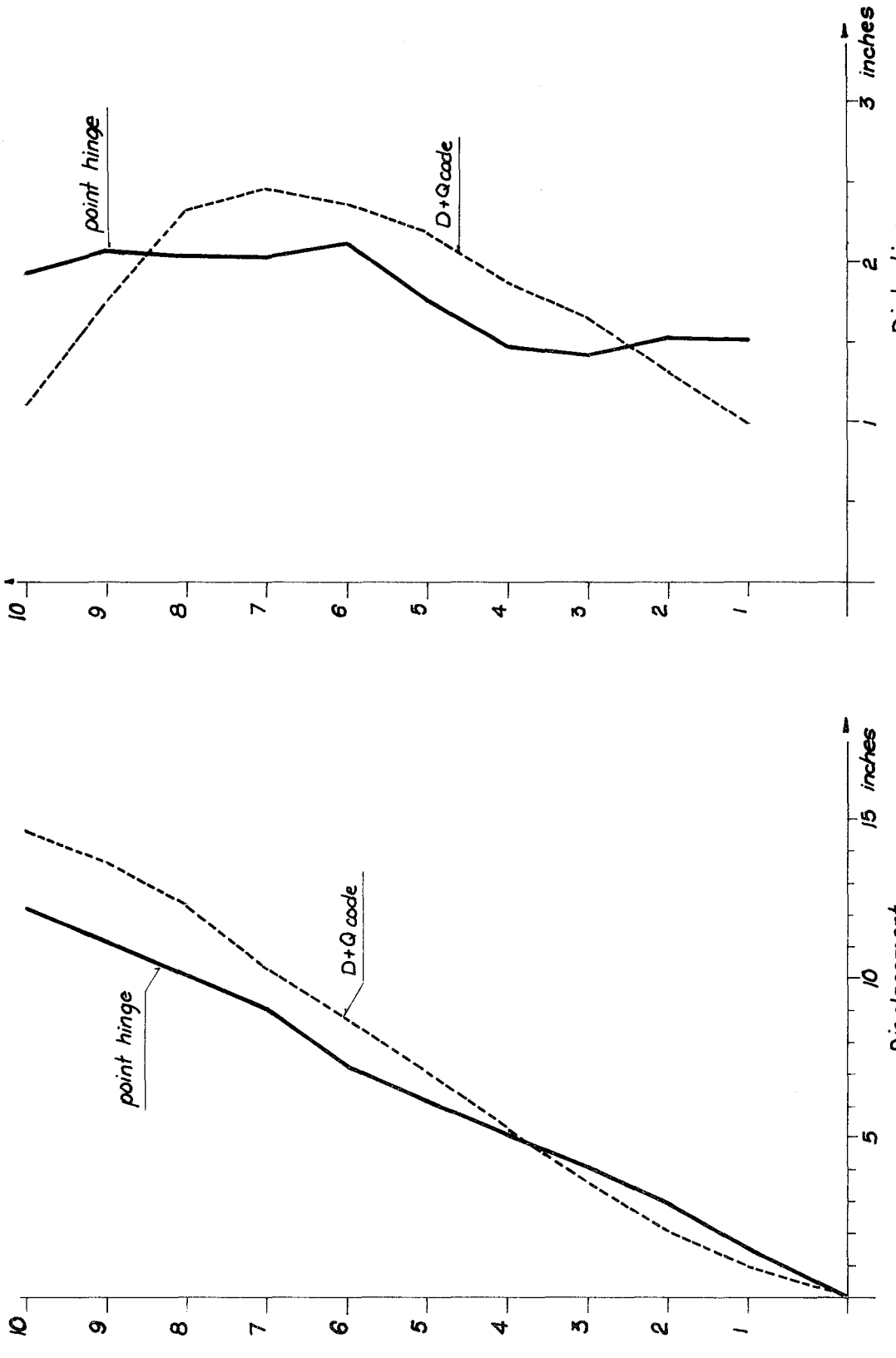

FIGURE 3.30 - KAMIL'S FRAME: POINT HINGE VS. MULTILINEAR. $D+Q_{code}$. INTERACTION. NO P-Δ. EL CENTRO

increase by about 30%. This results in a change in terms of agreements. The displacement envelope matches better in the lower stories than in the upper stories this time. The largest differences appear on the eighth to tenth floors, being of the order of 20%. The distortion envelopes show similar shapes from the third to eighth floors, the shear-beam model predicting larger values; but this tendency changes abruptly on the first two and the top two floors.

Figure 3.31 presents the results obtained using the bending yield criterion, without the P-Δ effect and gravity loads. Displacements are matched very well up to the sixth floor; then the shear-beam model predicts smaller displacements (by 10%) for the next two floors and larger displacement on the top (9%). The agreement overall, though, is good. This peculiar change of sign in predictions can be explained if a closer look is given to the distortion envelopes. Clearly the value for the top floor distortion is much larger in this case, forcing the total displacement to become also larger and forcing the envelop to "whip" towards the right when otherwise it would have stayed under the point-hinge envelope. Agreement in this case is not reasonable for distortions.

3.3.4 Sixteen-Story UBC Frame

Figure 3.32 shows the comparisons for the elastic case of the sixteen-story frame. The agreement for displacements is very good, the largest difference being in the top floor, but within ten percent of the point-hinge model. If compared with the other buildings, however, (four- and ten-story UBC) discrepancies are slightly larger in this case.

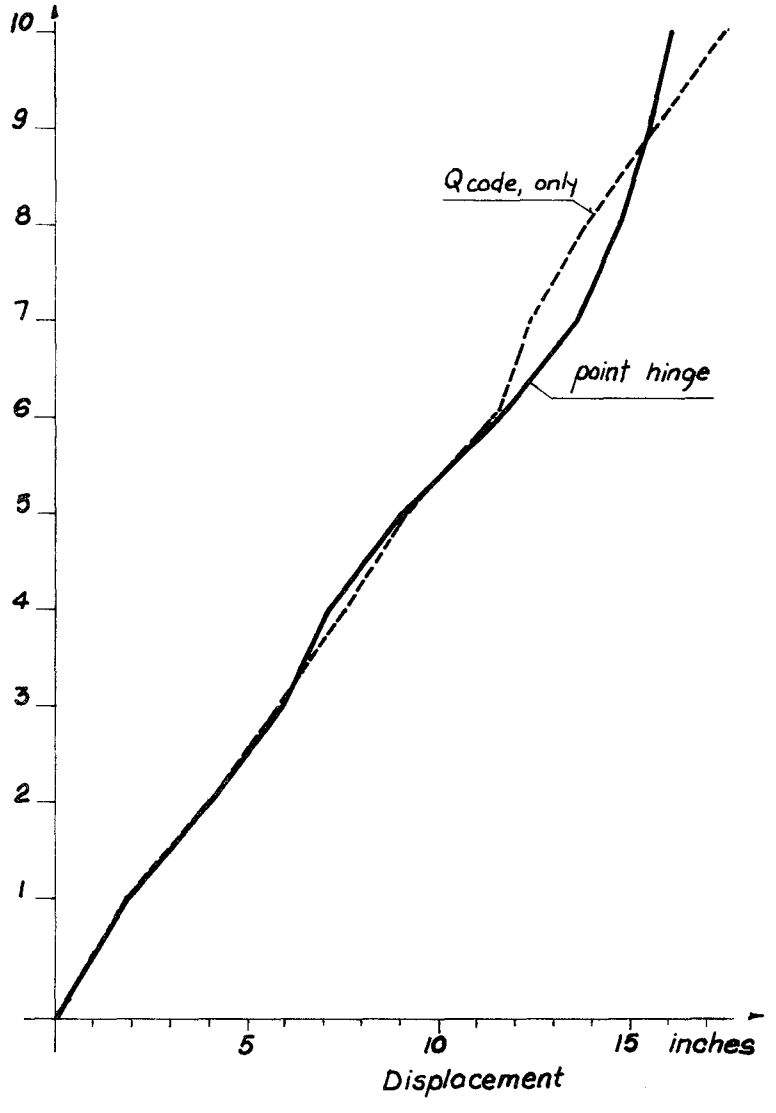

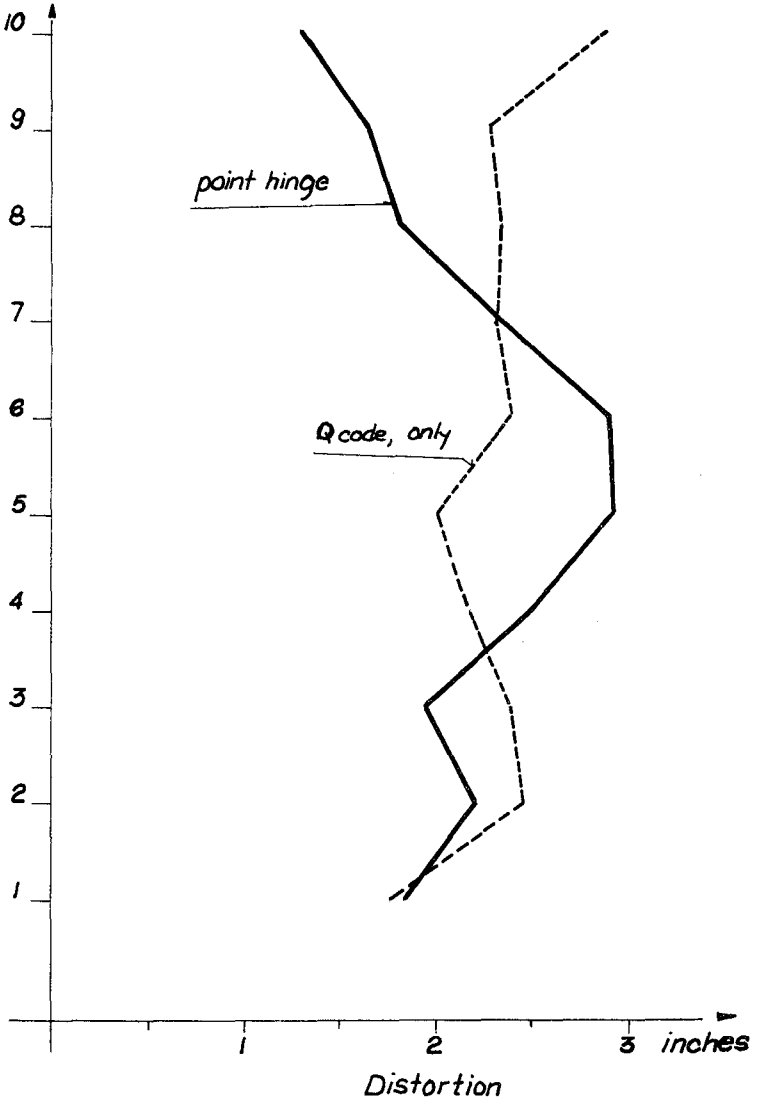

FIGURE 3.31 - KAMIL'S FRAME: POINT HINGE VS. MULTILINEAR. Q_{code} ONLY. BENDING MODEL. EL CENTRO.NO P-Δ

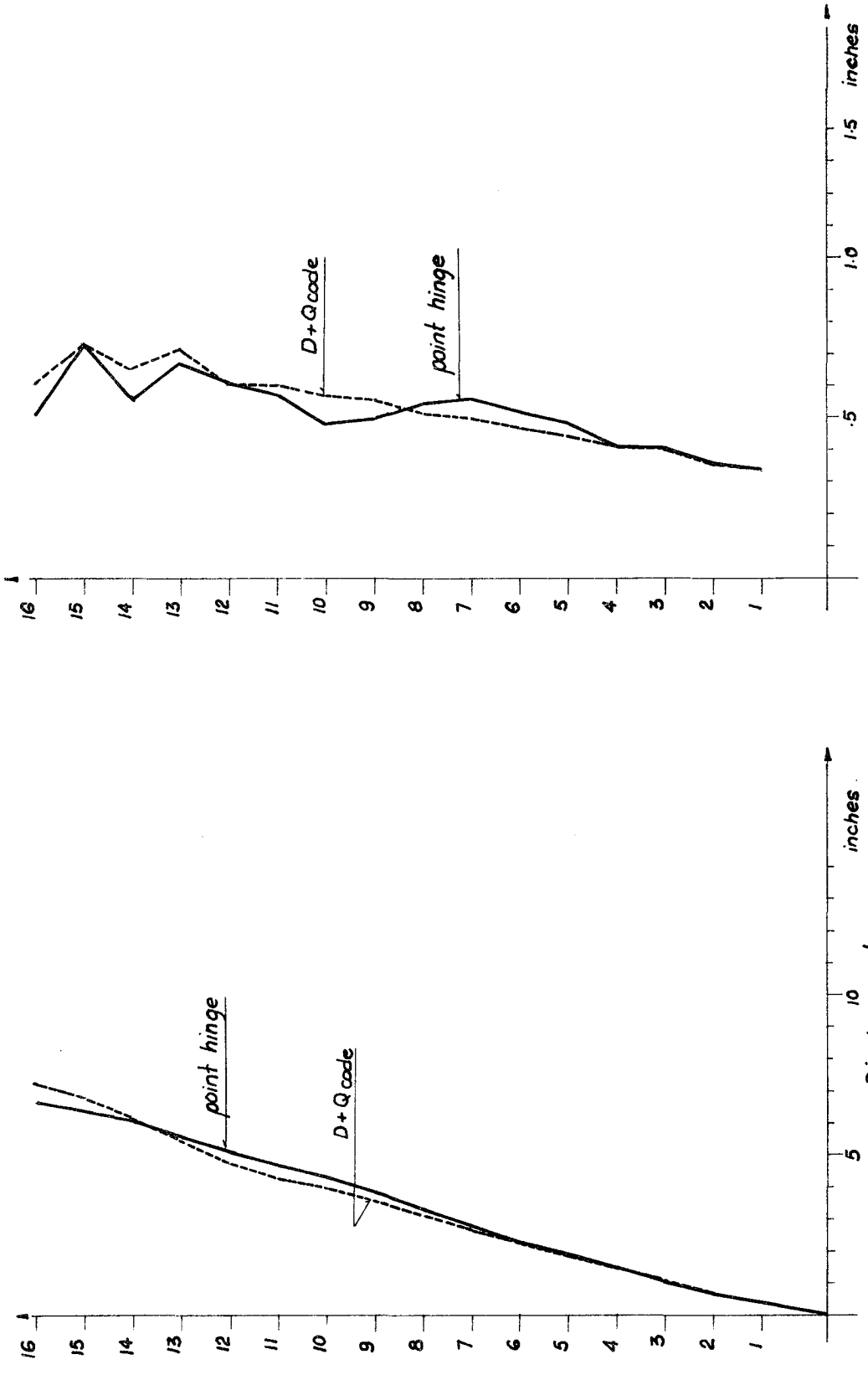

FIGURE 3.32 - 16-STORY UBC FRAME: POINT HINGE VS. MULTILINEAR. $D+Q_{code}$. ELASTIC. 1/4 EL CENTRO. P-Δ INTERACTION

The curves for distortions show a disagreement between floors four and twelve, although the magnitude of distortions considered is rather small (1/2 inch).

Figures 3.33 show the results for the point-hinge model and the shear-beam model using springs from the uniform and ATC-3 distributions. On Figure 3.34 the results obtained with springs from the UBC code and SRSS of all modes distributions are presented, all cases with the interaction yield criterion and including P-Δ effect. For the displacement envelopes the results show very good agreement in all floors. Differences are never larger than 11%. The shape of the curves is fully reproduced with the inflection points characteristic of the "bending behavior." The maximum displacement at the top is 19 inches. Distortions are also reproduced well for most distributions, the only exception being again the uniform distribution which shows rather large discrepancies when compared with other distributions and the point-hinge model. The shape of the curves is reasonably similar for a taller building like this; however, a "phase shift" can be observed between floors five and nine, where the shear-beam results move upwards, although with the same shape. On floor thirteen there is also a larger discrepancy for the UBC code and the uniform distribution, but overall agreement between the two models seems to be acceptable. Figure 3.35 illustrates the formation of hinges on this frame, corresponding to maximum displacements. The case where neither P-Δ effects nor gravity loads were included was also analyzed for this building, and the results are presented on Figure 3.36. There is very little change as compared to the case where these effects

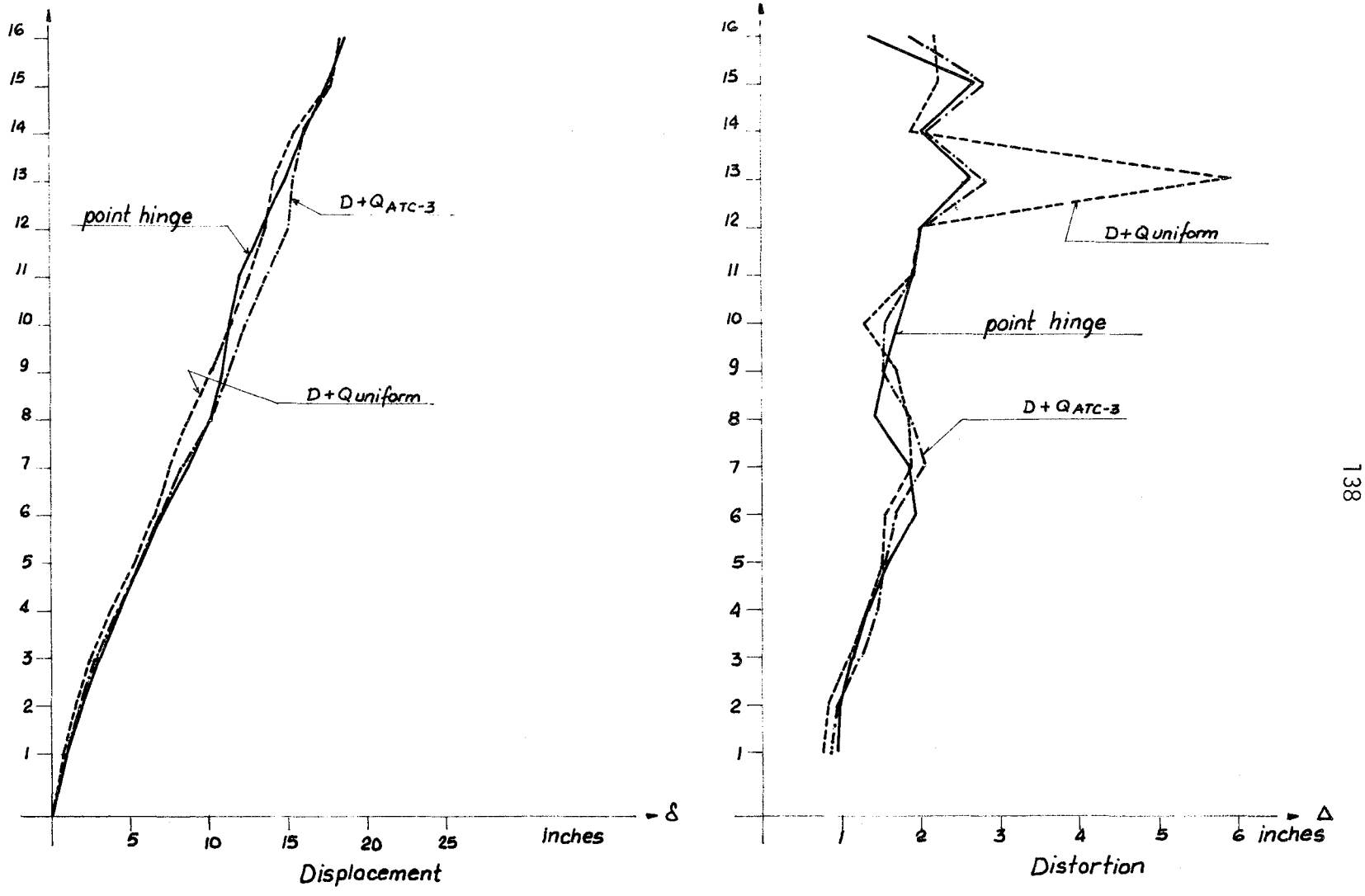

FIGURE 3.33 - 16-STORY UBC FRAME: POINT HINGE VS. MULTILINEAR. $D+Q_{uniform}$, $D+Q_{ATC-3}$. INTERACTION EL CENTRO. P-Δ

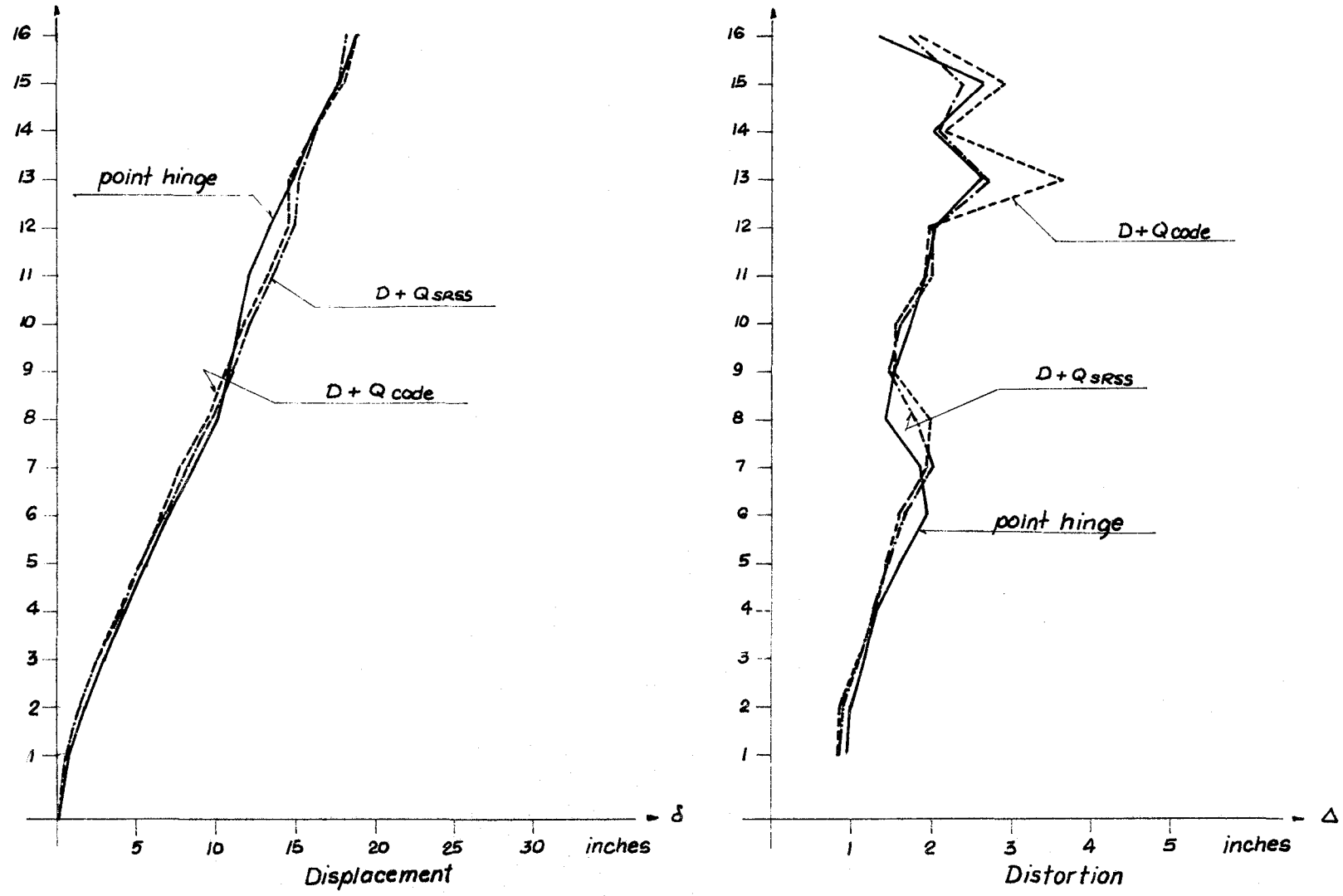

FIGURE 3.34 - 16-STORY UBC FRAME: POINT HINGE VS. MULTILINEAR. $D+Q_{code}$. $D+Q_{SRSS}$. INTERACTION. EL CENTRO. $P-\Delta$

are included. The point-hinge envelope for displacements diminishes slightly (less than 10%) and the shear-beam envelope changes only on the top story. The distortion in the sixteenth floor also changes for the shear beam from 1.9 to 2.9 inches, but remains almost unchanged for the rest of the floors. The overall agreement is quite good.

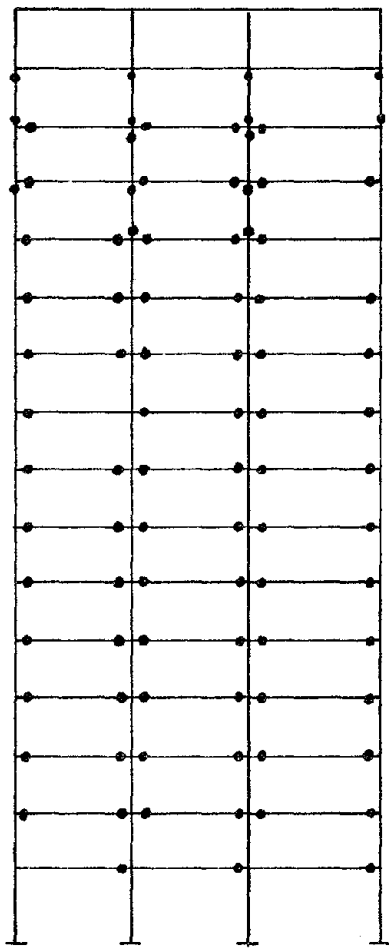

FIGURE 3.35 - HINGE FORMATION ON 16-STORY UBC FRAME

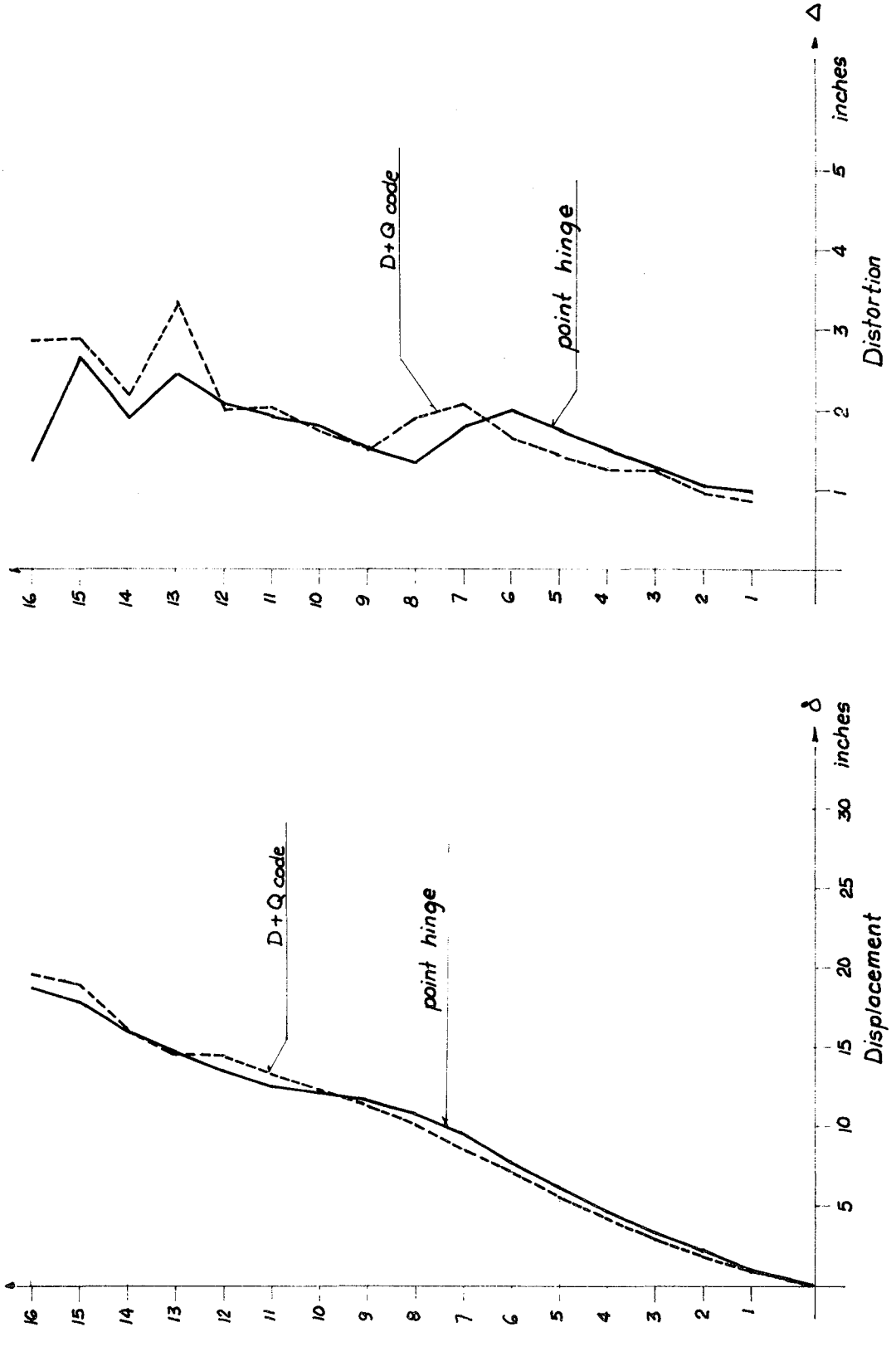

FIGURE 3.36 - 16-STORY UBC FRAME: POINT HINGE VS. MULTILINEAR $D+Q_{code}$. INTERACTION. EL CENTRO. NO P-Δ

Figure 3.37 shows the results obtained using the bending yield criterior, without gravity loads or P-Δ effects. The shape of the displacements envelope by the point-hinge model remains unchanged as compared to the case above, but the magnitude of the displacements is larger in all floors. The top displacement reaches 20.5 inches, and in most floors an increase of 14% over the case with interaction is maintained. The agreement with the shear-beam envelope is, however, good; and the shape of the curve is similar. Only on the top two stories does this model predict larger displacements, reaching 22.8 inches. In terms of distortions the shear-beam model overestimates them from the sixth floor up and underestimates them in the others. The shape of the curve is reproduced reasonably up to the tenth story.

Figure 3.38 shows the results obtained for 1.87 Taft without P-Δ effect, but using interaction and gravity loads. The maximum displacement predicted by the point-hinge model is 12.5 inches, smaller than for El Centro (18.6 inches). The shear-beam model predicts 15.3 inches; that is, 22% more. From the thirteenth to sixteenth floors this tendency is sustained, but for the lower floors the agreement is much better. The distortion envelopes have reasonable agreement up to the ninth floor. Figure 3.39 shows the results for a different peak acceleration using El Centro. P-Δ effect is not included. The agreement between both models is maintained for twice El Centro and is even improved in relative terms. The shape of the curves does not change basically, and the same "phase shift" appears on the distortion envelopes as before.

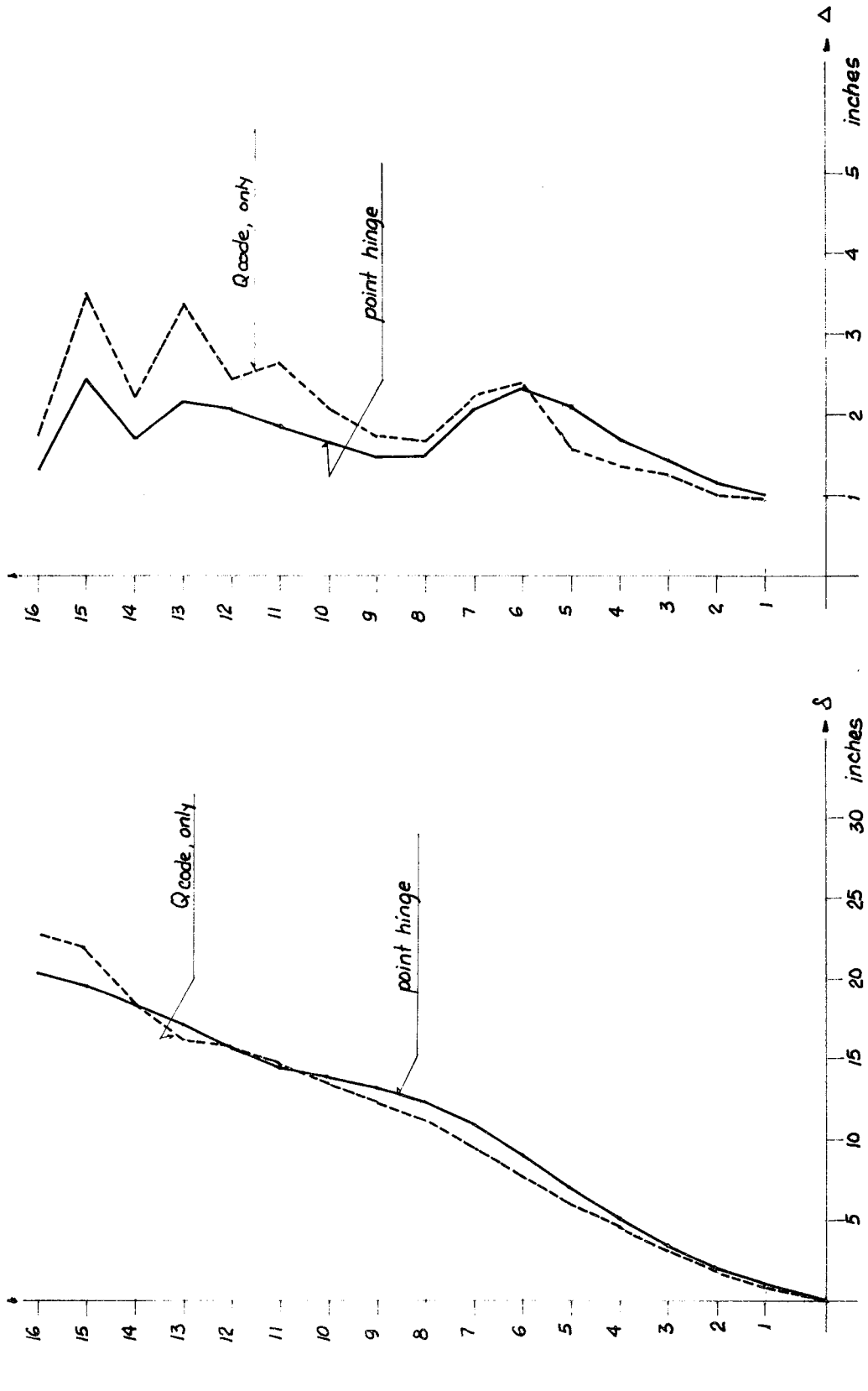

FIGURE 3.37 - 16-STORY UBC FRAME: POINT HINGE VS. MULTILINEAR. Q_{code}. BENDING. EL CENTRO. NO P-Δ

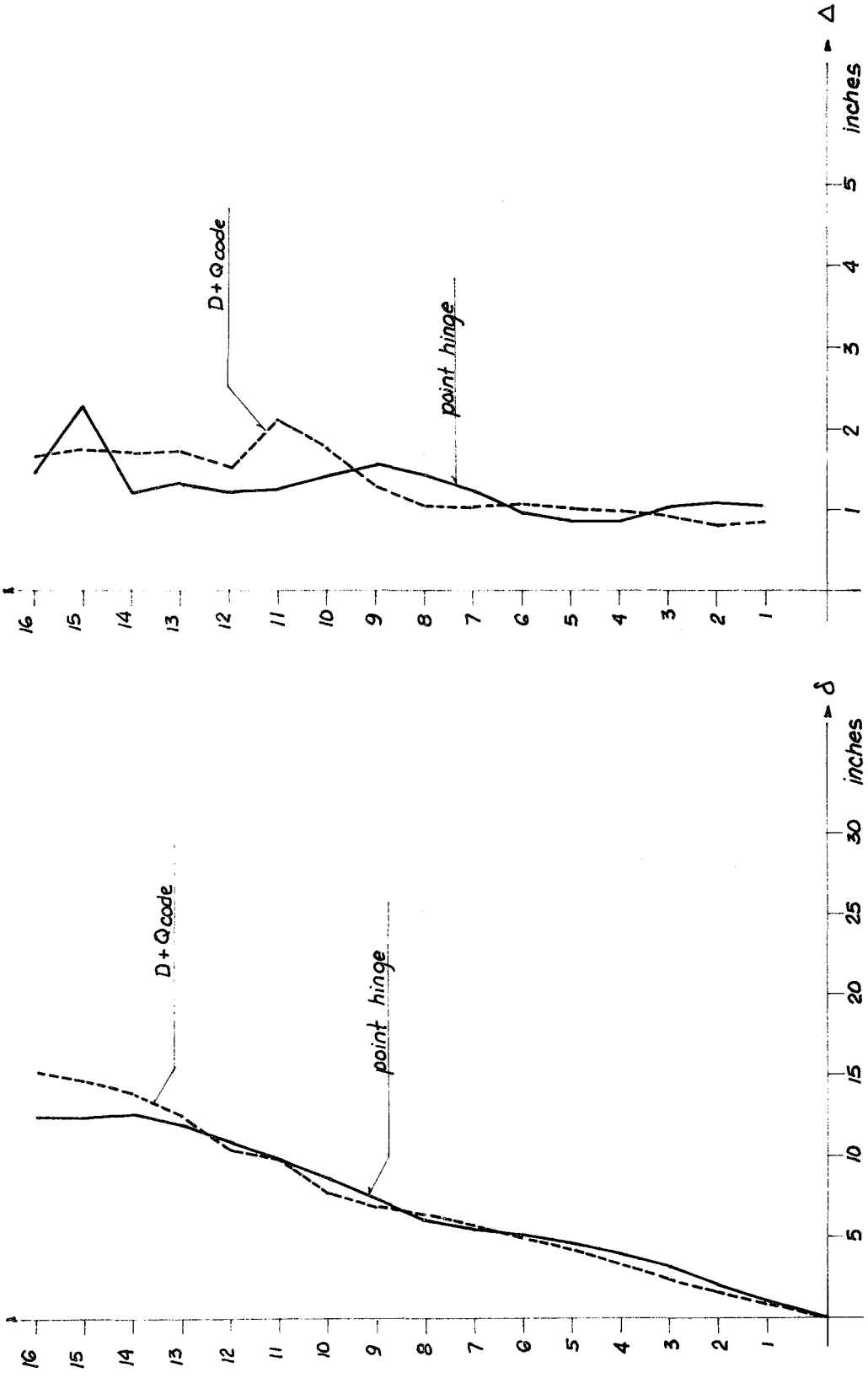

FIGURE 3.38 - 16-STORY UBC FRAME: POINT HINGE VS. MULTILINEAR. $D+Q_{code}$. INTERACTION. 1.87xTAFT. NO P-Δ

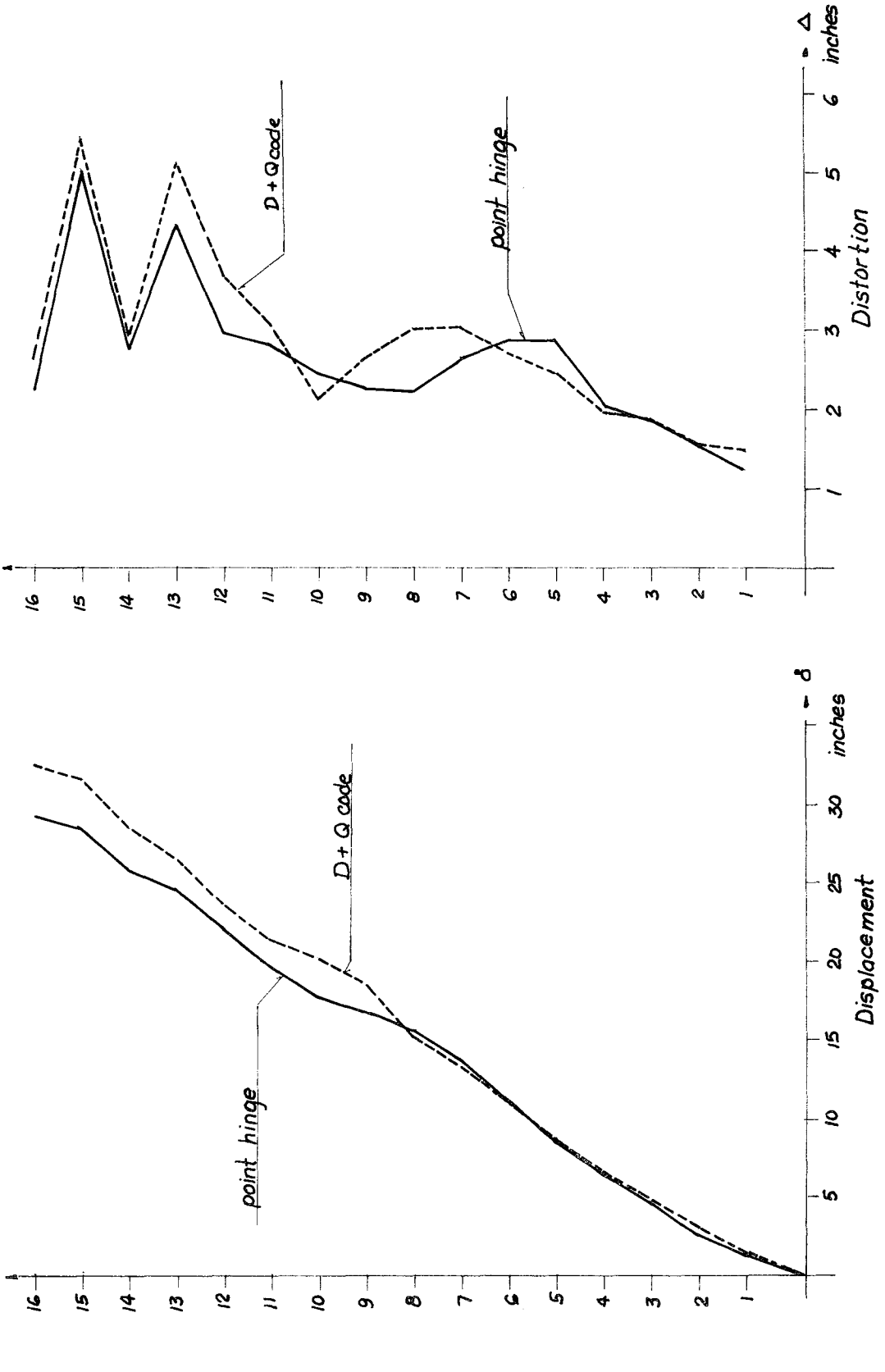

FIGURE 3.39 - 16-STORY UBC FRAME: POINT HINGE VS. MULTILINEAR. $D+Q_{code}$. INTERACTION. 2 x EL CENTRO. NO P-Δ

3.3.5 Influence of Lateral Load Distribution

Except for the springs obtained using a uniform lateral load distribution, all of the others predicted very similar results. For the three buildings analyzed, four- ten- and sixteen-story UBC frames, all displacement envelopes were clustered into a single group. Some scatter was sometimes present, but it was insignificant in terms of magnitude. The uniform distribution did not follow the same pattern, and also did not agree with the point-hinge model response, which suggests it is inappropriate to be used in the estimation of floor shear springs. In terms of distortions the same pattern was found, the uniform distribution springs predicting a different response than the others. As a result it was thought to be sufficient to use the lateral force distribution given by the UBC code, and this one was used in the additional analysis presented in section 3.3.4.

3.3.6 Influence of Earthquake Intensity

For the three frames studied under different peak accelerations, displacements did not increase proportionally as expected. However, the ratio of their increment varied for the two models. The shear-beam model predicted smaller responses for one times El Centro, but would tend to predict larger values for twice El Centro. Agreement, however, was maintained in most cases, and only in the ten-story frame was this change more significant. The overall shape of the envelopes remained unchanged, varying only in magnitude.

Responses predicted using the Taft record scaled to have the same

Arias intensity as El Centro were in all cases much lower, varying from 70% in the sixteen-story frame to 50% in the ten-story frame--a radical variation if due notice is given to the fact that differences between the two models are rarely larger than 30%.

3.3.7 Estimation of Local Ductilities Based on Shear-Beam Analysis.

At the end of each increment of loading in the static analysis, rotation and moment ductilities are computed for all members and printed at every given number of steps. Also the corresponding floor and interstory displacements are printed. These values are used to estimate dynamic member ductilities based on the maximum floor or interstory displacements from the dynamic analysis using the shear-beam model.

For a given floor, the predicted maximum distortion or floor displacement is taken, and its value compared to the closest smaller and larger values in the static analysis where ductilities have been printed out; a linear interpolation is then performed to compute all of the member ductilities of that floor, both based on moments and rotations.

These calculations were carried out for the four-, ten- and sixteen-story UBC frames, based on both floor displacements and distortions as predicted by the shear-beam dynamic analyses using springs from the UBC code distribution and without P-Δ effect.

Figures 3.40 and 3.41 show envelopes of maximum moment and rotation ductilities per floor in the four-story frame based on distortions and floor displacements. Figures 3.42 to 3.45 show the same for the ten-story UBC frame and Figures 3.46 to 3.49 for the sixteen-story frame.

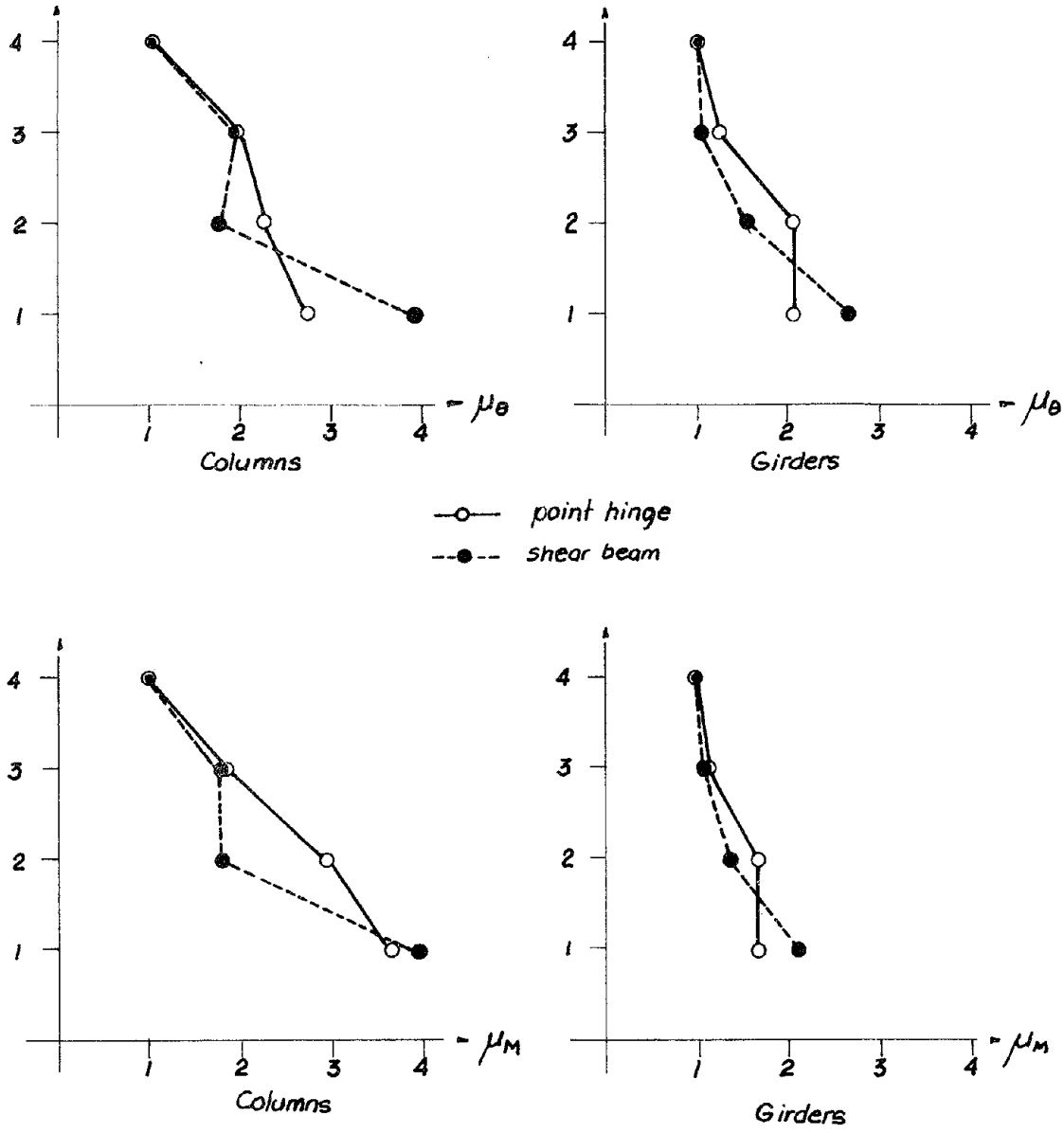

FIGURE 3.40 - 4-STORY UBC FRAME: MAX. DUCTILITIES. POINT HINGE VS. MULTILINEAR. BASED ON DISTORTIONS

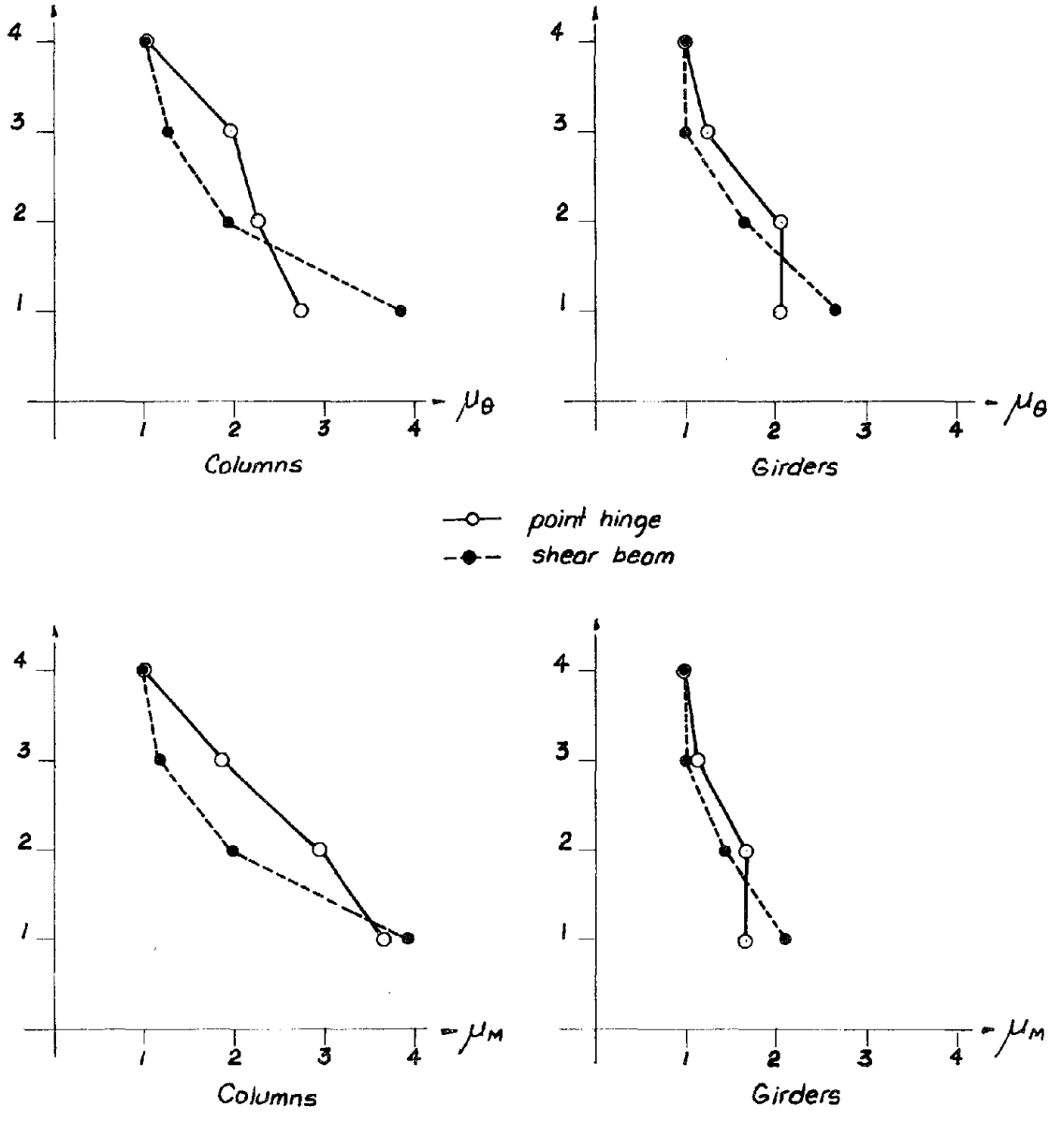

FIGURE 3.41 - 4-STORY UBC FRAME: MAX. DUCTILITIES. POINT HINGE VS. MULTILINEAR. BASED ON DISPLACEMENTS

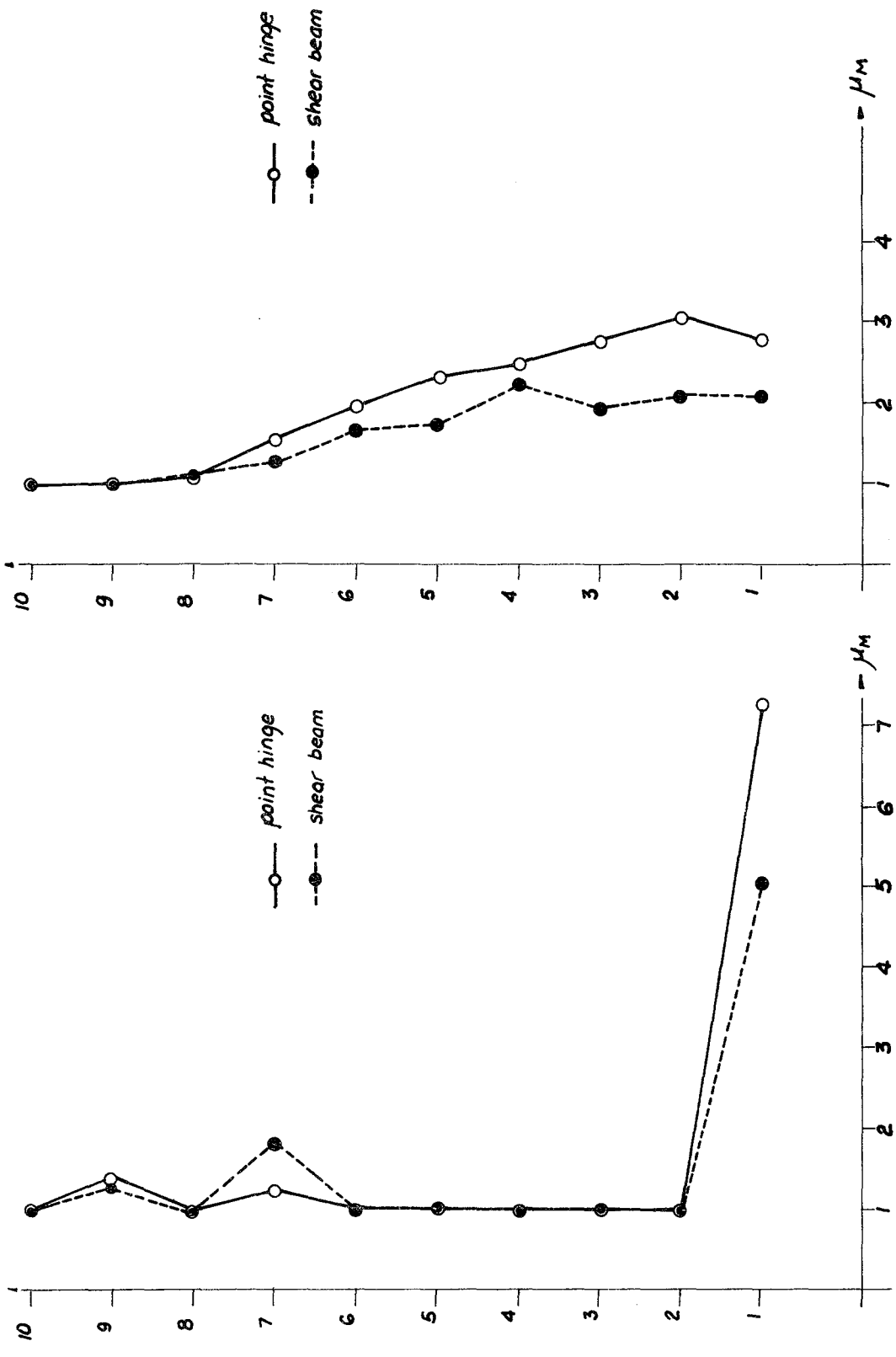

FIGURE 3.42 - 10-STORY UBC FRAME; MOMENT DUCTILITIES BY MULTILINEAR DISTORTIONS VS. POINT HINGE

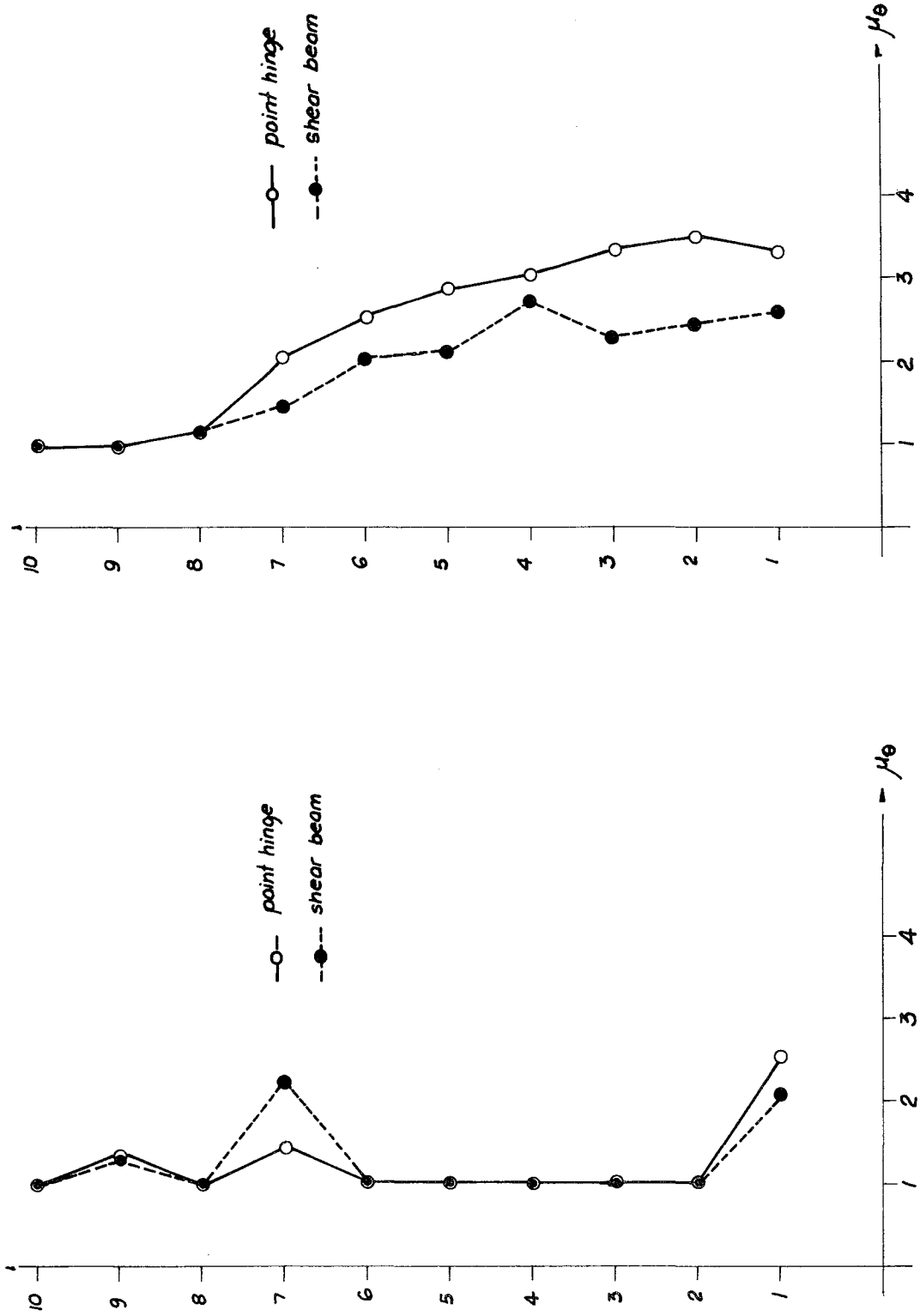

FIGURE 3.43 - 10-STORY UBC FRAME: ROTATION DUCTILITIES BY MULTILINEAR DISTORTIONS VS. POINT HINGE

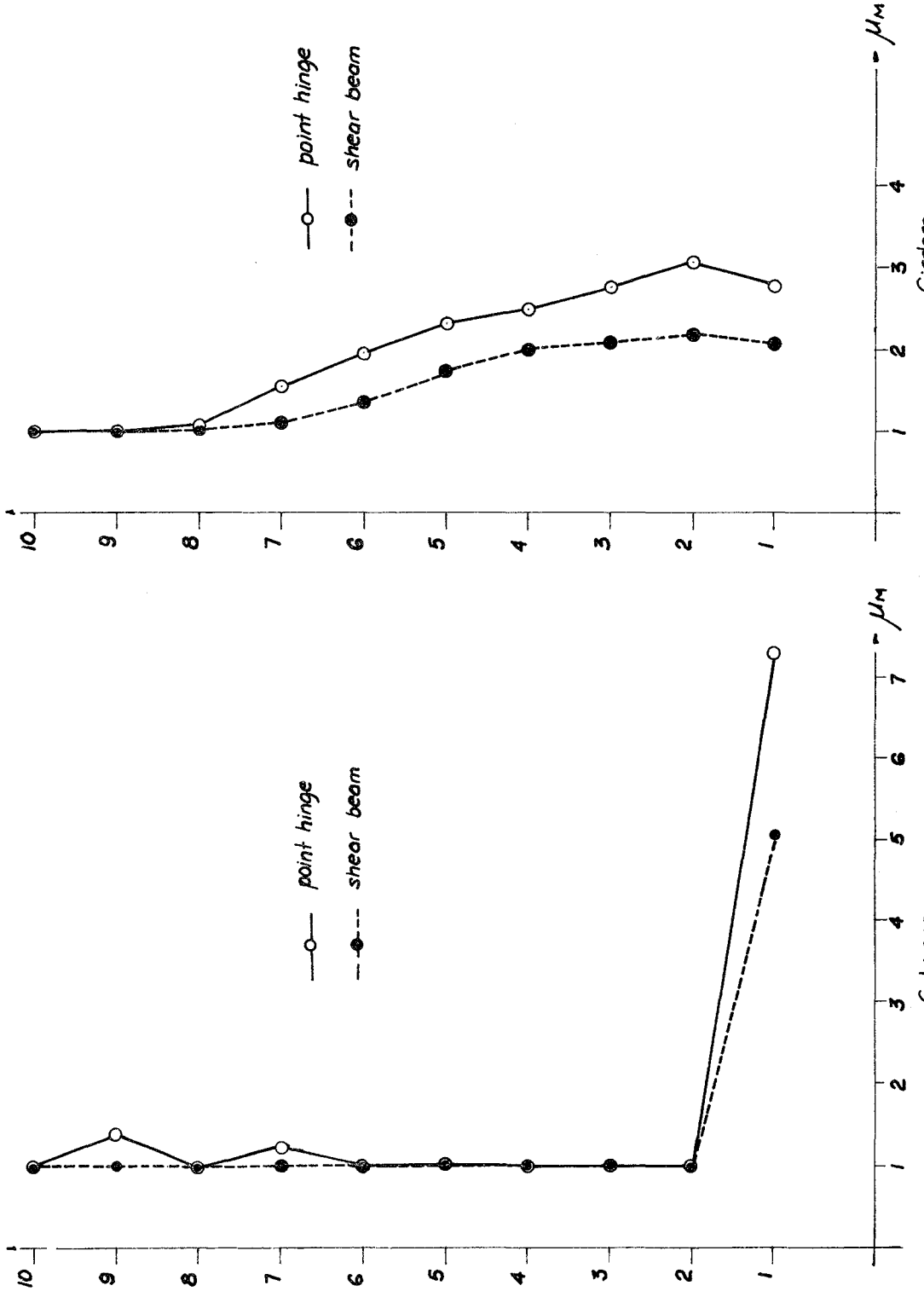

FIGURE 3.44 - 10-STORY UBC FRAME: MOMENT DUCTILITIES BY MULTILINEAR DISPLACEMENTS VS. POINT HINGE

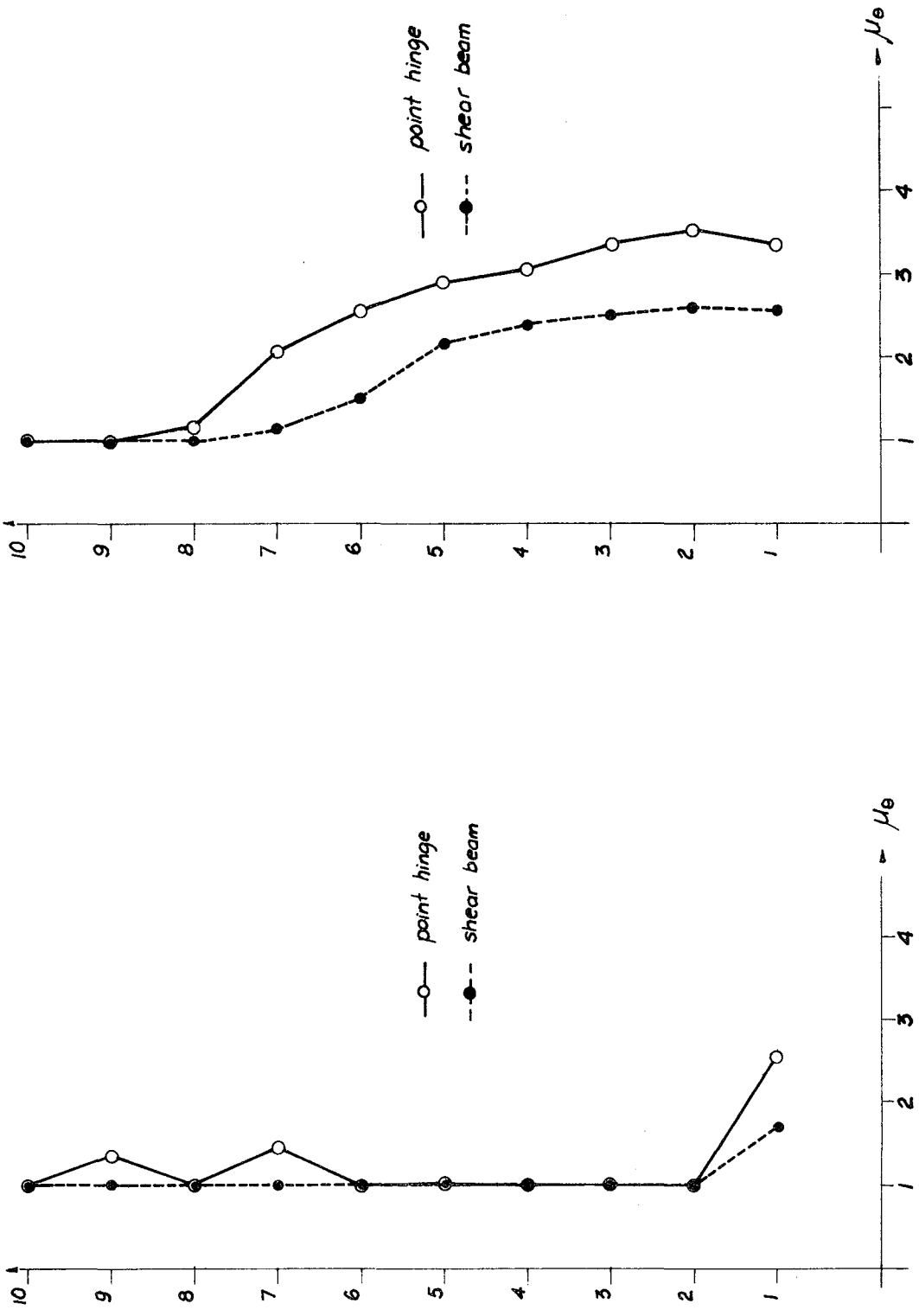

FIGURE 3.45 - 10-STORY UBC FRAME: ROTATION DUCTILITIES BY MULTILINEAR DISPLACEMENTS VS. POINT HINGE

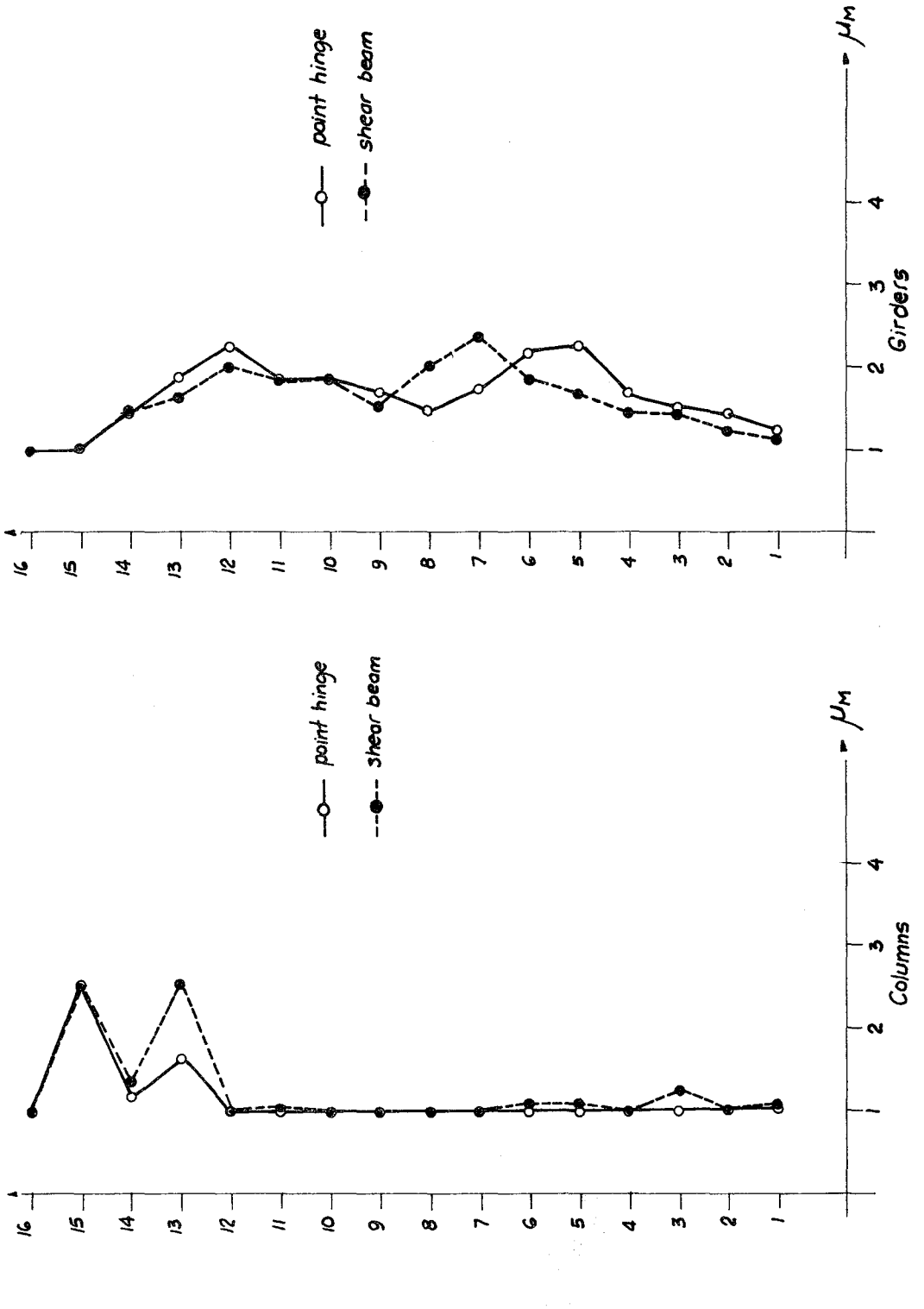

FIGURE 3.46 - 16-STORY UBC FRAME: MOMENT DUCTILITIES BASED ON MULTILINEAR DISTORTIONS

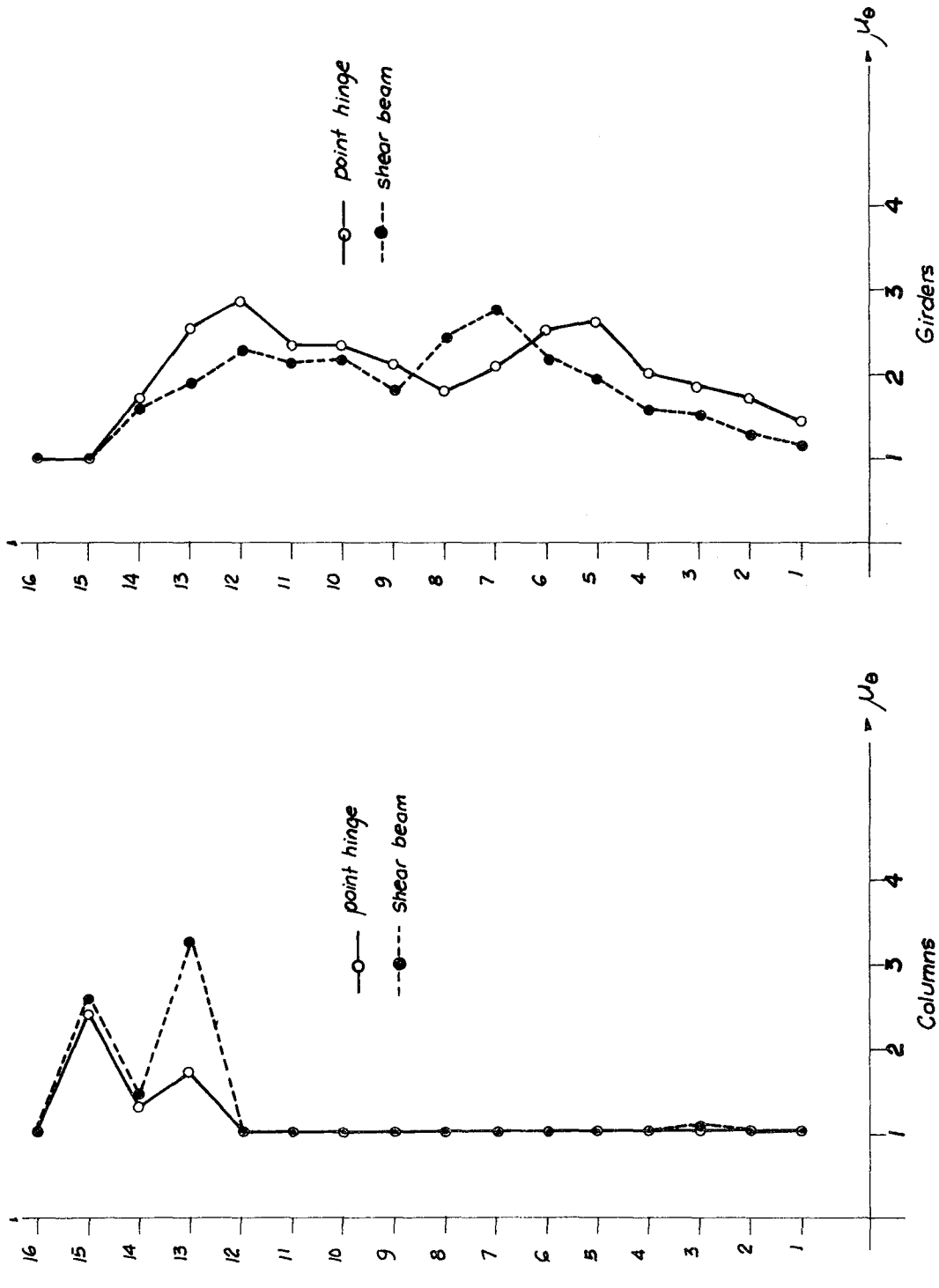

FIGURE 3.47 - 16-STORY UBC FRAME: ROTATION DUCTILITIES BASED ON MULTILINEAR DISTORTIONS

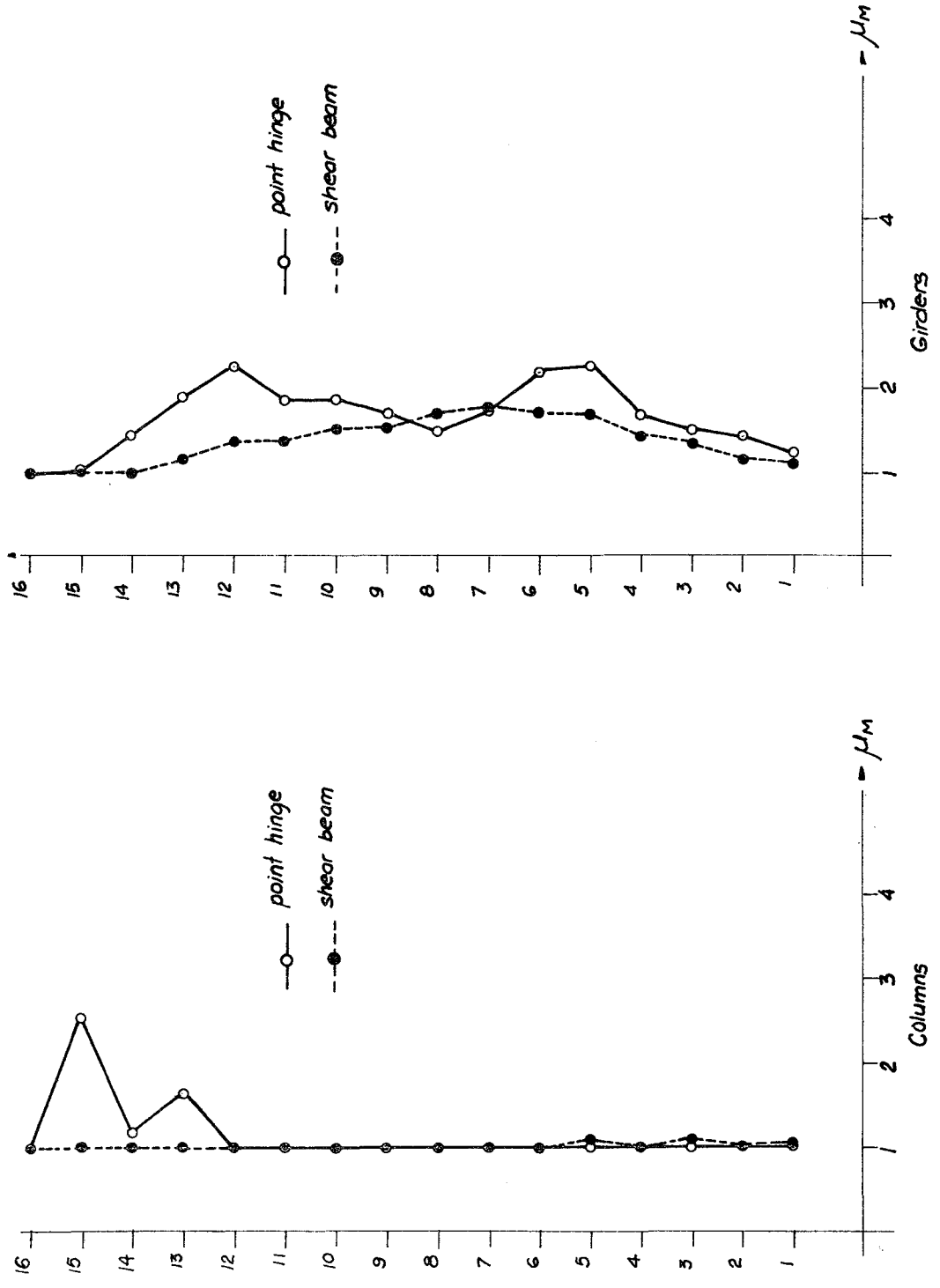

FIGURE 3.48 - 16-STORY UBC FRAME: MOMENT DUCTILITIES BASED ON MULTILINEAR DISPLACEMENTS

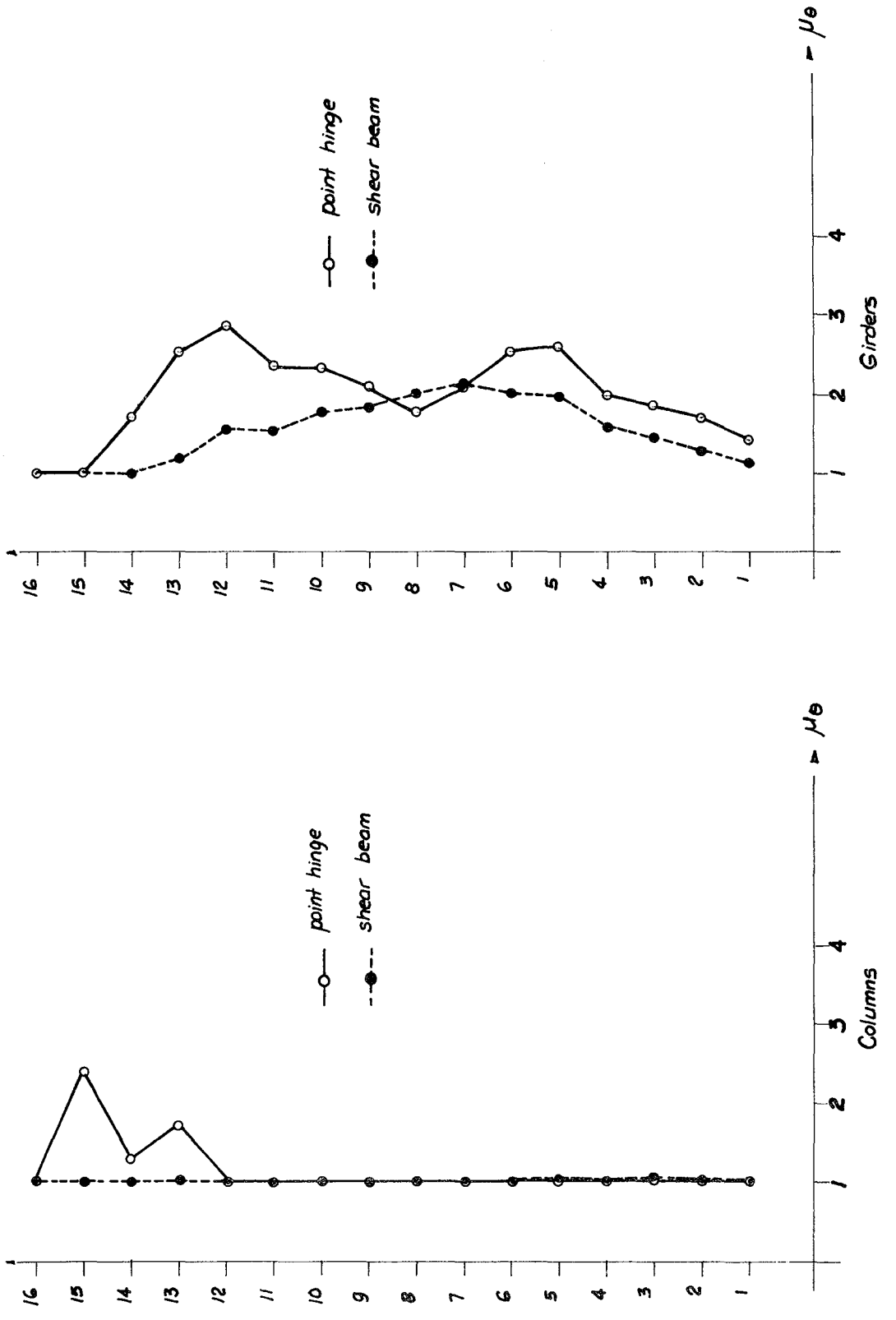

FIGURE 3.49 - 16-STORY UBC FRAME: ROTATION DUCTILITIES BASED ON MULTILINEAR DISPLACEMENTS

Reasonable agreements are found for all buildings. When distortions are used for the computations, results agree better than when using floor displacements. This is more so for the upper stories, where a moderate displacement in the static analysis does not represent the same for distortions resulting in smaller ductilities. Most results follow the same kind of correlation found for displacements and distortions, giving smaller values when distortions are smaller and larger when they are larger. This indicates that the procedure to estimate member ductilities given the "correct" floor distortions is adequate, and the discrepancies found are those inherent in the results of the shear-beam model. To illustrate this point, ductilities were computed and compared with the point-hinge model predictions using the distortions obtained by this model. Figures 3.50 to 3.54 present these results. It can be seen that the agreement in these cases improves substantially and is quite good everywhere. Some discrepancies found are due to the linear interpolation procedure when the end values are too far apart.

3.4 EVALUATION OF THE SHEAR-BEAM MODEL PERFORMANCE

A primary objective of this research was to determine the ability of the shear-beam model to predict dynamic responses similar to those given by the point-hinge model. By using the procedures presented in Chapters 2 and 3, uncertainties in the performance of the shear-beam model due to spring determination have been reduced to a minimum, allowing the results to be interpreted as a measure of the adequacy of the model. As a general conclusion for all the structures analyzed and the

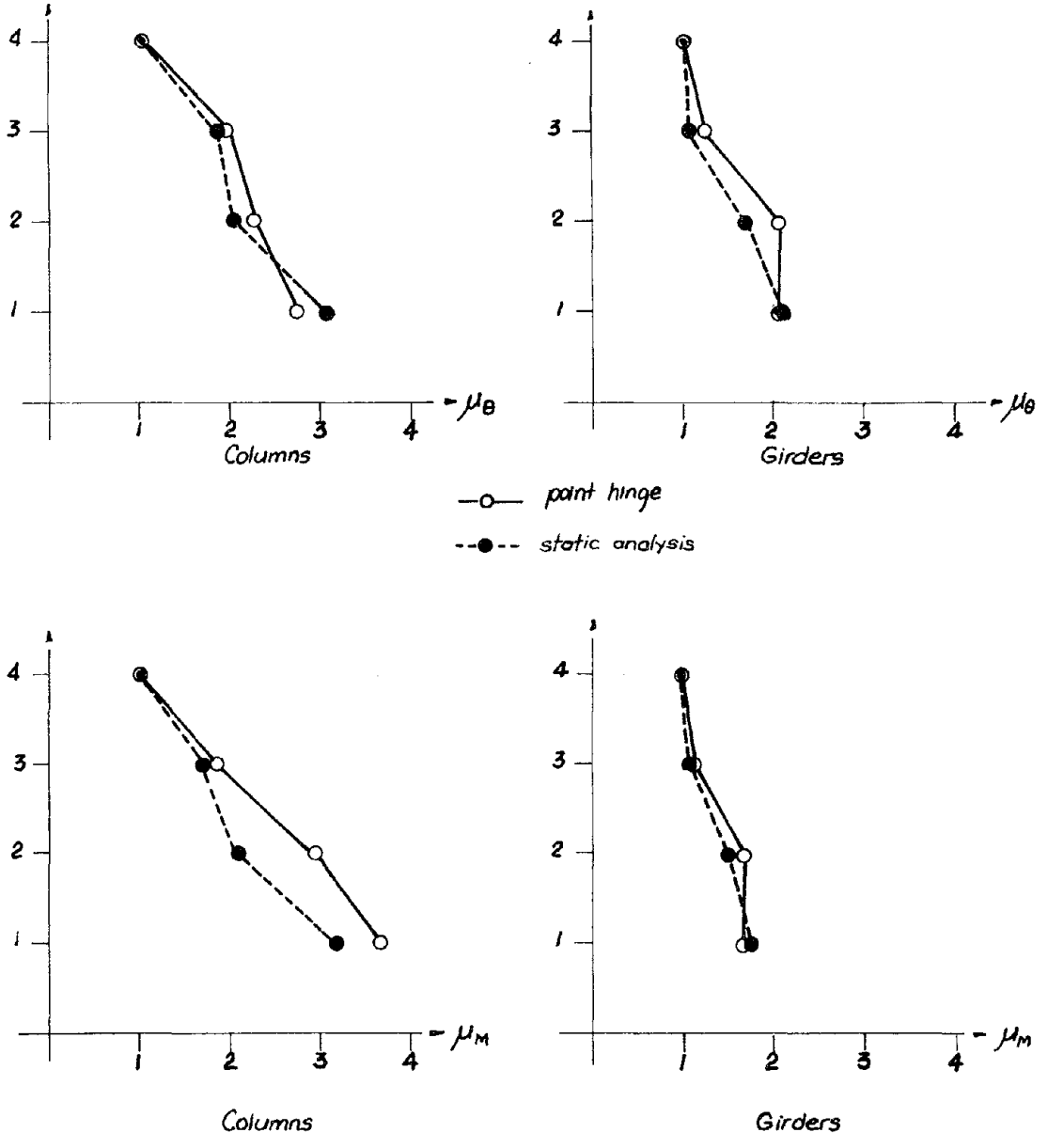

FIGURE 3.50 - 4-STORY UBC FRAME: DUCTILITIES BASED ON FRIEDA DISTORTIONS

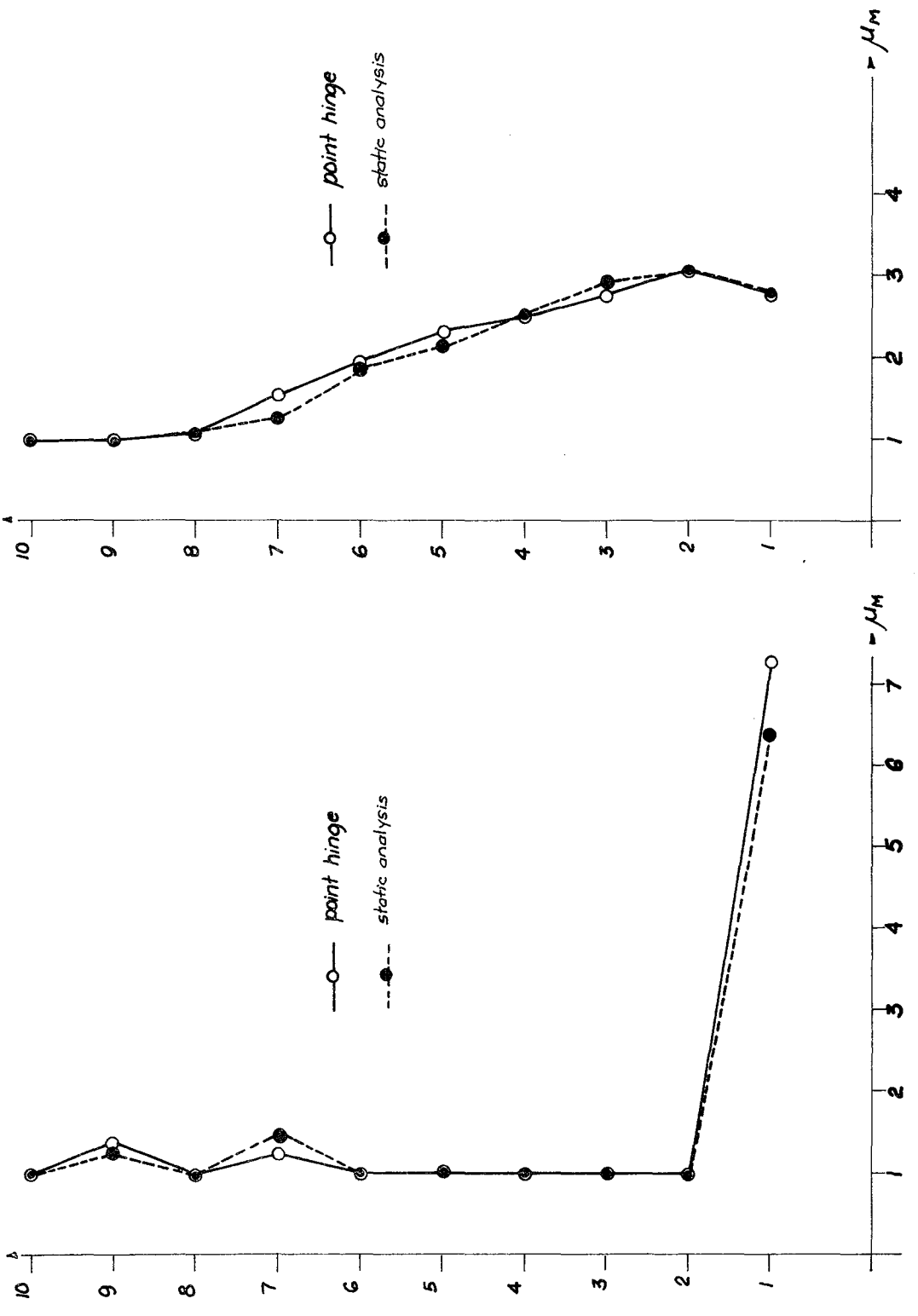

FIGURE 3.51 - 10-STORY UBC FRAME: MOMENT DUCTILITIES BASED ON FRIEDA DISTORTIONS

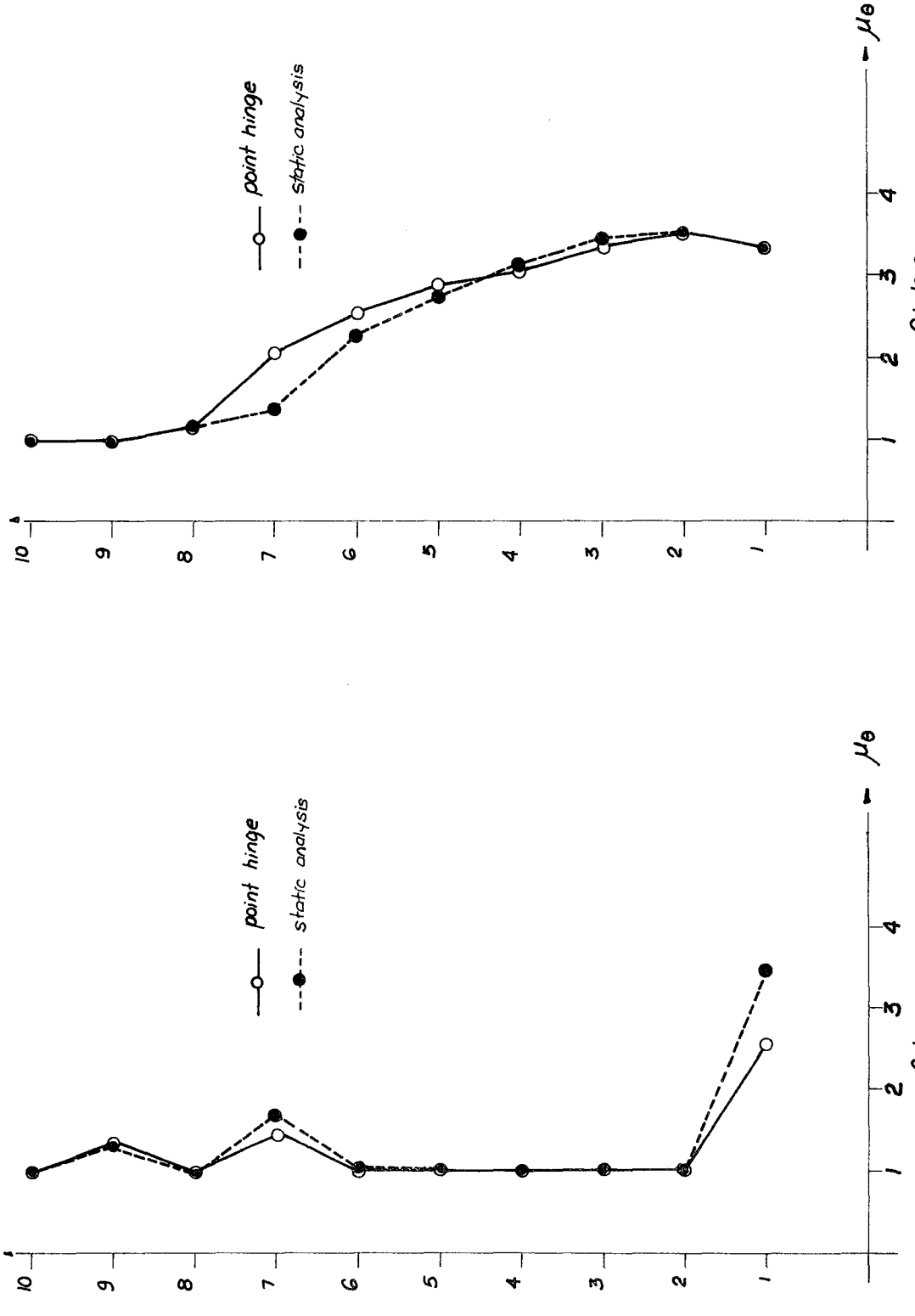

FIGURE 3.52 - 10-STORY UBC FRAME: ROTATION DUCTILITIES BASED ON FRIEDA DISTORTIONS

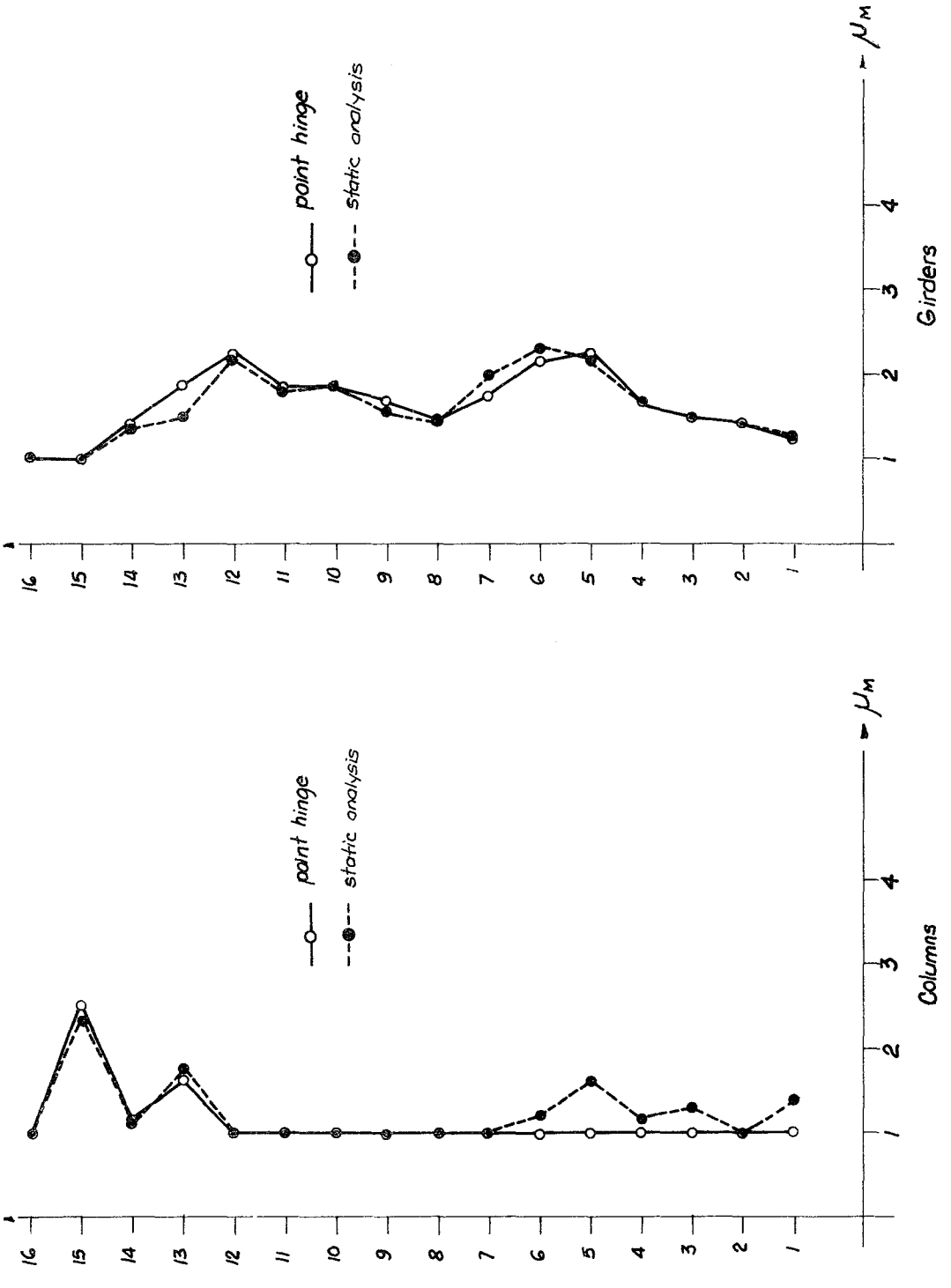

FIGURE 3.53 - 16-STORY UBC FRAME: MOMENT DUCTILITIES BASED ON FRIEDA DISTORTIONS

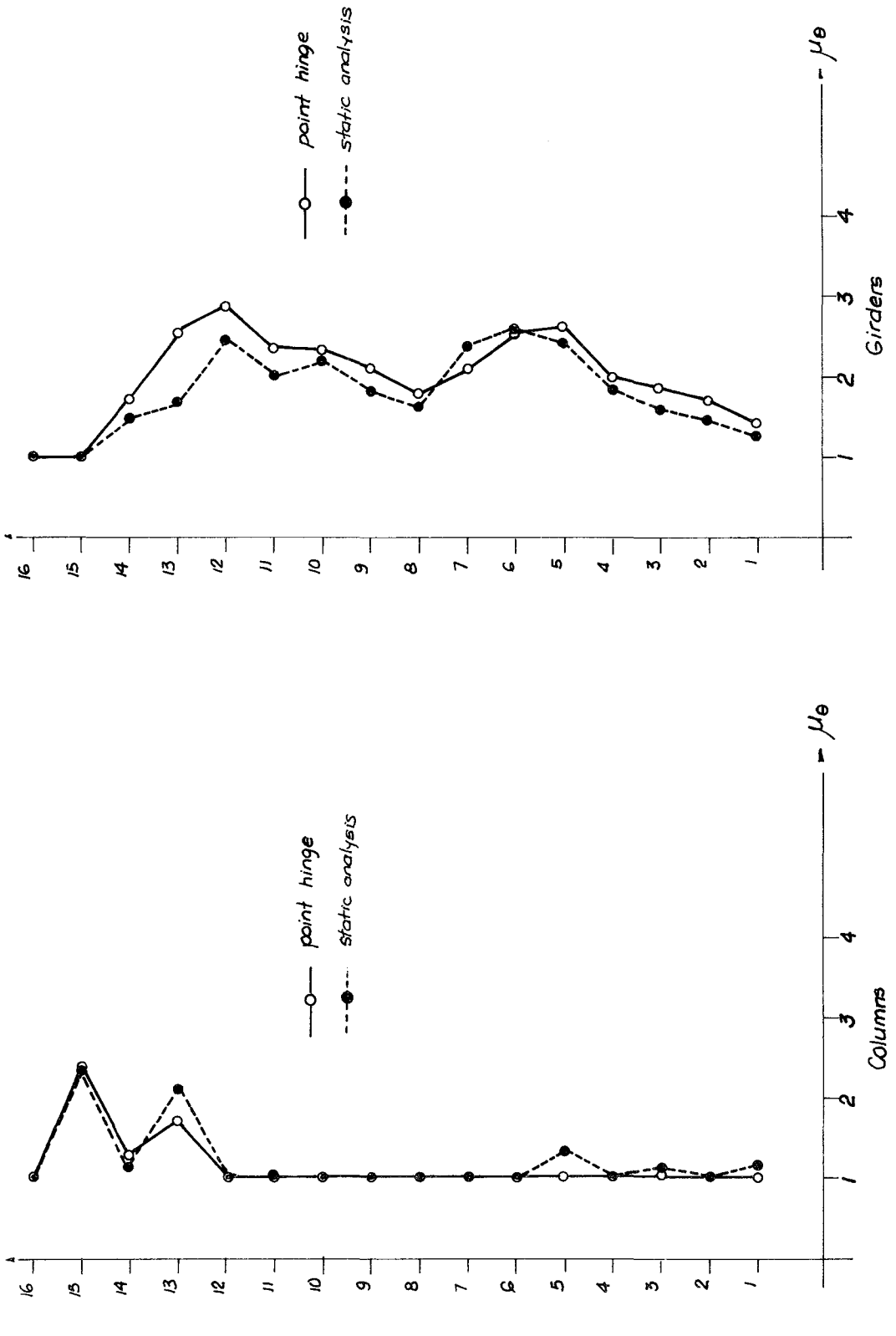

FIGURE 3.54 - 16-STORY UBC FRAME: ROTATION DUCTILITIES BASED ON FRIEDA DISTORTIONS

different cases of load distribution and intensity of motion, it appears that the shear-beam model is adequate to predict dynamic response within reasonable limits.

The ability of the model to reproduce the overall shape of maximum floor displacements is quite good. It has been seen that by using the shear springs computed from the solution of the entire structure, deformed shapes other than the first mode of a shear beam can be modeled appropriately. Local discrepancies in magnitude are not rare, but the overall shapes of the displacement envelopes are in the majority of cases close or proportional. For some structures and particular values of earthquake peak acceleration, differences up to thirty percent with respect to the point-hinge model have been encountered. This seems to be acceptable in view of the fact that much larger differences occur due to the ground motions themselves, even though they may be of the same intensity.

Distortions are reproduced with more scatter than displacements, but a general pattern of agreement is found with local higher differences than for displacements.

When used to compute local ductilities, the predictions of the shear-beam model provide reasonable estimations in comparison to the point-hinge model. For the same structure, even when using artificial motions that match the same response spectrum, a much larger variation is found, as reported by Luyties et al. [18] and Haviland [35]. Following a different approach, Haviland [35] has shown that the shear-beam model provides response entirely comparable to those of the point-hinge model when adequate properties are used. In his case, bilinear springs were estimated

from the story shear-distortion curves obtained directly from the dynamic analysis with the point-hinge model. Shear-beam dynamic analyses were then performed using these springs, and floor displacements were reproduced within a ten percent margin.

3.5 CONCLUSIONS

The following conclusions can be drawn from the results of this Chapter:

- The shear-beam model provides reasonable estimations of maximum floor displacements and distortions when appropriate floor springs are used.

- Floor springs obtained by using the UBC code lateral force, the first mode shape, the SRSS of all modes, or ATC-3 distributions give very similar results in the dynamic analysis.

- The uniform lateral load distribution gives results that differ from both the point-hinge model and from the shear-beam analysis with the other distributions, suggesting that it produces inadequate floor springs.

- P-Δ effects have relatively minor effect on displacements and distortions except for some specific cases where the structures have peculiar configurations. The shear-beam model as implemented here seems to be less sensitive to this effect than the point-hinge model. This may be a point that requires further study.

- Agreements using the bending yield criterion are overall better than using the interaction criterion. In some cases displacements predicted by it are larger than for the interaction case.

- Difference in the magnitude of displacements and distortions due to different ground excitations of the same intensity are substantial and can be as large as 50%.

- For different peak accelerations there is no clear trend that the shear-beam model underpredicts or overpredicts the response. The relative difference of the results is maintained regardless of the intensity of the earthquake.

- It is possible to estimate local ductilities based on the displacements and distortions predicted by the shear-beam model. The agreement between these and the ones predicted by the point-hinge model is comparable to the agreement between displacements.

CHAPTER 4

INELASTIC DYNAMIC ANALYSIS USING APPROXIMATE SPRINGS

4.1 INTRODUCTION

In Chapter 3 dynamic analyses using multilinear springs were performed to evaluate the close-coupled assumption of the shear-beam model. For actual applications, however, this becomes impractical and simpler approximations for floor springs, such as bilinear or trilinear relationships, are used. In this Chapter analyses performed using these two types of springs are presented and evaluated in terms of the point-hinge model response and that of the multilinear springs.

Section 4.2 describes the actual bilinear and trilinear approximations as applied to the shear-distortion curves obtained in Chapter 2. The results and comparison of the analyses with the point-hinge model and the multilinear springs is presented in sections 4.3 and 4.4. In section 4.5 an evaluation of the performance of the shear-beam model using approximate floor springs is presented, followed by a summary of the conclusions in section 4.6.

4.2 APPROXIMATION OF SHEAR-DISTORTION CURVES WITH BILINEAR AND TRILINEAR SPRINGS

A bilinear approximation to the actual shear-distortion curve is the simplest that can be used (an elastoplastic is not possible if a non-zero second slope is assumed for the M-θ relation in the static analysis). The initial stiffness is always known, but the second branch has to be selected based on a certain criterion. Figures 2.16 to 2.20 show a flat ultimate branch extending along most of the length of the curve. This corresponds to a percentage of the initial slope given in the static analysis, but it is only reached for very large values of interstory displacement. In most cases the distortions predicted in the dynamic analysis fall within a much smaller range. It would be more appropriate, then, to assume as the second branch or ultimate slope a line tangent to the V-Δ curve at the closest point where distortions will not be exceeded in the dynamic analysis. (A generous estimation of these values is essential). The slope of this line is larger than the actual ultimate slope, and when intersected with the initial stiffness prolongation a smaller

yield value is obtained than when using the actual one. (See Figure 4.1). Both approaches, selecting for the second branch the ultimate slope and a best fit over the region of interest were investigated. The bilinear spring is then fully defined by its initial stiffness, the second branch or ultimate stiffness and yield point where both intersect.

When examined at a larger scale most curves show a much smoother transition than that provided by a bilinear approximation. In some cases, like the Anderson frame (see, for example Fig. 2.20), a clear trilinear curve is evidently formed, but for most buildings the shape does not suggest a clear-cut approximation. A better reproduction of the actual curve can be obtained, however, by using trilinear springs.

Figure 4.1 shows a typical V-Δ curve, in this case for the second floor of the sixteen-story frame under dead plus code lateral loads. The point where the behavior ceases to be linear and the first change (decrease) in stiffness appears is for a shear equal to 157 Kips, but the curve does not substantially deviate from the initial stiffness until higher values of shear are reached. This fact suggested the use of two choices of trilinear springs. One, called "Trilinear A" obtained as the closest fit possible through the curve, and the second "Trilinear B" obtained by defining the first yield as the shear for which the floor stiffness becomes 50% of the initial one. In both cases the third branch or ultimate slope is the same one defined for the bilinear springs.

The initial stiffness being the same for all approximations, the remaining parameters to define completely a trilinear spring are the second branch and the ultimate yield.

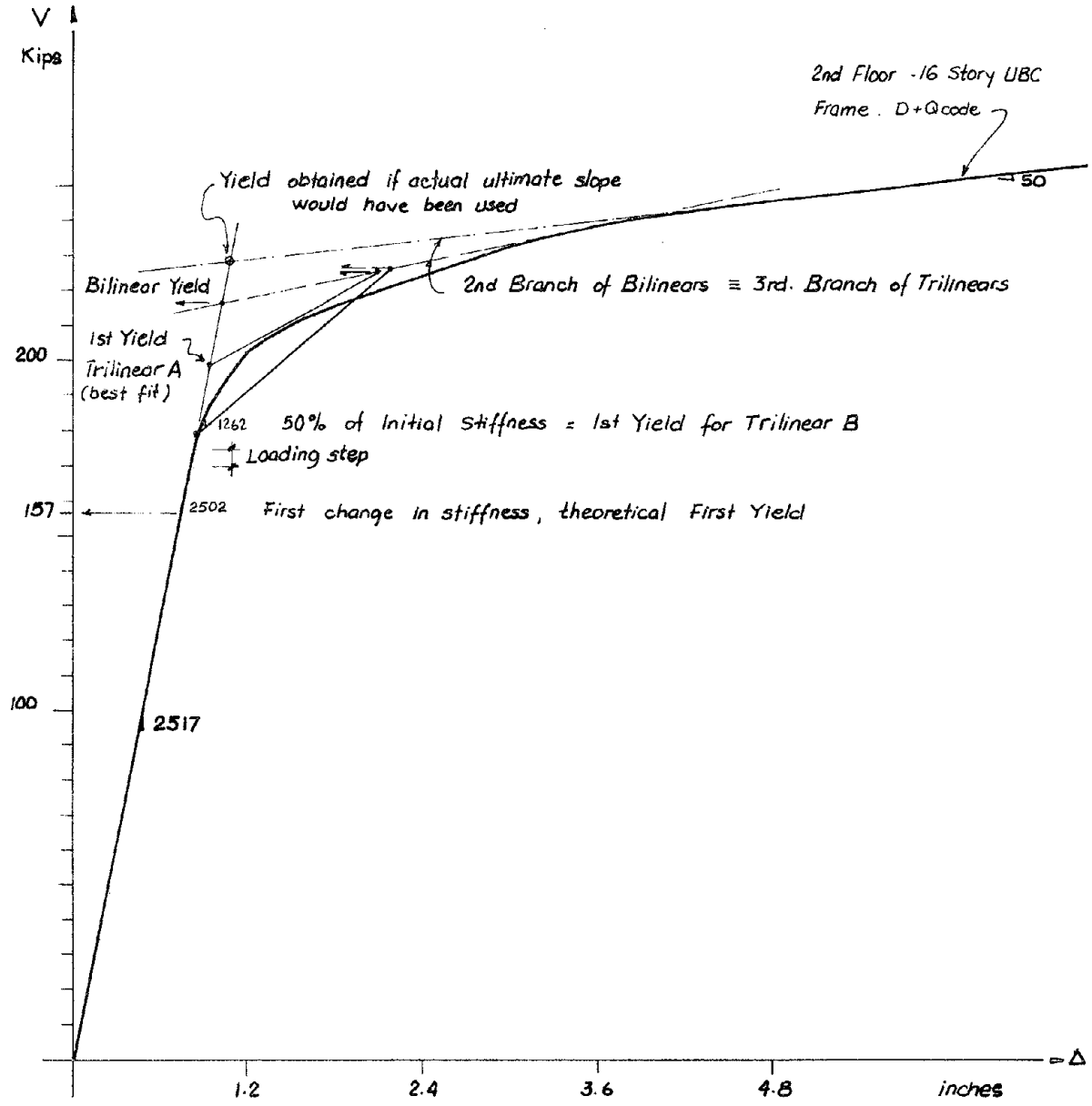

FIGURE 4.1 - APPROXIMATIONS FOR BILINEAR AND TRILINEAR SPRINGS "A" AND "B"

For the "Trilinear A" the second branch was chosen as the one which follows the V-Δ curve the closest. No unique answer could of course be found, but the criterion followed was to have balanced "unmatched" segments at both sides of this branch. The intersection of this line with the initial and ultimate stiffness defined the first and ultimate yield for this spring.

For the "Trilinear B" the second branch was a line from the point on the initial stiffness at first yield, as defined before, to the ultimate slope maintaining the areas (energy) above and below the curve equal. The ultimate yield would be defined then as the intersection of the second and ultimate branches.

4.3 COMPARISONS OF RESPONSES PREDICTED BY THE SHEAR-BEAM AND POINT-HINGE MODELS

4.3.1 Four-Story UBC Frame

All comparisons presented in this section were performed using the interaction yield criterion. Figure 4.2 shows the envelopes for displacements and distortions predicted by the shear-beam model using bilinear springs as compared to the point-hinge model. Springs obtained from three lateral load distributions were used, i.e., the UBC code, the first mode shape and the SRSS of all modes. The second slopes used with these bilinears were the ultimate slopes of the curves that extended along the large portion of the plot. The responses predicted by the shear-beam model using bilinear springs computed according to the formulas presented by Anagnostopoulos [2] is also shown. These springs will be referred to as the "original" bilinears.

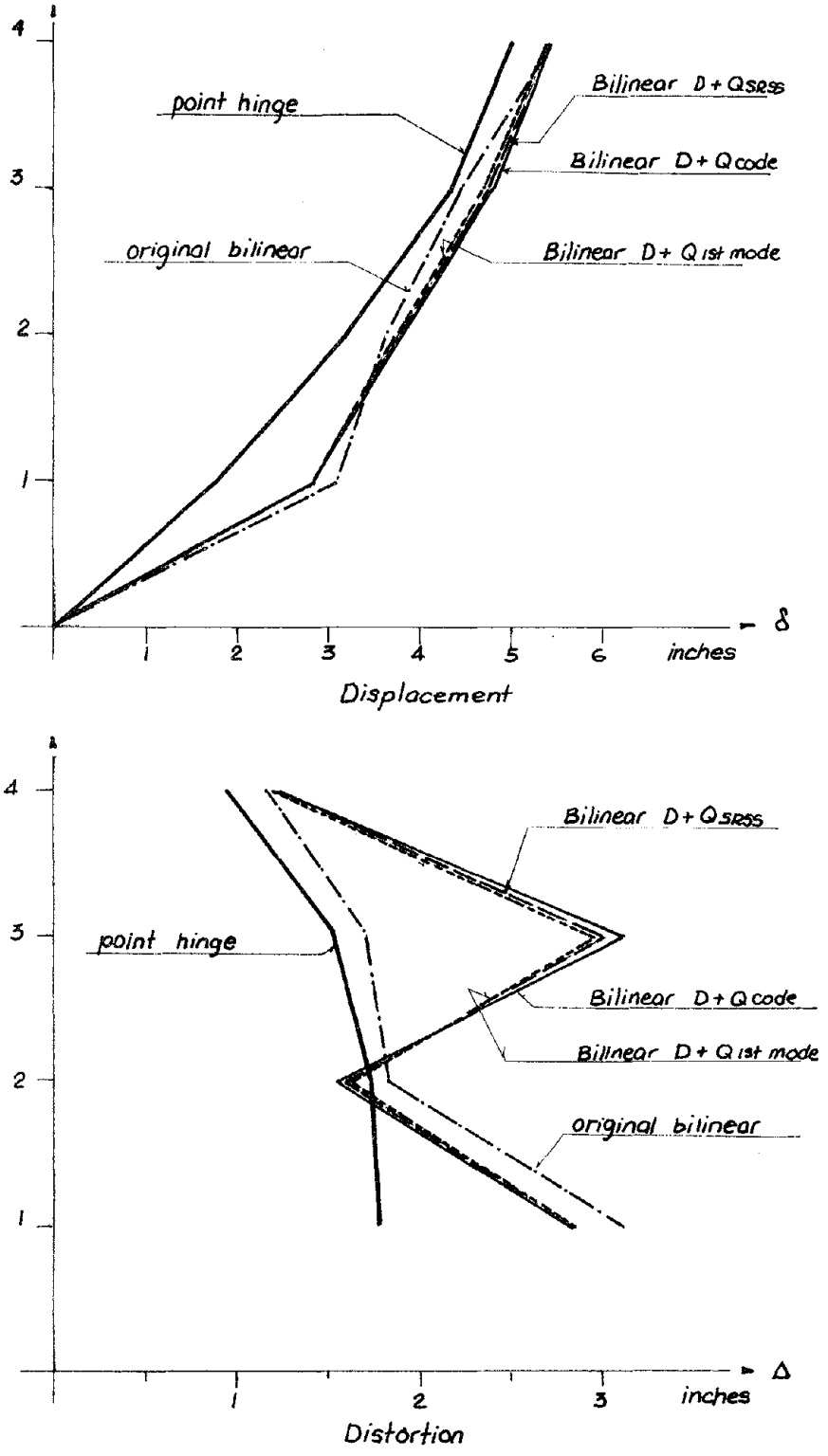

FIGURE 4.2 - 4-STORY UBC FRAME. POINT HINGE VS. BILINEAR SPRINGS.

EL CENTRO. P-Δ

Basically all three load distributions give the same results. The bilinear springs overestimate response (on the top floor the difference is 8% , increasing to 25% on the second floor and 50% on the first floor, all measured with respect to the point-hinge model predictions). The original bilinear gives closer results on the upper floors, but larger discrepancy on the first floor.

Distortions with the bilinear springs are reasonable on the second and fourth floors, but largely overpredicted on the first and third. However, the original bilinear behaves better on the three upper stories and only on the first floor exceeds the others.

On Figure 4.3 the results using a different second slope for the bilinear spring obtained from the code distribution are shown. The ultimate stiffness was estimated at the range of interest as explained in section 4.1. The agreement improves substantially for both floor displacements and distortions, with a maximum difference on the first story of 28%. The other floors show better agreement.

This seems to indicate that it would be more appropriate to limit the "length" of the spring to the range of interest and obtain a better representation of the actual curve in that area.

Figures 4.4, 4.5 and 4.6 show the comparisons using trilinear springs "A" and "B" for the same three lateral load distributions. There is a very small difference in the predicted behavior due to the lateral load distribution. The springs from the UBC code distribution give results in between the other two for both cases and effects.

The agreement is reasonably good for all floors but the first, where

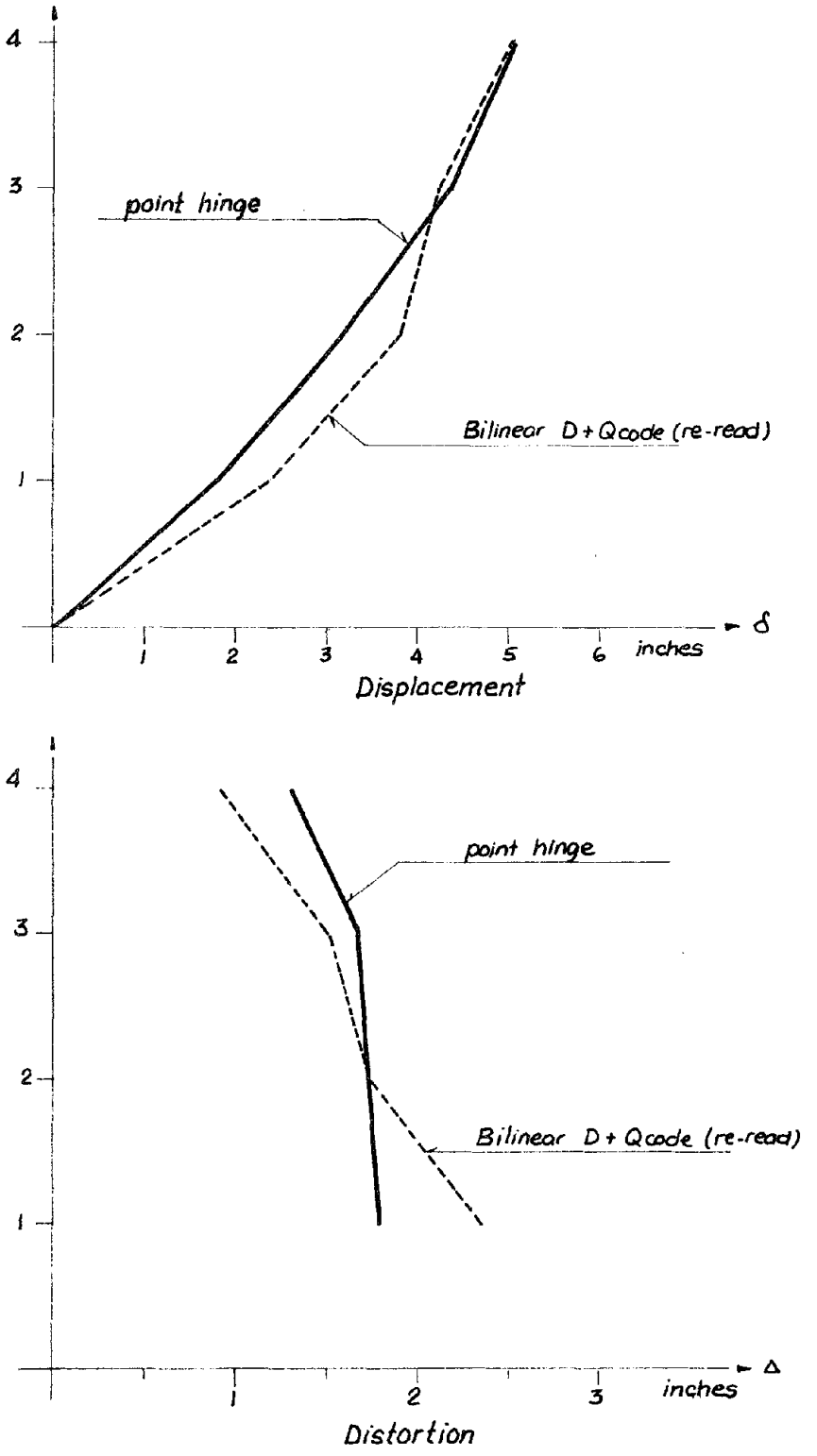

FIGURE 4.3 - 4-STORY UBC FRAME: POINT HINGE VS. RE-READ BILINEAR. EL CENTRO. P-Δ

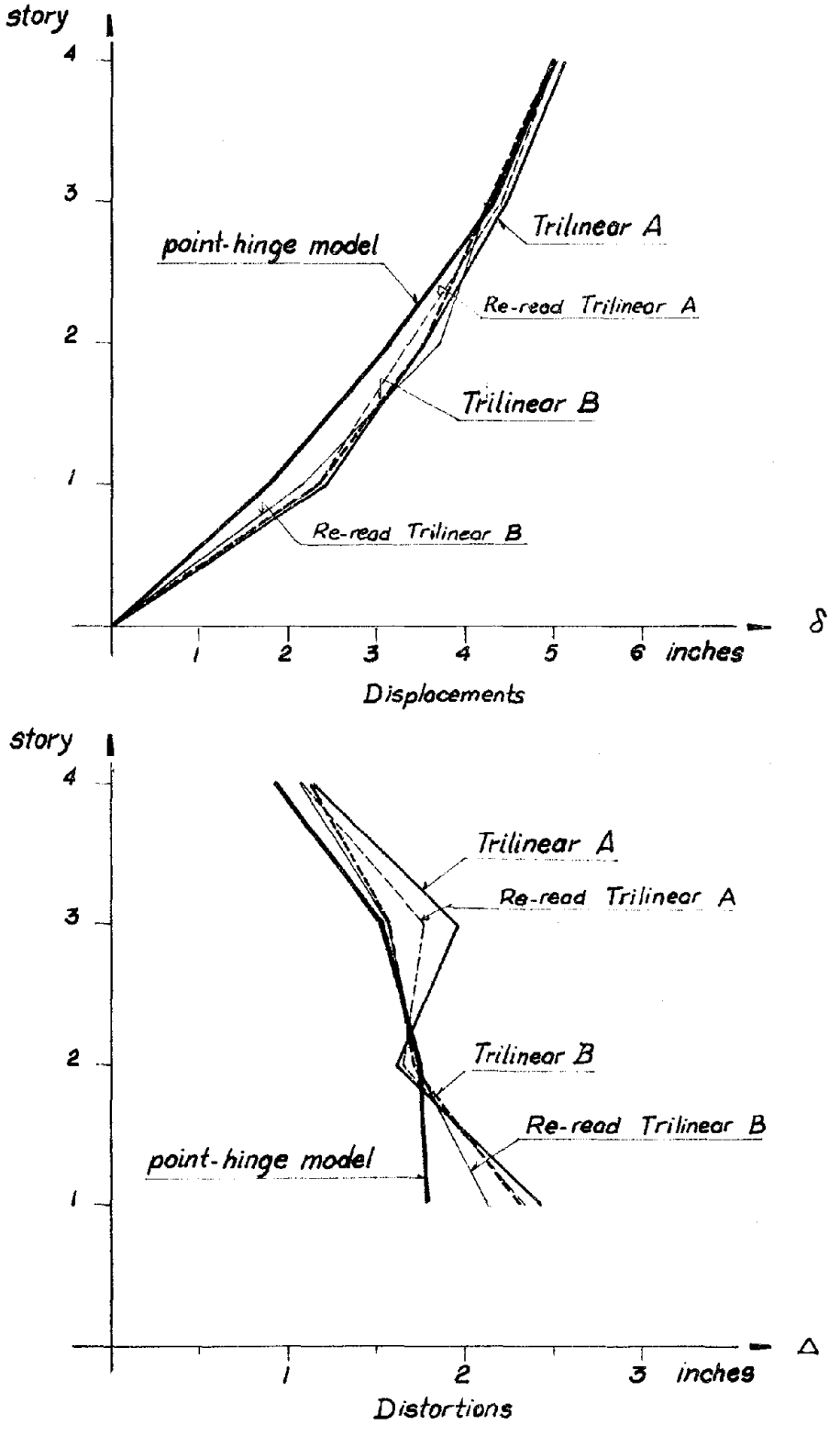

FIGURE 4.4 - 4-STORY UBC FRAME: POINT HINGE VS. TRILINEARS A AND B
D+Qcode. EL CENTRO. P-Δ

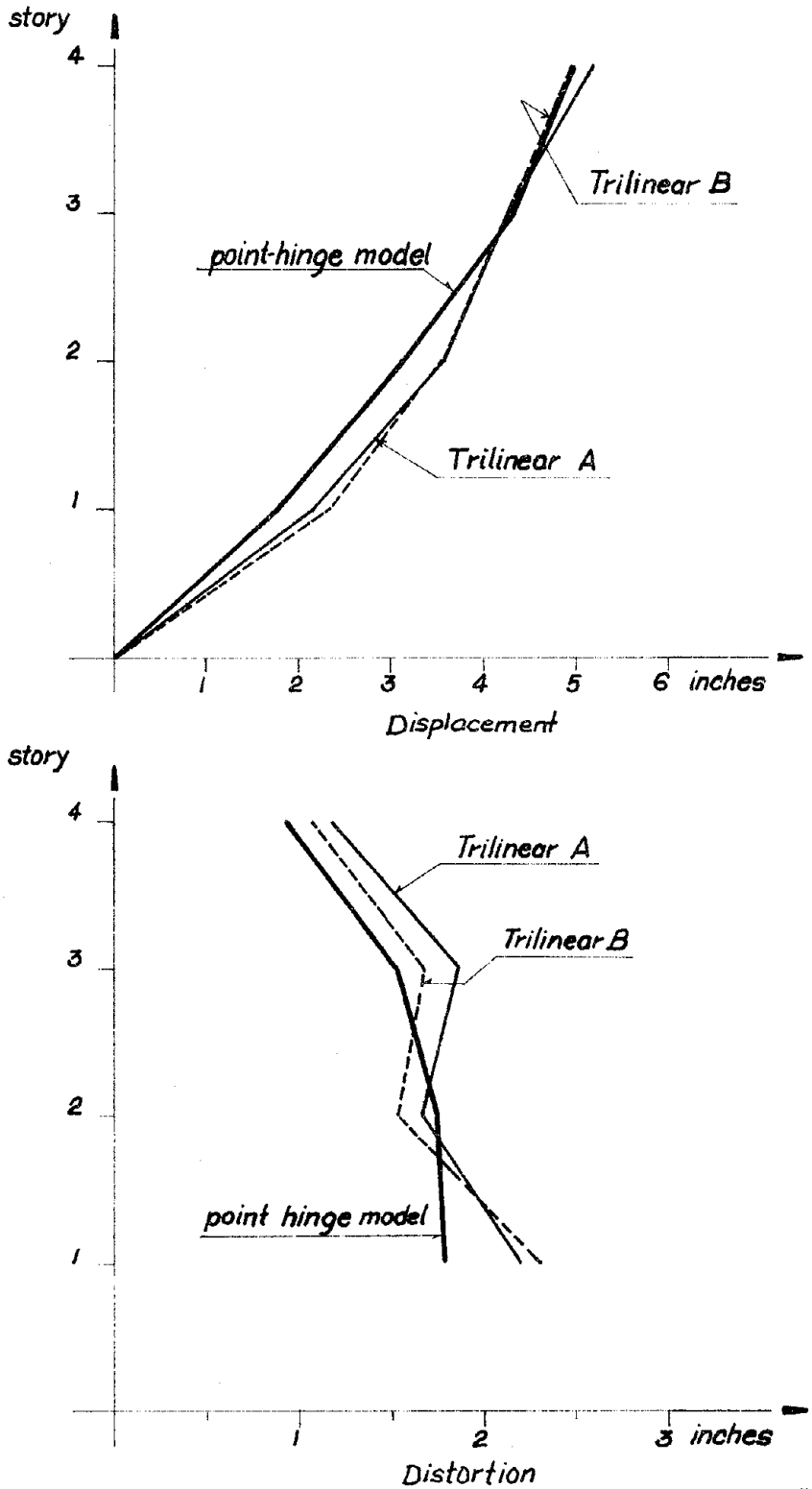

FIGURE 4.5 - 4-STORY UBC FRAME: POINT HINGE VS. TRILINEARS A AND B. $D+Q_{1st.\ mode}$. EL CENTRO. P-Δ

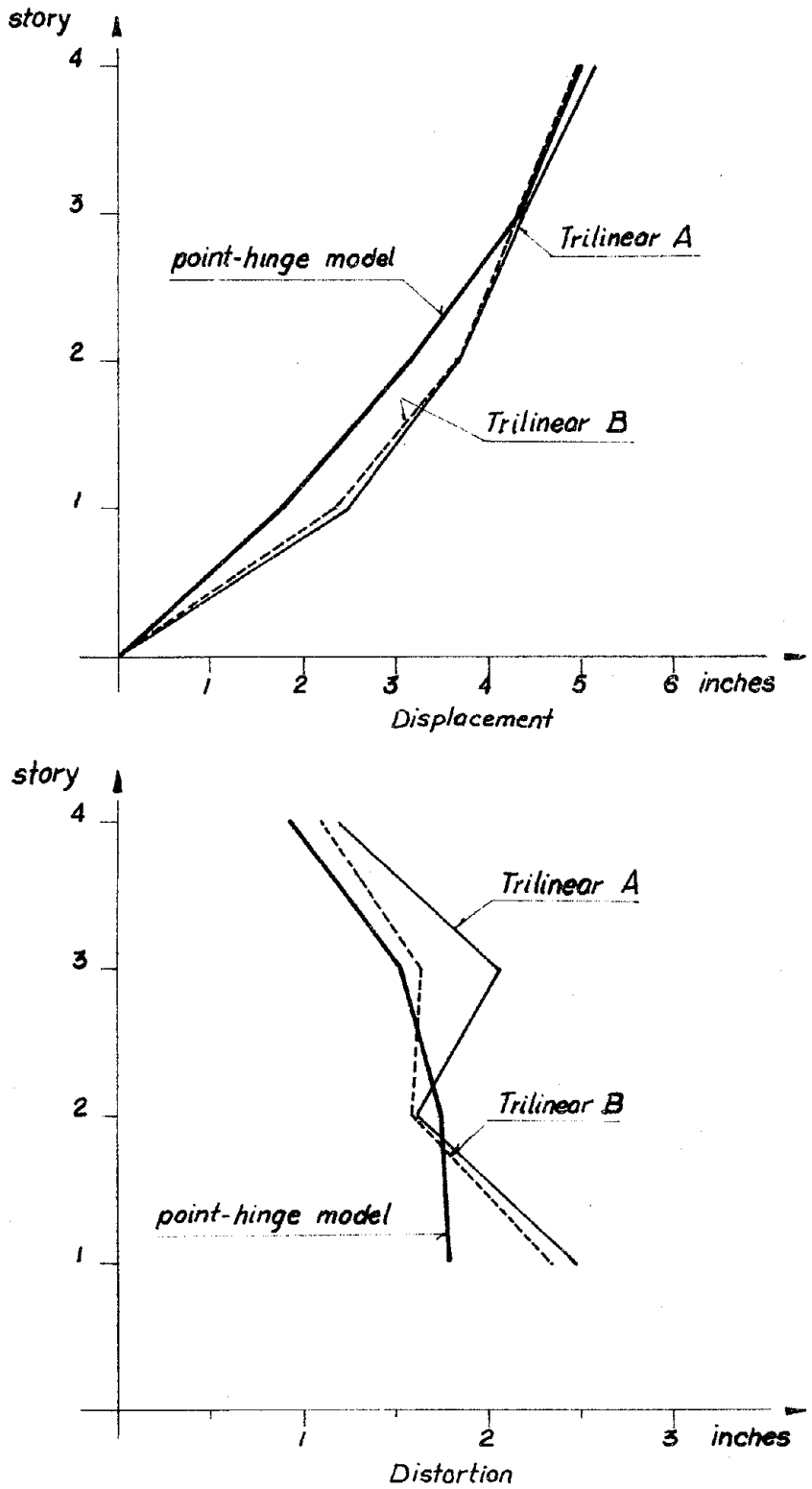

FIGURE 4.6 - 4-STORY UBC FRAME: POINT HINGE VS. TRILINEARS A AND B. $D+Q_{SRSS}$. EL CENTRO. P-Δ

the shear-beam model overestimates the response. The difference is within 30%, however. The trilinear springs B give a better agreement than the trilinear A in most cases and for both effects. Overall, the response using trilinear springs correlates better with the point-hinge response than using bilinear springs.

Figure 4.4 shows the response for the case of trilinears A and B from the code distributions with an ultimate slope within the range of interest. Results improved some in certain areas, but the difference is not as substantial as it was for the bilinear springs. The results of the analysis using the original trilinears are also included in this figure. It can be seen that the shape of the displacements envelope is not that of the point hinge or the other trilinears, but clearly that of a shear-beam first mode; although the actual magnitude of the displacements is in reasonable agreement with the point-hinge model. Distortions do not show the same correlation, but rather a shape shifted to the opposite side on the upper two stories and the same values on the first two.

Figures 4.7, 4,8, and 4.9 show results for the trilinears A and B from the three load distributions, but without including P-Δ effects. The floor displacements predicted by the point-hinge model are smaller by 10%; the shear-beam displacements, however, remain almost the same. Agreements between the two models is less close than for the cases with P-Δ effect. The trilinear B still provides the best correlation, except for the case using springs from the first mode shape distribution.

Distortions change less than displacements on the point-hinge model, and about the same for the shear-beam responses. This results in similar

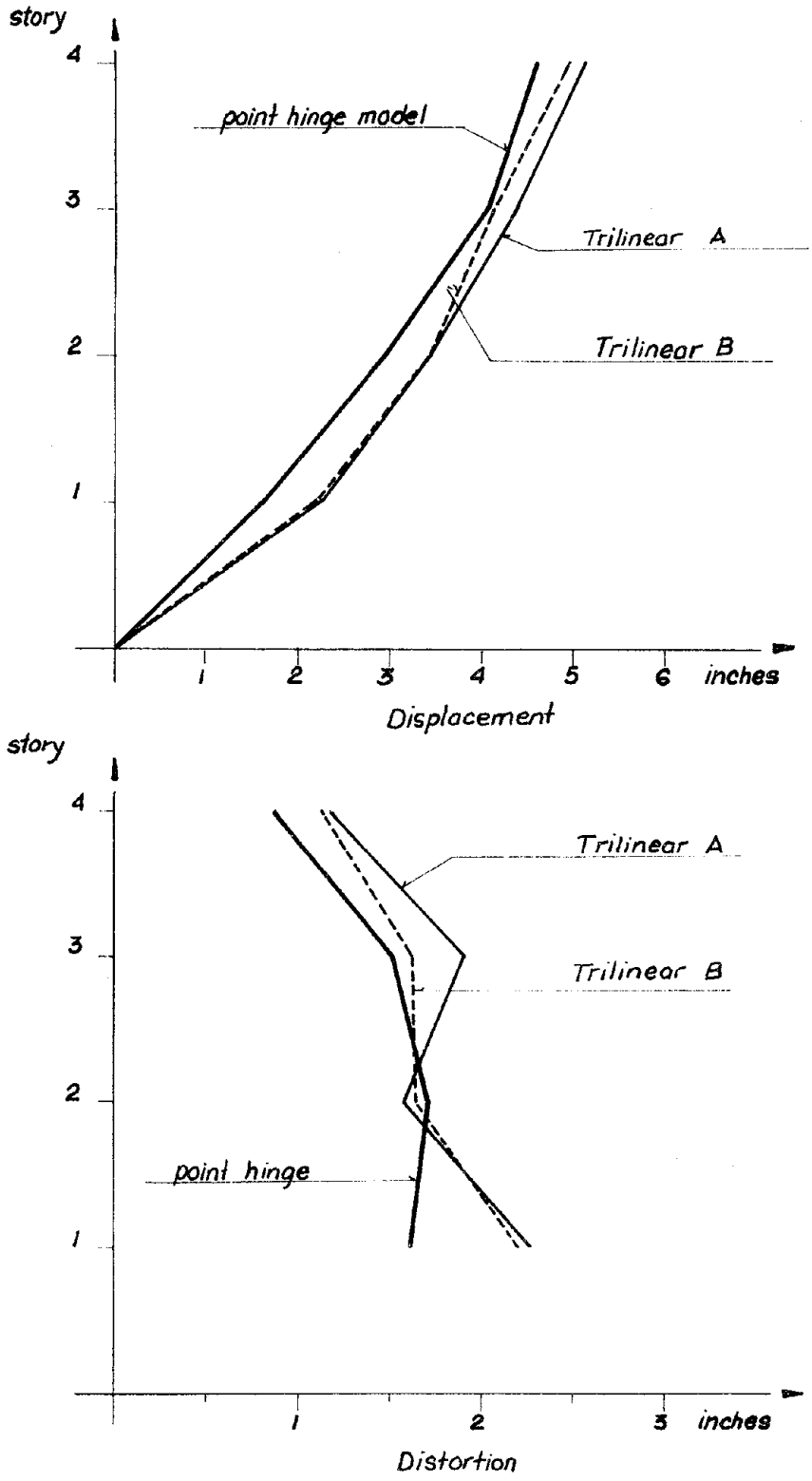

FIGURE 4.7 - 4-STORY UBC FRAME: POINT HINGE VS. TRILINEARS A AND B $D+Q_{code}$. EL CENTRO. NO P-Δ.

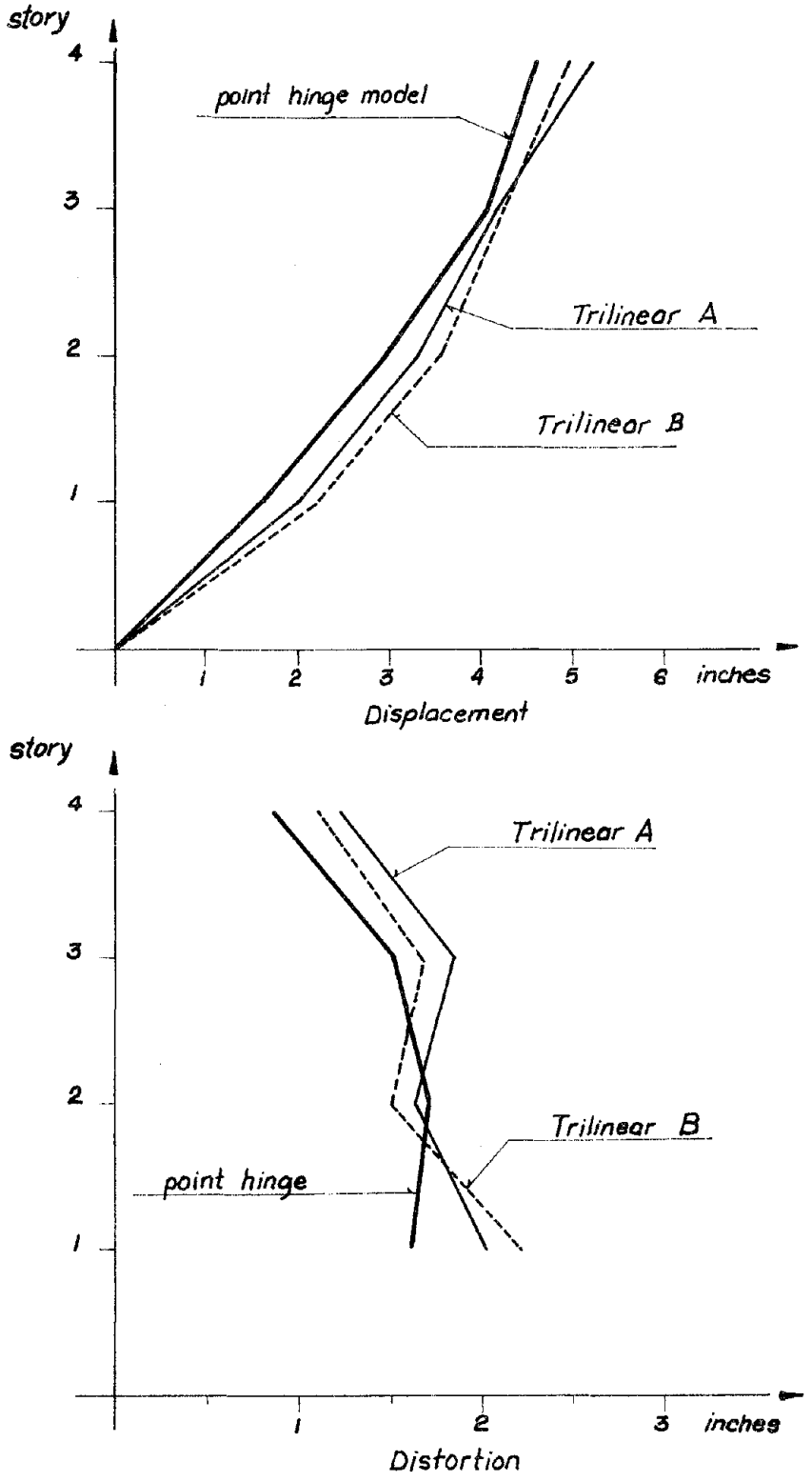

FIGURE 4.8 - 4-STORY UBC FRAME; POINT HINGE VS. TRILINEARS A AND B. $D+Q_{1st.\ mode}$. EL CENTRO. NO P-Δ

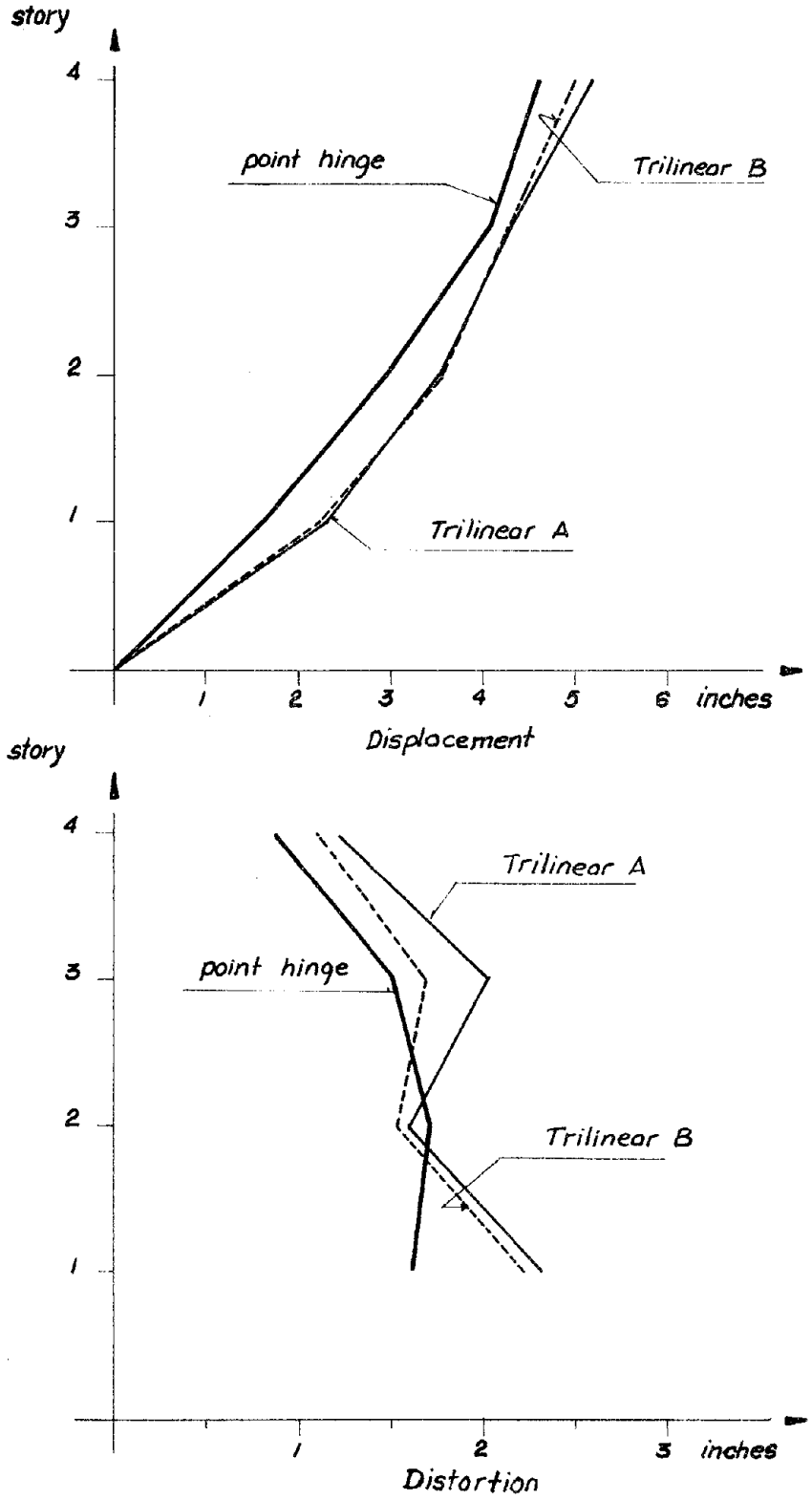

FIGURE 4.9 - 4-STORY UBC FRAME: POINT HINGE VS. TRILINEARS A AND B

$D+Q_{all\ modes}$. EL CENTRO. NO P-Δ

agreements as for the case with P-Δ effect.

The influence of the lateral load distribution on the response is also very small for this case, all of them producing similar results.

Figure 4.10 shows the response from the point-hinge model as compared to the bilinear and trilinears A and B for a ground excitation of twice El Centro. The springs were obtained using the code distribution. For displacements, the trilinear spring "B" gives the best agreement with the point-hinge model as it did in the preceding cases. The discrepancies are always below 14%. For distortions, however, the bilinear spring is the one whose predictions agree better with the point-hinge model. All the results maintain the same correlation as they did for once El Centro in terms of envelope shapes and relative magnitude of the responses.

4.3.2 Ten-Story UBC Frame

Figures 4.11 and 4.12 show the responses predicted by the bilinear springs from the code, first mode, and SRSS of all modes distributions, in comparison with the response using the point-hinge model. The results using the original bilinears are also presented in the same figures. All analyses were performed using the interaction yield criterion and including P-Δ effects. The ultimate slope of the plots was taken as the second branch of the bilinear springs. The envelopes from the code and first mode distributions give very similar responses. The bilinear from the SRSS of all modes gives slightly larger values than the other two. The agreement between this last one and the point-hinge model envelope for displacements is remarkably close. For the other distributions the agree-

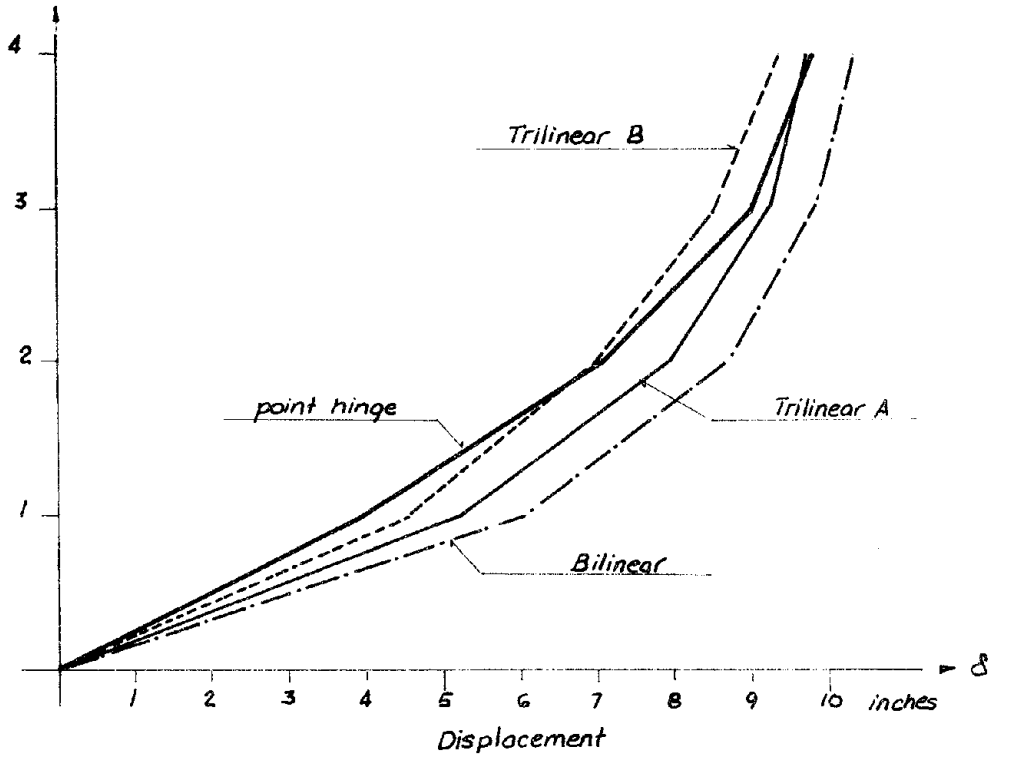

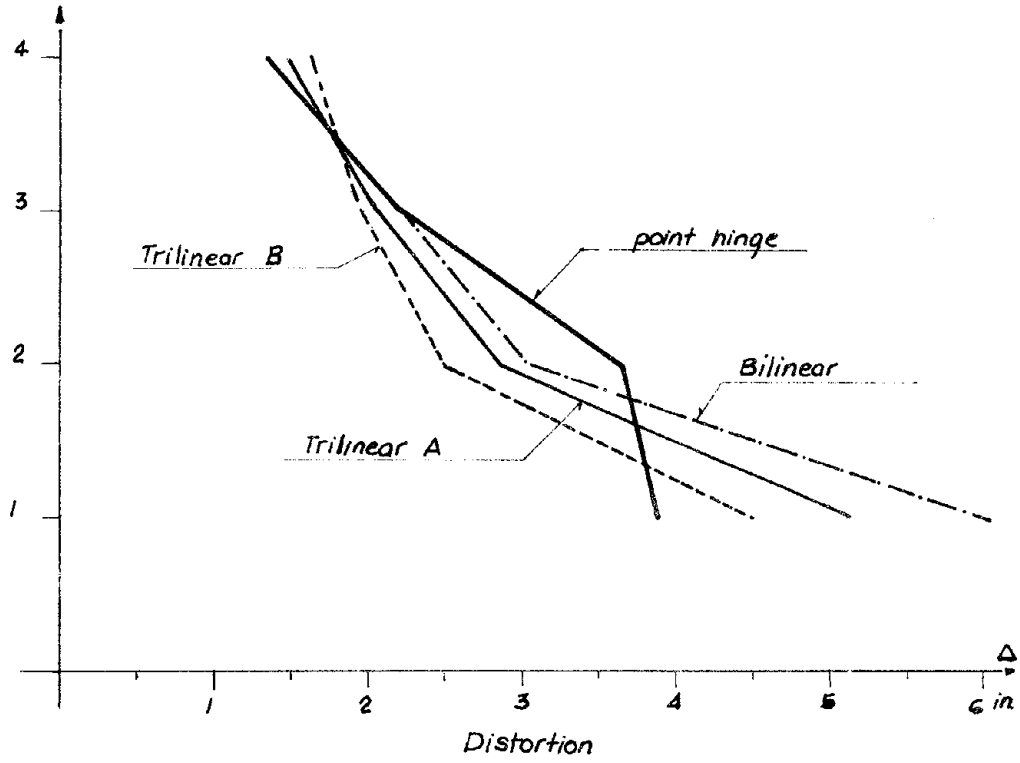

FIGURE 4.10 - 4-STORY UBC FRAME: POINT HINGE VS. BILINEAR, TRILINEAR A AND B. $D+Q_{code}$. 2 x EL CENTRO. P-Δ

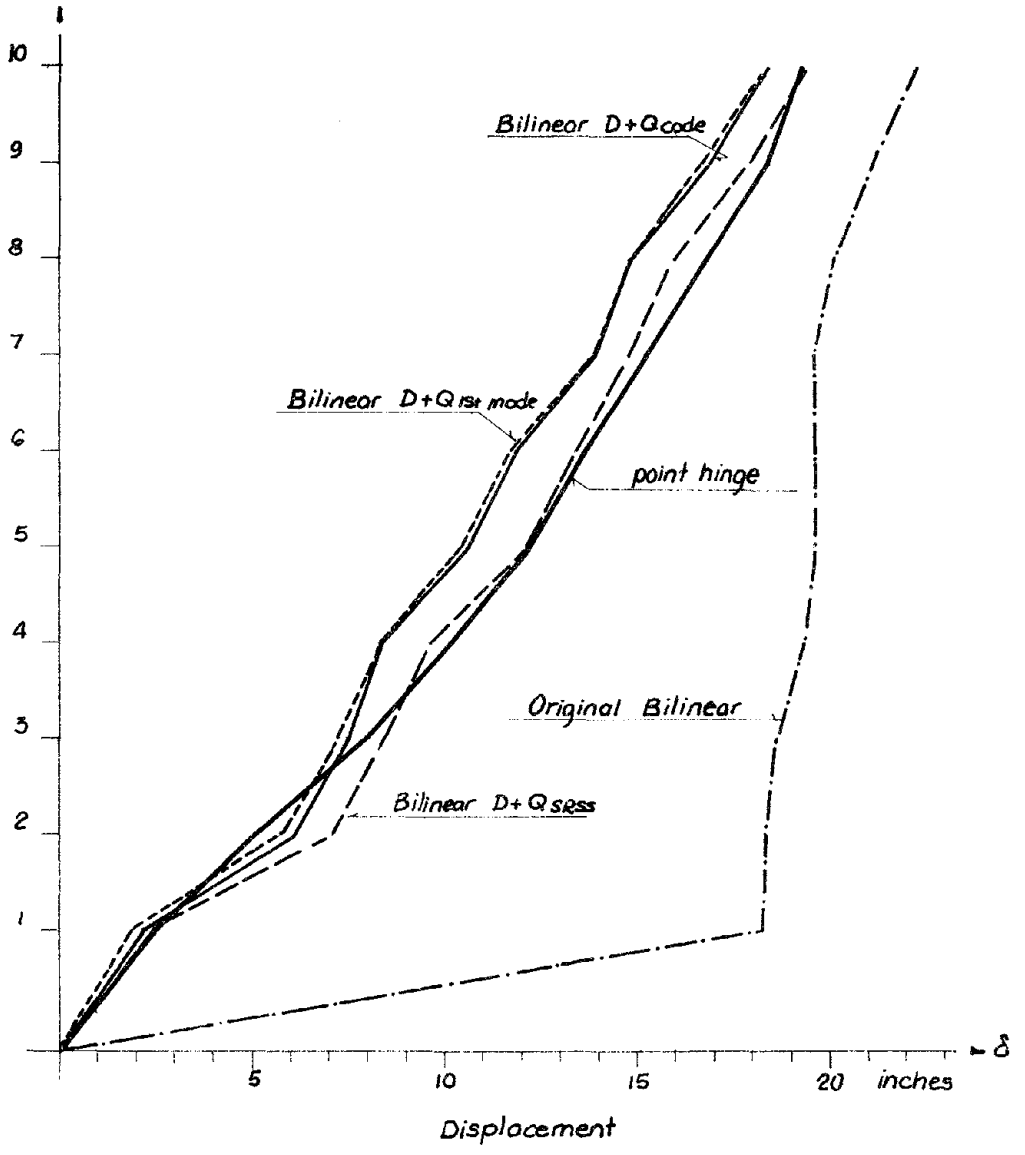

FIGURE 4.11 - 10-STORY UBC FRAME: FLOOR DISPLACEMENTS. POINT HINGE VS BILINEAR SPRINGS. EL CENTRO. P- △

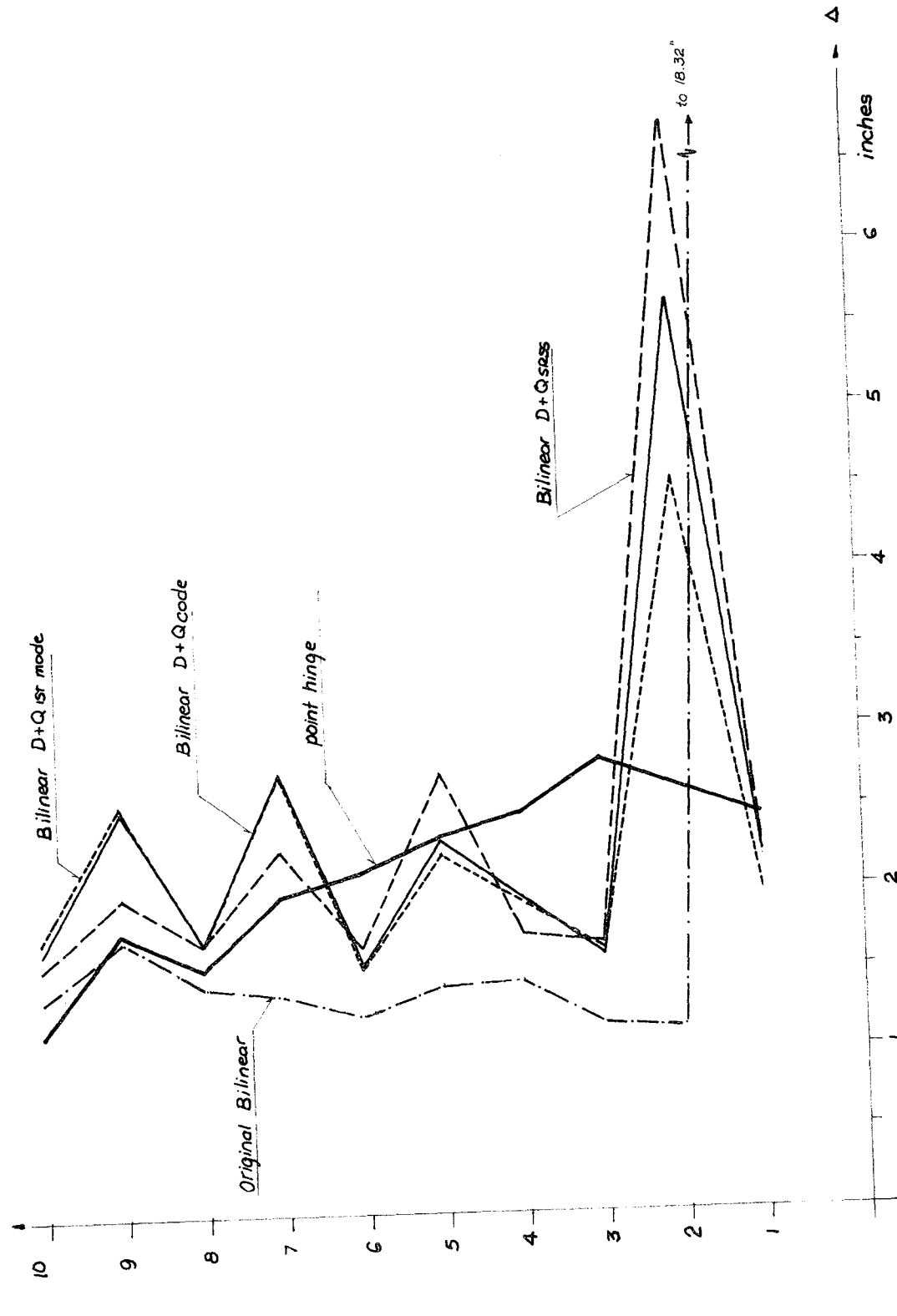

FIGURE 4.12 - 10-STORY UBC FRAME. DISTORTIONS. POINT HINGE VS. BILINEAR SPRINGS. EL CENTRO. P-Δ

ment is reasonable, remaining within 15%. An interesting fact must be noted, however, and that is the large interstory displacement for story two. This causes the whole upper part of the structure to shift closer towards the point-hinge envelope, resulting in good agreement on the upper floors. Had the second-story distortions remained of the same order as for the other floors, the bilinear springs would have underestimated the response as the other shear springs did for this particular frame.

The original bilinear predicts a very large first-story displacement, forcing the upper stories to a small additional displacement. The shape is in this case like the extreme case of a shear beam.

The distortion envelopes appear very jagged along the height. On the second floor a large value is recorded for the bilinear springs of the order of two-and-a-half the point-hinge prediction. Overall the agreement is rather poor.

Figures 4.13 to 4.18 show the envelopes for displacements and distortion obtained from the trilinear springs A and B for the code, first mode and SRSS of all modes distributions, all using the interaction yield criterion and including P-Δ effect.

Results for all distributions are very similar at all floors. In the case of distortions this also happens except for some specific floors. (The differences on these curves appear amplified because of the expanded scale for distortions in comparison to the one of displacements).

The shear-beam model underestimates the floor displacements at all floors, with differences of up to 30% found in some floors. The shape of

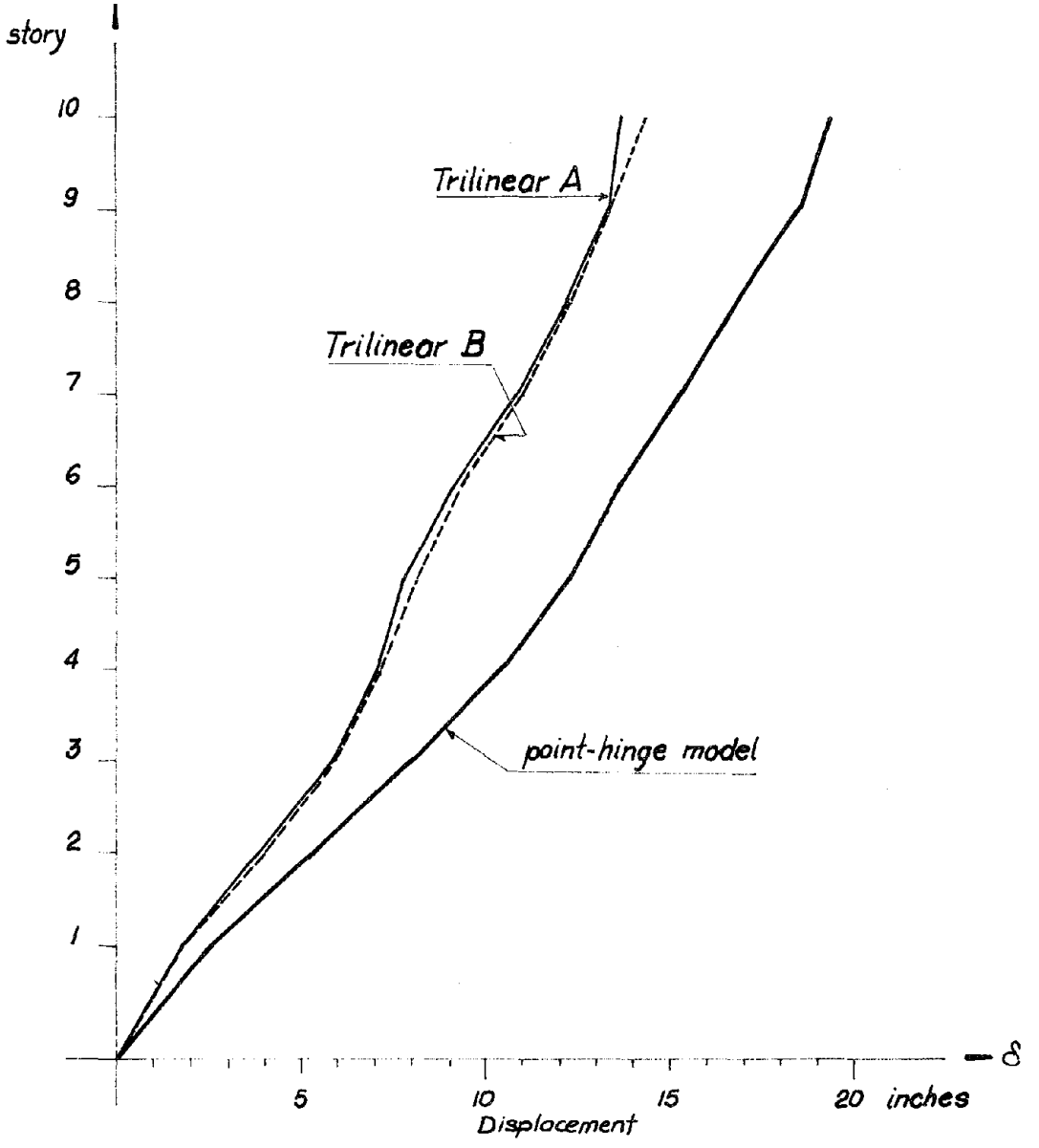

FIGURE 4.13 - 10-STORY UBC FRAME. FLOOR DISPLACEMENTS. POINT HINGE VS. TRILINEARS A AND B. $D+Q_{code}$. EL CENTRO. P-Δ

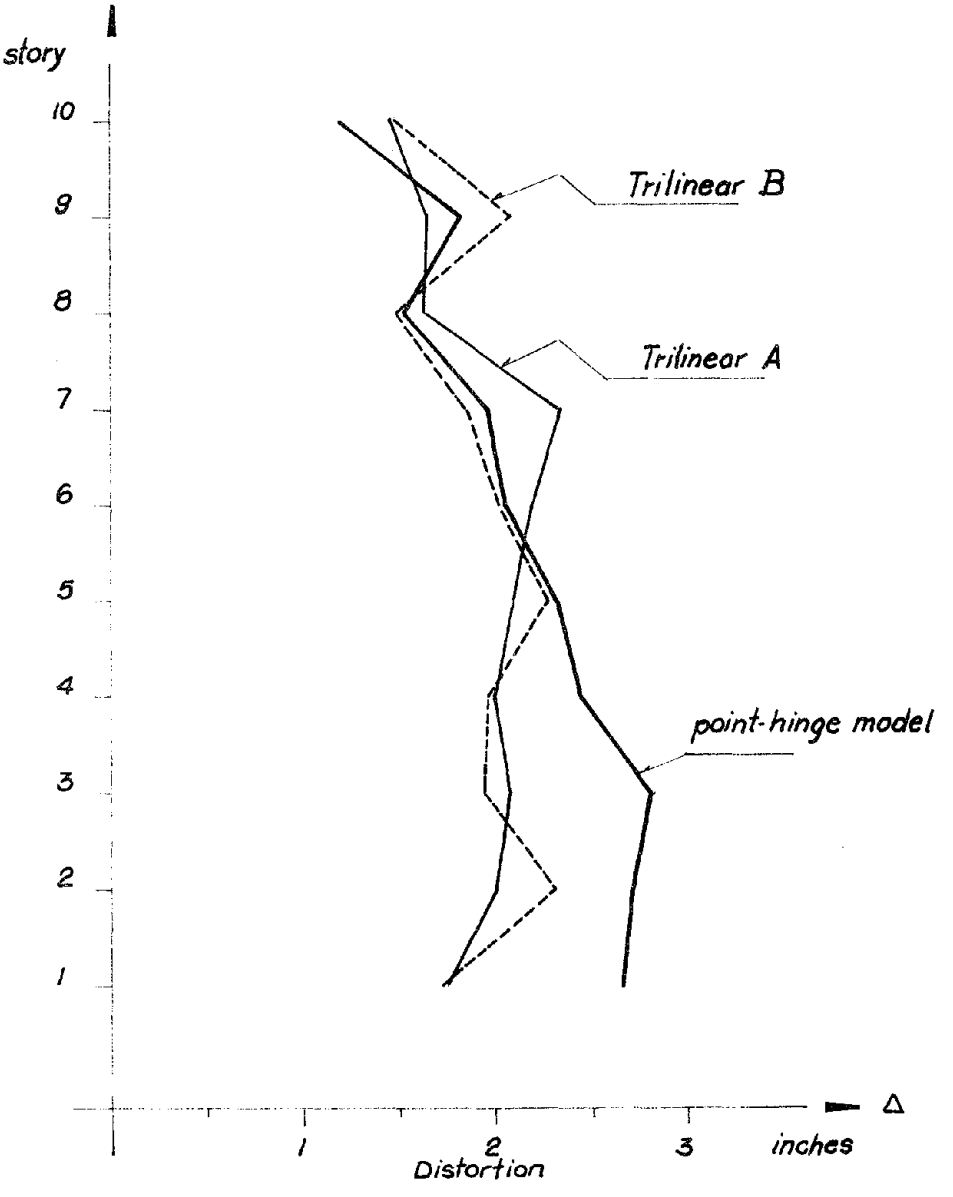

FIGURE 4.14 - 10-STORY UBC FRAME. DISTORTIONS. POINT HINGE VS. TRILINEARS A AND B. $D+Q_{code}$. EL CENTRO. P-Δ

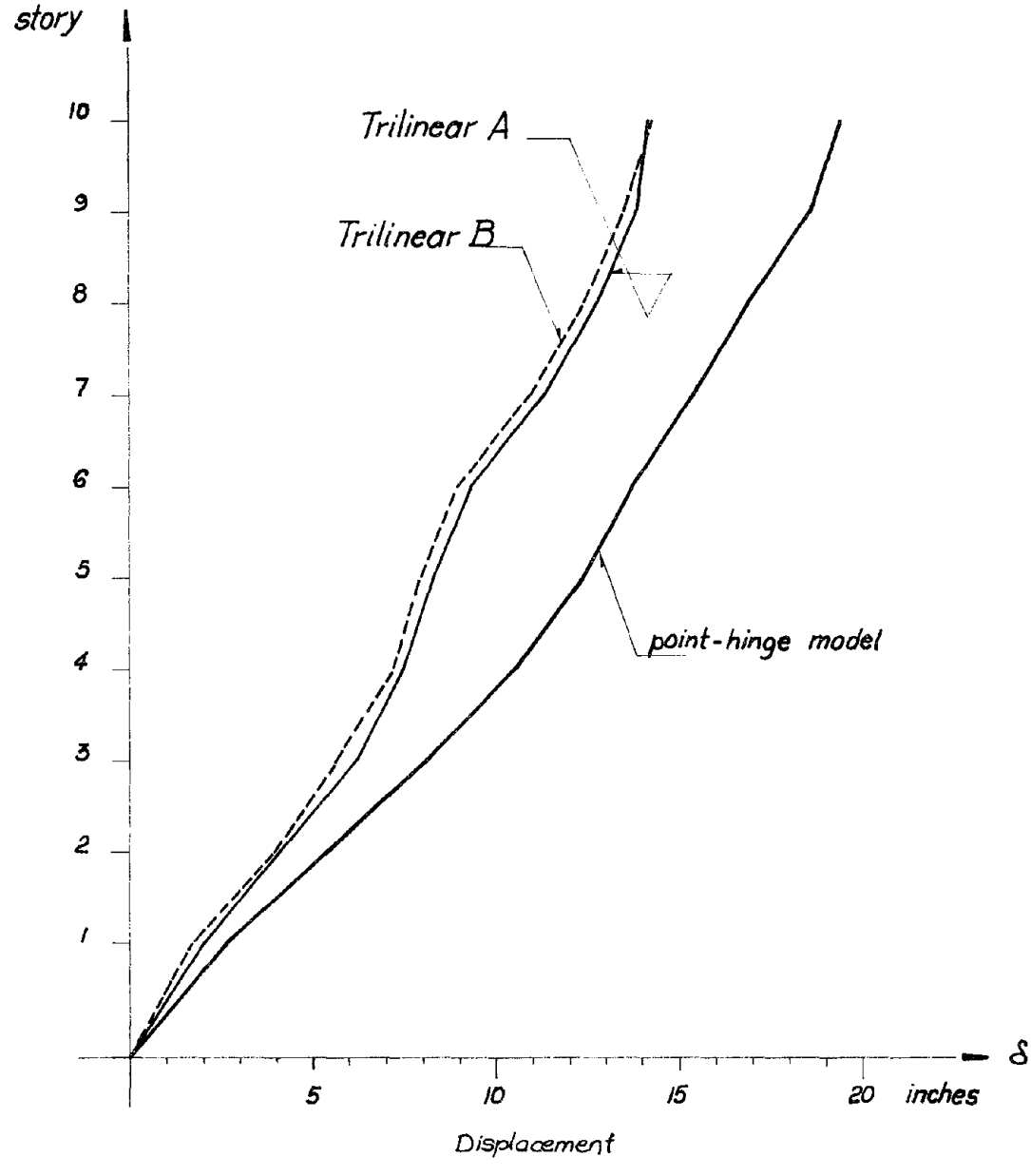

FIGURE 4.15 - 10-STORY UBC FRAME. FLOOR DISPLACEMENTS. POINT HINGE VS. TRILINEARS A AND B. $D+Q_{1st.\ mode}$. EL CENTRO. P-Δ

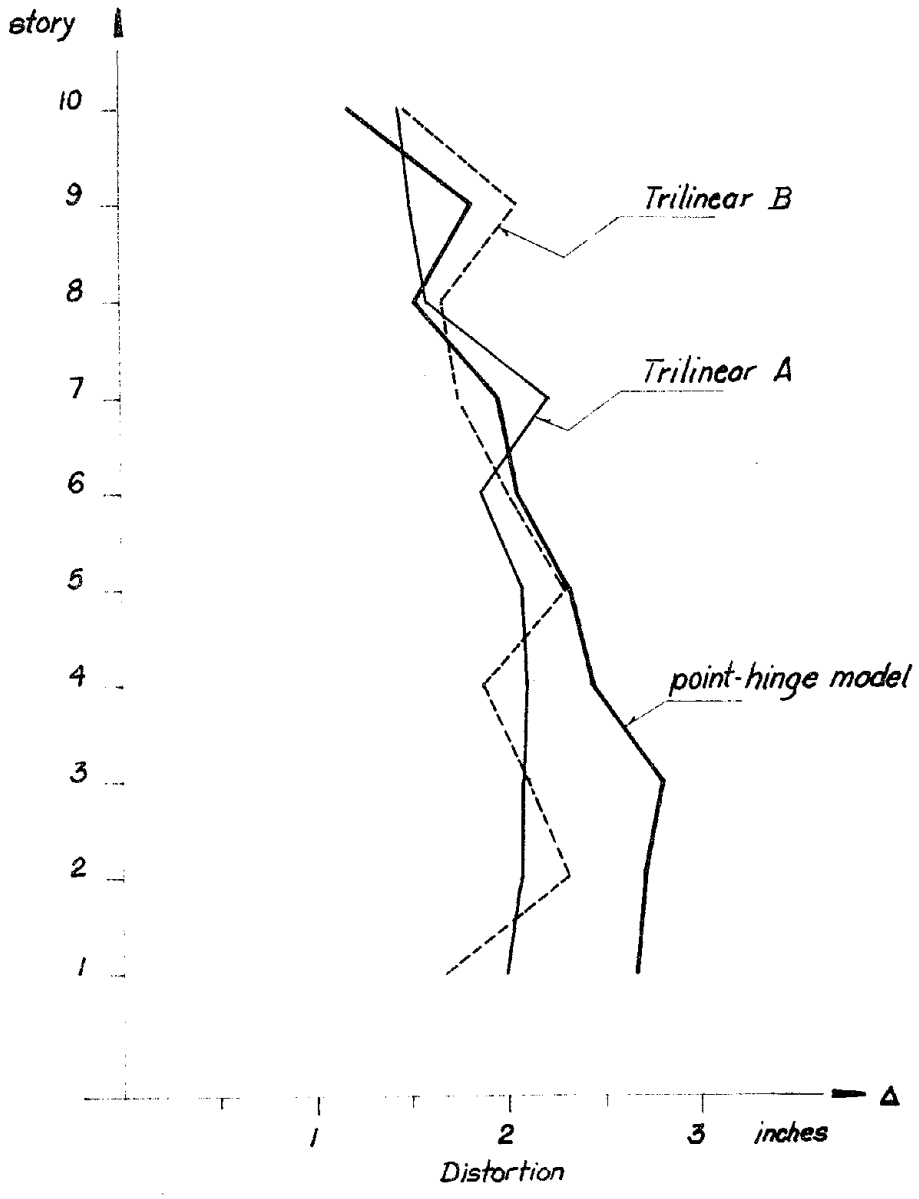

FIGURE 4.16 - 10-STORY UBC FRAME. DISTORTIONS. POINT HINGE VS. TRILINEARS A AND B. $D+Q_{1st.\ mode}$. EL CENTRO. P-Δ

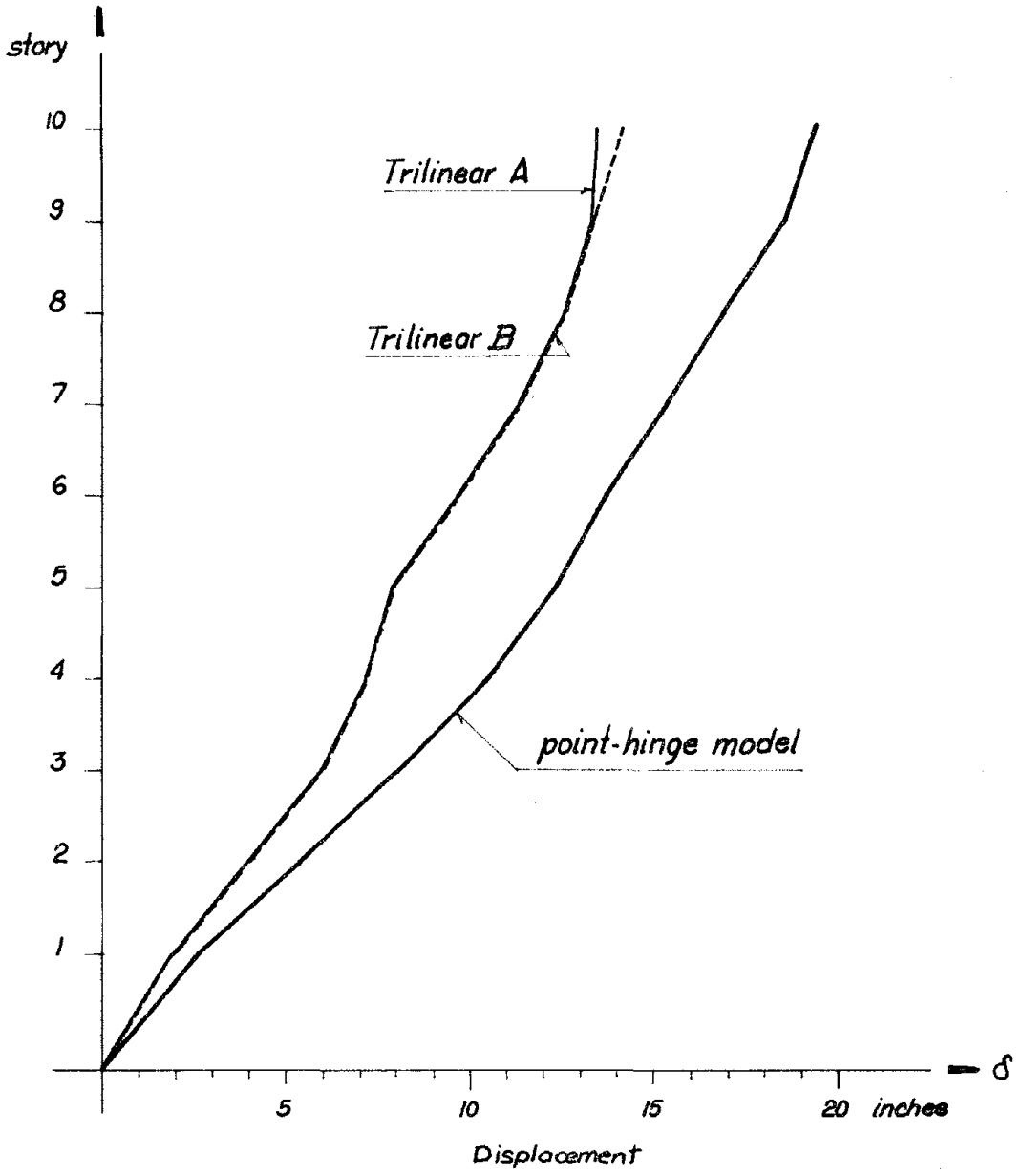

FIGURE 4.17 - 10-STORY UBC FRAME. FLOOR DISPLACEMENTS. POINT HINGE VS. TRILINEARS A AND B. $D+Q_{all\ modes}$. EL CENTRO. P-Δ

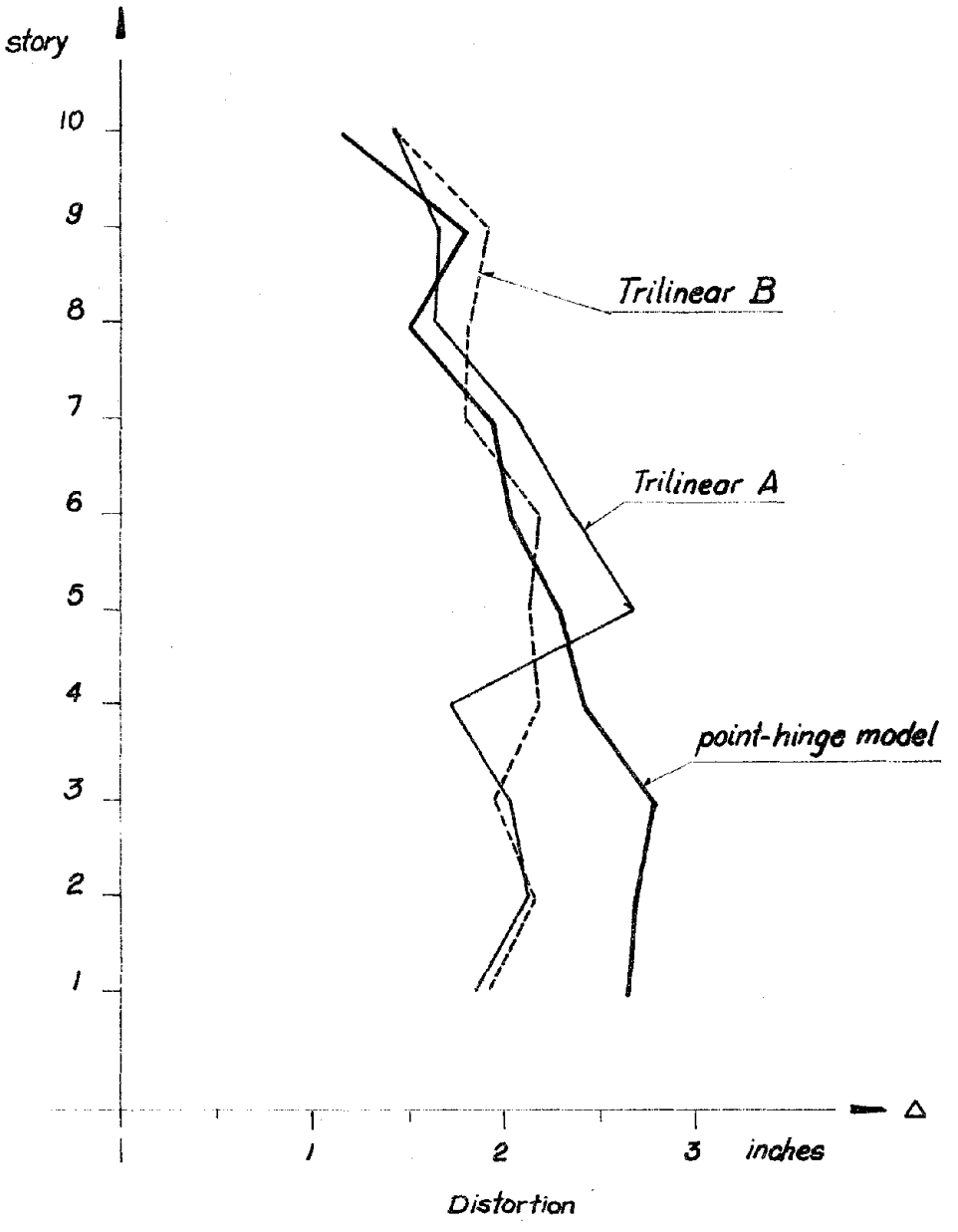

FIGURE 4.18 - 10-STORY UBC FRAME. DISTORTIONS. POINT HINGE VS. TRILINEARS A AND B. $D+Q_{all\ modes}$. EL CENTRO. P-Δ

the curve, however, is reasonably reproduced, and it is only from floors four to seven that there is a "curvature" reversal of the envelope.

Distortions are underestimated on the first four floors, the largest difference being on the first floor (30%). On the upper floors the agreement is reasonable once the shape of the curve is better reproduced, especially by the trilinear B of the code distribution. Taking the average distortion over height, the agreement is acceptable. The response predicted by these springs is very similar to the one predicted using multilinear springs as presented in Chapter 3 (see Figures 3.17 and 3.18). for example).

Figures 4.19 and 4.20 show the response from the bilinear and trilinear springs whose ultimate slope was read on the range of interest of the curves, all for the code distribution only. There are rather small changes in the response as when using the other ultimate slope.

The original springs give an envelope of displacements with a similar shape to the first mode of a shear beam, resulting in an overestimation of the response in the first two floors and an even larger underestimation of the response on the upper floors. The distortions predicted by the original trilinear are rather erratic at most levels, with little relation to either the point-hinge or the other shear-beam models.

Figures 4.21 and 4.22 show the results for the trilinear springs A and B from the code distribution but without including P-Δ effect. Changes on the displacement envelopes are very small for both models. Only stories seven to nine experience a small reduction in displacements.

In the case of distortions also very small variations occur,

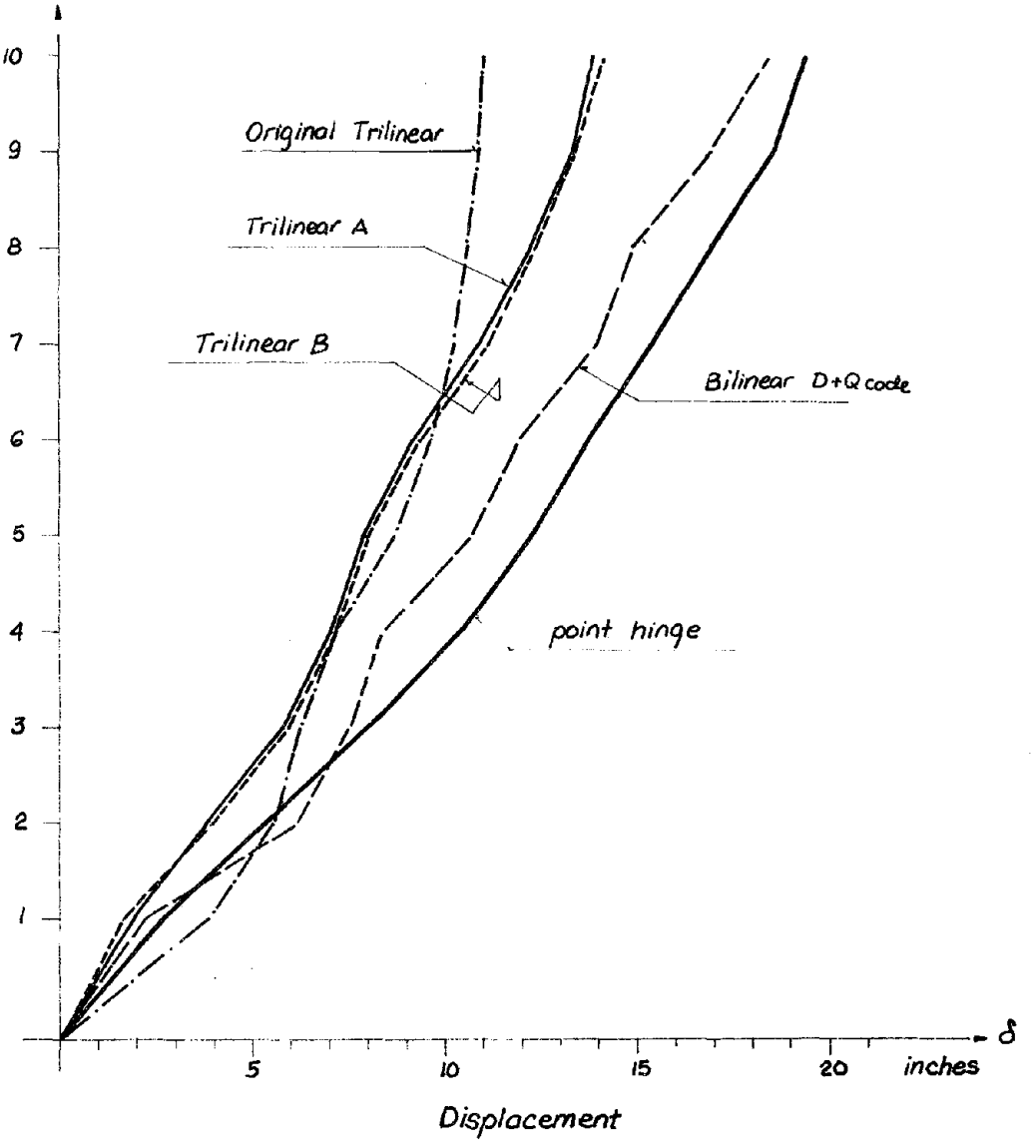

FIGURE 4.19 - 10-STORY UBC FRAME. FLOOR DISPLACEMENTS. POINT HINGE VS. BILINEAR AND TRILINEAR SPRINGS A AND B. EL CENTRO. P-Δ

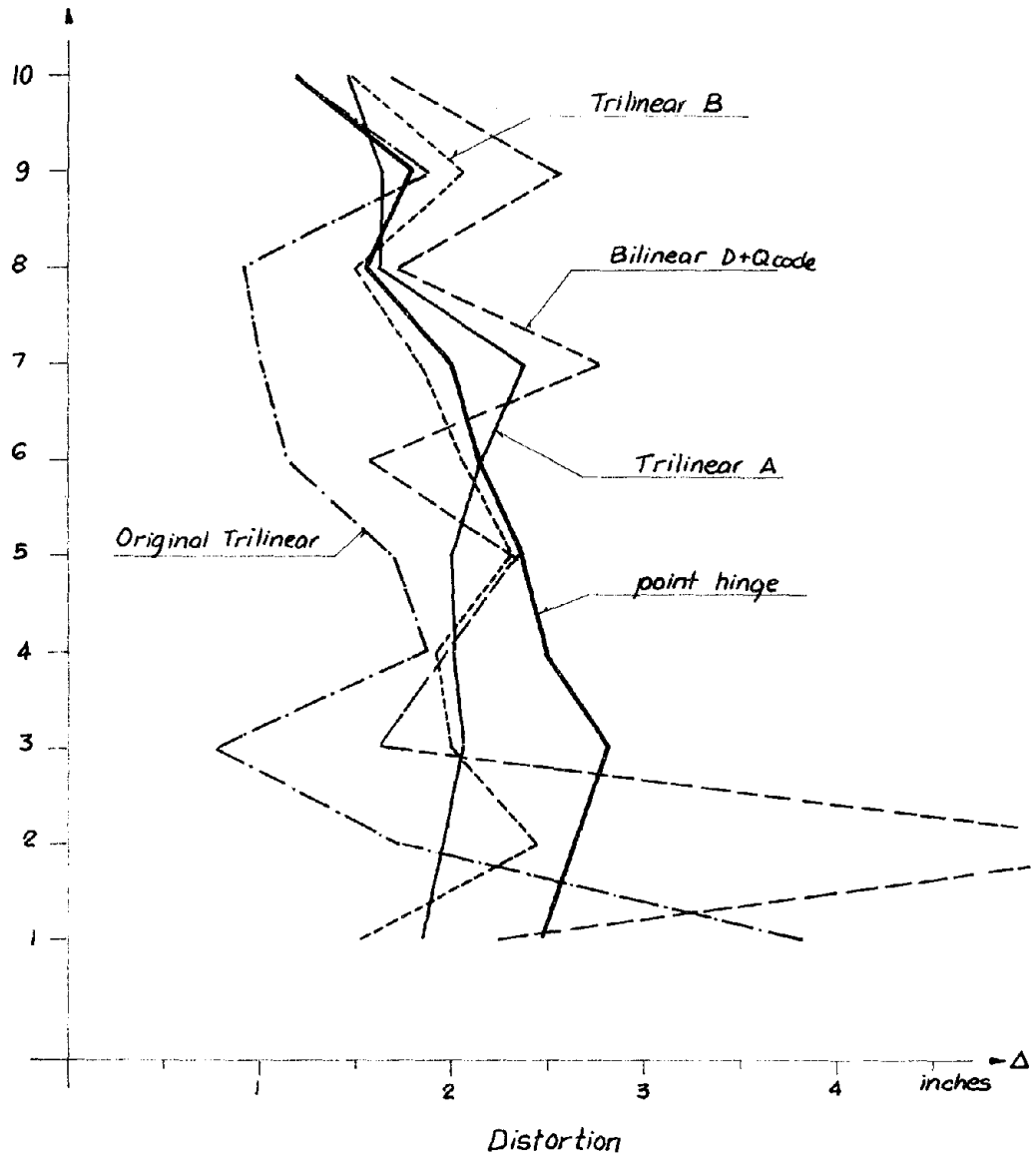

FIGURE 4.20 - 10-STORY UBC FRAME. DISTORTIONS. POINT HINGE VS. BILINEAR AND TRILINEAR SPRINGS A AND B. EL CENTRO. P-Δ

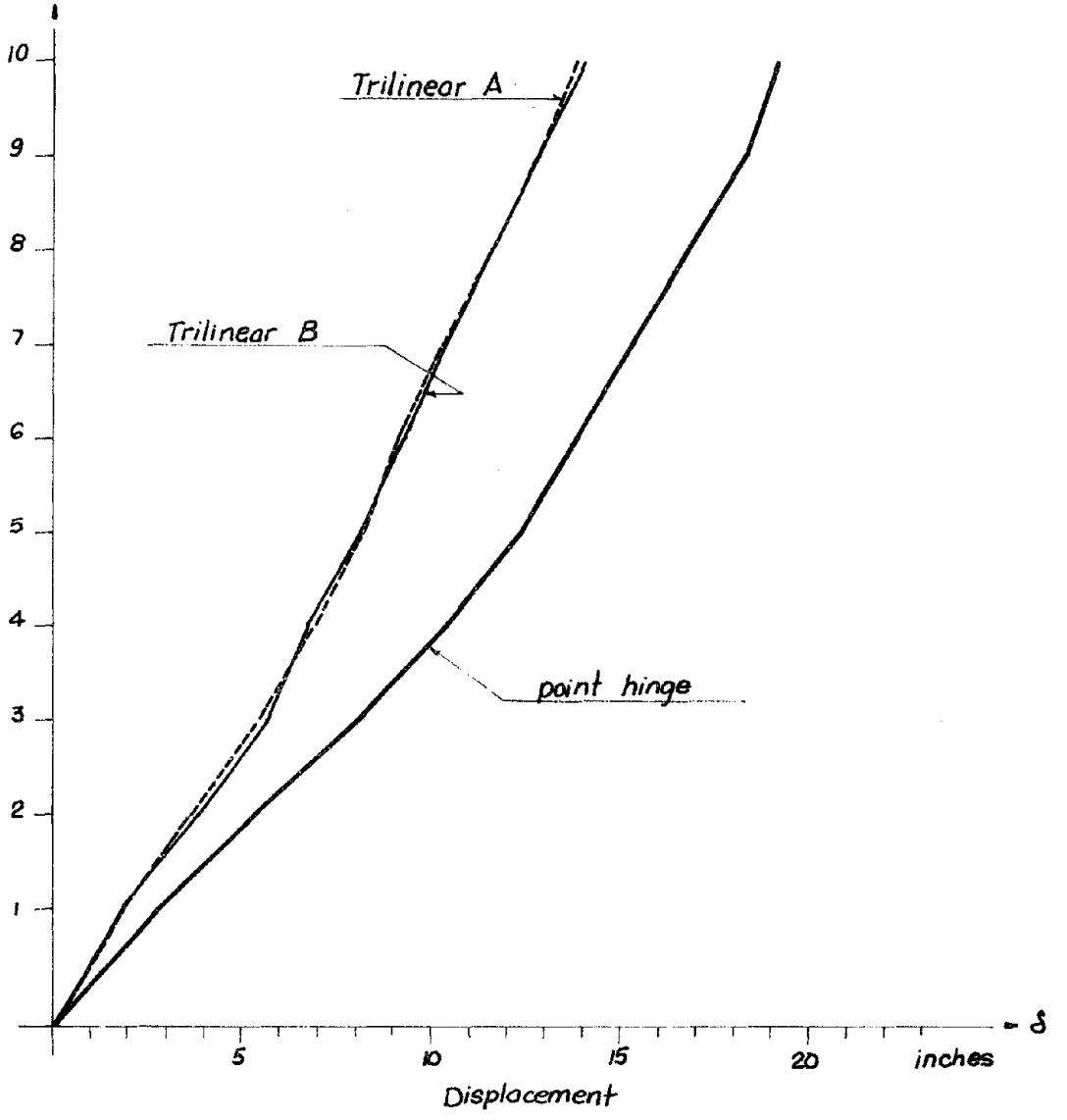

FIGURE 4.21 - 10-STORY UBC FRAME. FLOOR DISPLACEMENTS. POINT HINGE VS. TRILINEARS A AND B. $D+Q_{code}$. EL CENTRO. NO P-Δ.

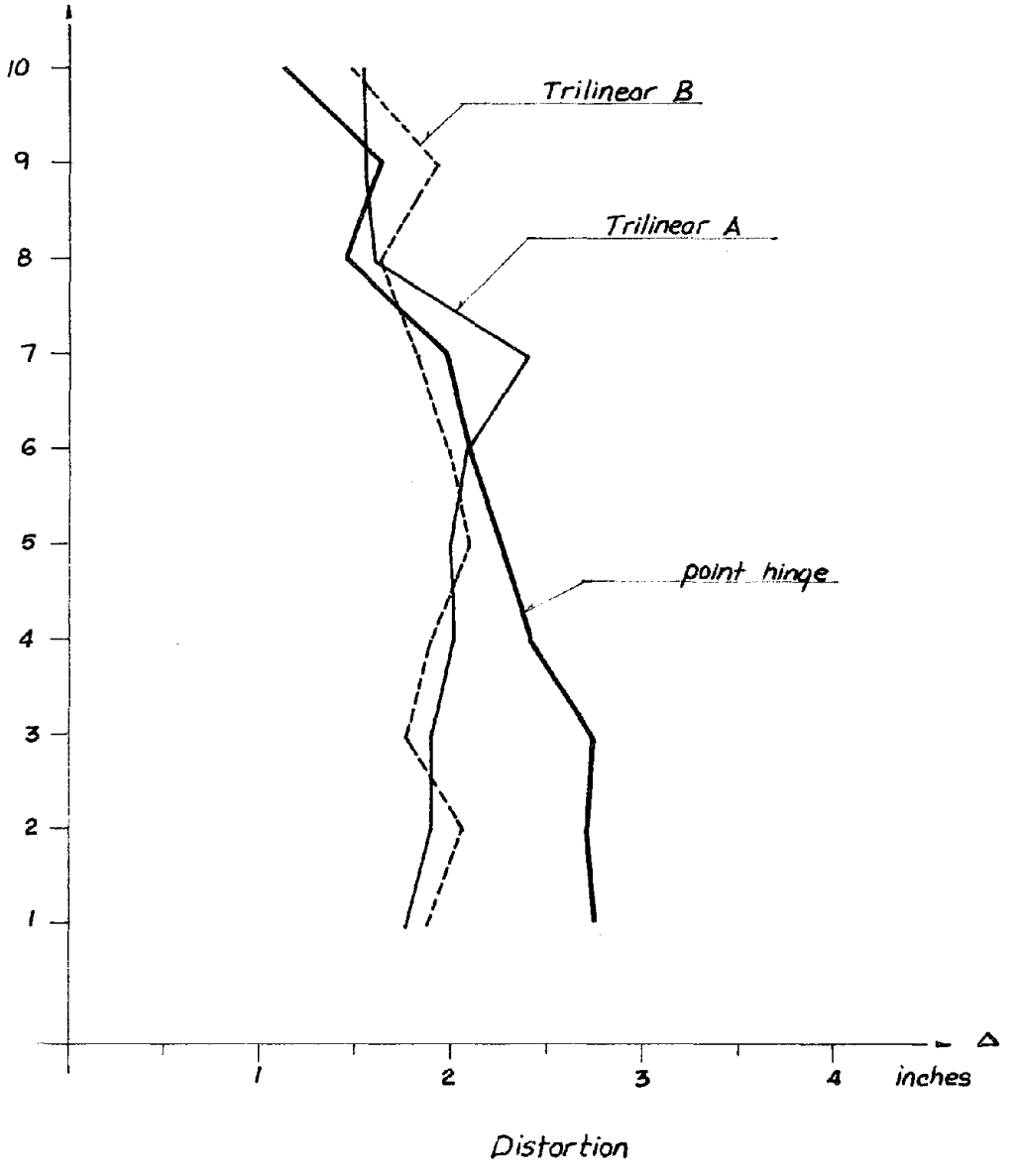

FIGURE 4.22 - 10-STORY UBC FRAME. DISTORTIONS. POINT HINGE VS. TRILINEARS A AND B. $D+Q_{code}$. EL CENTRO. NO P-Δ.

maintaining the same kind of agreement as for the cases with P-Δ. Similar behavior is obtained for the first mode and SRSS of all modes distributions for both trilinear springs.

4.3.3 Sixteen-Story UBC Frame

Figures 4.23 and 4.24 show the comparisons for the envelopes from the point-hinge model and the bilinear model corresponding to the code lateral load distribution. The second slope of the bilinear spring was estimated at the range of interest of the curve. The interaction yield criterion was used and P-Δ effects were included. The envelopes for displacements show reasonable agreement between the two curves. The shape of the shear-beam curve is not quite proportional over the height, since it underpredicts the response on the lower four stories and then crosses the point-hinge envelope, increasing its values as it goes upwards. Discrepancies accentuate on floors 10 to 12 and then at the top of the building. The maximum difference is 21% on the fifteenth story. In terms of distortions, however, there are some specific floors where the discrepancies are very large, as on floor thirteen, for example. The others show a jagged curve that does not follow the point-hinge envelope. This pattern of behavior predicted by the bilinear springs seems to be the same as for the ten-story frame: reasonable agreement on displacements, but some exaggerated discrepancies on distortions.

Figure 4.25 and 4.26 show the results of the analysis using the trilinear spring "A" from the same curves used above for the bilinear approximation. The agreement for displacements is very good, with only localized

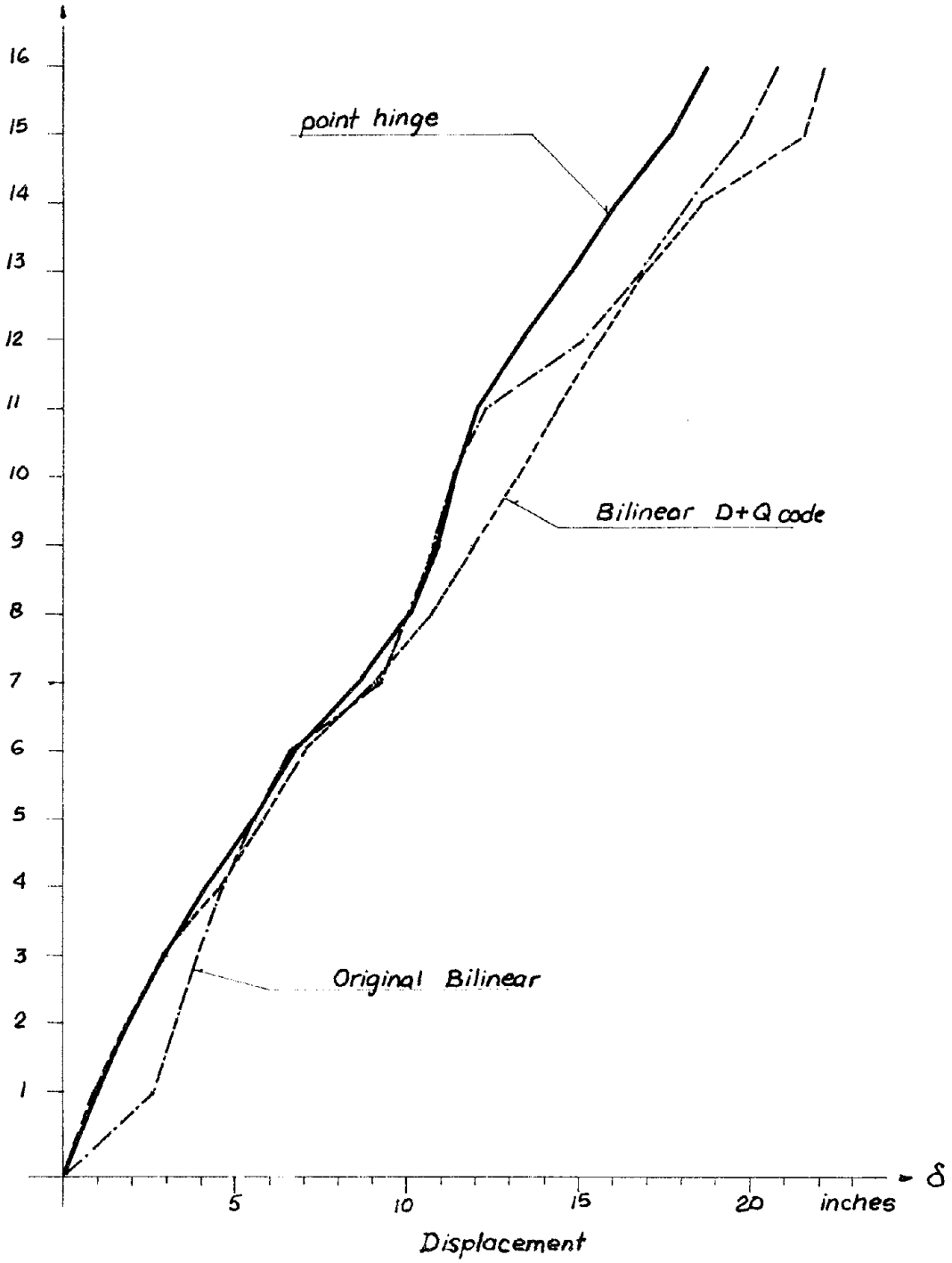

FIGURE 4.23 - 16-STORY UBC FRAME. FLOOR DISPLACEMENTS. POINT HINGE VS. BILINEAR SPRINGS. EL CENTRO. P-Δ.

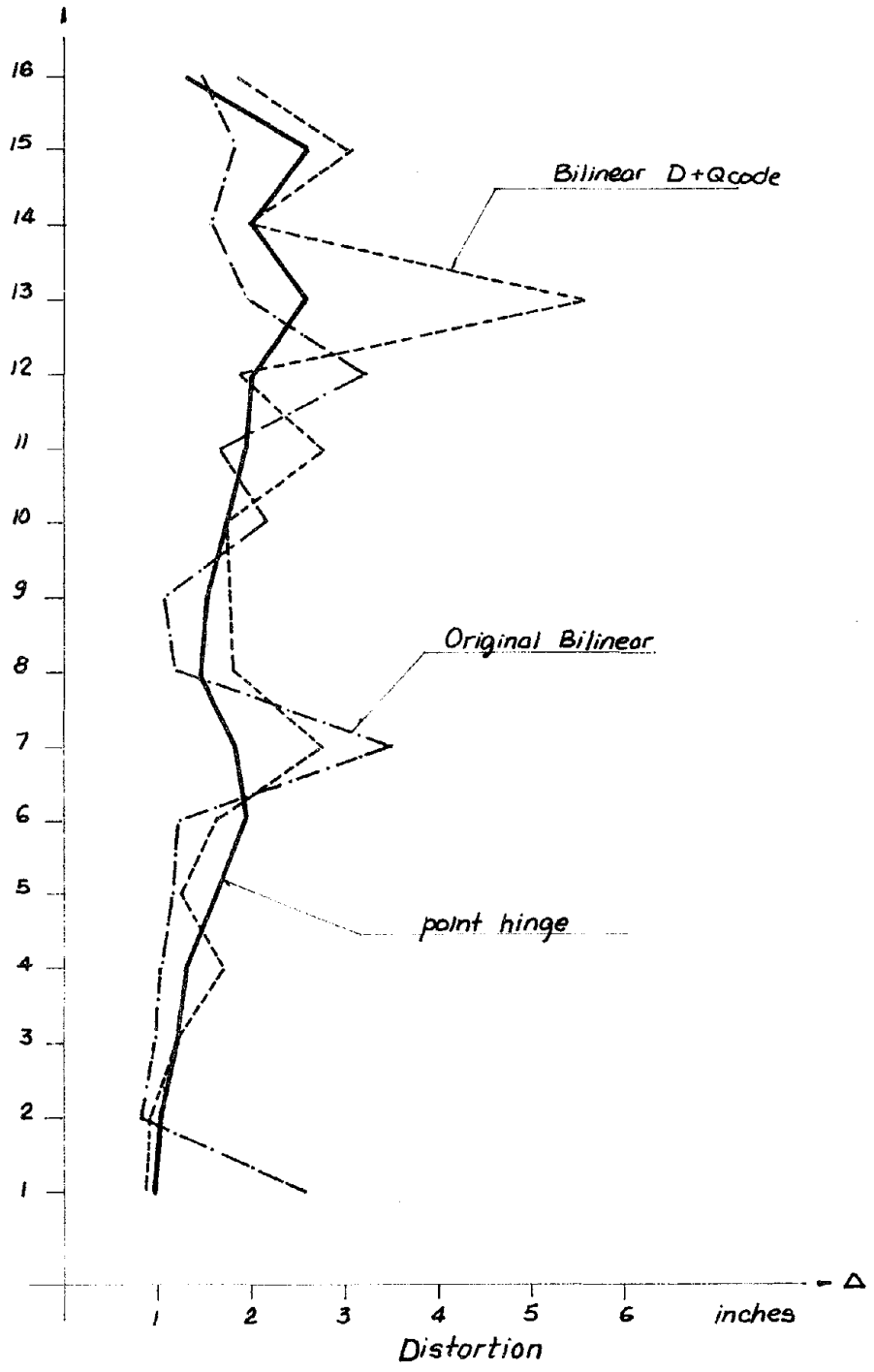

FIGURE 4.24 - 16-STORY UBC FRAME. DISTORTIONS. POINT HINGE VS. BILINEAR SPRINGS. EL CENTRO. P-Δ

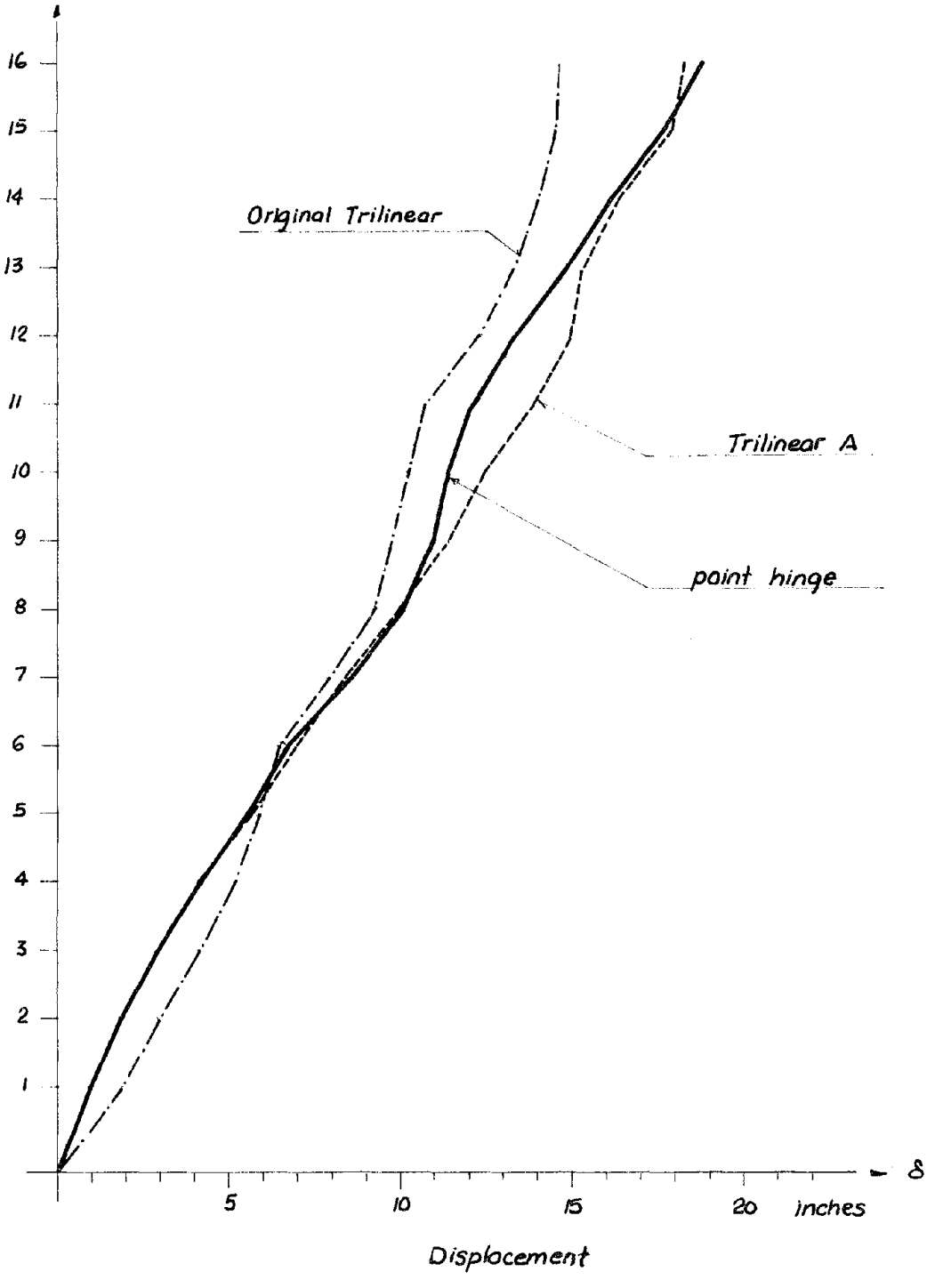

FIGURE 4.25 - 16-STORY UBC FRAME. FLOOR DISPLACEMENTS. POINT HINGE VS. TRILINEAR SPRINGS. EL CENTRO. P-Δ

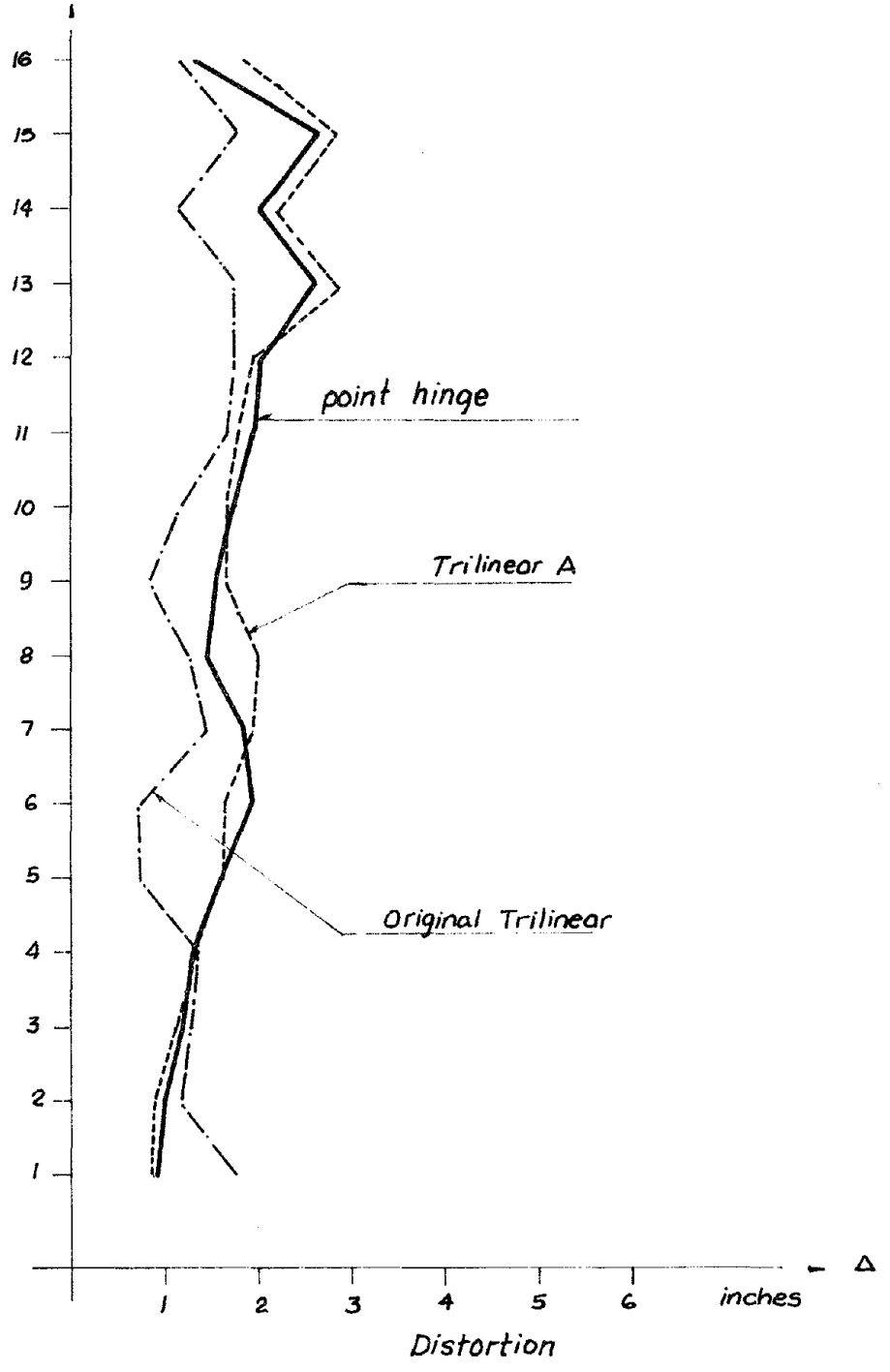

FIGURE 4.26 - 16-STORY UBC FRAME. DISTORTIONS. POINT HINGE VS. TRILINEAR SPRINGS. EL CENTRO. P-Δ

discrepancies as in floor eleven. This amounts to 13%, and less in all the other floors. Up to floor nine the shear-beam model gives smaller displacements than the point hinge, and from there up it gives larger displacements.

The agreement for distortions is also very reasonable; there are only a few levels where the response is exceeded (floors 8 and 16) but overall the results are much better than for the bilinear spring.

The original bilinear springs give larger floor displacements on the first three stories, agree quite well from floors four to eleven, and then predict larger values than the point-hinge model. The curve has sudden variations on floors seven and twelve. As for distortions, the first-floor response is overestimated, and on the other floors the response oscillates from one side of the point-hinge curve to the other. On the average, though, both agree within acceptable range. For the original trilinears the shear-beam shape is more evident, overestimating response on the lower floors, and underestimating it on the upper floors. The distortions have a smoother variation, and a closer shape to the point-hinge prediction is obtained, although smaller in magnitude from floors four to sixteen. Trilinear A gives better agreement than the original trilinears overall.

4.4 EVALUATION OF RESPONSES BY THE MULTILINEARS AND APPROXIMATE SPRINGS

In comparison to the responses predicted by the multilinear springs reported in Chapter 3, the analysis using bilinear and trilinear springs provides the following estimations:

Using bilinear springs, with the appropriate second slope in the range of interest, seems to provide reasonable results for the four-story frame, similar to those of the multilinear springs. It must be noted that this frame has a failure mechanism where columns develop large amounts of yielding, which may force a bilinear floor behavior. For the ten-story and sixteen-story frames, although displacements agreed reasonably well with the point hinge, there are rather sharp changes on inter-story displacement.

Using trilinear springs resulted in very similar responses to those of the multilinear springs, and this was consistent for all frames. Slightly better agreement was reached when the trilinear B was used. Similarly to the multilinear springs, the lateral load distribution did not influence the dynamic response of the frames. P-Δ effects were also unimportant in terms of the agreement between the two models. The original springs either bilinear or trilinear provided acceptable response for only the four-story frame, but not for the ten- or sixteen-story frames. The bilinear spring produced some localized extremely large distortions and the trilinear resulted in very jagged curves. The shear-beam shape was clearly in evidence in all cases, and when the actual situation demanded a "bending"-type curve, the shear-beam model using these springs was unable to reproduce it properly.

Since the response of both multilinear and trilinear springs is very similar, member ductilities computed using results from the trilinear springs are expected to be very close to those computed in Chapter 3. This means that the shear-beam model, even using simple force-deformation

relations can be used to estimate not only overall displacements and distortions, but also local member ductilities within a reasonable range of the point-hinge model predictions.

4.5 EVALUATION OF SHEAR-BEAM MODEL PERFORMANCE WITH APPROXIMATE SPRINGS

From the two approximations on the shear-distortion curves, the trilinear springs predict responses more consistent with the point-hinge model than the bilinear springs. The performance of the shear-beam model is studied, using the results from the trilinear springs. Since the results from the multilinear springs are very similar to the ones with the trilinear springs, the conclusions reached for the former in relation to overall performance are basically the same as for these. That is, the shear-beam model provides a reasonable estimation of the dynamic response when appropriate springs are used to represent floor behavior. Overall agreement for displacement envelopes is more consistent than for distortions, but in most cases the discrepancies encountered rarely exceed 30%.

4.6 CONCLUSIONS

The conclusions for these analyses can be summarized as follows:

- The shear-beam model predicts dynamic response with reasonable agreement with the point-hinge model, provided that appropriate springs are used.

- It is entirely feasible to use simple springs instead of the multilinear springs and still obtain response in good agreement with the point-hinge models.

- Trilinear springs as an approximation to actual shear-distortion curves give a good representation of floor behavior.

- Trilinears "B" gave better agreements with the point-hinge model than trilinears "A" in most cases.

- Bilinear springs seem to be limited to rather simple structures, since they tend to largely overpredict distortions in certain floors.

- The lateral load distribution used to obtain story shear-distortion curves has no significant influence in the dynamic response for the ranges considered.

- For the four-story frame, the correlation between the responses predicted by both models remained unchanged with earthquake peak acceleration (the 10- and 16-story frames were not studied with bilinear or trilinear springs for other motion intensities).

- For all practical purposes, P-Δ effects did not alter the response of the shear-beam model, but modified slightly the results of the point-hinge model. The agreement between both models was thus slightly damaged.

- Local member ductilities can be computed using the predicted distortions of the shear-beam model within a reasonable range of the point-hinge model predictions.

CHAPTER 5

EQUIVALENT SINGLE DEGREE OF FREEDOM SYSTEM FOR INELASTIC ANALYSIS OF MULTISTORY FRAMES

5.1 INTRODUCTION

An alternative simple model for the inelastic dynamic analysis of multistory frames is presented in this chapter. The procedure consists basically in the reduction of a given frame to an equivalent single-degree-of-freedom (E.S.D.O.F.) with a multilinear hysteretic force-deformation relationship. The time integration of the reduced single

equation of motion is performed in the conventional way, with the advantage of the simplicity and low cost of the analysis. From the relative displacement of the E.S.D.O.F., the displacements in all the floors are computed and also the interstory displacements. In addition, since this reduction is based on the deformed shapes for the building (resulting from the incremental static analysis of chapter 2), it is possible to use the predicted dynamic response (displacements or distortions) to estimate local member ductilities from the said static analysis.

The idea of reducing a frame to an equivalent S.D.O.F. has been presented by Biggs [8]. However, in the present formulation this concept has been extended to handle hysteretic force-deformation relationships of multiple branches representing the behavior of a frame at multiple stages of inelastic deformation. That is, the specific properties and inelastic response of any frame can be represented properly regardless of the shape of its "equivalent constitutive relation," without the limitation of simple springs.

Takizawa [4] presented another procedure based on the superposition of failure mechanisms as a set of springs acting in a series combination.

The mathematical formulation and governing equations are developed in the next section with a more detailed explanation of the input necessary for the analyses and the mechanics of the procedure.

In section 5.3 results of the analyses using this idealization and the point-hinge model are presented for comparison. All the frames described in chapter 2 are studied.

A comparison of the performance of the E.S.D.O.F. system with respect

to the traditional shear-beam model is presented in section 5.4. In section 5.5 local member ductilities evaluated using the results from these analyses are presented and compared with the results predicted by the point-hinge model. Section 5.6 discusses the performance and adequacy of this procedure to perform inelastic dynamic analyses, and section 5.7 summarizes the conclusions.

5.2 FORMULATION

As a result of an incremental inelastic static analysis, a set of corresponding deflected shapes U is obtained, the deflected shape being the set of lateral floor displacements. As long as the structure remains elastic, or as long as for a given number of loading steps no new hinges are formed on the members, the deflected shapes U will be proportional to each other. Every time a change on the yielding status of the frame occurs, the displacement vector U will have a different shape, the ratio between the floor displacements having changed.

In this analysis only those deflected shapes that limit each range of linear behavior are of interest, since in between them incremental displacements vary proportionally. Fig. 5.1 illustrates this process.

For example, in between curves number 5,$U(F_i)$ and 6,$U(F_{i+1})$ of Fig. 5.1 any deflected shape $U(F_i + \Delta F)$ can be expressed as:

$$U\ (F_i + \Delta F) = U(F_i) + \frac{\Delta F}{F_{i+1} - F_i}\ [U(F_{i+1}) - U(F_i)] \qquad (5.1)$$

$$0 \leq \Delta F \leq F_{i+1} - F_i$$

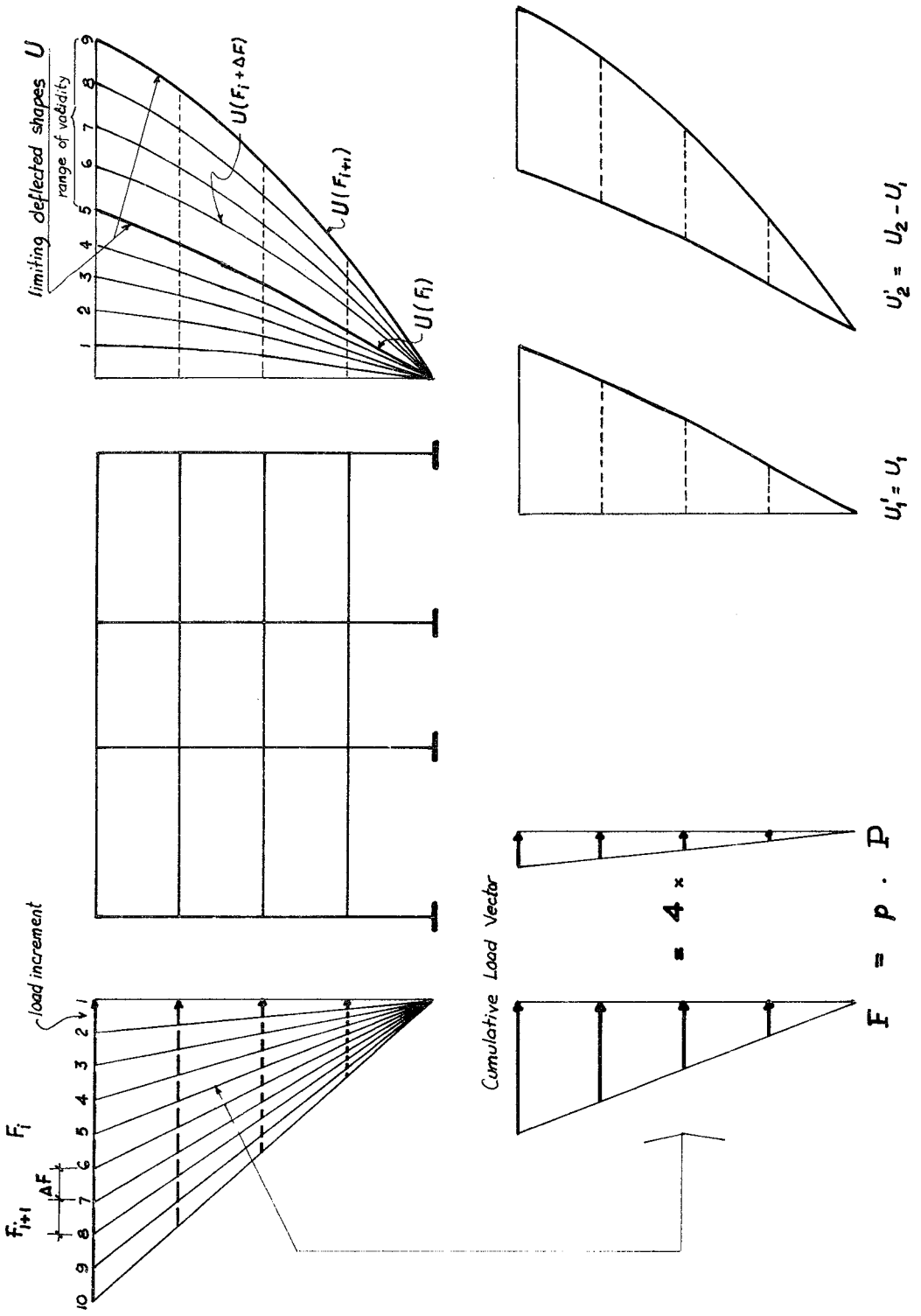

FIGURE 5.1 - DEFLECTED SHAPES FROM INCREMENTAL STATIC ANALYSIS

The lateral loads applied on incremental steps have a known distribution in height which remains unchanged during the analysis. So at any step of the procedure these loads constitute a vector (F) which can be represented as

$$F = p \cdot P \tag{5-2}$$

where p is a scalar which multiplies the vector of lateral load increments, P.

Corresponding to each limiting deflected shape, there is a vector of forces which is fully defined by the scalar p. The information used in the dynamic analysis is then:

- A vector of increments of load.
- A set of limiting deflected shapes U, as many as necessary to cover the expected maximum displacements, and
- The corresponding scalars p_i of the force vectors F_i.

The procedure described here is an incremental dynamic analysis in which the governing equations are assumed to be valid and the properties of the system linear during a given time step. From the set of limiting deflected shapes, the difference between adjacent curves is computed:

$$U'_j = U_j - U_{j-1} \tag{5-3}$$

defining a new set of shapes that remain constant during a given range.

The number of ranges and curves U'_j is the same as the number of limiting deflected shapes. The first curve U'_1 is equal to U_1. What follows is applicable to a particular range "j".

The incremental equations of motion for a multistory frame with lumped masses is

$$M \ \Delta\ddot{U} + \Delta F = - MI \ \ddot{u}_G \tag{5-4}$$

where M is the mass matrix, $\Delta\ddot{U}$ the vector of incremental accelerations, ΔF the vector of incremental restoring forces, I a unit vector, and $\ddot{u}_G$ the ground acceleration.

Expressing the incremental displacements as

$$\Delta U = \frac{U_j'}{\sqrt{U'^T M U_j}} \ \Delta u \tag{5-5}$$

$$\Delta\ddot{U} = \frac{U_j'}{\sqrt{U'^T M U_j'}} \ \Delta\ddot{u} \tag{5-6}$$

$$\Delta F = \Delta p \cdot P \tag{5-7}$$

Substituting Equations (5-6) and (5-7) in (5-4)

$$\frac{M U_j'}{\sqrt{U_j'^T M U_j'}} \ \Delta\ddot{u} + \Delta p \cdot P = - M I \ \ddot{u}_G \tag{5-8}$$

Premultiplying by $\dfrac{U_j'^T}{\sqrt{U_j'^T M U_j'}}$, equation (5-8) becomes

$$\frac{U_j'^T M U_j'}{U_j'^T M U_j'} \ddot{\Delta u} + \Delta p \frac{U_j'^T P}{\sqrt{U_j'^T M U_j'}} = - \frac{U'^T M I}{\sqrt{U_j'^T M U_j'}} \Delta \ddot{u}_G \tag{5-9}$$

$$\Delta \ddot{u} + \Delta p \frac{U_j'^T P}{\sqrt{U_j'^T M U_j'}} = - \frac{U'^T M I}{\sqrt{U_j'^T M U_k'}} \Delta \ddot{u}_G \tag{5-10}$$

If we visualize the force-deformation relation for this system as a multilinear curve, each branch corresponding to a range of validity for U_j', then a tangential stiffness k_{tj} of branch "j" is defined as

$$k_{tj} = \frac{\Delta P}{\Delta u} \tag{5-11}$$

Introducing (5-11) into (5-10)

$$\Delta \ddot{u} + \underbrace{\frac{U_j'^T P}{\sqrt{U_j'^T M U_j'}}}_{FR_j} k_{ij} \Delta u = - \underbrace{\frac{U_j'^T M I}{\sqrt{U_j'^T M U_j'}}}_{F\Delta_j} \Delta \ddot{u}_G \tag{5-12}$$

or $$\Delta \ddot{u} + K_{equiv.} \Delta u = - M_{equiv.} \Delta \ddot{u}_G \tag{5-13}$$

which is the governing equation. Actually the computer solution used here is based on equation (5-12) for simplicity, where k_{ij} and Δu are evaluated using the multilinear spring of Fig. 5-2.

The total displacements are computed by superposition of the incremental displacements of equation (5-5). This implies of course the possibility of discontinuities in the zone of transition from branch to branch.

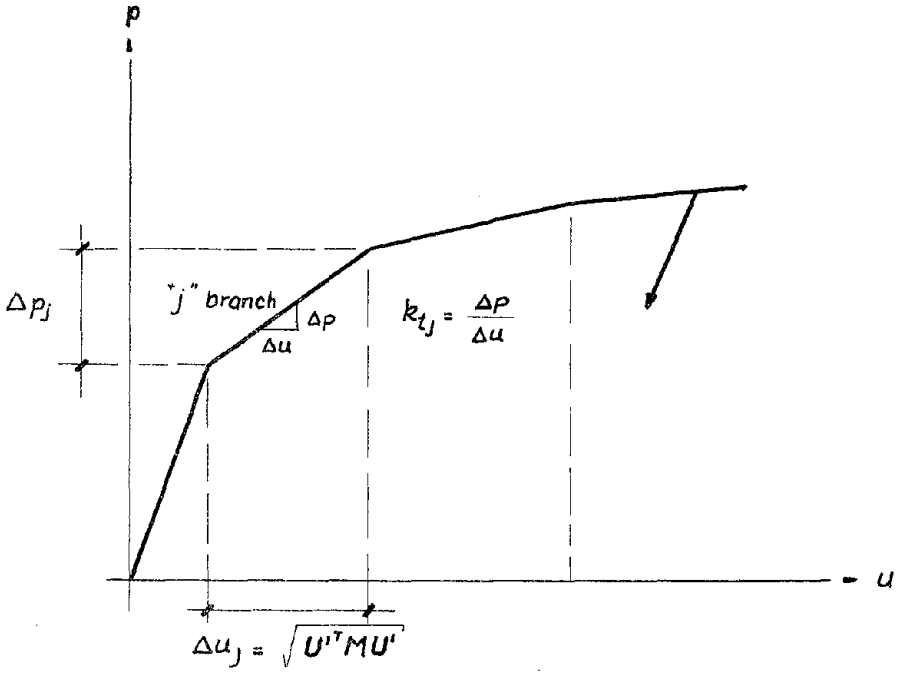

FIGURE 5.2 - HYSTERETIC MULTILINEAR RESISTANCE CURVE FOR EQUIVALENT SINGLE-DEGREE-OF-FREEDOM (E.S.D.O.F.) SYSTEM

It is possible to obtain similar governing equations by assuming alternative expressions for ΔU. Biggs, for example, takes the displacement at the top floor (u'_{jn}) as a normalizing factor. In that case equation (5-5) becomes

$$\Delta U = \frac{U'_j}{u'_{jn}} \Delta u \qquad (5\text{-}14)$$

An alternative assumption would be

$$\Delta U = \frac{U'_j}{\sqrt{U'^T_j U'_j}} \Delta u \qquad (5\text{-}15)$$

Any of the above would result in different force-deformation relations for the E.S.D.O.F., but the reduction would be the same. In the present studies only the reduction based on equation (5-5) was used.

Damping can be introduced in the s.d.o.f. governing equation by simply adding the corresponding term $2\beta\omega$. ω could be the equivalent natural frequency of the system at each instant based on its tangent stiffness, or can be considered as the initial frequency ω_1 in the elastic range. Since this damping is intended to reproduce the dissipation of energy under small vibrations, and is not due to inelastic action, the second approach was followed.

5.3 COMPARISON OF ANALYSIS WITH THE POINT-HINGE MODEL

The analyses reported in this section were performed with two percent damping, and without including P-Δ effect. Static analyses presented in chapter 2 were performed also without P-Δ effect for reasons explained there, and P-Δ effects were not explicitly incorporated in the formulation of the E.S.D.O.F.

It should be decided on further research wheather to implement P-Δ effects on the model itself or to include it in the static analysis.

El Centro and Taft were used for ground motions, both scaled to the same Arias intensity.

5.3.1 Four-Story UBC Frame

Figure 5.3 shows the envelopes of maximum floor displacement and distortion as given by the E.S.D.O.F. and the point-hinge model, using one quarter El Centro to guarantee elastic behavior. The agreement is

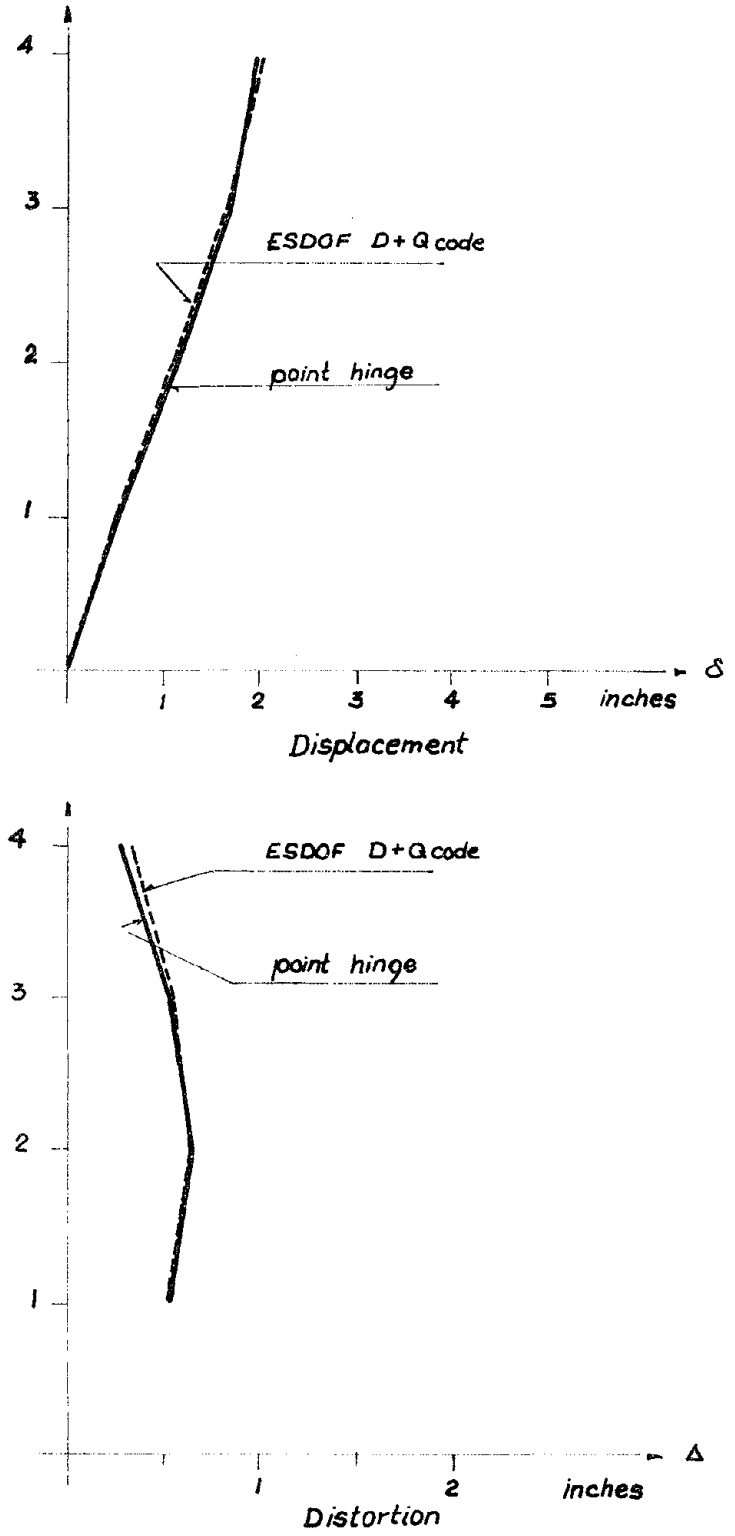

FIGURE 5.3 - 4-STORY UBC FRAME. POINT HINGE VS. E.S.D.O.F. $D+Q_{code}$. INTERACTION. ELASTIC. ¶/4 EL CENTRO

very good for both displacements and distortions at all floors. It can be noticed, however, that the shape of the displacement envelope is not exactly proportional, but crosses the point-hinge envelope on the top. This is a function of the load distribution. In this case, the deflected shapes used as input are obtained from the code lateral load distribution.

Figures 5.4 and 5.5 show the comparisons between both models for the code, first mode, uniform and SRSS of all mode distributions.

A similar situation arises for distortions: the uniform distribution gives results apart from the others. For the other distributions the agreement is good on the first two stories and deteriorates on the top. These distortions become smaller than those of the point-hinge model by 30%. This appears to be a limitation of the model. Since the dynamic analysis is based on deflected shapes of the building (displacement envelopes), distortions in the upper stories will be less sensitive to wave propagation through the height of the building. This forces them to be very similar to the interstory displacements on the deflected shapes and in most cases these are small for the top stories.

Figure 5.6 shows the comparisons between the point-hinge model and the E.S.D.O.F. for the code lateral load distribution under 1.87 Taft (same Arias intensity as El Centro).

The shape of the displacement envelope as predicted by the S.D.O.F. system is slightly different from that of the point-hinge model. On the first two stories, values are underestimated, and on the fourth story they are overestimated. The "curvature" of the envelope is somewhat

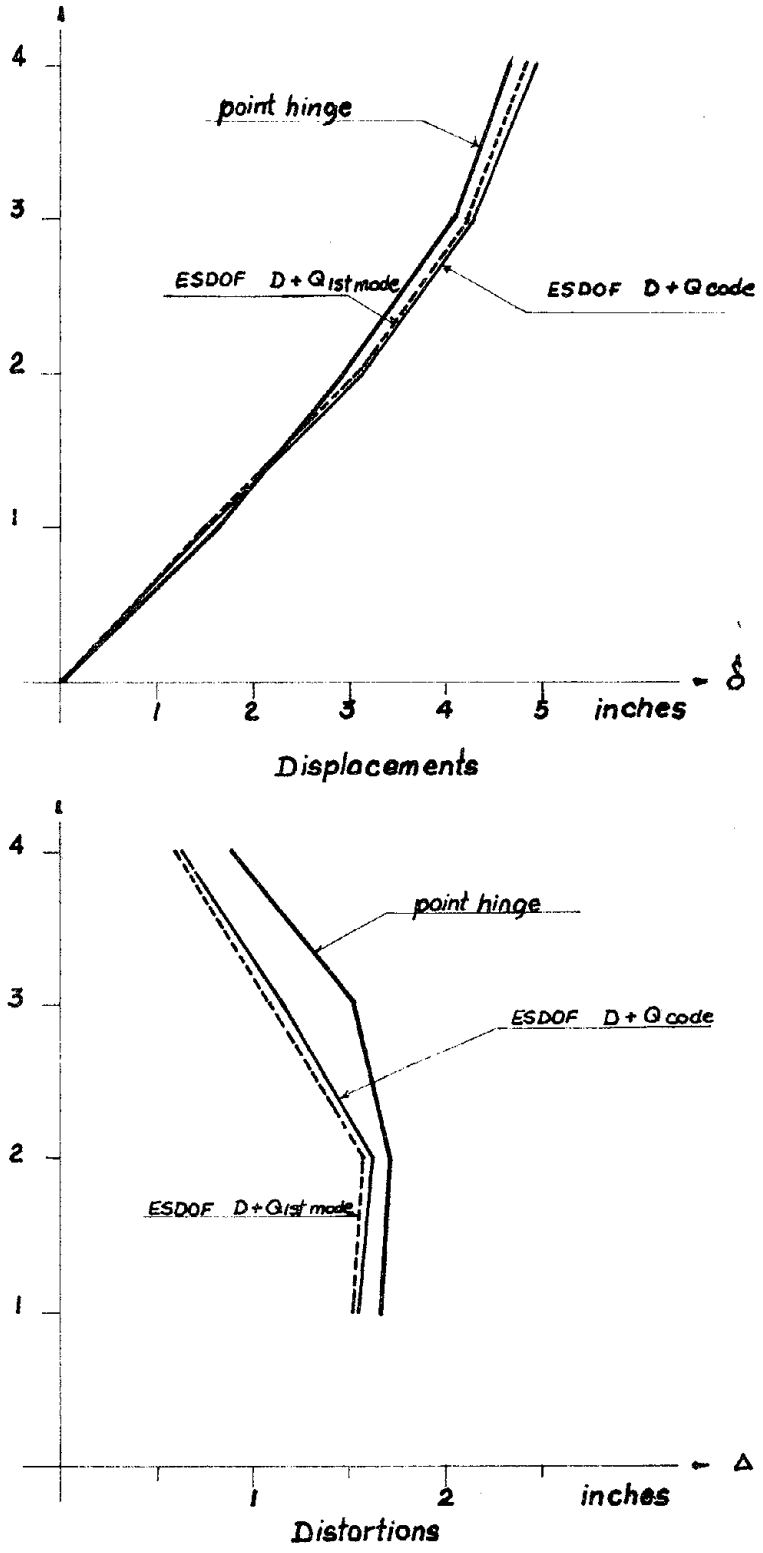

FIGURE 5.4 - 4-STORY UBC FRAME: POINT HINGE VS. E.S.D.O.F. $D+Q_{code}$. $D+Q_{1st.\ mode}$. INTERACTION. EL CENTRO

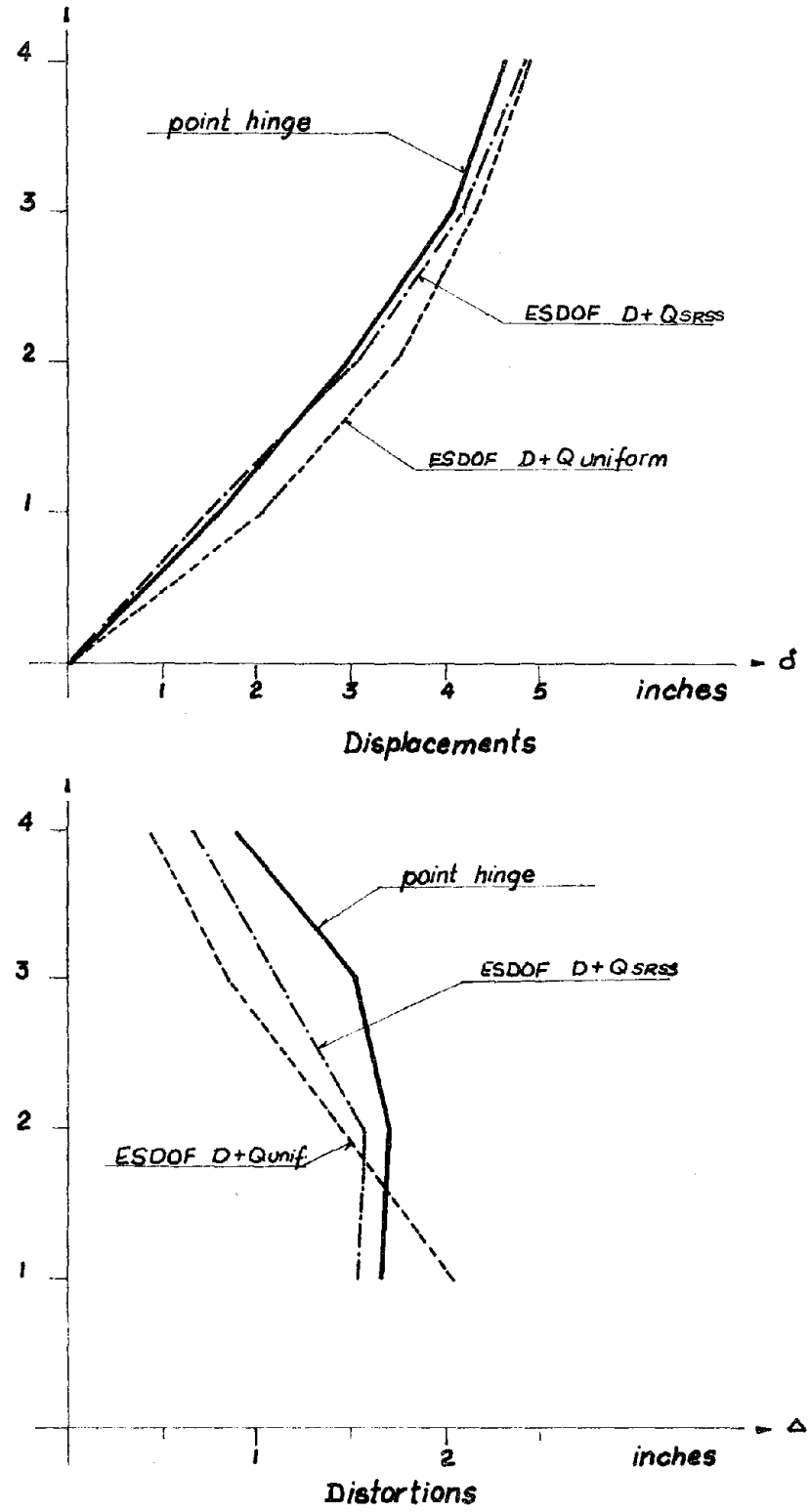

FIGURE 5.5 - 4-STORY UBC FRAME: POINT HINGE VS. E.S.D.O.F. $D+Q_{uniform}$, $D+Q_{SRSS}$, INTERACTION. EL CENTRO

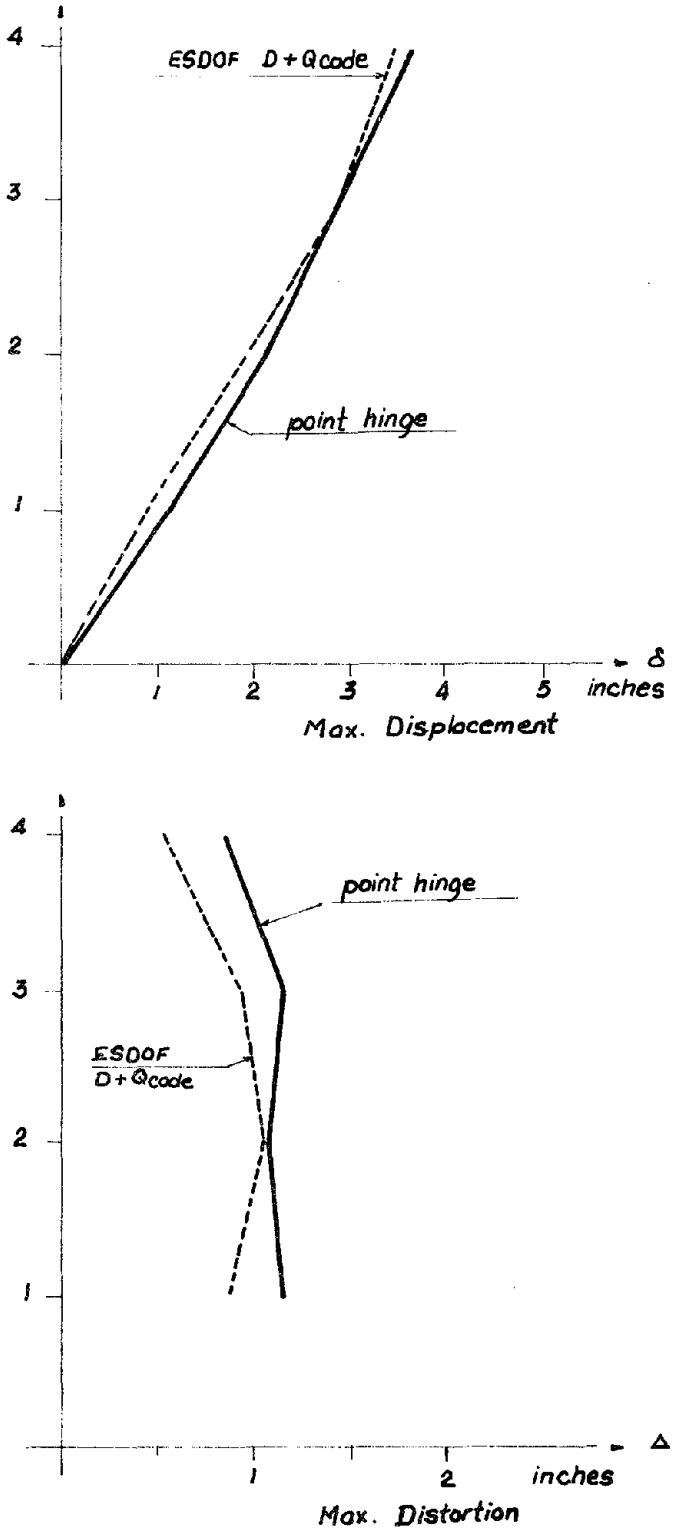

FIGURE 5.6 - 4-STORY UBC FRAME: POINT HINGE VS. E.S.D.O.F. $D+Q_{code}$. INTERACTION. 1.87 x TAFT

different; this was also in evidence for the comparisons under El Centro, but the predicted displacements were closer to the point-hinge model than for this case. In any case the agreement is still good, with a maximum discrepancy on the first floor of 25%.

For distortions the shape of the envelope predicted by the E.S.D.O.F. is different on the lower stories, and in all cases the values of distortions are underestimated. The largest discrepancies appear again at the top floors, being in this case of the order of 30%.

5.3.2 Ten-Story UBC Frame

Figure 5.7 presents the results for the comparisons in the elastic range of the two models, point hinge and E.S.D.O.F. (under one-quarter El Centro) using deflected shapes from the code load distribution. The overall agreement in the displacements envelope is good. Up to the eighth floor the displacements predicted by the E.S.D.O.F. are smaller, and on floors nine and ten they are slightly larger. The shape of the envelope itself is closely related to the load distribution, although magnitudes agree within a reasonable range.

For distortions, a good agreement is found up to the seventh floor, where they become smaller. The shape of the envelope is similar to that of the point-hinge model, but it deviates proportionally on the stories mentioned before. Figures 5.8 and 5.9 show the results of both models under El Centro, using different load distributions: the UBC code and ATC-3 on Figure 5.3 and the uniform and SRSS of all mode distributions on Figure 5.9.

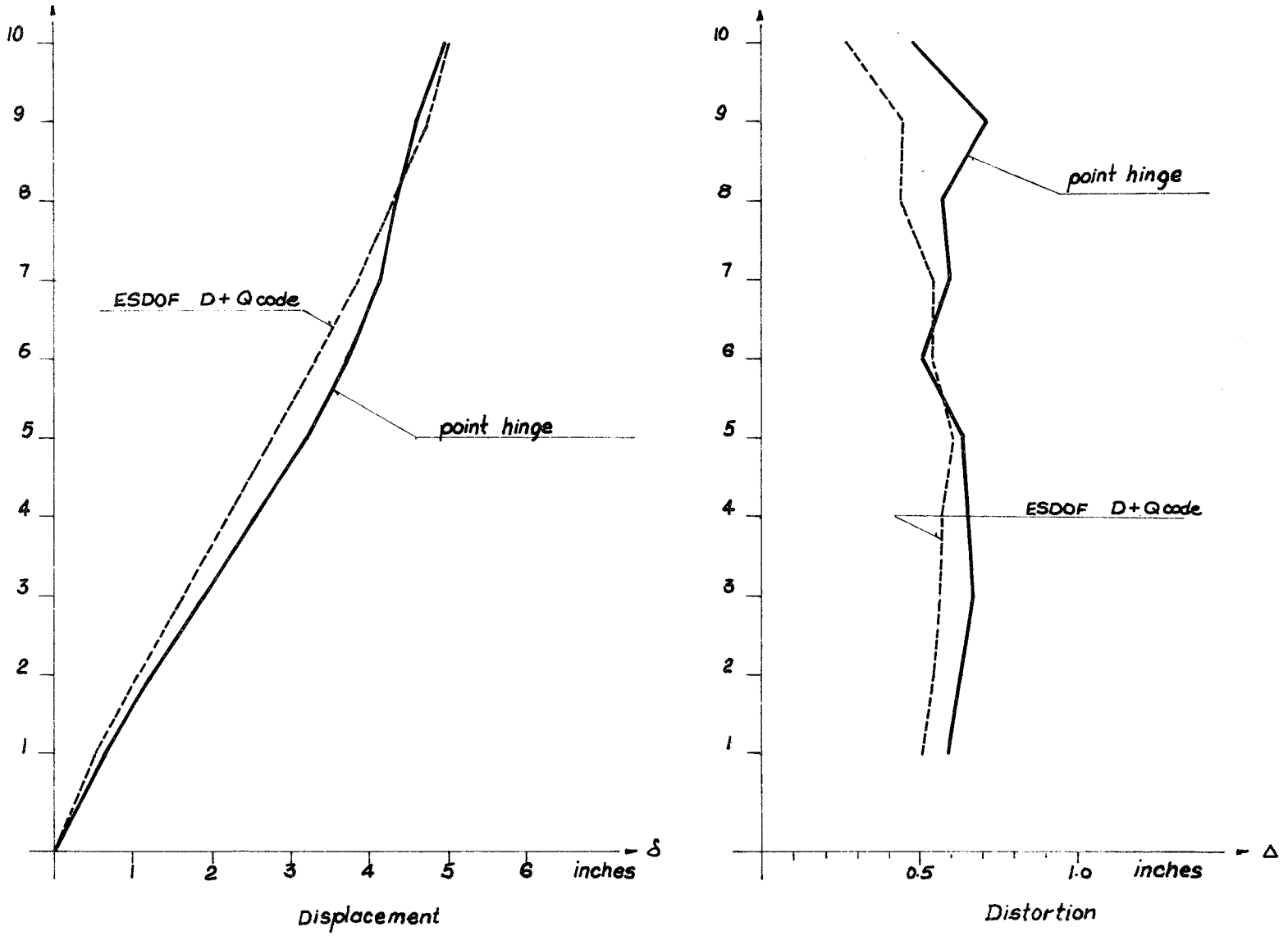

FIGURE 5.7 -10-STORY UBC FRAME: POINT HINGE VS. E.S.D.O.F. $D+Q_{code}$. INTERACTION. ELASTIC. 1/4 EL CENTRO

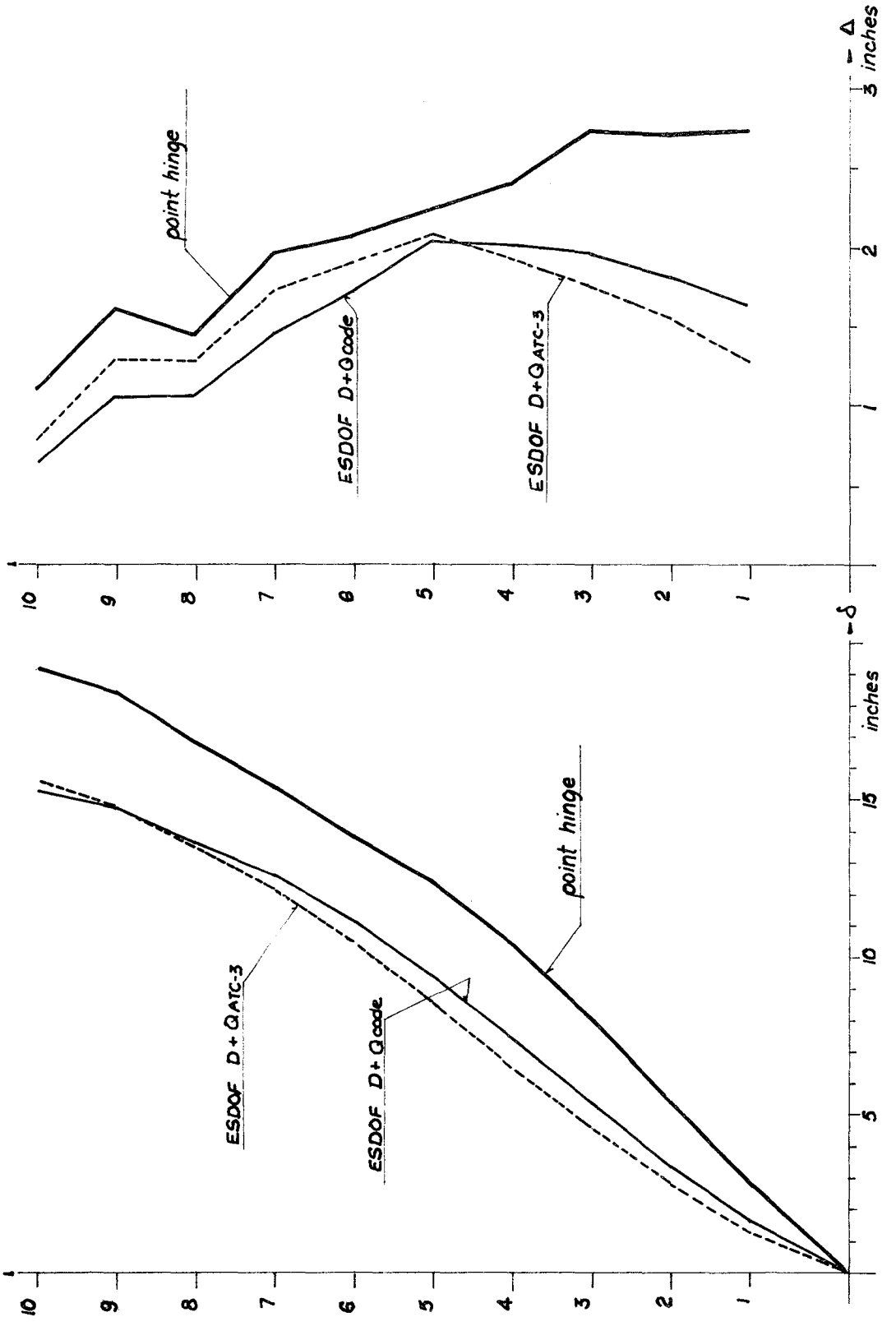

FIGURE 5.8 - 10-STORY UBC FRAME: POINT HINGE VS. E.S.D.O.F. $D+Q_{code}$, $D+Q_{ATC-3}$, INTERACTION. EL CENTRO

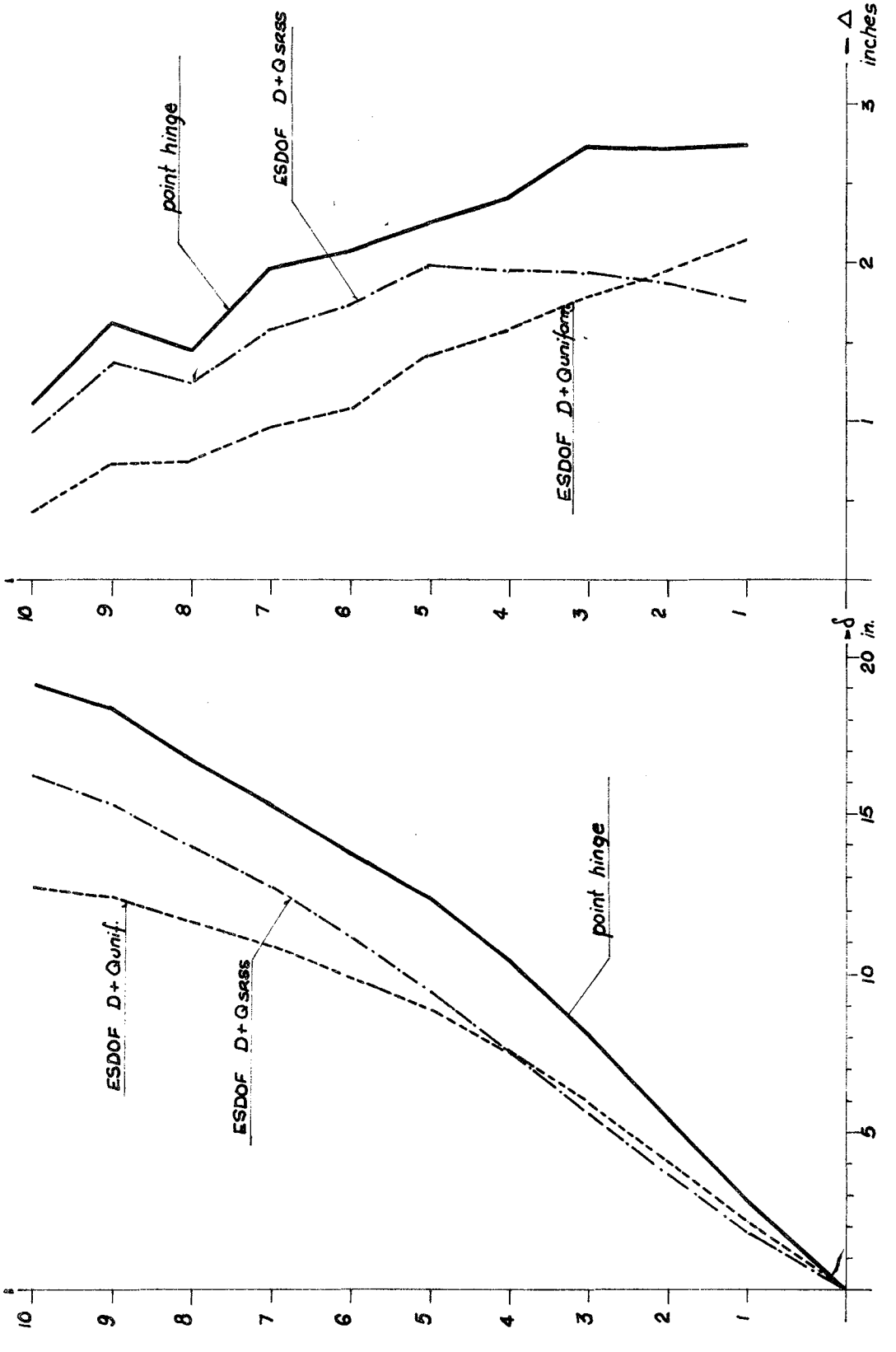

FIGURE 5.9 - 10-STORY UBC FRAME: POINT HINGE VS. E.S.D.O.F. $D+Q_{SRSS}$, $D+Q_{uniform}$, INTERACTION. EL CENTRO

The envelope of displacements obtained using the SRSS distribution curves gives the closest agreement to the point-hinge model. For distortions, however, the results of this distribution are closer for the top and lower stories, but the code distribution is better in between. The overall shape of the displacement envelope is similar to the point-hinge envelope, but the values are underestimated at all floors. The maximum difference is below 24%.

The code distribution has a slightly different shape, resulting in smaller displacements at the lower and top three stories. The differences are not very significant, however. The ATC-3 distribution displacement envelope changes more than the others with a larger negative curvature on the lower stories, clearly indicating the influence of the lateral loads (2nd degree parabola vs. triangular). The uniform distribution gives rather different results. The discrepancies are twice as large as for the other distributions and the shape resembles more that of a shear-beam with positive curvature all along the height.

For distortions the shapes are proportional on the upper five floors, but they curve inwards going down. The ATC-3 shows this trend more markedly. The uniform distribution gives an envelope which is almost parallel to the point-hinge model, but the values are largely underestimated. In all cases the largest discrepancies appear at the bottom stories and are not as large at the top. This may have a correlation with the fact that the relative differences in displacements are the largest at the bottom stories.

In Figure 5.10 the results using the bending yield criterion are presented. The load distribution used for the deflected shapes of the

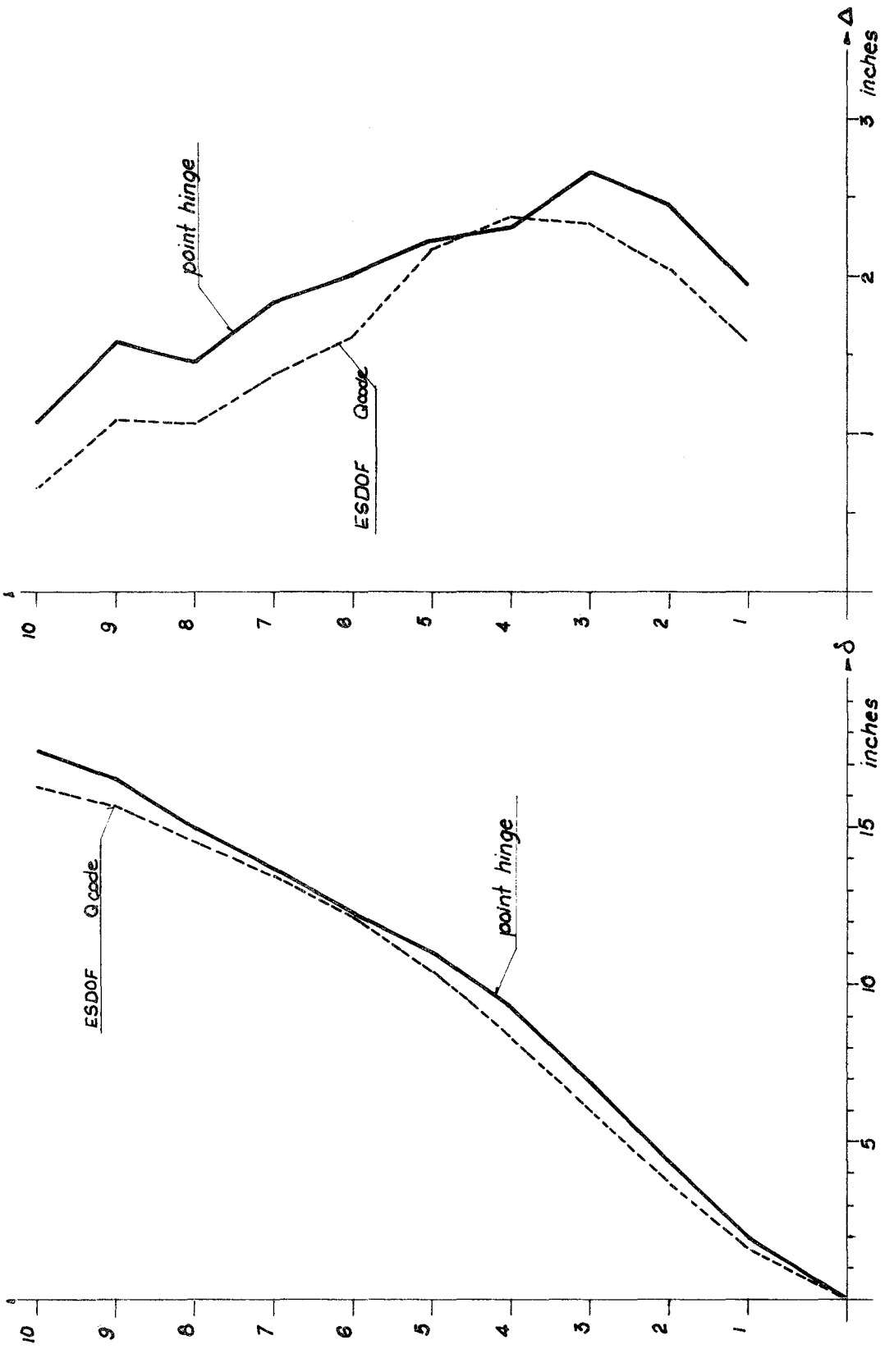

FIGURE 5.10 - 10-STORY UBC FRAME: POINT HINGE VS. E.S.D.O.F. Q_{code}. BENDING. EL CENTRO

E.S.D.O.F. was the one of the UBC code.

The agreement in terms of displacements is very good, better than for the interaction model. The shape of the envelopes is similar with only a minor difference from floors five to eight, in which the point-hinge model envelope changes curvature.

The envelopes of distortions are proportional at all floors except four and five. In relative terms the largest differences appear at the top, but the curve seems to be shifted towards the left of the point-hinge envelope.

Figure 5.11 shows the results for the analyses under 1.87 Taft. The envelope of displacements has a good agreement, although the shape of the curve is different. The E.S.D.O.F. predicts smaller displacements on the lower half of the building and larger on the upper part. The differences are smaller than 15% in all levels.

For distortions the curves show reasonable agreement up to the sixth floor and from there up the E.S.D.O.F. underestimates the response.

5.3.3 Anderson Frame

Figures 5.12 and 5.13 show the comparisons between the results of the point-hinge model and the E.S.D.O.F. for Anderson's frame. The first is for the case with interaction as yield criterion; the second uses the bending yield criterion.

For the case with interaction, the shape of the envelope of displacements from the E.S.D.O.F. shows a different curvature from the second to the seventh floor, resulting in larger discrepancies than for the other

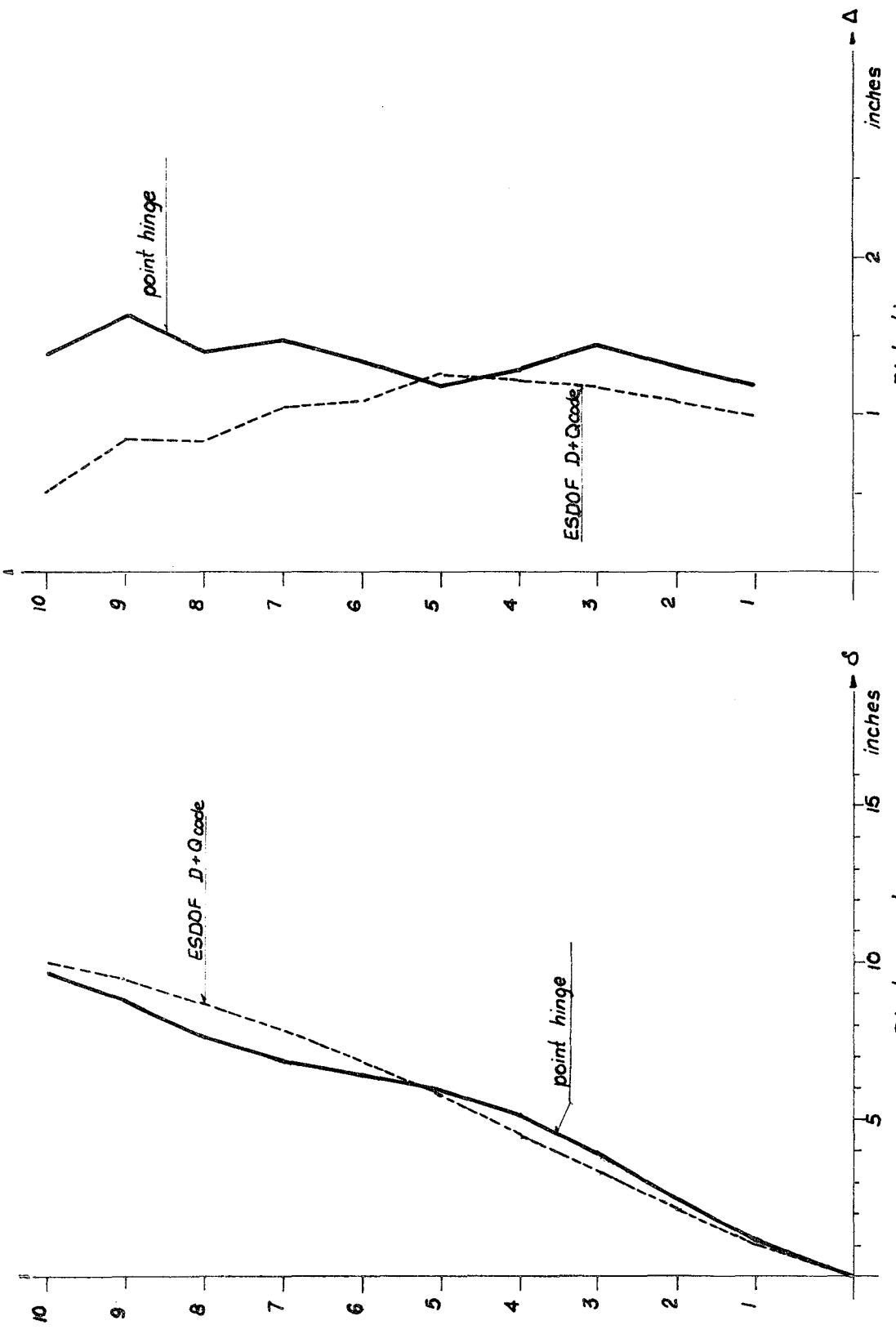

FIGURE 5.11 - 10-STORY UBC FRAME: POINT HINGE VS. E.S.D.O.F. $D+Q_{code}$. INTERACTION. 1.87 x TAFT

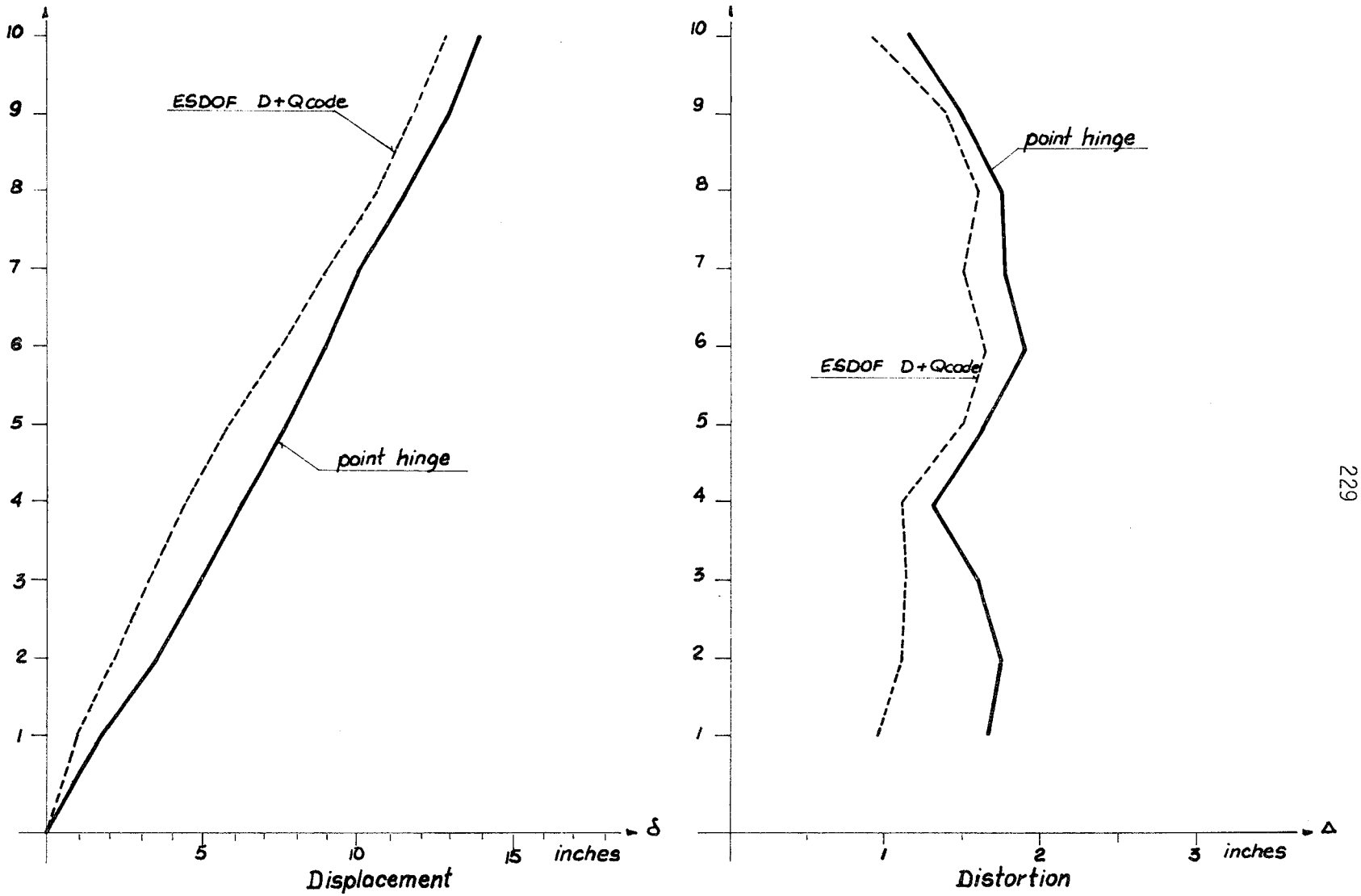

FIGURE 5.12 - ANDERSON FRAME: POINT HINGE VS. E.S.D.O.F. $D+Q_{code}$. INTERACTION. EL CENTRO

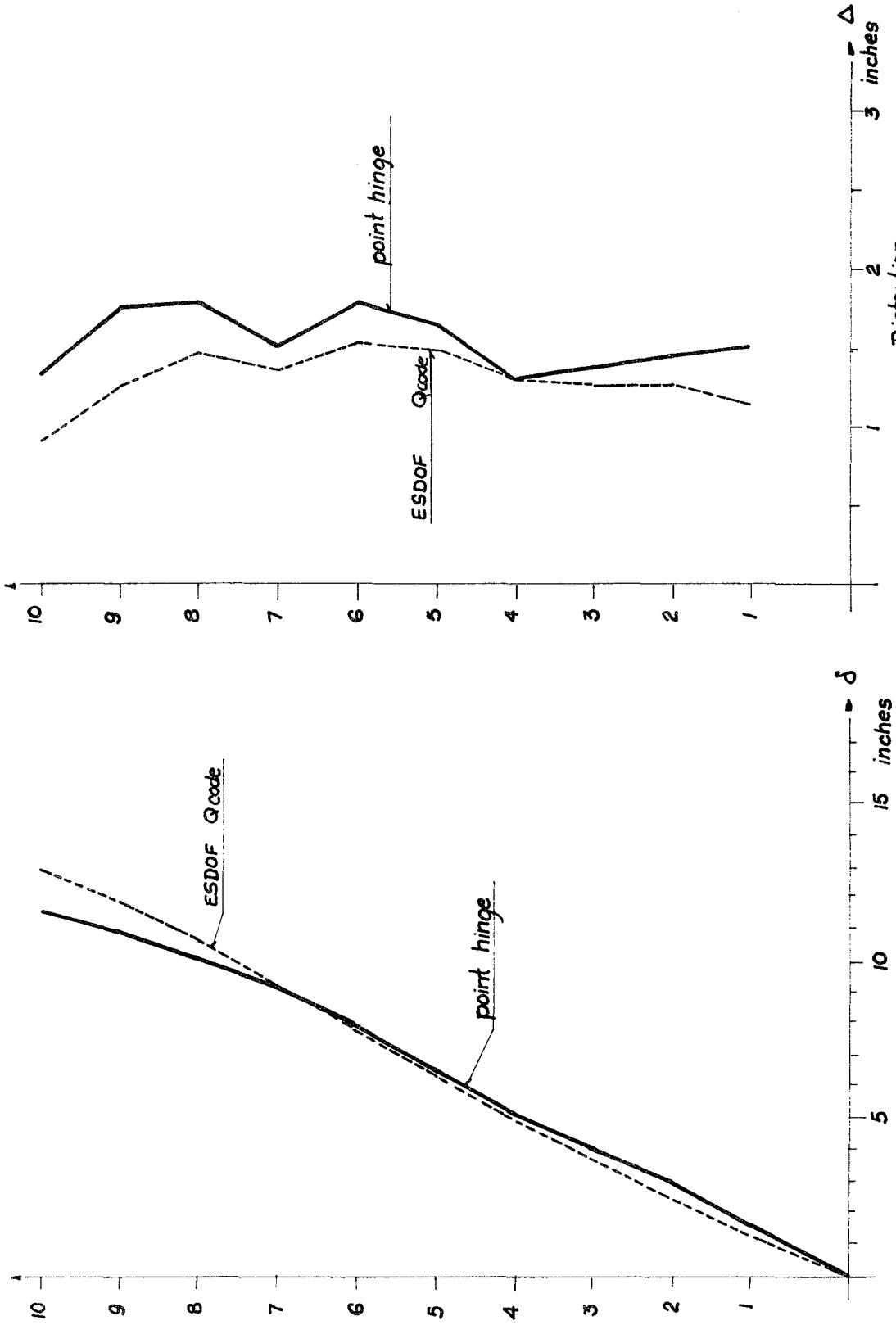

FIGURE 5.13 - ANDERSON FRAME: POINT HINGE VS. E.S.D.O.F. Q_{code}. BENDING. EL CENTRO

floors. The curves run parallel, however, with the point-hinge envelope, predicting larger displacements at all heights.

The envelopes for distortions show the E.S.D.O.F. having a proportional curve on the side of smaller values, but with a similar shape. The lower stories, however, have larger discrepancies. It is interesting to notice that for this frame distortions on the upper floors correlate better than for the frames described before.

In the case of the bending model the correlation in terms of floor displacements is much better than for the case above, with the difference that the envelopes cross each other at the sixth floor. The point-hinge envelope shows a marked positive curvature from there up which is sharper than for the E.S.D.O.F., resulting in smaller displacements. The actual relative difference never exceeds 25%.

The shape of distortion envelopes is proportional from floors four to ten, with the largest difference on the top floor. The agreement on the lower stories is better than for the interaction case, and overall it is acceptable.

For displacements the change in response due to the yield criterion is more significant using the point-hinge model than using the E.S.D.O.F. This model predicts smaller response with the interaction criterion as opposed to the point-hinge, which predicts a larger response in that case. For distortions, though, there is not a clear trend in this respect.

5.3.4 Kamil Frame

Figures 5.14 and 5.15 show envelope comparisons for Kamil's frame. Both cases are presented: the interaction and the bending yield criteria.

In the first case, the E.S.D.O.F. overestimates the floor displacements from floor three to the top, only the first three stories showing good agreement. On the others the discrepancies are considerable. The shape of the envelopes is different, with a pronounced slope on the E.S.D.O.F. envelope from floor two to six. For distortions the agreement is rather poor, having underestimated considerably the values on the top three stories. Both shapes present different characteristics.

In the bending case the results are different, mainly because the point-hinge model response changes a great deal. Displacements for this case are substantially larger than for interaction (around 25%), and the shape of the envelope also changes. The distortion envelope changes also its shape and magnitudes.

The agreement with the E.S.D.O.F. is good for displacements, and both shapes are very much alike. The values are always smaller when using the simple model. The shape of the distortion envelope is similar from floors four to ten, but fails to reproduce a "dip" on floor three. The values are also on the smaller side. In terms of magnitude the discrepancies are much larger than for displacements, reaching up to 65% on the top floor.

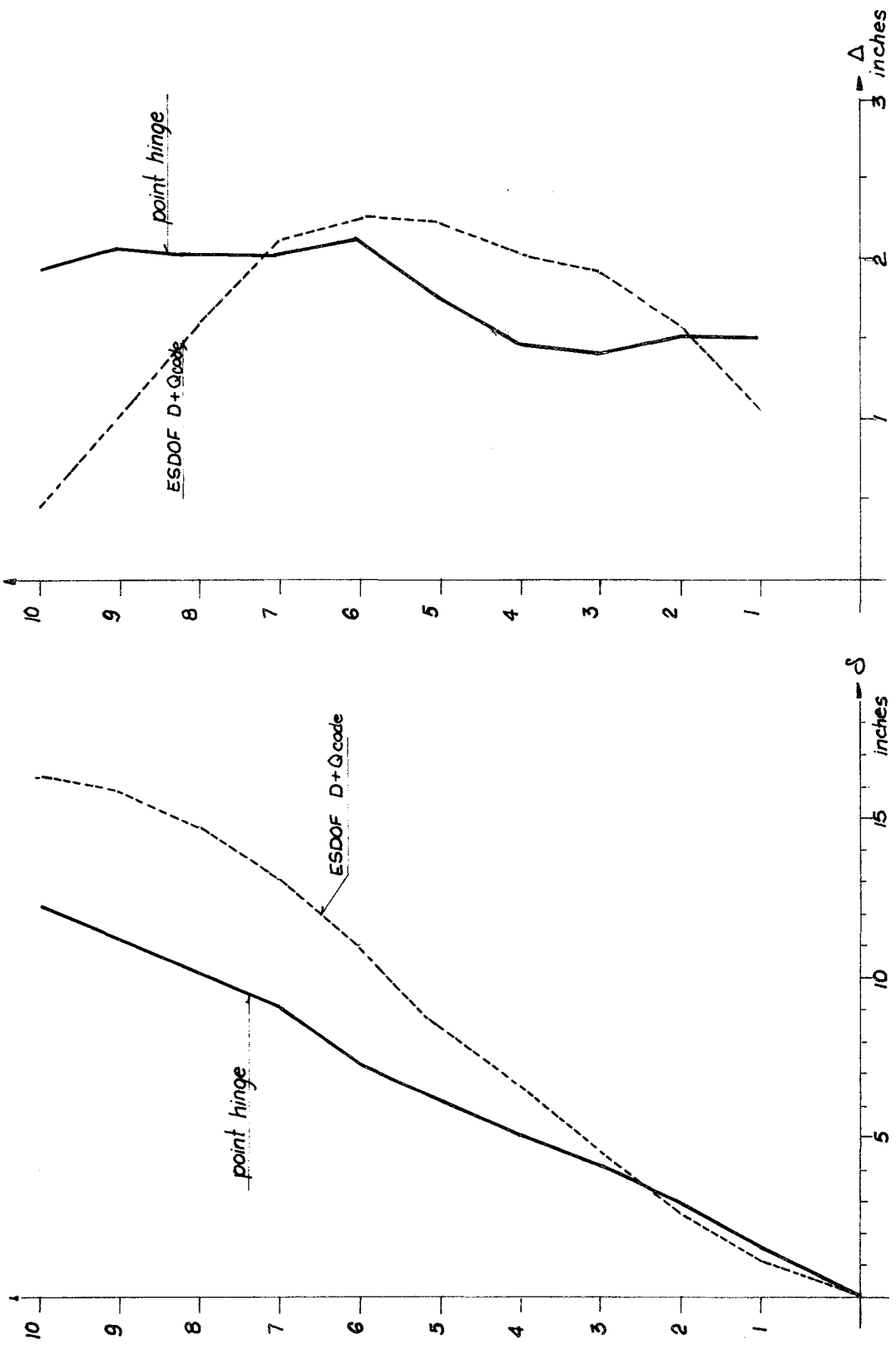

FIGURE 5.14 - KAMIL FRAME: POINT HINGE VS. E.S.D.O.F. $D+Q_{code}$ INTERACTION. EL CENTRO

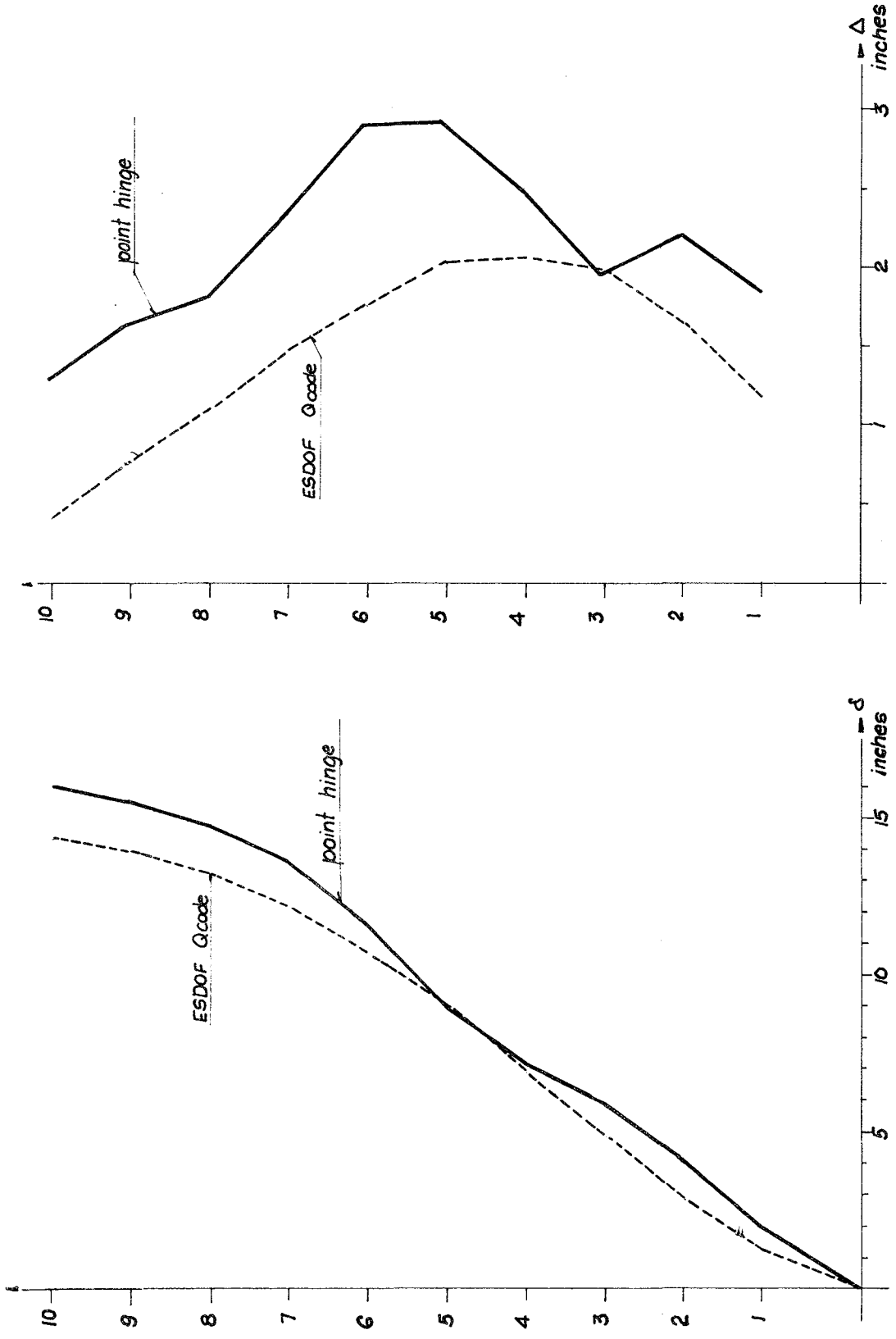

FIGURE 5.15 - KAMIL FRAME: POINT HINGE VS. E.S.D.O.F. Q_{code}, BENDING, EL CENTRO

5.3.5 Sixteen-Story UBC Frame

Figure 5.16 shows the comparisons between the point-hinge model and E.S.D.O.F. responses in the elastic range. The analyses were done under one quarter El Centro, using curves from the code distribution and the interaction yield criterion.

The agreement in the displacement envelopes is quite good, the E.S.D.O.F. giving smaller values all the way up to floor fourteen, where it crosses the point-hinge envelope. For distortions the agreement is good until floor eleven, where the E.S.D.O.F. shows a tendency to underestimate the response. The shape of the curve shows the same peaks as the point-hinge model, but always underpredicting their magnitude.

Figure 5.17 shows the results for El Centro, using the code-distribution deflected shapes and the interaction yield criterion. Figure 5.18 shows the same for the ATC-3 and uniform distributions.

The code distribution gives the best agreement of all. As for other cases, the E.S.D.O.F. system underpredicts the response on the lower nine stories, then crosses the point-hinge envelope and gives larger results from then up. Better agreement is encountered on the lower stories. The model (E.S.D.O.F.) is unable to reproduce the negative curvature that appears from floors ten to fourteen on the point-hinge envelope. The largest difference is registered in floor twelve (20%).

In the case of distortions, the E.S.D.O.F. envelope does not follow the shape of the point-hinge model from floors six to twelve. On the remaining ones the curves are similar in shape, with largest discrepancies on the top floors.

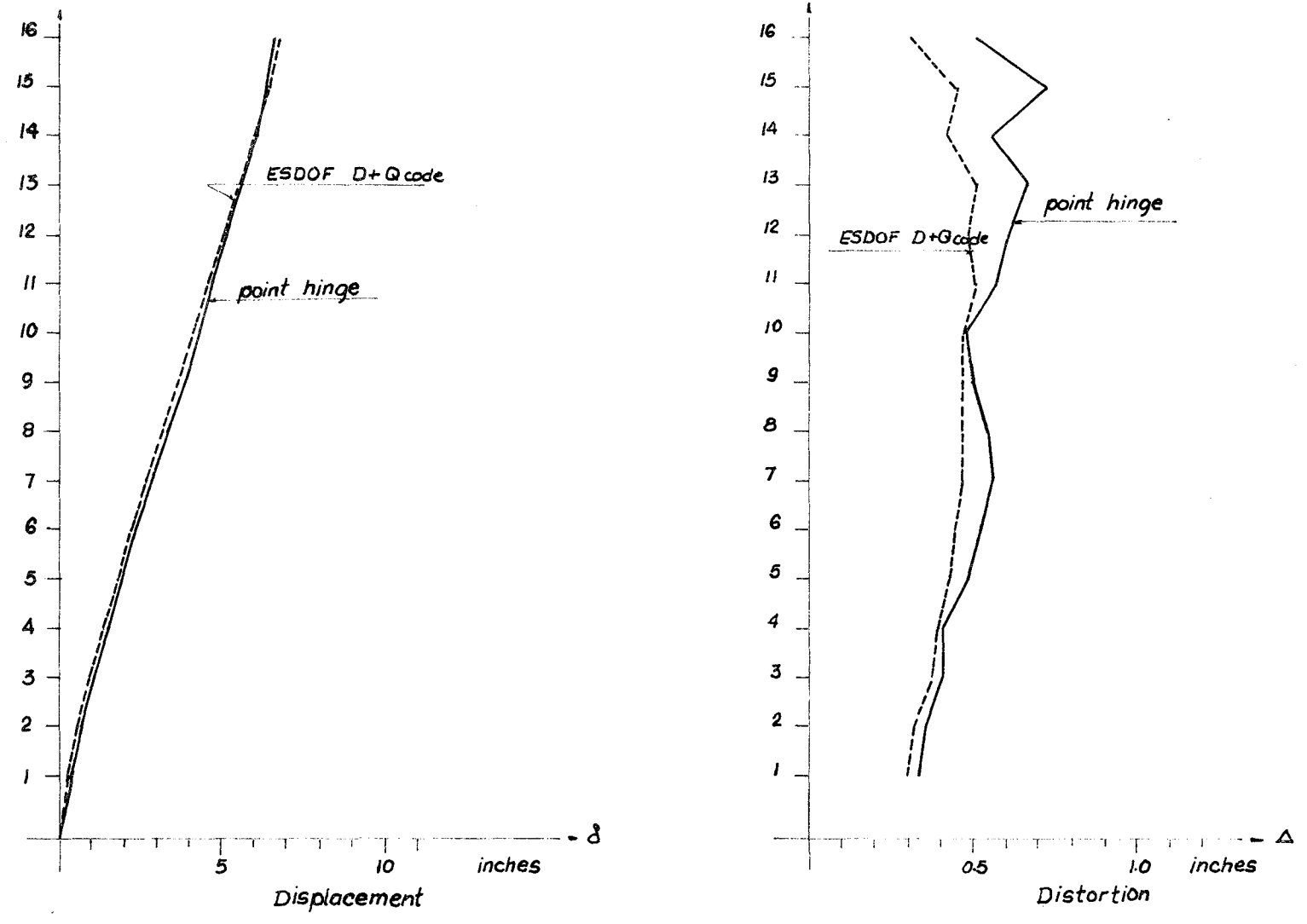

FIGURE 5.16 - 16-STORY UBC FRAME: POINT HINGE VS. E.S.D.O.F. $D+Q_{code}$. INTERACTION. ELASTIC. 1/4 EL CENTRO

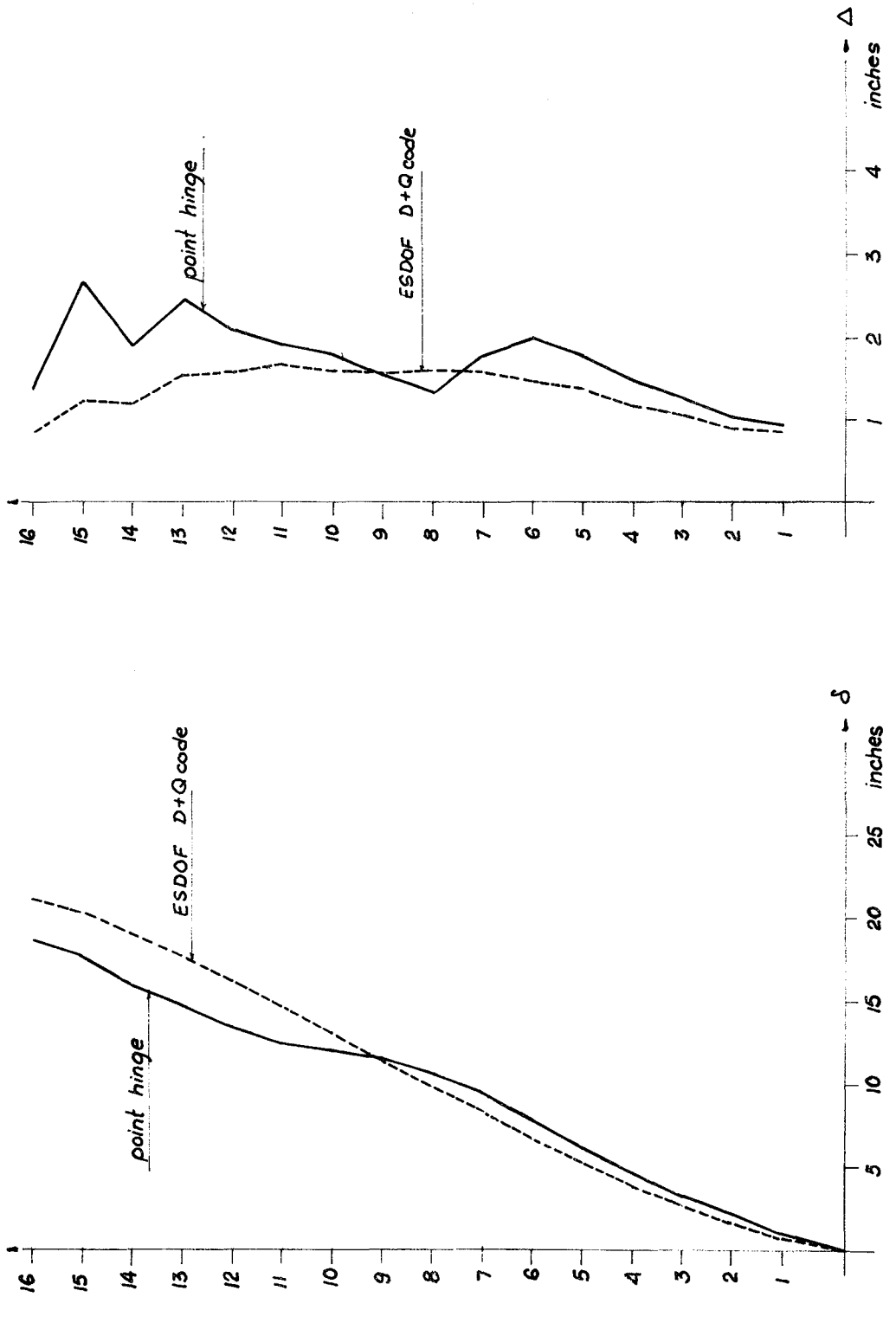

FIGURE 5.17 - 16-STORY UBC FRAME; POINT HINGE VS. E.S.D.O.F. $D+Q_{code}$. INTERACTION. EL CENTRO

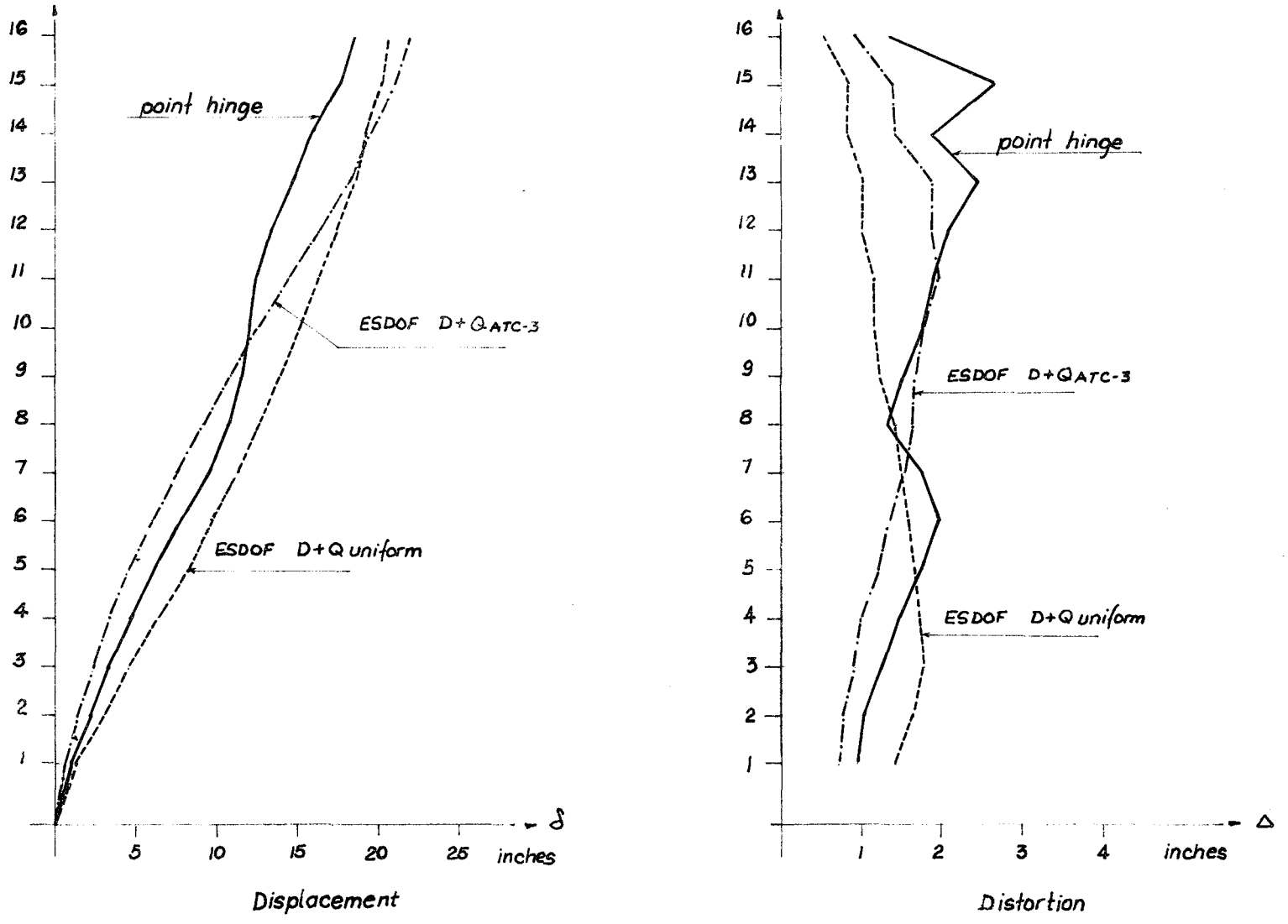

FIGURE 5.18 - 16-STORY UBC FRAME: POINT HINGE VS. E.S.D.O.F. $D+Q_{ATC-3}$. $D+Q_{uniform}$. INTERACTION. EL CENTRO

The results using the ATC-3 distribution show clearly the influence of the shape of the lateral load distribution. There is a noticeable change in curvature of the predicted displacement envelopes, which results in larger discrepancies with the point-hinge model, mainly on the lower floors. The results for distortion are similar in shape to the ones predicted using the code distribution, but with the difference that values are lower on the first seven stories, and higher on the upper ones. This amounts to a better agreement on the top floors, but a worse one for the bottom stories.

The uniform distribution gives very different results. The shape of the displacement envelope is mostly a shear-beam first mode (except on the first two floors), and it overestimates the response at all floors. The envelope for distortions is also very different, with much smaller values at the top and larger at the bottom. The shape does not resemble that of the point-hinge model.

Figure 5.19 shows the results for the case using the bending yield criterion, with the code distribution and under El Centro. Displacements predicted by both models are larger than for the interaction case, but the agreement between displacements and distortion envelopes is the same as the one obtained there. Figure 5.20 presents the responses obtained with both models for 1.87 Taft. The deflected shapes used are those from the code distribution.

The agreement for displacements is very good. Only in the top two stories, where the point-hinge model envelope shows a peculiar turn to the left, the E.S.D.O.F. fails to reproduce it properly. The discrepancies, however, are under 20% for most parts of the building, and slightly

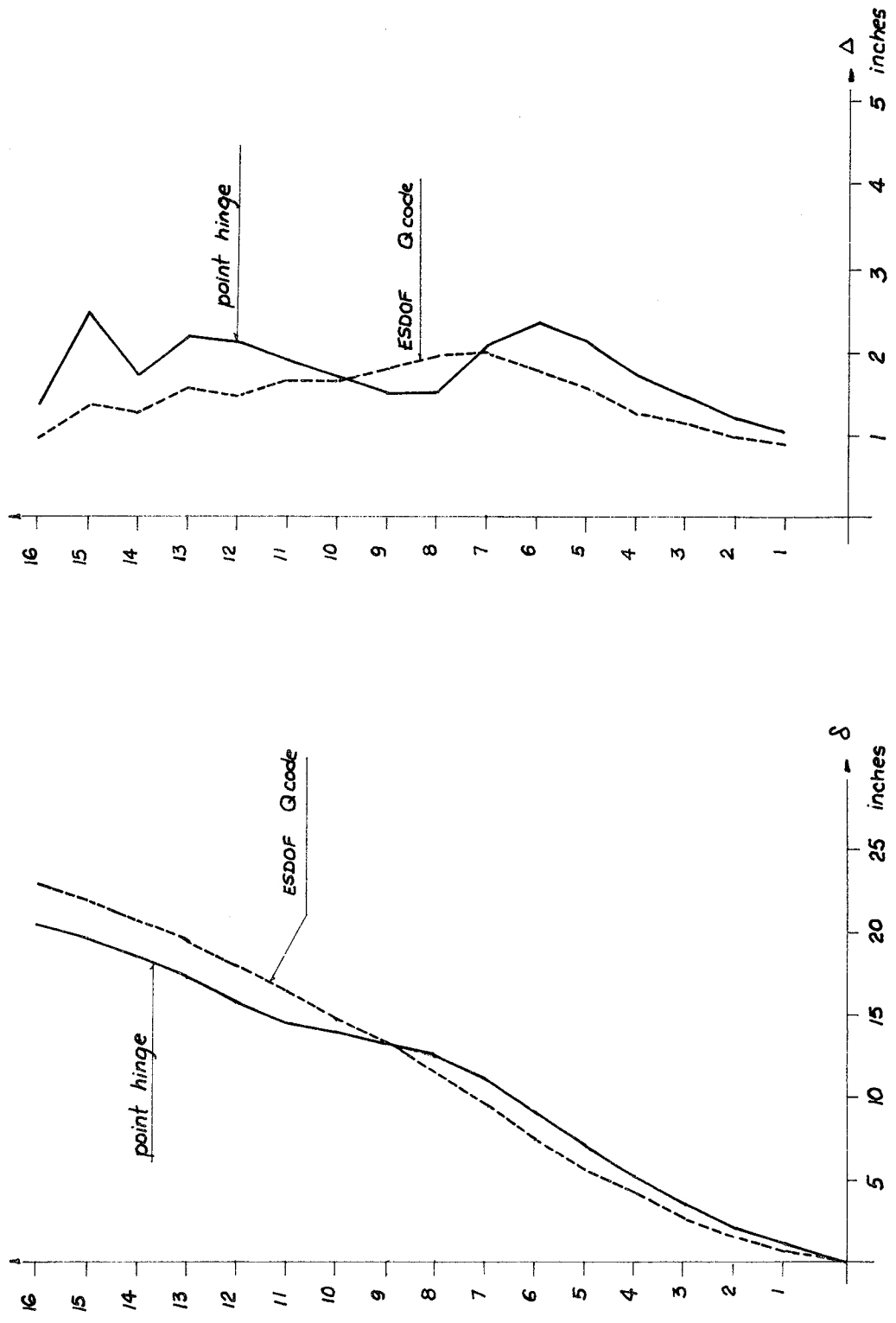

FIGURE 5.19 - 16-STORY UBC FRAME: POINT HINGE VS. E.S.D.O.F. Q_{code}. BENDING. EL CENTRO

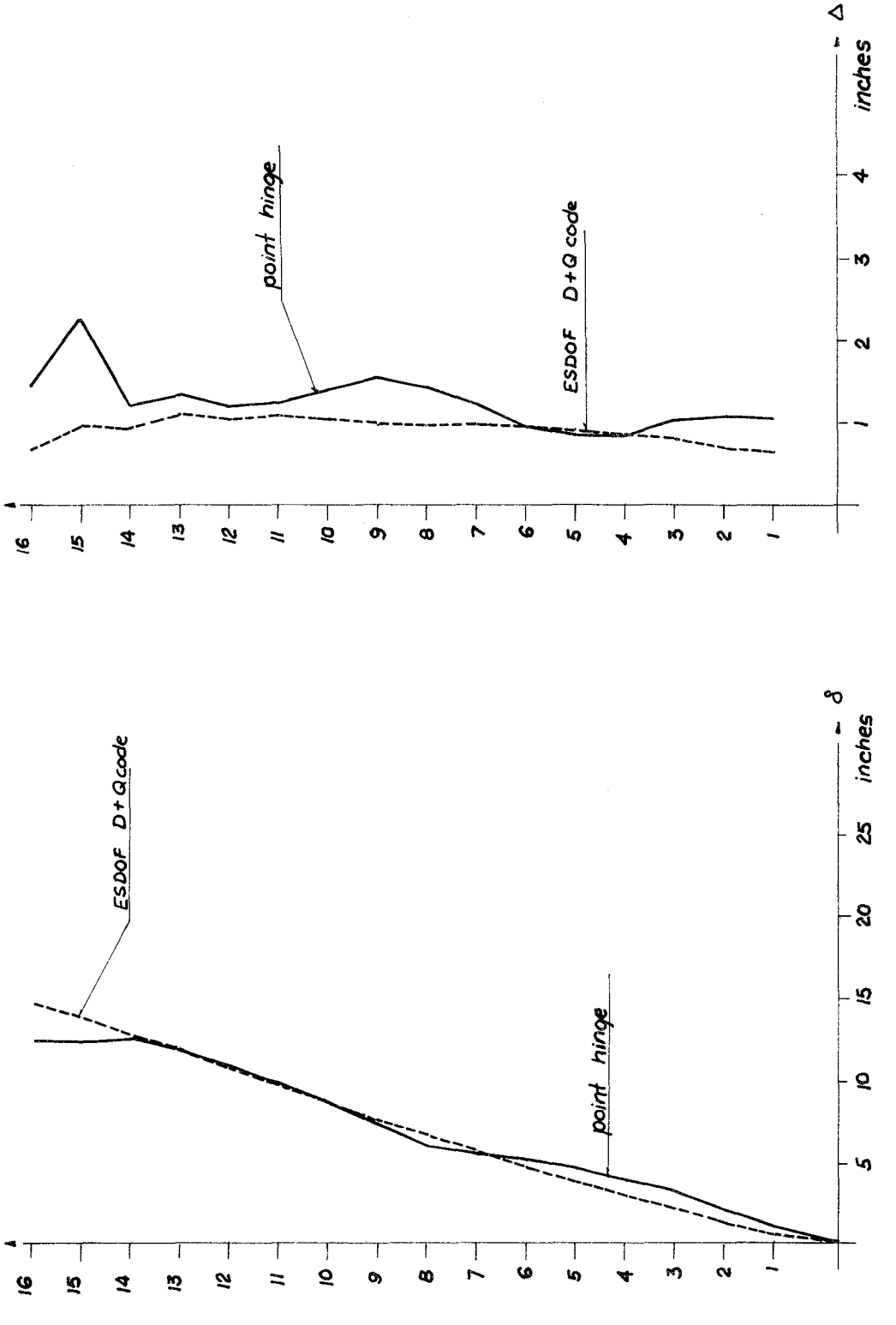

FIGURE 5.20 - 16-STORY UBC FRAME: POINT HINGE VS. E.S.D.O.F. $D+Q_{Code}$ INTERACTION. 1.87 x TAFT

larger in the lower stories. The envelope for distortions predicted by the E.S.D.O.F. is almost linear all the way up, and therefore does not reflect the variations that the point-hinge curve shows.

5.4 COMPARISON OF THE PERFORMANCE OF THE E.S.D.O.F. WITH THE SHEAR-BEAM ANALYSIS WITH MULTILINEAR SPRINGS

The ability of the E.S.D.O.F. to predict envelopes of maximum floor displacements is as good and in some cases even better than that of the multilinear shear beam. This is more noticeable for the four- and ten-story frames. In the taller frame the agreement is not as good on the upper six stories (compare, for example, Figures 3.10 and 3.11 with Figures 5.4 and 5.5 for the four-story frame; Figure 3.20 with Figures 5.8 and 5.9 for the ten-story UBC frame; Figure 3.26 with 5.12 for the Anderson frame; Figure 3.30 with 5.14 for Kamil's frame; and 3.36 with 5.17 for the sixteen-story UBC frame). When using the bending yield criterion, the E.S.D.O.F. compares even better than the multilinear shear beam in most cases (see Figures 3.21, 3.28, 3.31, and 3.37, and compare them with Figures 5.10, 5.13, 5.15, and 5.19). In the case of the sixteen-story frame, results compare well up to the tenth story and then the multilinear springs show better agreements.

When using 1.87 Taft, results are comparable; for the sixteen-story frame they show even better agreement than the multilinear springs.

Overall the shape of the envelopes predicted by the E.S.D.O.F. systems have different curvatures than those obtained from the multilinear dynamic analysis, but the agreements are of the same kind and the difference in terms of percentage usually smaller.

5.5 ESTIMATION OF DUCTILITIES BASED ON THE E.S.D.O.F. SYSTEM

Following the same procedure as for the multilinear springs, local member ductilities were computed using the predicted dynamic response of the E.S.D.O.F. Both floor displacement and interstory distortions were used in the computation.

Figures 5.21 and 5.22 present the results for the four-story UBC frame. Figure 5.21 shows the estimates based on the maximum floor displacements predicted by E.S.D.O.F. for rotation and moment ductilities. Agreements with the point-hinge model are acceptable in this case. The E.S.D.O.F. underestimates the magnitude practically at all floors. The maximum discrepancies are of the order of 30%. However, when compared to similar predictions obtained using the multilinear springs (Figure 3.41) the results are almost identical except for the first floor, where E.S.D.O.F. shows a closer correlation. Ductilities based on the maximum predicted distortions are presented in Figure 5.22. There is little change between these estimations and the ones based on displacements (Figure 5.21). However, for girder ductilities E.S.D.O.F. shows slightly better agreement than the multilinear springs (Figure 3.40), and for columns the envelopes show a smoother variation, although underestimating the magnitudes. This is not surprising, since the envelopes for distortion themselves are always smoother in the case of the E.S.D.O.F.

Figures 5.23 to 5.26 show ductilities for the ten-story UBC frame. The first two figures are for computations based on distortions. Predictions based on the E.S.D.O.F. give very similar results to the multilinear springs (Figures 3.42 and 3.43) for moment and rotation ductili-

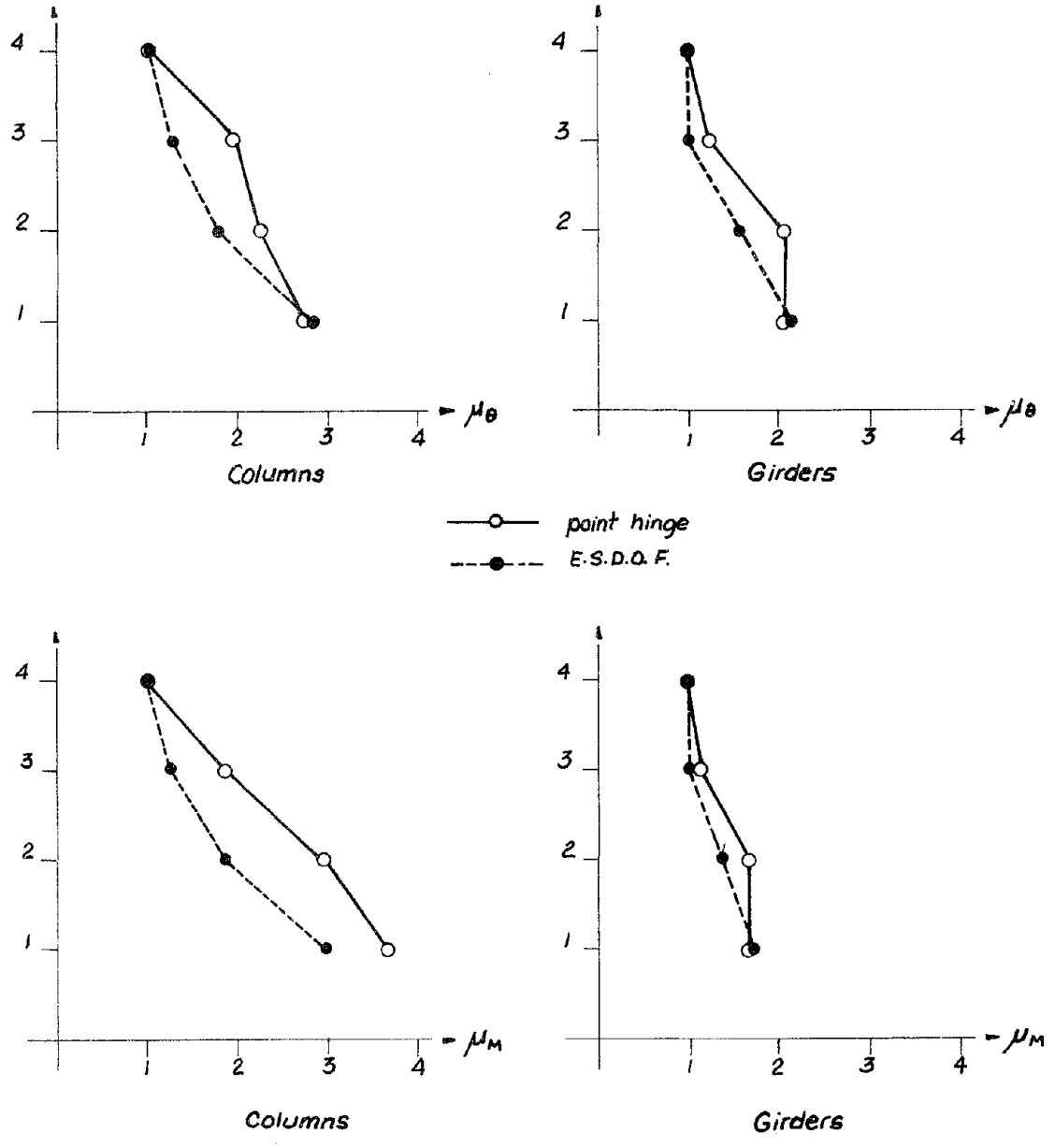

FIGURE 5.21 - 4-STORY UBC FRAME: MAX. DUCTILITIES BASED ON E.S.D.O.F. DISPLACEMENTS

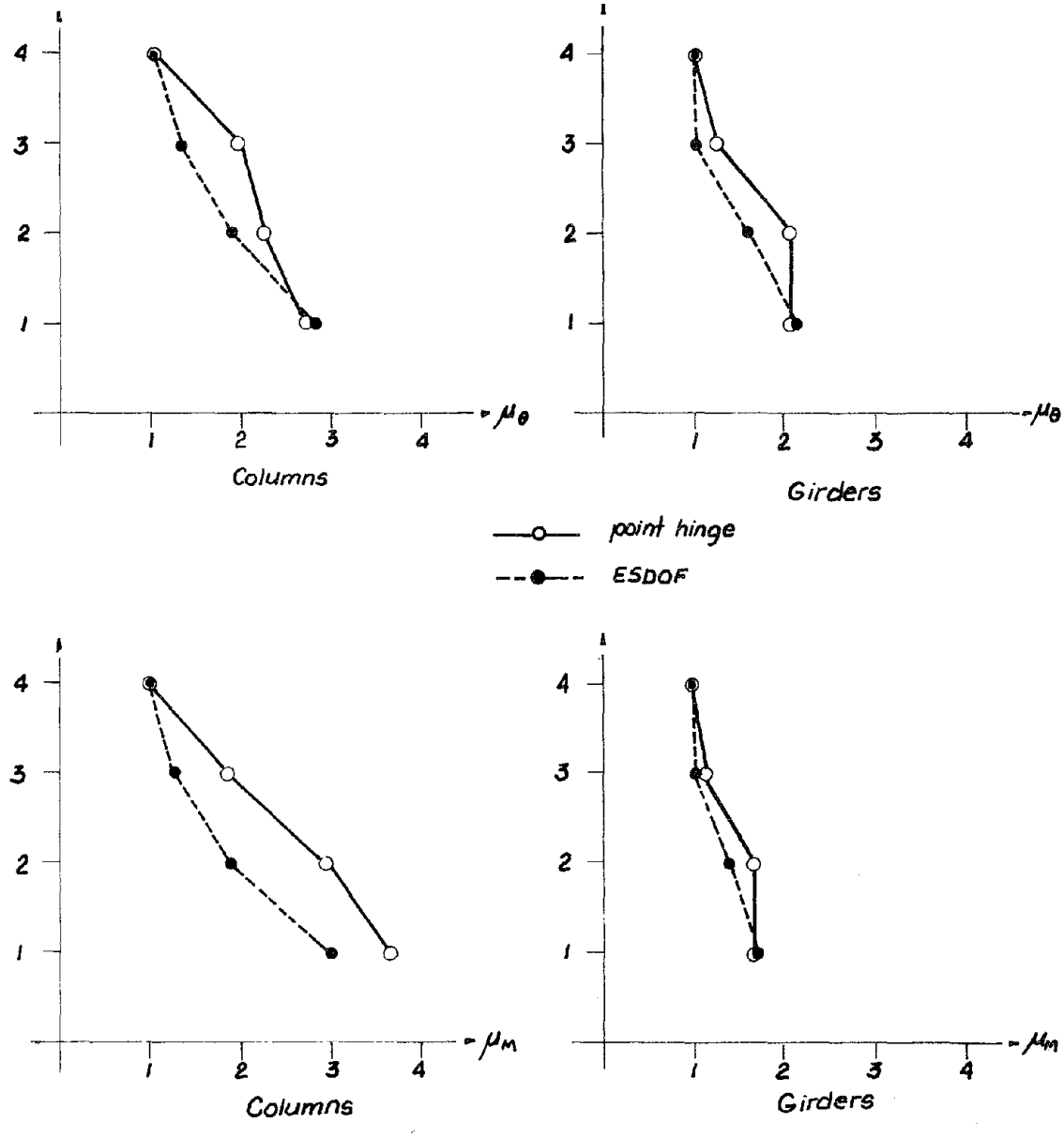

FIGURE 5.22 - 4-STORY UBC FRAME: MAX. DUCTILITIES BASED ON E.S.D.O.F. DISTORTIONS

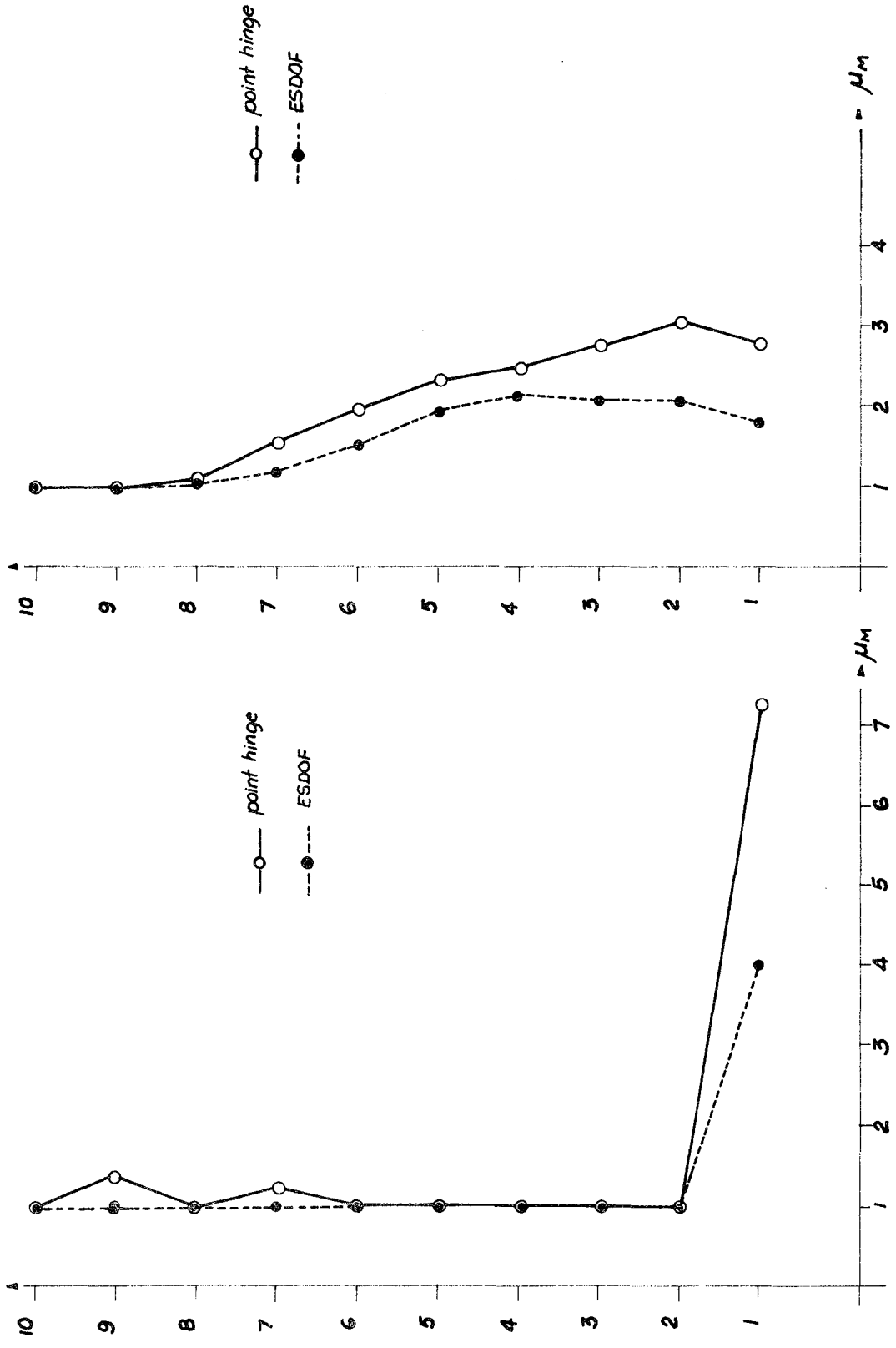

FIGURE 5.23 - 10-STORY UBC FRAME: MOMENT DUCTILITIES BASED ON E.S.D.O.F. DISTORTIONS

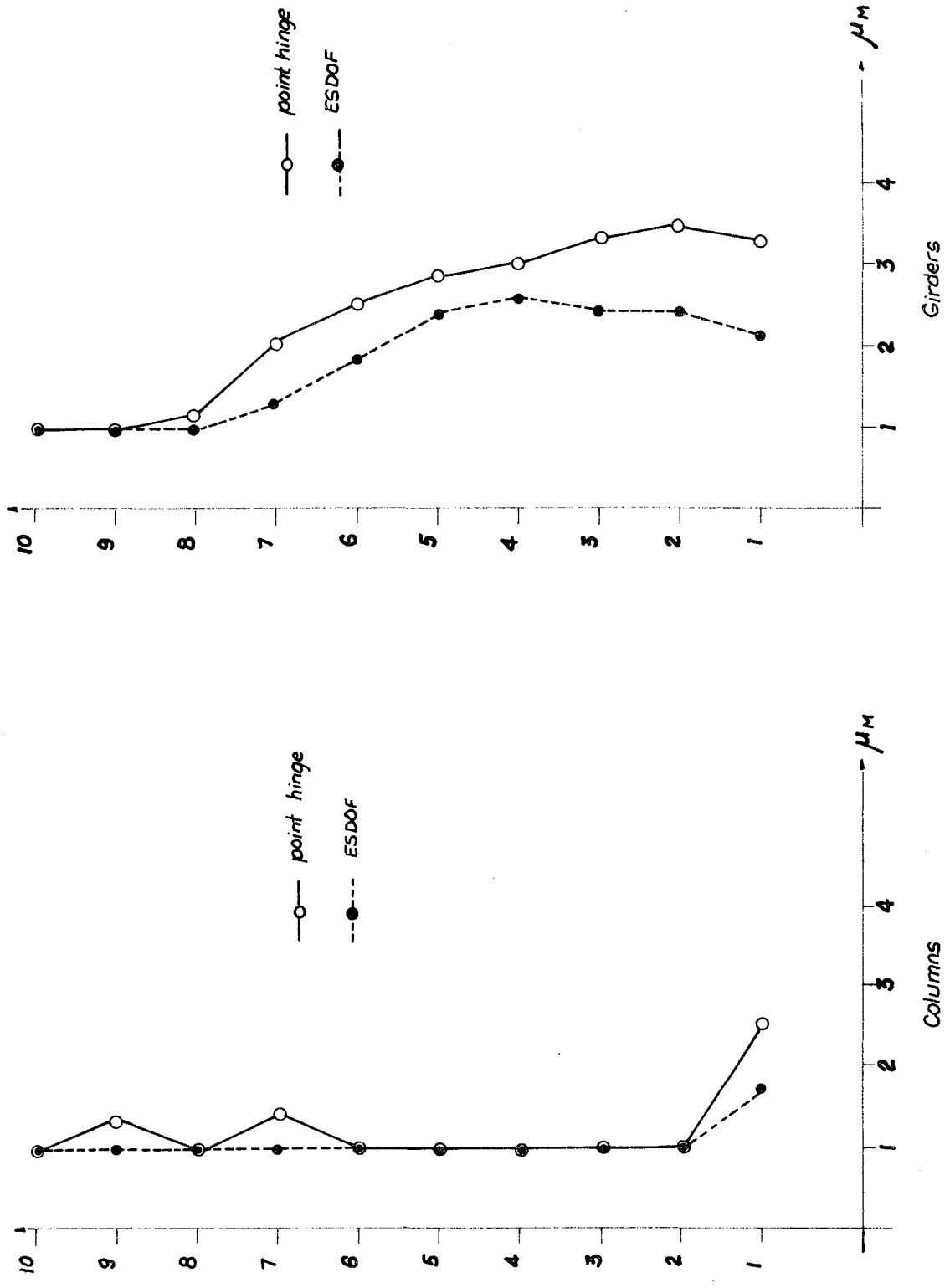

FIGURE 5.24 - 10-STORY UBC FRAME: ROTATION DUCTILITIES BASED ON E.S.D.O.F. DISTORTIONS

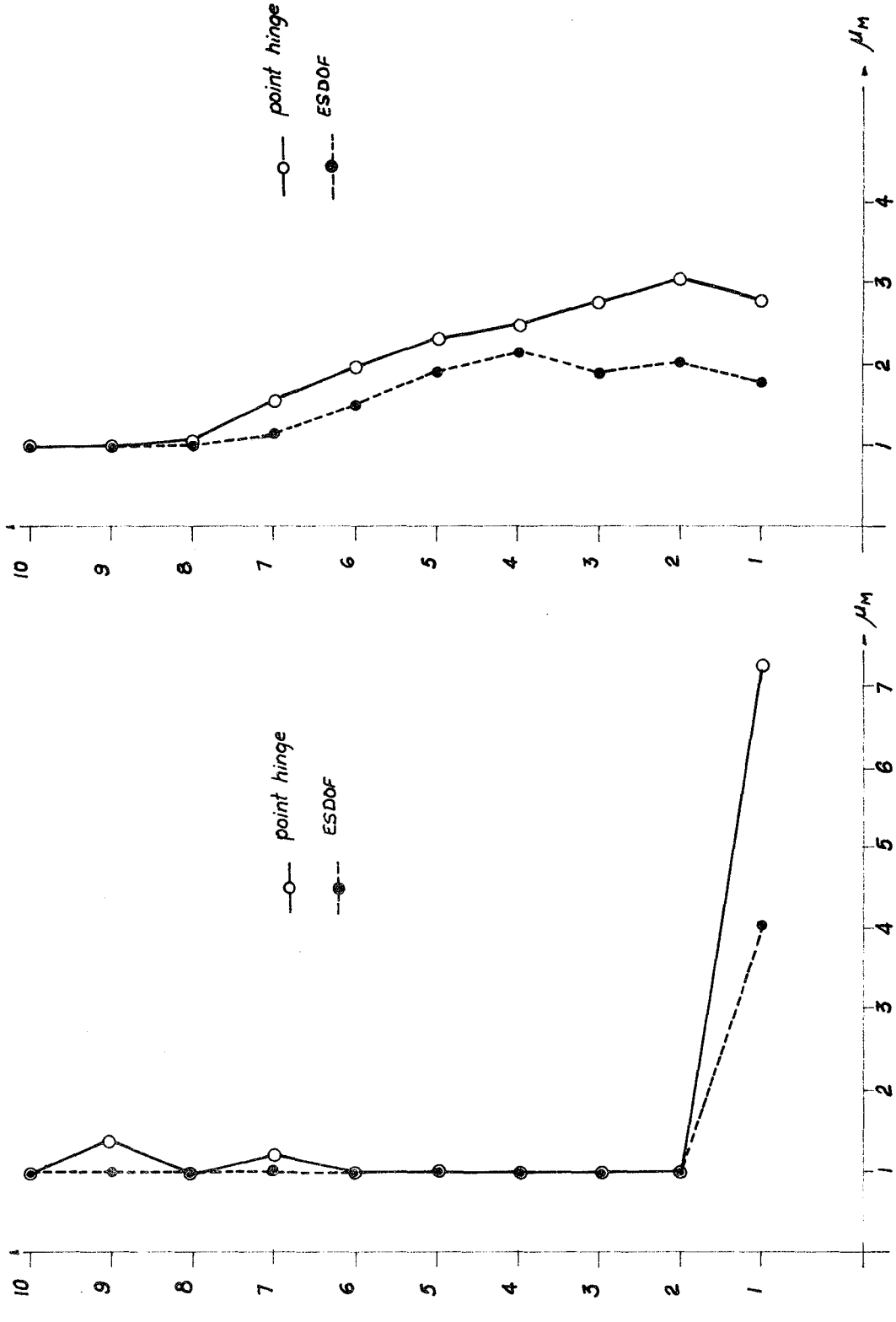

FIGURE 5.25 - 10-STORY UBC FRAME: MOMENT DUCTILITIES BASED ON E.S.D.O.F. DISPLACEMENTS

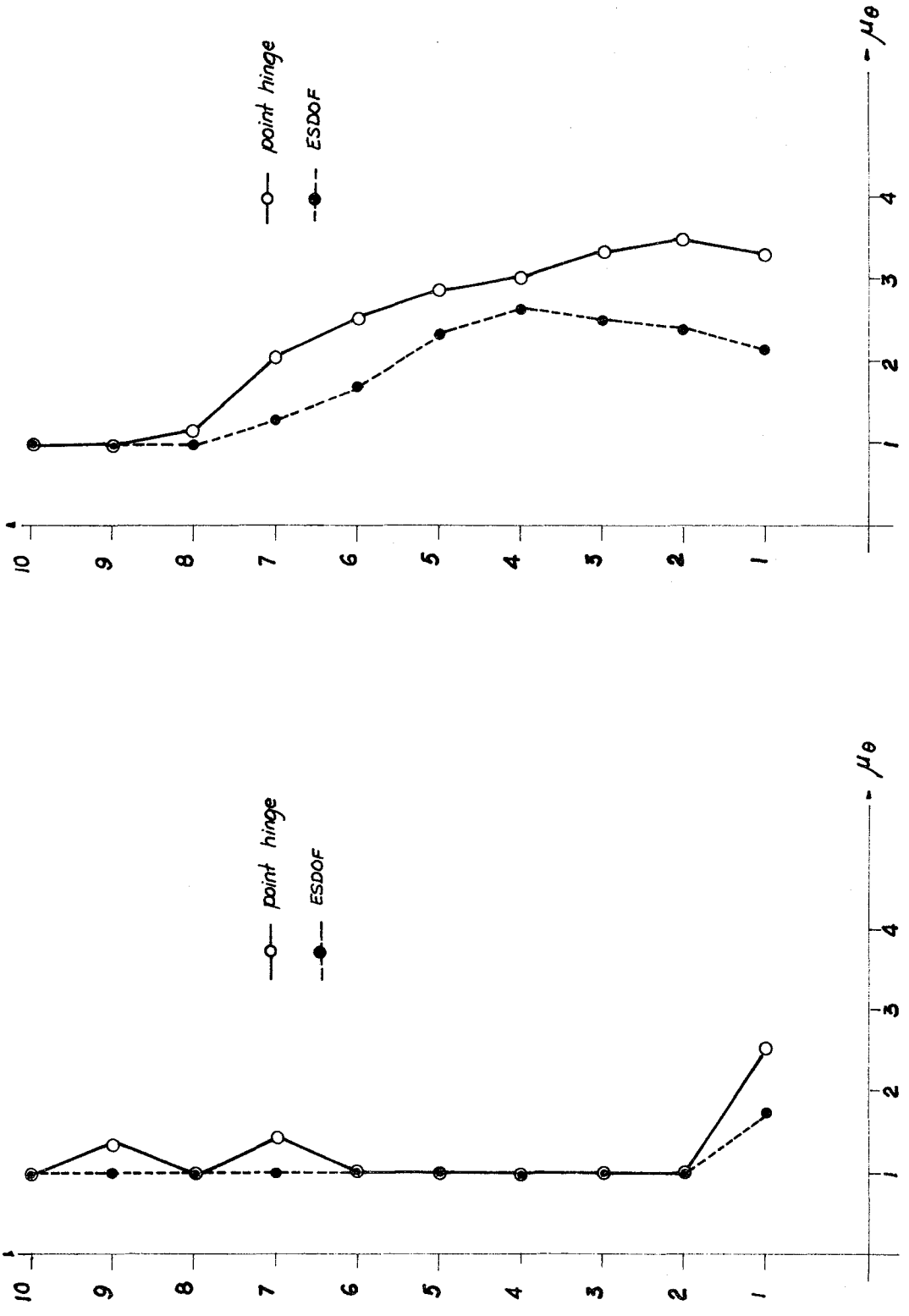

FIGURE 5.26 - 10-STORY UBC FRAME; ROTATION DUCTILITIES BASED ON E.S.D.O.F. DISPLACEMENTS

ties in the case of the girders. For the columns the agreement on the upper stories is not as good, the E.S.D.O.F. failing to reproduce the sudden changes that appear on the point-hinge envelope. When displacements are used, the ductilities predicted by the E.S.D.O.F. are very similar to those predicted by the multilinear springs (Figures 3.44 and 3.45). In the upper stories the agreement with the point-hinge ductilities is even better.

Figures 5.27 to 5.30 show the results for the sixteen-story UBC frame. Values computed based on distortions show acceptable correlation on the lower eleven stories, but discrepancies become large on the upper stories. For column ductilities, again the E.S.D.O.F. does not register ductilities larger than one on the upper floors. The multilinear springs show better agreement in this case.

When floor displacements are used in the estimations (Figures 5.29 and 5.30), a slightly better agreement is obtained for girders, but no change in the column ductilities is experienced. Moment ductilities show a better agreement with the point-hinge model than for the multilinear springs (when using also displacements, Fig. 3.48). Rotation ductilities show a better agreement, although in both cases the upper stories have rather large discrepancies.

5.6 EVALUATION OF THE E.S.D.O.F. SYSTEM PERFORMANCE

As compared to the dynamic response predicted by the point-hinge model, the E.S.D.O.F. gives reasonable agreements in terms of maximum floor displacements. The absolute differences encountered are acceptable

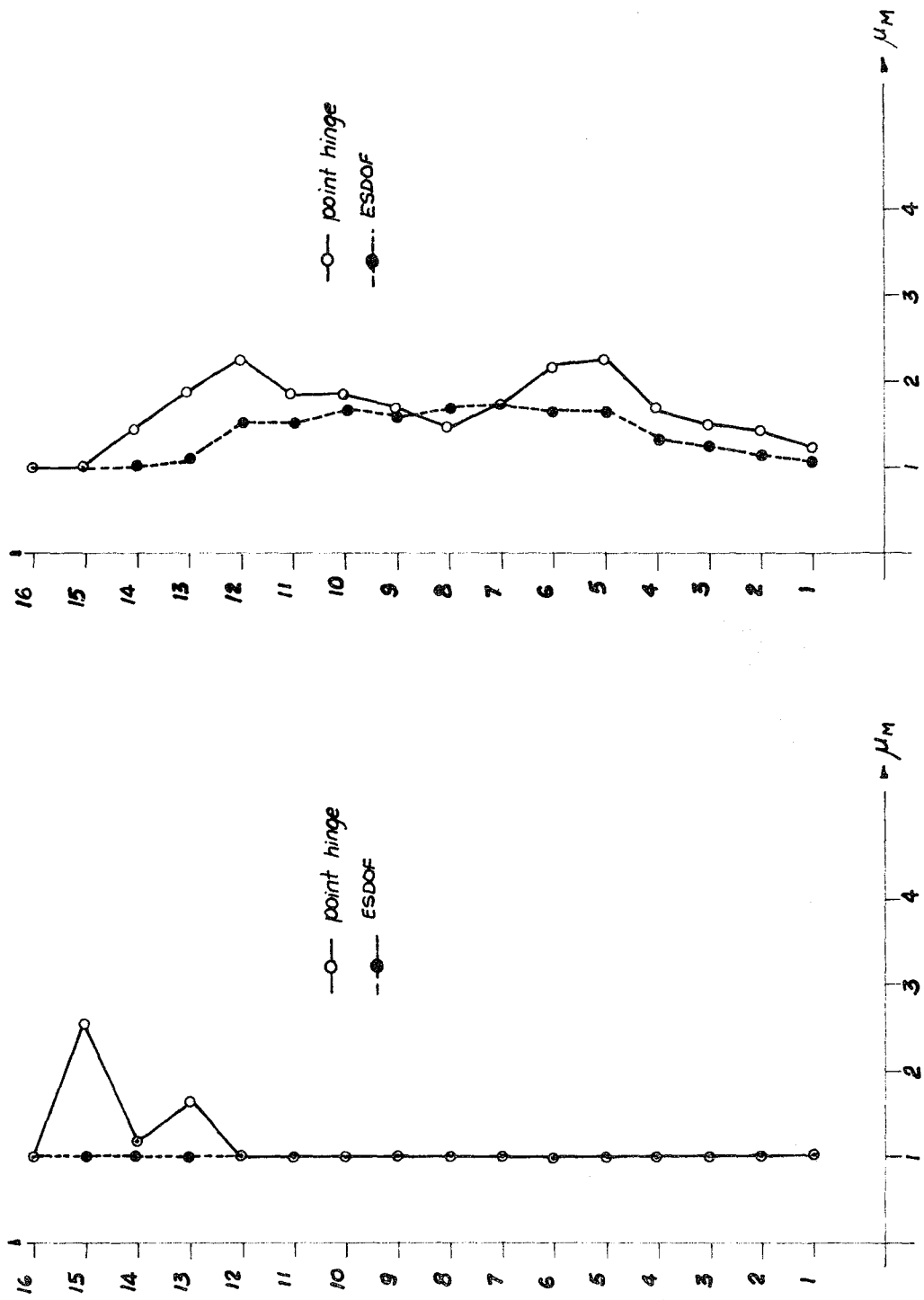

FIGURE 5.27 - 16-STORY UBC FRAME: MOMENT DUCTILITIES BASED ON E.S.D.O.F. DISTURTIONS

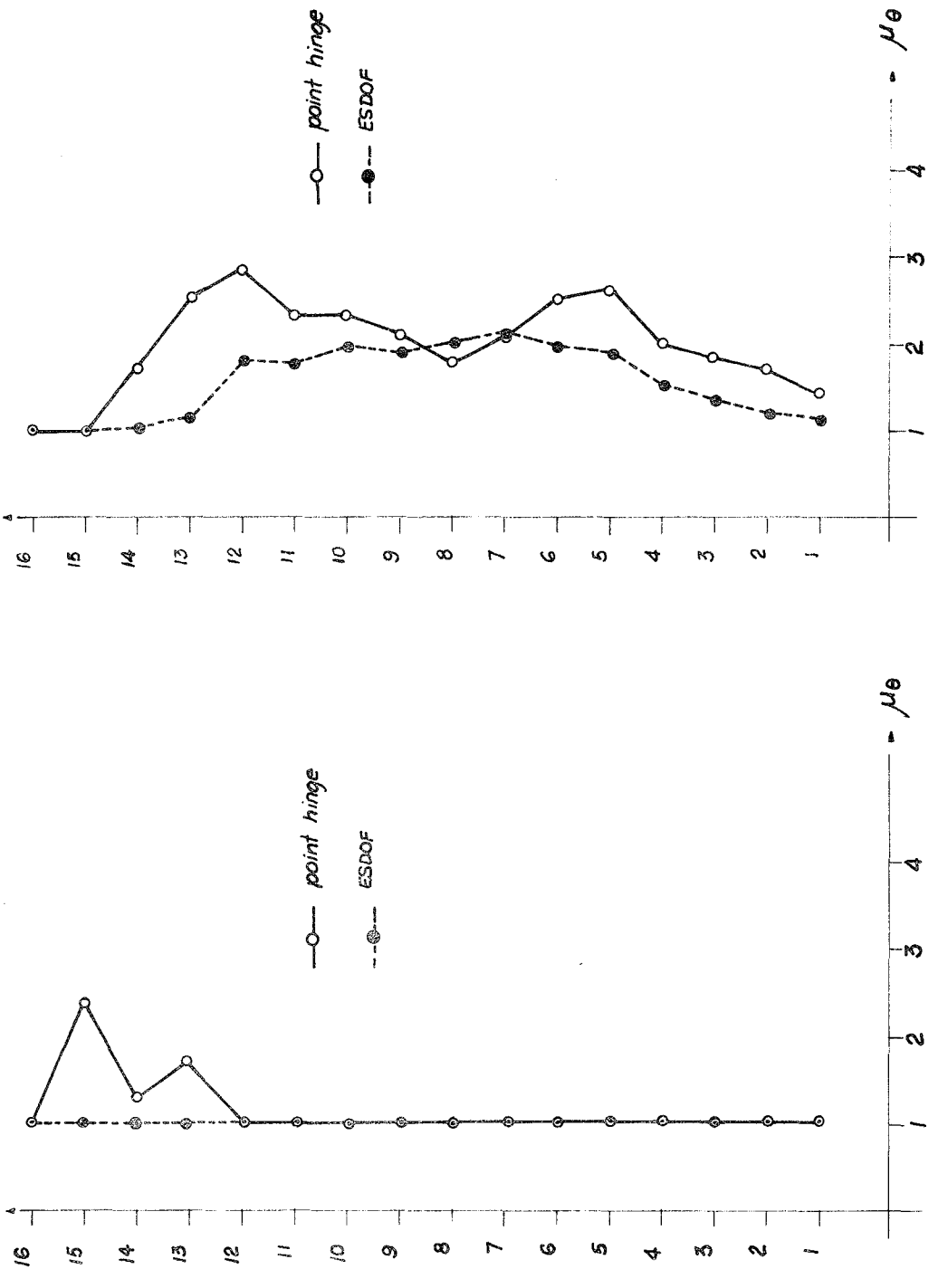

FIGURE 5.28 - 16-STORY UBC FRAME: ROTATION DUCTILITIES BASED ON E.S.D.O.F. DISTORTIONS

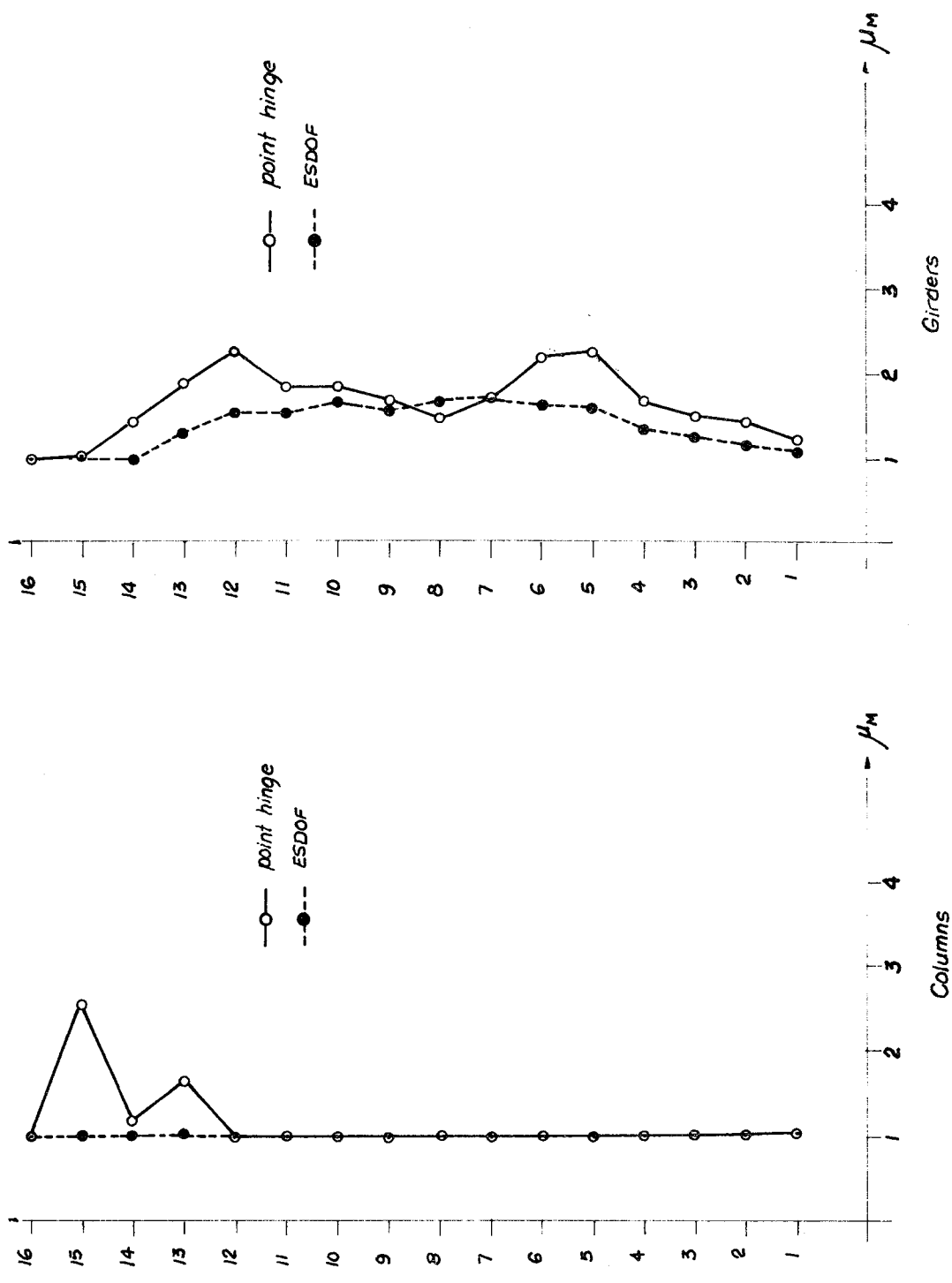

FIGURE 5.29 - 16-STORY UBC FRAME: MOMENT DUCTILITIES BASED ON E.S.D.O.F. DISPLACEMENTS

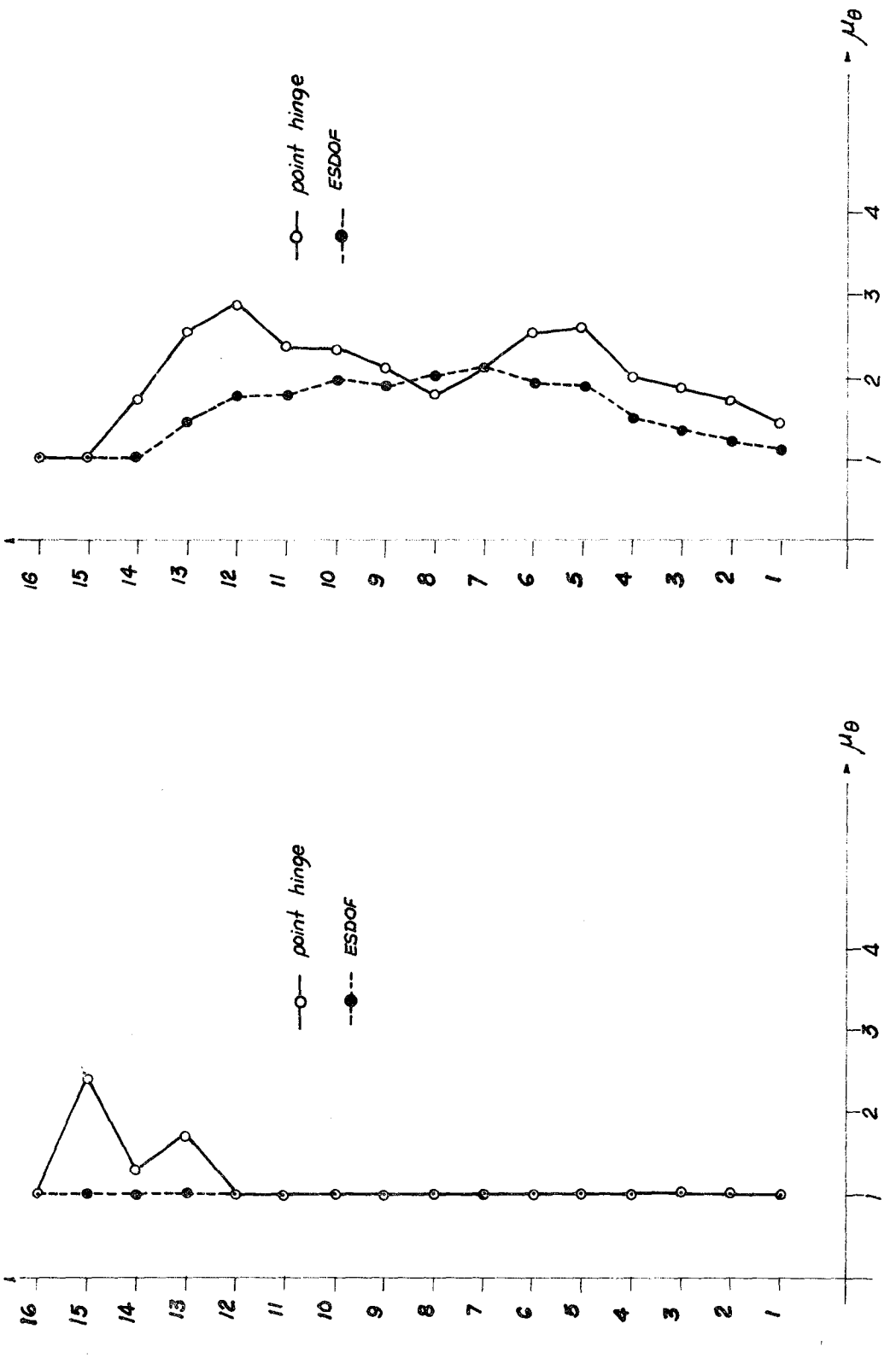

FIGURE 5.30 - 16-STORY UBC FRAME: ROTATION DUCTILITIES BASED ON E.S.D.O.F. DISPLACEMENTS

and always within the range of variation from one earthquake record to the other. In most cases, however, displacements are underestimated on the lower floors and overestimated on the upper floors, providing a shape for the envelopes with different curvature on the upper stories than the point hinge.

Since distortions are related to the deflected shapes used in the analysis, the model seems unable to represent properly reversals in the envelope of displacements and therefore, the magnitude of distortions on the upper floors. In most cases the E.S.D.O.F. underestimates the response on the top floors.

For the sixteen-story frame, where a negative curvature in the displacements envelope is almost always present, the model shows discrepancies (overestimations) which are larger for the upper stories. This seems to indicate a tendency to obtain predictions with less accuracy than for shorter structures.

For the four- and ten-story frames the E.S.D.O.F. shows comparable or even better agreement than the multilinear springs.

The local distribution used to obtain the deflected shapes had a larger influence on the dynamic response predicted by E.S.D.O.F. because the shape of the envelopes is closely related to the load distribution as opposed to the case of the shear-beam analysis, where the floor springs did not change substantially with the load.

The code and the SRSS of all modes distributions give the best agreements. Since the latter requires a previous elastic dynamic analysis, it seems appropriate enough to use the shapes obtained from the code loads.

Distortions were not estimated with the same agreement as displacements, being in most cases underestimated and limited in modeling the shape of the envelope. When the bending model was used, better agreements were found, in most cases.

When used to estimate ductilities, the performance of this model is again comparable to that of the multilinear springs when using displacements. The agreements are acceptable in general, although in most cases results are underestimated. There is very small difference in ductilities computed using displacements or distortions in most cases, though slightly better agreement will be found if displacements are used for this purpose, contrary to what was observed for the shear-beam model.

5.7 CONCLUSIONS

The conclusions for this chapter can be summarized as follows:

- A single-degree-of-freedom system can be used to study the inelastic dynamic response of a multidegree-of-freedom system,given a set of deflected shapes from a static analysis.

- Predictions in terms of displacements using this E.S.D.O.F. show reasonable agreement with the point-hinge model. In some cases the agreement is even better than using the shear-beam model. When using the bending model, the response was closer to the point-hinge predictions than with the interaction yield criterion.

- For taller frames, deviations are larger at the top floors, overestimating the response. The model is more appropriate for short or intermediate height buildings.

- The load distribution influences the response, resulting in different shapes for the displacement envelopes. The best agreement is found with the SRSS and code distributions. The uniform load distribution gives results very different from the others, and the poorest correlation with the point-hinge model.

- The shape of the displacement envelopes crosses that of the point-hinge model at about two-thirds of the building height. Displacements are underestimated at the bottom stories and overestimated at the top.

- Distortions are usually underestimated on the upper floors. On the lower floors the agreement is acceptable.

- Local ductilities estimated using the E.S.D.O.F. predicted displacements show reasonable agreement with the point-hinge model ductilities. The estimations using the multilinear springs are very similar to the ones from the simple model. Ductilities based on predicted distortions are not different from the ones based on displacements, but worse than those obtained with the shear-beam model (where the use of distortions represented in improvement over the use of displacements).

CHAPTER 6

CONCLUSIONS and RECOMENDATIONS

6.1 CONCLUSIONS

An evaluation of simple models to predict the inelastic dynamic response of frames has been presented in this study. Two types of models were considered, a shear-beam model with the floor springs determined on the basis of an incremental inelastic static analysis, and an equivalent one-degree-of-freedom system resulting from the same

analysis. This latter model would be easier to relate to code type design procedures.

The structures considered herein were: a four-story frame designed according to the UBC code (1973), three ten-story frames (one designed by UBC, Anderson's frame, and Kamil's frame), and a sixteen-story frame designed by UBC. All were steel moment-resisting frames. These frames were subjected to a very small intensity of motion so as to remain elastic, to the N-S component of the El Centro 1940 earthquake, to the N69W component of the Taft earthquake scaled to have the same Arias intensity as El Centro and to the El Centro earthquake scaled by a factor of 2.

For the cases studied it appears that the simple models can provide a reasonable approximation to the response. The ten-story frames under El Centro were the ones that showed larger differences, with a supposedly more rigorous point-hinge (dual-component) model. The maximum discrepancies in this case were of the order of 27% in floor displacements. The solutions obtained with the equivalent single-degree-of-freedom system are comparable to those of the shear-beam model. For the four- and ten-story frames, the results were even better as far as floor displacements are concerned; however, they deteriorate slightly for taller frames (16 stories). The model is less accurate in reproducing interstory distortions, and it is more sensitive to the assumed shape of the lateral loads used in the static analysis.

When the earthquake intensity was changed, the degree of accuracy of the results remained essentially the same (for the ten-story UBC

frame the agreement improved for larger motion intensity). For the two different earthquakes with the same intensity, the same was true (for the ten-story UBC frame again better agreement was obtained with Taft and also for the four-story frame). The structural responses were, however, very different for the two earthquakes.

The simple models behave better when using a bending yield criterion. Although the interaction with axial loads was accounted for in the static analysis, it would seem that the effect in the dynamic response was different.

Local ductilities were estimated, using the simple model predictions and the incremental static analysis. The results are acceptable in comparison to the point-hinge model predictions.

6.2 RECOMMENDATIONS

Continuing research is suggested in the following areas:

- Additional studies on the variation of response parameters with earthquake intensity is necessary to compare the trends in the response predicted by each model. Since the results seem to be very sensitive to the nature of the ground motion, it is further suggested that these studies be repeated for different earthquakes.

- Simpler approximate procedures to estimate the floor springs to use with the shear-beam model should be developed, based on the information provided by the more complete analysis.

- This study should be extended to buildings designed under different philosophies, and also to structures such as concrete building frames or shear walls with different force-deformations (stiffness degrading).

- Additional investigation is recommended on the simulation of the interaction effect in the simple models and mainly to include P-Δ effects.

- An extension of the single-degree-of-freedom reduction to a two- or three-degree-of-freedom equivalent systems in order to account for higher modes contribution, mainly for taller frames.

REFERENCES

1. Veletsos, A.S. and Newmark, N.M., "Effect of Inelastic Behavior on the Response of Simple Systems to Earthquake Motions," Proceedings of Second World Conference on Earthquake Engineering, Vol. II, 1961 (Tokyo).

2. Anagnostopoulos, S.A., Non-Linear Dynamic Response and Ductility Requirements of Building Structures Subjected to Earthquakes, Research Report R72-54, M.I.T. Department of Civil Engineering, Publication No. 349, September 1972.

3. Veletsos, A.S., "Maximum Deformations of Certain Non-Linear Systems," Proceedings of the Fourth World Conference on Earthquake Engineering, Vol. II, 1969 (Santiago, Chile).

4. Takizawa, Haruo, "Non-Linear Models for Simulating the Dynamic Damaging Process of Low-Rise Reinforced Concrete Buildings during Severe Earthquakes," International Journal of Earthquake Engineering and Structural Dynamics, Vol. 4, pp. 73-94, September 1975.

5. Iwan, W.D., "A Model for the Dynamic Analysis of Deteriorating Structures," Proceedings of the Fifth World Conference on Earthquake Engineering, Vol. II, pp. 1782-1791 (Rome, 1973).

6. Nielsen, N.N. and Imbeault, F.A., "Validity of Various Hysteretic Systems," Proceedings of the Third Japan Earthquake Engineering Symposium, 1970, pp. 707-714.

7. Clough, R.W. and Johnston, S.B., "Effect of Stiffness Degradation on Earthquake Ductility Requirements," Proceedings of the Japan Earthquake Engineering Symposium, 1967.

8. Biggs, J. M., Introduction to Structural Dynamics, McGraw-Hill, New York, 1964.

9. Clough, R.W. and Benuska, K.L., FHA Study of Seismic Design Criteria for High-Rise Buildings, HUD TS-3, August 1966.

10. Anderson, J.C. and Bertero, V.V., Seismic Behavior of Multistory Frames Designed by Different Philosophies, Report No. EERC-69-11, Earthquake Engineering Research Center, University of California at Berkeley, October 1969.

11. Giberson, Melbourne F., "Two Nonlinear Beams with Definitions of Ductility," Journal of the Structural Division, ASCE, ST2, February 1969, pp. 137-157.

12. Goel, S.C., Response of Multistory Steel Frames to Earthquake Forces, Steel Research for Construction Bulletin 12, November 1968.

13. Kamil, H., "Optimum Inelastic Design of Unbraced Multistory Frames Under Dynamic Loads," Ph.D. Thesis, University of California, Berkeley, June 1972.

14. Fukada, Y., "Study on the Restoring Force Characteristics of Reinforced Concrete Buildings," Proceedings Kant. Dist. Symposium, Architectural Institute of Japan (1965).

15. Takeda, T., Sozen, M.A. and Nielsen, N., "Reinforced Concrete Response to Simulated Earthquakes," Proceedings of the Third Earthquake Engineering Symposium, 1970, pp. 357-364.

16. Aziz, Tarek, S.A., Inelastic Dynamic Analysis of Building Frames, Sc.D. Thesis, Department of Civil Engineering, M.I.T., Sept. 1974.

17. Mahin, S.A. and Bertero, V.V., An Evaluation of Some Methods for Predicting Seismic Behavior of Reinforced Concrete Buildings, Report No. EERC 75-5, University of California, Berkeley, February 1975.

18. Luyties, W.H.III, Anagnostopoulos, S.A. and Biggs, J.M., Studies on the Inelastic Dynamic Analysis and Design of Multistory Frames, Report No. R76-29, M.I.T. Department of Civil Engineering, July 1976.

19. American Institute of Steel Construction (AISC), Specification for the Design, Fabrication and Erection of Structural Steel for Buildings, AISC, New York, February 1969.

20. American Concrete Institute (ACI), Building Code Requirements for Reinforced Concrete (ACI 318-71), ACI, Michigan, 1971.

21. Perez, Fernando and Roesset, J.M. (Supervisor), "Comportamiento Plástico de Pórticos Bajo Carga Dinámica," Engineering Thesis, Universidad Católica de Chile, Santiago, Chile, 1968.

22. LaTona, R.W., and Roesset, J.M., Non-Linear Analysis of Building Frames for Earthquake Loading," Research Report R70-65, M.I.T. Department of Civil Engineering, September 1970.

23. Adams, John, "Non-Linear Behavior of Steel Frames," Ph.D. Thesis, M.I.T. Department of Civil Engineering, June 1973.

24. Mark, Kenneth, "Nonlinear Dynamic Response of Reinforced Concrete Frames," Sc.D. Thesis, M.I.T. Department of Civil Engineering, September 1974.

25. Unemura, H., Aoyama, H., Takizawa, H., "Analysis of the Behavior of Reinforced Concrete Structures During Strong Earthquakes Based on Empirical Estimation of Inelastic Restoring Force Characteristics of Members," Proceedings Fifth World Conference on Earthquake Engineering, 1973 (Rome).

26. Luyties, W.H. III, Anagnostopoulos, S.A., and Roesset, J.M., FRIEDA - A Computer Program for Frame Inelastic Earthquake Dynamic Analysis - Documentation and User's Guide (to be published) M.I.T. Department of Civil Engineering.

27. Uniform Building Code, International Association of Building Officials, California, 1973.

28. SEAOC, (Structural Engineers Association of California), Recommended Lateral Force Requirements and Commentary, San Francisco, California, 1974.

29. Applied Technology Council, Working Draft of Recommended Seismic Design Provisions for Buildings, ATC-3-04, San Francisco, January, 1976.

30. Roesset, J.M.,"APPLE PIE", Computer Program for Linear Dynamic Analysis for Tri-dimensional Structures, M.I.T. Dept. of Civil Engineering, 1972.

31. Przemieniecki, J.S., Theory of Matrix Structural Analysis, McGraw Hill, New York, 1968.

32. Connor, J.J. Jr., Structural Member Systems, Ronald Press, New York, January 1976.

33. Roesset, J.M., Class notes on Structural Dynamics, M.I.T., 1969.

34. Crandall, S.H., Engineering Analysis, McGraw-Hill, New York, 1956.

35. Haviland, R.W., "Inelastic Response Spectrum Design Procedures for Steel Frames," M.S. Thesis, M.I.T. Department of Civil Engineering, August, 1976.

36. Kubori, T., Minai, R., and Fujiwara, T., "Earthquake Response of Frame Structures Composed of Inelastic Members," Proceedings of the Fifth World Conference on Earthquake Engineering, Vol. II, pp. 1772-1781, 1974 (Rome).

37. Arias, A., "A Measure of Earthquake Intensity," in Seismic Design for Nuclear Power Plants, R. J. Hansen, Editor, MIT Press, Cambridge, Massachusetts, 1969.

38. United States Steel, Column Design Curves, Pittsburgh, 1969.

APPENDIX A

A.1 FOUR-STORY UBC FRAME

In Figures 2.1 and 2.2 the plan and elevation of the four-story frame are shown. The design is based on the specifications of the Uniform Building Code, 1973 version [27].

The loads used were:

dead load	80 psf	
live load	40 psf	for typical floor
	20 psf	for roof.

Lateral loads were computed as for zone 3 following the code distribution.

A preliminary design was performed using full dead and live load in all members, using approximate coefficients to determine maximum moments in girder sections. All girder spans in a given floor were assigned the same section, since it was thought impractical to have different profiles at every span.

Code Lateral Loads:

Dead Load on Girders:	352 kips
Girders and Columns:	15 kips
	367 kips

Base Shear: $V = ZKCW$

$Z = 1$ (Zone 3)

$K = 0.67$ (Moment-Resisting Frame)

$$C = \frac{0.05}{\sqrt[3]{T}}, \quad T = 0.1N = 0.4 \text{ secs.}$$

$C = 0.0679$

$V = 0.67 \times 0.0679 \times 367 = 16.7$ kips

$$V = 16.7 \text{ kips}$$

Code Distribution $F_i = \frac{W_i h_i}{\Sigma W_i h_i}$

Story	F_i (kips)	Mass (K-sec^2/ft)
1	1.67	2.83
2	3.34	2.83
3	5.01	2.83
4	6.68	2.80

The AISC specifications were used for the design requirements on steel sections. Yield stress was 36 Ksi for all sections and frames. The sections were assumed properly braced against lateral buckling, so that they could be considered "compact" for working stresses. For girders F_b = 24 Ksi.

For the combination of dead plus live load plus earthquake (D+L+Q) the allowable increase in working stress of 33% was followed (See 2303 UBC) or a reduction in acting moments.

Analysis using the properties from the preliminary design were done using a computer program for the following combinations

D + L in all spans
D + L in alternate spans (max. positive)
D + L in two adjacent spans (max. negative)
3/4(D + L + Q)

Designs were done for the maximum effects of these combinations. For girder design, the maximum moments were used to proportion the sections and then checked for shear and deflections (due to live load) limitations.

Girders	Story	Max. M_{D+L} (Kip-ft)	Max. $M_{3/4(D+L+Q)}$ (Kip-ft)	Section
	1	80.6	75	W16 x 31
	2	80.6	76	W16 x 31
	3	80.5	70.7	W16 x 31
	4	67.33	56.0	W16 x 26

The first- , second- , and fourth-story girders were changed (reduced) as compared to the preliminary design.

Columns

For column design, the frame was assumed to be fully braced in the out-of-plane direction (Y-direction) and therefore K_y for all columns was taken as 1. K_x was computed according to the AISC procedure. The section properties were obtained by using a Handbook for Column Design by U.S. Steel [38], which contains interaction diagrams prepared, based on the AISC code specifications. Table A.1 shows the maximum effects and design profiles. For practical purposes sections were maintained at least for two stories, even though they may not have been needed.

INTERIOR COLUMN

Story	K_x	D + L		3/4 (D + L + Q)		Section
		P	M	P	M	
4	1.42	35.7	24.1	24.0	40.0	W10 x 33
3	1.52	78.1	13.8	57.8	24.7	W10 x 33
2	1.52	120.6*	18.7	89.2	32.0	W10 x 39
1	1.42	163.2*	12.9	120.0	23.2	W10 x 39

EXTERIOR COLUMN

Story	K_x	D + L		3/4 (D + L + Q)		Section
		P	M	P	M	
4	1.89	19.2	52.5	15.0	44.2	W10 x 33
3	2.08	42.9	31.0	33.0	31.5	W10 x 33
2	2.02	66.4	41.2	52.5	39.0	W10 x 39
1	1.65	89.8	28.4	72.0	27.7	W10 x 39

(*) No live load reduction included

TABLE A.1 - COLUMN DESIGN. FOUR-STORY FRAME

All of these column sections were smaller than the ones used in the preliminary design. The analysis was repeated with these new properties, and it was found that no changes were required.

A constant wind pressure of 20 psf was used to check the capacity of the structure, and all sections were found satisfactory.

Lateral deflections were computed under lateral loads from earthquakes and wind to check against drift requirements. No changes were necessary.

The limiting criteria for interstory drift and total drift was

$$\frac{\Delta_i}{i} \leq \frac{1}{350} \qquad \frac{\delta_{top}}{h_t} \leq \frac{1}{350} \quad \text{for wind} \tag{A-1}$$

$$\frac{\Delta_i}{h_i} \leq \frac{1}{500} \qquad \frac{\delta_{top}}{h_t} \leq \frac{1}{500} \quad \text{for earthquake} \tag{A-2}$$

DEFLECTIONS (in)

Floor	Earthquake	Wind
1	0.16	0.13
2	0.36	0.26
3	0.53	0.36
4	0.64	0.39

A.2 TEN-STORY FRAME

The plan and elevation of this frame are shown in Figures 2.3 and 2.4. The loads used for this design were

dead load	80 psf	
live load	50 psf	on typical floors
	20 psf	on roof
wind load	20 psf	uniform

Sections were initially determined based on an approximate analysis for full dead plus live loads. The same criterion in terms of keeping girders the same for all spans in a given floor, and columns every two stories as for the four-story frame, was used.

Code Lateral Loads

Total Weight

dead load on girders	960 kips
girders and columns	48 kips
	1008 kips

Base Shear

$Z = 1$, $K = 0.67$, $T = 0.1N = 1$ sec. , $C = 0.05$

$$V = ZKCW = 0.67 \times 0.05W = 0.0335\ W$$

$$V = 0.0335 \times 1008 = 33.77 \text{ kips}$$

$$\underline{V = 33.77 \text{ kips}}$$

Code Distribution

$$F_i = \frac{W_i\ h_i}{\Sigma W_i h_i} \qquad (h/D < 3)$$

Story	F_i (kips)	Mass (kips-sec^2/ft)
1	0.75	3.14
2	1.33	3.14
3	1.92	3.14
4	2.51	3.14
5	3.10	3.14
6	3.68	3.14
7	4.27	3.14
8	4.86	3.14
9	5.45	3.14
10	5.91	3.07

The same criteria in terms of allowable stresses and load combinations as for the four-story frame were used in this case.

Girder Design

Table A.2 shows the maximum effects on girders and the results of the first analysis. It also shows the changes that resulted from the analysis using these new properties as the sections resulting from a combination of D+L+W (wind). These last were the final properties. No changes were required by drift limitations.

Column Design

Columns were assumed to be properly braced in the out-of-plane direction (Y); K_y was taken as 1. K_x was computed according to the AISC procedure described in the Commentary to the Specifications. Interaction diagrams were used in the design and the maximum effects of the different load combinations were taken. Tables A.3 and A.4 present the moments and loads from the maximum vertical load effects (whatever load pattern

Story	Max. Moment K-' D+L	3/4(D+L+Q)	Section Profile 1st Trial	2nd Trial	D+L+W Final
1	93.5	117.2	W18 x 40 *	W18 x 40	W18 x 40
2	91.7	116.9	W18 x 40 *	W18 x 40	W18 x 40
3	92.4	115.5	W18 x 35	W18 x 35	W18 x 40
4	92.7	112.6	W18 x 35	W18 x 35	W18 x 35
5	93.2	109.0	W18 x 35	W18 x 35	W18 x 35
6	94.0	104.2	W18 x 35	W18 x 35	W18 x 35
7	93.7	98.7	W18 x 35	W18 x 35	W18 x 35
8	93.6	91.9	W16 x 31 *	W18 x 35	W18 x 35
9	93.2	84.2	W16 x 31 *	W18 x 35	W18 x 35
10	73.8	61.3	W16 x 26 *	W16 x 31	W18 x 35

(*) Changed from preliminary design

TABLE A.2 - TEN-STORY FRAME. GIRDER DESIGN

Story	K_x	D+L		3/4 (D+L+Q)		Section
		P**	M	P	M	
1	1.48	426.8	2.5	391.5	72.3	W14 x 95Q*
2	1.70	381.6	3.7	351.0	52	W14 x 95Q*
3	1.70	336.4	2.7	311	48.7	W14 x 78Q*
4	1.63	291.2	2.7	271	46	W14 x 78Q*
5	1.59	294.9	3.1	231	43	W14 x 61Q
6	1.55	208.0	3.2	155.2	44.6	W14 x 61Q*
7	1.5	166.4	3.4	123.8	40.5	W14 x 43D*
8	1.45	124.8	3.2	91	31.6	W14 x 43D
9	1.41	88.8	3.0	59.8	28.9	W10 x 35D*
10	1.36	41.6	5.8	27.9	18.6	W10 x 33D*

TABLE A.3 - TEN-STORY FRAME, INTERIOR COLUMN DESIGN

Story	K_x	D+L		3/4 (D+L+Q)		Section
		P	M	P	M	
1	1.61	208.0	26.6	215.0	63.0	W14 x 68Q*
2	2.02	187.2	44.7	192.0	58.5	W14 x 68Q*
3	2.02	166.4	38.7	168.0	53.9	W14 x 61Q
4	1.97	145.6	35.8	144.7	51.5	W14 x 61Q*
5	1.90	124.8	38.8	121.5	51.9	W14 x 48Q*
6	1.82	104.0	34.5	99.0	46.5	W14 x 48Q*
7	1.78	86.8	35.6	76.5	43.5	W10 x 39D*
8	1.78	68.0	35.8	55.5	42.0	W10 x 39D*
9	1.78	46.0	34.4	34.5	36.0	W10 x 33D*
10	1.67	20.8	48.2	15	42.0	W10 x 33D*

TABLE A.4 - TEN-STORY FRAME, EXTERIOR COLUMN DESIGN

** Includes Live load reduction

* Changed from preliminary design

Q = Controlled by 3/4 (D+L+Q)

D = Controlled by D+L

gave the largest loads and moments) and the ones from the combination of maximum dead, live and earthquake loads. The resulting section profiles for the most unfavorable situation are also shown. Design was controlled by lateral loads up to the sixth floor; D+L thereafter. The analyses were repeated using these new properties, and no changes were required on the columns. Also an analysis for the combination of dead, live and wind loads was carried out, and the sections did not have to be changed in this other case. Drift computations for wind and earthquake gave the following results; all were within the tolerances specified by equations (A-1) and (A-2). Table A.5 contains the results.

DEFLECTIONS (in)

Floor	Earthquake		Wind	
	Δ	δ_T	Δ	δ_T
1	0.35	0.35	0.48	0.48
2	0.33	0.68	0.40	0.88
3	0.35	1.03	0.40	1.28
4	0.35	1.38	0.37	1.65
5	0.34	1.72	0.33	1.98
6	0.31	2.03	0.27	2.25
7	0.30	2.33	0.25	2.51
8	0.25	2.58	0.18	2.69
9	0.24	2.82	0.15	2.84
10	0.13	2.95	0.05	2.89

TABLE A.5 - LATERAL DEFLECTIONS. TEN-STORY FRAME

A.3 SIXTEEN-STORY UBC FRAME

The plan and elevation of this building are shown on Figures 2.3 and 2.7. The loads used in the design were:

dead load	80 psf	
live load	50 psf	on typical floors
	20 psf	on roof
wind loads	20 psf	stories 1 to 3
	25 psf	stories 4 to 8
	30 psf	stories 9 to 16

Properties for the first trial analysis were determined based on an approximate analysis using full dead plus live loads in all spans. All girder sections in a given floor were chosen to be the same in all spans, and columns were taken equal at least every two stories.

Code Lateral Loads

Total Weight

dead load on girders	1536 kips
girders and columns	92.9 kips
	1628.9 kips

Base Shear

$Z = 1$, $K = 0.67$, $T = 0.1N = 1.6$ sec. , $C = 0.0427$

$$V = ZKCW = 0.67 \times 0.0427W = 0.0286\ W$$

$$\underline{V = 46.65 \text{ kips}}$$

Code Distribution

$$F_i = (V - F_t) \frac{W_i\ h_i}{\Sigma W_i h_i}$$

$$F_t = 0.004V \left(\frac{h}{D}\right)^2 = 0.004\ (3.25)^2\ V = 0.0423V$$

$$F_t = 1.97 \text{ kips}$$

Story	F_i (kips)	Mass (kips-sec^2/ft)
1	0.41	3.14
2	0.74	3.14
3	1.06	3.14
4	1.39	3.14
5	1.71	3.14
6	2.03	3.14
7	2.34	3.14
8	2.67	3.14
9	2.97	3.14
10	3.28	3.14
11	3.58	3.14
12	3.90	3.14
13	4.19	3.14
14	4.51	3.14
15	4.80	3.14
16	7.07	3.07

Actually the masses vary slightly from top to bottom, due to the change in profile sizes, but for simplicity a constant typical value was used in the analysis as shown above.

Analyses were performed for the same different load combinations as for the other frames. For most floors the wind load was the critical lateral load.

Lateral Load

Table A.6 shows the maximum moments used to design the girders, as well as the sections after the second analysis with modified properties was performed and the lower floors increased due to drift.

Story	Max. Moment K-'		Section Profile		
	D+l	3/4(D+L+Q or W)	1st Trial	2nd Trial**	Drift = Final
1	95.4	64.4 Q	W21 x 55*	W21 x 55*	W24 x 55
2	93.8	89.8 Q	W21 x 55*	W21 x 55*	W24 x 55
3	94.4	97.2 W	W21 x 55*	W21 x 55*	W21 x 55
4	93.8	106.9 W	W21 x 55*	W21 x 55*	W21 x 55
5	94.0	115.8 W	W21 x 49*	W21 x 49*	W21 x 49
6	94.1	124.1 W	W21 x 49*	W21 x 49*	W21 x 49
7	92.9	133.1 W	W21 x 44*	W21 x 44*	W21 x 44
8	93.2	146.6 W	W21 x 44*	W21 x 44*	W21 x 44
9	93.4	154.4 W	W21 x 44*	W21 x 44*	W21 x 44
10	93.4	159 W	W18 x 40*	W18 x 40*	W18 x 40
11	93.9	177.7 W	W18 x 40*	W18 x 40	W18 x 35
12	95.9	182.7 W	W18 x 35	W18 x 35	W18 x 35
13	99.2	188.9 W	W18 x 35	W18 x 35	W18 x 35
14	99.9	202.0 W	W18 x 35	W18 x 35	W18 x 35
15	100.8	206.9 W	W18 x 35	W18 x 35	W18 x 35
16	78.2	209.0 W	W18 x 31	W18 x 31	W16 x 31

(*) Changed from preliminary design (increased)

(**) Control by D+L+W

TABLE A.6 - SIXTEEN-STORY FRAME. GIRDER DESIGN

Column Design

For this case also, the frame was assumed to be properly braced in the out-of-plane direction (Y) and K_y taken as 1. K_x were determined using the AISC procedure. The columns were designed using interaction diagrams [38] with the maximum effects of different load combinations. Tables A.7 and A.8 show the maximum effects from vertical and lateral load for the interior and exterior column lines. Designs were controlled by wind up to floor 12, and by vertical loads thereafter. Drift requirements imposed some changes on the interior columns, but none on the exterior ones. Deflections by wind (which was more critical than earthquake at all times) are given in Table A.9.

DEFLECTIONS (in)

Floor	Δ	δ
1	0.49	0.49
2	0.44	0.94
3	0.47	1.41
4	0.46	1.87
5	0.47	2.34
6	0.45	2.78
7	0.44	3.22
8	0.40	3.62
9	0.36	3.99
10	0.36	4.34
11	0.36	4.70
12	0.31	5.02
13	0.31	5.33
14	0.22	5.56
15	0.21	5.77
16	0.12	5.89

Story	K_x	D+L		3/4(D+L+W)		Section Profile		
		P	M	P	M	1st Trial	2nd Trial	Drift (Final)
1	1.48	683	18.1	518.7	218.5	W14 x 167*	W14 x 167*	W14 x 167
2	1.64	639	11.9	484.8	147.8	W14 x 167*	W14 x 167*	W14 x 167
3	1.62	555	14.4	421.1	142.9	W14 x 119*	W14 x 119*	W14 x 127
4	1.61	551	13.2	417.5	135.6	W14 x 119*	W14 x 119*	W14 x 127
5	1.61	507	14.3	384.0	127.1	W14 x 111*	W14 x 111*	W14 x 111
6	1.61	464	13.5	351.2	115.4	W14 x 111*	W14 x 111*	W14 x 111
7	1.60	421	15.5	318.3	107.3	W14 x 95	W14 x 95	W14 x 95
8	1.60	378	13.3	285.8	99.8	W14 x 95	W14 x 95	W14 x 95
9	1.57	336	14.7	253.8	92.1	W14 x 84*	W14 x 84*	W14 x 84
10	1.60	294	12.4	221.8	78.2	W14 x 84*	W18 x 84*	W14 x 84
11	1.61	252	14.3	190.0	71.5	W14 x 68*	W14 x 68*	W14 x 68
12	1.58	210	12.5	158.0	57	W14 x 68*	W14 x 68*	W14 x 68
13	1.58	168	15.6	126.4	53.4	W14 x 48	W14 x 48	W14 x 48
14	1.40	126	13.8	95.1	37.4	W14 x 48	W14 x 48	W14 x 48
15	1.25	89.6	8.9	67.7	21.5	W10 x 33	W10 x 33	W10 x 33
16	1.15	42	11.1	31.6	13.2	W10 x 33	W10 x 33	W10 x 33

(*) Changed from preliminary design.

TABLE A.7 - SIXTEEN-STORY FRAME. INTERIOR COLUMN DESIGN

Story	K_x	D+L		3/4(D+L+W)		Section Profiles	
		P	M	P	M	1st Trial	2nd Trial (Final)
1	1.58	341.5	29.5	380.5	151.9	W14 x 127*	W14 x 127*
2	1.88	319.5	39.7	350.0	99.3	W14 x 127*	W14 x 127*
3	1.85	297.5	34.7	319.7	95.7	W14 x 87*	W14 x 95
4	1.82	275.5	35.5	289.8	92.2	W14 x 87*	W14 x 95
5	1.80	253.5	35.7	261.3	88.9	W14 x 78*	W14 x 78*
6	1.78	232.0	35.6	206.7	80.3	W14 x 78*	W14 x 78*
7	1.78	210.5	36.7	206.7	75.0	W14 x 68	W14 x 74
8	1.83	189.0	37.2	181.5	71.9	W14 x 68	W14 x 74
9	1.80	168.0	36.1	157.2	71.7	W14 x 61	W14 x 61
10	1.80	147.0	36.8	133.7	62.6	W14 x 61	W14 x 61
11	1.80	126.0	35.0	111.5	59.8	W14 x 48	W14 x 48
12	1.60	105.0	36.9	90.2	50.3	W14 x 48	W14 x 48
13	1.55	87.6	27.6	72.8	39.9	W10 x 39	W10 x 39
14	1.40	68.6	29.1	55.3	33.8	W10 x 39	W10 x 39
15	1.37	46.4	25.6	36.4	30.7	W10 x 33	W10 x 33
16	1.30	21.0	31.5	16.1	25.4	W10 x 33	W10 x 33

(*) Changed from preliminary design.

TABLE A.8 - SIXTEEN-STORY FRAME. EXTERIOR COLUMN DESIGN